ESTIMATION OF CATALYST ACTIVITY PROFILES AND DEACTIVATION PARAMETERS FROM REACTOR OPERATING DATA WITH APPLICATIONS TO NAPHTHA REFORMING

Thesis by

George Chi Hsu

In Partial Fulfillment of the Requirements

For the Degree of

Doctor of Philosophy

California Institute of Technology
Pasadena, California

1972

(Submitted December 16, 1971)

This thesis is dedicated

to my parents

and

to my wife, Ingrid

ACKNOWLEDGMENTS

I wish to express my sincere appreciation to my research advisor, Professor G. R. Gavalas, for his invaluable patience, encouragement, and guidance throughout the course of this work. Moreover, his stimulating philosophy on research and education has motivated my interest in applied research. I am especially grateful to Professor J. H. Seinfeld for his many helpful discussions and valuable advice. He and Professor Gavalas have led me to the interesting field of parameter estimation. I would like also to thank other members of the faculty who have helped strengthen my education and have enriched my past four and one-half years in Pasadena.

Financial support from the California Institute of Technology in the form of Graduate Research and Teaching Assistantships, and from the National Science Foundation Grant GK10136 is gratefully acknowledged.

I wish to express special appreciation to my master-degree advisor, Professor R. C. Kintner, at the Illinois Institute of Technology, with whose encouragement I came to Caltech. Finally, I feel indebted to Dr. R. G. Lindgren for his assistance in correcting the English and to Mrs. Ruth Stratton for her excellent typing of this thesis.

ABSTRACT

Techniques are developed for estimating activity profiles in fixed bed reactors and catalyst deactivation parameters from operating reactor data. These techniques are applicable, in general, to most industrial catalytic processes. The catalytic reforming of naphthas is taken as a broad example to illustrate the estimation schemes and to signify the physical meaning of the kinetic parameters of the estimation equations. The work is described in two parts. Part I deals with the modeling of kinetic rate expressions and the derivation of the working equations for estimation. Part II concentrates on developing various estimation techniques.

Part I: The reactions used to describe naphtha reforming are dehydrogenation and dehydroisomerization of cycloparaffins; isomerization, dehydrocyclization and hydrocracking of paraffins; and the catalyst deactivation reactions, namely coking on alumina sites and sintering of platinum crystallites. The rate expressions for the above reactions are formulated, and the effects of transport limitations on the overall reaction rates are discussed in the appendices. Moreover, various types of interaction between the metallic and acidic active centers of reforming catalysts are discussed as characterizing the different types of reforming reactions.

Part II: In catalytic reactor operation, the activity distribution along the reactor determines the kinetics of the main reaction and is needed for predicting the effect of changes in the feed state and the operating conditions on the reactor output. In the case of a

monofunctional catalyst and of bifunctional catalysts in limiting conditions, the cumulative activity is sufficient for predicting steady reactor output. The estimation of this cumulative activity can be carried out easily from measurements at the reactor exit. For a general bifunctional catalytic system, the detailed activity distribution is needed for describing the reactor operation, and some approximation must be made to obtain practicable estimation schemes. This is accomplished by parametrization techniques using measurements at a few points along the reactor. Such parametrization techniques are illustrated numerically with a simplified model of naphtha reforming.

To determine long term catalyst utilization and regeneration policies, it is necessary to estimate catalyst deactivation parameters from the current operating data. For a first order deactivation model with a monofunctional catalyst or with a bifunctional catalyst in special limiting circumstances, analytical techniques are presented to transform the partial differential equations to ordinary differential equations which admit more feasible estimation schemes. Numerical examples include the catalytic oxidation of butene to butadiene and a simplified model of naphtha reforming. For a general bifunctional system or in the case of a monofunctional catalyst subject to general power law deactivation, the estimation can only be accomplished approximately. The basic feature of an appropriate estimation scheme involves approximating the activity profile by certain polynomials and then estimating the deactivation parameters from the integrated form of the deactivation equation by regression techniques. Different bifunctional systems must be treated by different estimation algorithms,

which are illustrated by several cases of naphtha reforming with different feed or catalyst composition.

TABLE OF CONTENTS

1. INTRODUCTION

Catalysts lower the activation energy barrier of a reaction without any effect on the overall free energy change of the reaction. As a result, under given operating conditions, they usually serve the purpose of promoting reactions which otherwise are slow, or do not proceed at all. The catalyst can also influence product distribution and, in some cases, slow down certain undesired reactions. Thus, the objective of utilizing catalysts in a chemical process is both to increase the yield and to enhance the selectivity.

Catalyst deactivation has been the subject of many recent investigations. Primary interest has been focussed on the determination of optimal operating and regenerating policies, e.g., references [1,2,3,4,5]. Such optimization studies are open loop in the sense that they predict the catalyst activity distribution along the reactor on the basis of an a priori deactivation model. The optimal policies derived in this manner are usually subject to errors due to the variations in the deactivation parameters as a result of changes in deactivation conditions. To provide a closed loop feedback of the information about catalytic behavior of the system, it is essential to estimate the catalyst activity distribution directly from the operating data. Based upon the estimated activity profile, operating conditions can be adjusted appropriately and the deactivation model can be updated periodically. Prompted by these considerations, the present work is concerned particularly with the estimation of catalyst activity profiles and deactivation parameters from current operating measurements.

On the other hand, the scheme for optimizing the operating and regenerating policies of a catalytic reactor may be of steady state or of dynamic nature. Steady state optimization seeks to adjust the operating conditions in accordance with the current distribution of catalyst activity without considering a deactivation model. Therefore, the estimation of catalyst activity profiles is required for short term optimization of catalytic reactor operations. Appropriate estimation schemes are presented in Chapter 6 and by Gavalas et al. [6]. A dynamic optimization takes into consideration both operating conditions and deactivation, and thus requires a deactivation model. An appropriate kinetic model of deactivation would be a differential equation describing the change in catalyst activity in terms of the local activity, temperature, and concentrations. Based upon this deactivation model and the conservation equations of mass and energy, a dynamic optimization can be carried out to determine catalyst utilization and regeneration policies. To carry out long term system optimization, it is thus essential to estimate the kinetic parameters of the catalyst deactivation model. The proposed estimation schemes for monofunctional and bifunctional catalysts are discussed in Chapter 7 and Chapter 8, respectively, and by Gavalas et al. [7].

The estimation techniques presented in this work are all based on operating reactor data, which are available in reality as thermocouple recording of temperature and gas chromatographic analysis of concentrations at the reactor exit or at several points along the reactor. These measured states are coupled with the catalyst activity through the conservation equations. Estimates of activity profiles

and deactivation parameters can thus be obtained by minimizing the error between predicted and measured operating data. For a bifunctional catalytic system, the determination of operating and regenerating policies generally requires the knowledge of the detailed activity profiles for which observations at an infinite number of positions along the reactor would be required in principle. However, in reality, only a limited number of temperature and concentration measurements are available. Therefore, approximation must be used to obtain practicable estimation schemes with a reasonable amount of operating data.

As will be described in the text, the plug flow equations of fixed bed reactors consist of a set of quasi-linear hyperbolic partial differential equations. Several studies have been made for parameter estimation in partial differential equations, e.g., Seinfeld et al. [8,9.10], Pell and Aris [11]). However, for systems of partial differential equations such as those encountered in this study and for more than one parameter, the computational requirements of implementing an estimation algorithm become prohibitive. Therefore, alternative estimation methods which utilize special features of the pertinent partial differential equations must be sought. For the special cases where the declining catalyst activity is uniform along the fixed bed, the estimation of deactivation parameters has been discussed by Gavalas and Seinfeld [12]. The present work extends their study to the generalized cases of position-dependent catalyst deactivation and of bifunctional catalysts. For monofunctional catalytic systems, analytical techniques are presented to transform the partial differential equations to ordinary

differential equations which admit more feasible estimation schemes. For certain limiting cases of bifunctional catalytic systems, the transformation with the help of approximations may still be possible. However, in general, a transformation cannot be carried out for a bifunctional catalyst. Estimation of deactivation parameters in this case is accomplished through approximating the activity profile with certain polynomials and then estimating the deactivation parameters from the integrated form of the deactivation equation by regression techniques. The estimation techniques used in ordinary differential equations are not discussed in this work as they constitute a well-studied topic in the literature. The essential and novel aspects of Part II are: the reduction of the parameter estimation for fixed bed reactors, described by partial differential equations, to one involving ordinary differential equations and the delineation of approximations and types of measurement required in each class of problems.

In order to carry out the above estimation, a set of system equations is always necessary. To describe the estimation schemes consistently and effectively it is desirable to deal with a concrete catalytic process, and preferably a real industrial process. This process should contain more than one catalytic deactivation phenomenon and include several individual reactions to be of sufficiently broad scope. On the other hand, the process should be approximately described by relatively simple kinetic models so that the estimation techniques can be demonstrated clearly. The catalytic reforming of naphtha is chosen in this study as it possesses the above desirable properties. However, it should be kept in mind that the proposed estimation schemes

are applicable to most other catalytic processes.

One of the important refinery processes for the production of high-octane gasoline is naphtha reforming, which employs metallic-acidic bifunctional catalysts. In order to derive the system equations for naphtha reforming, the modeling of the pertinent reaction rates and the derivation of catalyst deactivation equations have to be performed first. Therefore, Part I of this work deals with the kinetic modeling of catalytic naphtha reforming and two catalyst deactivating mechanisms, namely coking on alumina active centers and sintering of platinum particles. Moreover, a fundamental basis for general catalytic rate expressions is discussed qualitatively in the beginning of Part I to provide a consistent background for the derivations. The effect of transport limitations on the overall reaction rates is discussed in the appendices.

For the convenience of readers, this work is presented in two parts which are complete in themselves and may be referred to independently. Nevertheless, an understanding of the modeling described in Part I is important for the application of the proposed estimation schemes to other processes, and consequently a complete reading of both parts is strongly recommended.

PART I

MODELING OF CATALYTIC NAPHTHA REFORMING PROCESSES

2. BASIS OF KINETIC EXPRESSIONS FOR CATALYTIC REACTIONS

Description of Catalytic Kinetics of the Main Reactions in Terms of Active Site Densities

Despite various arguments concerning the nature of catalyst activity in terms of surface imperfections and geometric and electronic factors [13,14,15,16,17,18], the assumption of active sites as a representation of catalyst activity is a working one in catalysis. In general, the active sites of a catalyst include sites that are either unoccupied or are reversibly occupied by reactants, products, intermediates, or poisons.

A catalyst may contain sites of different types or strengths, characterized by different kinetic parameters. The density of active sites of i^{th} type or i^{th} strength will be denoted by s_i, its associated vector of kinetic parameters by p_i. In general, the intrinsic rate of a heterogeneous catalytic reaction has a form

$$r' = f(s,p,x) \tag{2.1}$$

where x is a state variable vector whose components are

concentrations and temperature, i.e., $x = (c_1,\cdots,c_N,T)$

s is a vector of the densities of active sites of different strengths or types

p is a compound vector whose components are p_i, the kinetic parameter vectors

Consider monofunctional catalysts first. The intrinsic reaction rate due to active sites of kinetic parameter vector p_j is proportional to the density of active sites of that kind, s_j, under the

following assumption, according to Gavalas [19]:

> There is no interaction between species adsorbed on neighboring sites. This requires that no elementary step involves more than one site and that the kinetic parameters do not depend on surface coverage.

Therefore, the overall rate of an intrinsic reaction is the summation over all sites of different strengths

$$r' = \sum_{j=1}^{k} s_j f_j(p_j,x) \tag{2.2}$$

Assuming that the surface is uniform or more generally that the relative densities of sites of different strengths do not depend on the extent of deactivation, expression (2.2) can be simplified to

$$r' = sf(p,x) \tag{2.3}$$

Now for a uniform polyfunctional catalyst of n different types, the intrinsic reaction is catalyzed by a portion or all of n types as

$$r' = f(s_1,\cdots,s_m;p_1,\cdots,p_m;x) \quad , \quad m \leq n \tag{2.4}$$

Note that a uniform bifunctional catalyst could have more than two types of active sites. Again, for a uniform surface with no interaction between neighboring occupied sites, the factorization of site densities is justified and

$$r' = \sum_{i=1}^{m} s_i f_i(p_i,x) \quad , \quad m \leq n \tag{2.5}$$

The equations describing a chemical reactor are formulated in terms of global pseudo-homogeneous rates. In the absence of transport limitations the global rate is proportional to the intrinsic rate. In the presence of transport limitations the separability of s no longer holds, and one must consider the distribution of site density inside the catalyst pellet. Under certain limiting conditions (see [6]) the following modified separable form for the global reaction rate is justified

$$r = \phi(s)\ \tilde{f}(p,x) \tag{2.6}$$

Throughout the main chapters of this work, the following three assumptions are adopted in expressing the overall reaction rates:

(i) The reaction is rate determining.

(ii) The surface is uniform. Non-uniform surfaces often behave as uniform, as reported by Halsey [20] and Boudart [21] so that this assumption may often be quite good.

(iii) There is no interaction between species adsorbed on neighboring sites.

As far as the concentration dependence in a catalytic rate expression is concerned, the reaction rate can usually be expressed as a product of powers of the concentrations. The Langmuir-Hinshelwood type equations describing the kinetics of heterogeneous catalytic reactions are not separable with respect to the concentration terms. However, as observed by Weller [22] and Kabel [23], many such reactions can be reasonably well represented by the simpler power expressions. Indeed, they found that in some cases the power model gave a better fit

of the data than the Langmuir-Hinshelwood model. Theoretical justification for these findings was given in the work of Kwan [24], Ozaki, Taylor and Boudart [25], and Temkin and Pyzhev [26].

General Description of Catalyst Deactivation

The mechanisms contributing toward catalyst deactivation are coking, sintering, retardation, sublimation, and poisoning, where the poison may be the result of feed impurities, reaction products, or reaction intermediates. As far as a single active site is concerned, the deactivation taking place by combination with a deactivating species may occur either instantaneously or gradually. Moreover, there are two possible types of instantaneous deactivation. The active site of one type loses its activity completely as a whole, while that of the other reduces its activity only partially to a lower value. In this work the former case of abrupt deactivation is considered for simplicity. Most of the models of catalyst deactivation available in the literature are also limited to this type of instantaneous loss of activity. On the other hand, the deactivation by gradual loss of activity, which may be characterized by a continuous change of kinetic parameters in the deactivation model, is too complicated for the purposes of analysis.

In general, the rate of catalyst decay depends on the catalyst and fluid conditions in a nonlinear fashion

$$\frac{ds}{dt} = g(s,q,x) \tag{2.7}$$

where q is a vector whose components are the deactivation parameters. Here and throughout the rest of this work surface uniformity is

assumed for simplicity. An additional assumption required for simplification of the general expression (2.7) is that each site deactivates independently of its neighbors.

Wojciechowski [27,28] first proposed a simple adsorption controlled deactivation

$$\frac{ds}{dt} = - k_d s^m \tag{2.8}$$

A more general separable model was proposed by Szepe and Levenspiel [29,30] to describe many cases of catalyst deactivation

$$\frac{ds}{dt} = - k_d'(T)\ s^m \tag{2.9}$$

where $$k_d'(T) = k_d \exp(-E_d/RT) \tag{2.10}$$

m , a non-negative constant, is called the deactivation order

E_d is called the activation energy for catalyst decay so that the vector of deactivation parameters q consists of k_d, m, E_d .

In this work a more complex deactivation model which includes a concentration dependent term is used

$$\frac{ds}{dt} = -k_d \exp(-E_d/RT)\ s^m\ \phi(x) \tag{2.11}$$

where $\phi(x)$ is usually in its simplest form, a power function.

3. NATURE OF BIFUNCTIONAL CATALYSTS AND CATALYTIC REACTIONS IN NAPHTHA REFORMING

Literature Review of Bifunctional Catalytic Reforming Reactions

Excellent reviews of both the theoretical and practical aspects of bifunctional catalysis have been given by Ciapetta et al. [31], Weisz [32], Haensel [33], Sinfelt [34], and Thomson and Webb [35]. While other examples of bifunctional catalysis are known [36], the application in catalytic reforming is by far the best known and the one in which most research work has been done. Recently an updated review of the chemistry involved in catalytic reforming was presented by Pollitzer and co-workers [37]. A valuable description of industrial naphtha reforming processes and proven catalysts was given by Thomas [38].

Sinfelt et al. [39] and Lyster et al. [40] have investigated independently the kinetics and mechanism of n-pentane isomerization over a platinum reforming catalyst. Sinfelt and co-workers [41,42] also carried out studies on the role of dehydrogenation activity in the isomerization and dehydrocyclization of hydrocarbons. Nix and Weisz [43] studied the hydrocarbon reaction path with dual functional catalyst component mixtures. The dehydrogenation of cycloparaffins has been studied by several workers. Among them, Jenkins and Thomas [44], Ross and Valentine [45] looked into the kinetics, Graham et al. [46] set up a transport controlled model, and Hawthorn et al. [47] presented a mathematical model for packed bed reactors. The kinetics of catalytic dehydrocyclization of n-paraffins has been investigated

by Davis and Venuto [48] over "nonacidic" supported platinum catalysts, while Rohrer and co-workers [49] carried out a study over regular platinum reforming catalysts. The article by Langlois and Sullivan [50] serves as a good review for the chemistry of catalytic hydrocracking of hydrocarbons over various catalysts. The kinetics of n-heptane hydrocracking were discussed by Myers and Munns [51].

Industrial reports on the reactions involved in catalytic reforming have been given by several workers. Hettinger et al. [52] discussed thoroughly the effects of certain catalyst properties and poisons in the reforming reactions, Donaldson et al. [53] studied the dehydrocyclization in reforming, Heinemann et al. [54] examined the reforming of hydrocracked naphthas, Beyler et al. [55] investigated the aromatization in reforming, and a review on the overall reforming reactions was given by Hatch [56]. Flow charts and some economic or technical data on industrial reforming processes appeared in Hydrocarbon Processing [57,58,59,60,61]. Information on the thermodynamic properties of hydrocarbons can be obtained from Rossini et al. [62].

Description of Bifunctional Reforming Catalysts

The bifunctional catalysts consist of a metallic hydrogenation-dehydrogenation component, for example platinum, palladium, or nickel, supported on an oxide acidic component such as alumina or silica-alumina. The catalysts frequently contain a small amount of halogens, such as chlorine or fluorine which serve as effective promoters for acid-catalyzed reactions. However, in this work, only pure platinum on alumina catalyst is considered for simplicity.

The amount of platinum present is commonly within the range of 0.3 to 1.0 wt. % in the form of fine dispersion on an acidic alumina (γ or η) . The aluminas commonly used have surface areas in the range of 150 to 300 m^2/gm, corresponding to average pore radii of 60 to 30 angstroms. The reforming catalysts used commercially are in the form of cylindrical pellets about 1/16 × 1/8 inch in size. One common method of preparing such a catalyst involves impregnation of alumina with chloroplatinic acid, followed by calcination in air at temperatures in the range 550 to 600°C.

The degree of platinum dispersion in reforming catalysts must be large, for on freshly prepared catalysts, hydrogen chemisorption is extensive; it amounts to about one hydrogen atom per platinum atom [63]. Thus if the platinum is in crystallite form, it must have a crystal size of about 10 angstroms.

The alumina support has been shown to be acidic in nature. An acid is defined as a species capable of accepting electron pairs (Lewis acid definition) or as one capable of donating protons (Brønsted acid definition). The solid state structure of alumina is reminiscent of organic polymers in the sense that one or more characteristic groups (e.g., an alumina atom coordinated with four or six oxygen atoms) are linked and repeated in two-dimensional or three-dimensional networks.

Description of Catalytic Reforming Reactions

Some of the typical reforming reactions catalyzed by platinum on alumina catalysts, along with specific examples of each are listed below:

(i) Dehydrogenation of cycloparaffins to aromatics

Methylcyclohexane ——> Toluene + $3H_2$

Cyclohexane ——> Benzene + $3H_2$

(ii) Dehydroisomerization of alkylcycloparaffins to aromatics

Methylcyclopentane ——> Benzene + $3H_2$

(iii) Isomerization of alkylcycloparaffins to cycloparaffins

Methylcyclopentane ——> Cyclohexane

(iv) Isomerization of n-paraffins to branched paraffins

n-heptane ——> iso-heptane

n-hexane ——> iso-hexane

(v) Dehydrocyclization of paraffins to aromatics

n-heptane ——> toluene + $4H_2$

N-hexane ——> benzene + $4H_2$

(vi) Hydrocracking to low molecular weight paraffins

n-heptane + H_2 ——> butane + propane

n-hexane + H_2 ——> 2 propane

Of all the reactions taking place in catalytic reforming, the dehydrogenation of cycloparaffins to aromatics occurs by far the most readily. Isomerization reactions also occur readily, but not nearly as fast as dehydrogenation of cycloparaffins. The reactions of dehydrocyclization and hydrocracking, generally occur at much lower rates. The improvement of the octane number in commercial gasoline arises from

the formation of aromatics, and to a lesser extent from isomerization of straight-to-branched chains and cracking of high molecular weight fractions.

General Aspects of Reaction Mechanisms

Ciapetta [31] observed that olefins were isomerized over nickel-silica-alumina catalysts at appreciably lower temperatures than were the corresponding saturated hydrocarbons and suggested that olefins were intermediates in the reaction. Sinfelt et al. [39] and Weisz [32] confirmed experimentally the existence of olefin intermediates via gas phase in trace concentrations corresponding to equilibrium.

Ciapetta [31] also suggested that the rearrangement of the carbon skeleton took place via a carbonium ion mechanism. A carbonium ion refers to a hydrocarbon carrying a positive charge on one of its carbon atoms. The formation of carbonium ions from neutral olefins requires the availability of protons, or other carbonium ions.

The mechanisms involved in the reactions of a complex reforming process can be classified into the following four categories, according to how the two catalytic functions of catalyst are utilized:

(i) Dehydrogenation of cycloparaffin to aromatics requires the dehydrogenation metal function only.

(ii) Hydrocracking can take place either on platinum sites or on acidic sites [51], once the olefin intermediates are formed.

(iii) Isomerization of saturated hydrocarbons proceeds via a succession of steps between the two functions. It involves dehydrogenation to an olefin on platinum sites, followed by desorption and subsequent diffusion through

the gas phase to acidic sites, where the isomerization step takes place, then the isomerized olefin can diffuse through the gas phase to a platinum site, where it undergoes hydrogenation to form the final product.

(iv) Dehydrocyclization takes place only on bifunctional catalysts where sites of the two functions exist in close proximity [64]. It proceeds via formation of an olefin, followed by migration to an acidic site by surface diffusion or interaction with an acidic site in very close proximity to the platinum [65], and then cyclization takes place on acidic centers. The reaction is completed with conversion to benzene via gas phase intermediates and dehydrogenation on metal sites.

Interrelation of Metal and Acidic Centers

Generally speaking, platinum sites and acidic sites act independently. Weisz and Swegler [66] and Hindin [67] have shown that mechanical mixtures in which the dehydrogenation and acidic functions were present on separate particles were active for isomerization or dehydroisomerization of saturated hydrocarbons, provided the catalyst particles were small enough. The independence of two functional sites means that the reactions catalyzed can proceed via gas phase intermediates, which diffuse from one type of site to the other.

The dehydrocyclization reaction does not proceed via gas phase intermediates. According to the description in the last section, it involves a surface migration step from a metal site to a neighboring acidic site. The occurrence of dehydrocyclization thus requires the presence of a platinum-acid co-site, or complex. The density of this postulated co-site should in principle depend upon the detailed site

distributions of both functions, the geometric structure of the catalyst, the surface diffusion mechanism, and the mobility of an adsorbed species on a heterogeneous surface. However, due to the lack of information for the above items, in this work the platinum-alumina co-site density is approximated by the product of platinum and alumina site densities. This co-site acts as a third type of catalytic site in addition to the platinum and alumina sites. Therefore, a bifunctional catalyst may indeed involve more than two types of catalytic sites.

Thermodynamic Considerations

The thermodynamics of the more important reactions in naphtha reforming can be discussed conveniently by referring to the equilibria involved in the various interconversions among the existing hydrocarbons. Some thermodynamic equilibrium constants and heats of reaction at 500°C are given in Table 1. The equilibrium between methylcyclopentane and cyclohexane favors the former, indicating that the five-membered ring structure is more stable than the six-membered ring. In the case of the equilibria between n-hexane and methylpentanes, it can be seen that the 2-methylpentane is the favored isomer over 3-methylpentane. On the other hand, a strong kinetic barrier resists the transformation of a singly branched to doubly branched isomer [31], which prevents the further isomerization to dimethylparaffins. The equilibria of isomerization reactions are much less temperature sensitive than those of dehydrogenation reactions, since the heats of reaction are quite small.

The dehydrogenation and dehydrocyclization to aromatics is seen to be strongly endothermic, so that increasing temperature has a marked

TABLE 1

THERMODYNAMIC DATA FOR TYPICAL REFORMING REACTIONS*

Reaction	K at 500°C	ΔH K_{cal}/g_{mole}
Cyclohexane ——> benzene + $3H_2$	6×10^5	52.8
Methylcyclohexane ——> toluene + $3H_2$	2×10^6	≈53
Methylcyclopentane ——> cyclohexane	0.086	-3.8
n-Hexane ——> benzene + $4H_2$	0.78×10^5	63.6
n-Hexane ——> 2-methylpentane	1.1	-1.4
n-Hexane ——> 3-methylpentane	0.76	-1.1
n-Pentane ——> iso-pentane	2.0	-1.8
n-Hexane ——> 1-hexene + H_2	0.037	31.0

*Data from Rossini et al. [62]

effect on improving the extent of conversion. Hydrogen partial pressure obviously has a marked effect on the extent of formation of aromatics too, and from the viewpoint of equilibrium alone, it is advantageous to operate at as high a temperature and as low a hydrogen partial pressure as possible to maximize the yield of aromatics. However, catalyst deactivation due to formation of carbonaceous residues on the surface and catalyst thermal damage due to high temperature or hot spots impose a practical lower limit on the hydrogen partial pressure and an upper limit on the operating temperature.

The dehydrogenation of paraffins to olefins, which occurs only to a small extent, is of importance from the viewpoint of the reaction path. The thermodynamics of olefin formation can play an important role in determining the rates of these reactions which proceed via olefin intermediates, since it sets an upper limit on the attainable concentration of olefins.

Characterization of the Overall Reaction Schemes

The overall reaction schemes for C_7 and C_6 hydrocarbons are presented schematically in Figures 1 and 2. The type of active sites which catalyzes each individual reaction is indicated, along with the corresponding rate constant. Here s_1 stands for the dimensionless site density of platinum and s_2 stands for that of alumina.

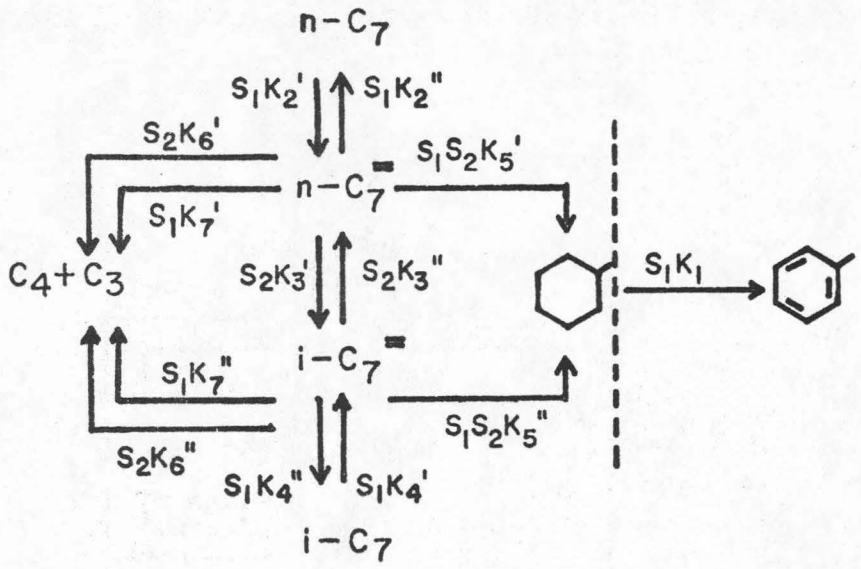

Fig. 1. Reaction Mechanism in the Reforming of C_7 Hydrocarbons

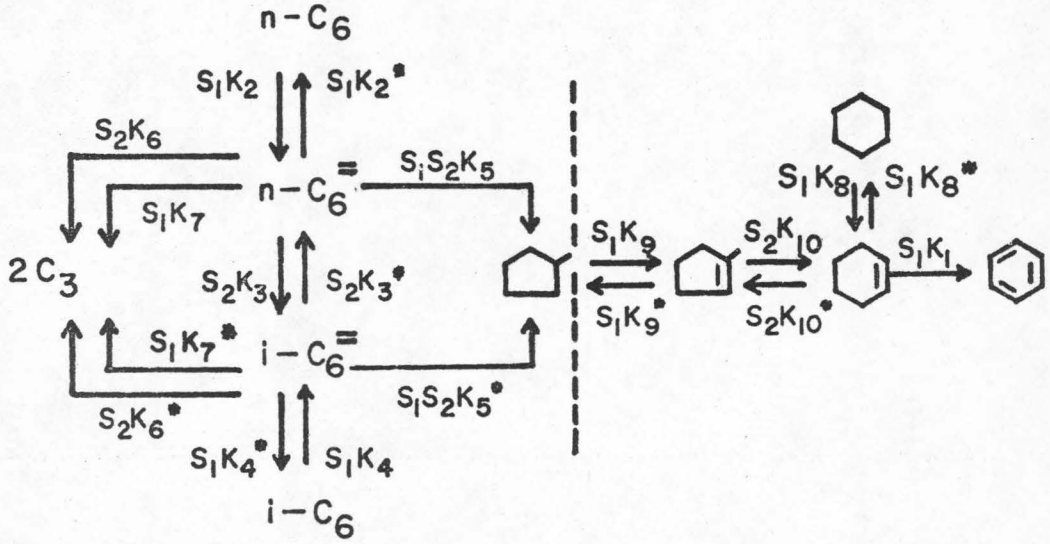

Fig. 2. Reaction Mechanism in the Reforming of C_6 Hydrocarbons

4. CATALYST DEACTIVATION IN NAPHTHA REFORMING

Literature Review of Catalyst Deactivation

Because of its great importance, the deactivation of catalyst pellets in fixed bed reactors has been studied widely both experimentally and theoretically. Many models have been proposed to describe the phenomena of catalyst deactivation. The early approaches tended to concentrate on empirical correlations and these are still favored as first approximations in industrial work. Wheeler [68] has proposed an important model of catalyst deactivation based on the increase in diffusional resistance as deposits accumulate in catalyst pores. A second important approach is that of Froment and Bischoff [69] who have developed a model based on the amount of coke deposited on the catalyst due to reaction. The third and best known model describes catalyst deactivation by competitive adsorption of reactant and poison molecules on active sites. The theory of Langmuir-Hinshelwood type of poison adsorption was fully described by Laidler [70], and its mechanism and kinetics were recently studied by Tan [71] and Forni et al. [72]. Chu [73] has also used a Langmuir-Hinshelwood kinetic model to study the effect of adsorption on three types of catalyst fouling, i.e., series, parallel, and independent.

Wheeler [74] extended Thiele's work [75] on pore diffusion to include nonuniform poisoning in the Langmuir-Hinshelwood model, and discussed the effects of catalyst poisoning on reaction rates. He distinguished between those cases in which activity was linearly related to the fraction of active sites or surface poisoned and those in which poisoning of a small fraction of sites resulted in a large decrease in activity.

These two situations were termed nonselective and selective poisoning, respectively. Recently Carberry and co-workers [76,77] have used the "shell-progressive rate mechanism" to describe the deactivation characteristics of pore-mouth poisoned catalysts. This approach showed the time-dependent effect of pore-mouth poisoning on the activity of catalysts. The effects of the "pore-mouth poisoning" on the overall reaction rate and catalyst selectivity were discussed by Petersen [78] and Sada et al. [79]. An experimental technique has been developed to differentiate between uniform poisoning and pre-mouth poisoning for a first-order reaction by Balder and Petersen [80].

As to the effects of poisoning in fixed bed reactors, Wheeler and Robell [81] recently combined much of the previous theory to describe activity decline in a fixed bed reactor with poison in the feed. Haynes [82] extended their model to include the case of transport limitation. Froment and co-workers [83,84] have studied the unsteady state behavior of a fixed catalytic reactor by coupling the rate equation for the formation of the catalyst fouling compound to the material balance of the main reaction. The expressions derived by Froment and Bischoff were used by Massamune and Smith [85] to evaluate the performance of a pellet in terms of the effectiveness factor which is a function of time and Thiele modulus. Using the same procedure as above, Sagara et al. [86] extended the study to evaluate the effects of non-isothermal operation of catalysts on deactivation. Weekman [87] studied the dynamics of catalytic cracking in fixed bed, moving bed, and fluidized bed reactors. Olson [88] and Kunugita et al. [89] evaluated the performance of fixed bed reactors with catalyst fouling.

Bischoff [90] obtained a general solution of equations representing the catalyst regeneration process in poisoned fixed beds, and Ozawa [91,92] applied the Legendre transformation to describe the above phenomena.

Deactivation of the Acidic Component

It is well known that when hydrocarbons are dehydrogenated over an oxide catalyst a hydrogen deficient carbonaceous residue is deposited upon the catalyst surface resulting in a decrease in catalyst activity. This phenomenon is called coking or fouling. Fouled catalysts may be regenerated by burning off the carbonaceous substance, usually with air.

According to Thomas [38] the coke tends to form primarily on the acidic alumina. It has been reported [73,83,87] that coking leads to a linear decrease of alumina activity with respect to the prevailing activity and an exponential decay of activity with respect to catalyst on-stream time. Therefore, the following simplest form of first order deactivation is adopted for alumina activity:

$$\frac{ds_2}{dt} = - k_{d2} s_2 \exp(-E_{d2}/RT) \qquad (4.1)$$

A more general deactivation model should include the role of concentration variables. However, just which concentration terms should be included is open to question due to the fact that the exact chemical constituents of coke and the detailed coking mechanism are still unknown. Nevertheless, based on the following limited experimental information, a simplified mechanism for coke formation is postulated

in this work.

It is widely accepted that coke is formed via polymerization. As suggested by Peri [93], Hall and co-workers [94,95], and Ozaki [96] it is possible that coke is a polymeric carbonium ion formed by reaction of an olefin with a Brønsted acidic site. This theory has been recently supported experimentally by Leftin and Hermana [97] and Hightower [98]. As to the coking precursor, according to Hightower and Emmett [99], olefins are by far the most active compounds in forming coke. Aromatics appear to be second in coke-forming activity with an average magnitude ten times less than that of olefins. They claimed that most of the coke appears to be formed not by alkylation of benzene or toluene into condensed polycyclic compounds, but rather by polymerization of straight olefinic species.

As an illustration, the following simplified coking mechanism is postulated for a system of C_7 hydrocarbons:

(i) Dehydrogenation of n-paraffin to olefin

$$C_7H_{16} \underset{s_1k_a^*}{\overset{s_1k_a}{\rightleftharpoons}} C_7H_{14} + H_2 \qquad (4.2)$$

(ii) Formation of carbonium ion due to the transfer of a proton from acidic site

$$C_7H_{14} + [H^+] \underset{s_2k_b^*}{\overset{s_2k_b}{\rightleftharpoons}} [C_7H_{15}^+] \qquad (4.3)$$

(iii) Irreversible polymerization of carbonium ion on alumina site with olefin from gas phase to form coke

$$[C_7H_{15}^+] + C_7H_{14} \xrightarrow{s_2 k_c} [C_{14}H_{29}^+] \tag{4.4}$$

where the brackets refer to species on the surface. The product $[C_{14}H_{29}^+]$, an unsaturated polymeric carbonium ion deposited on the active alumina surface, is a coking substance . Denote the concentrations of C_7H_{16}, C_7H_{14}, $[C_7H_{15}^+]$, $[C_{14}H_{29}^+]$, and H_2 by c_2, c_a, c_b, c_c, and c_7 . Assuming that the linear velocity does not vary along the tubular reactor, material balances can be set up under the usual assumptions as follows:

$$u \frac{dc_2}{dz} = - (k_a c_2 - k_a^* c_a c_7) s_1 \tag{4.5}$$

$$u \frac{dc_a}{dz} = (k_a c_2 - k_a^* c_a c_7) s_1 - (k_b c_a - k_b^* c_b) s_2 - k_c c_a c_b s_2 \tag{4.6}$$

$$u \frac{dc_b}{dz} = (k_b c_a - k_b^* c_b) s_2 - k_c c_a c_b s_2 \tag{4.7}$$

$$u \frac{dc_c}{dz} = k_c c_a c_b s_2 \tag{4.8}$$

Here the rate constants k_a, k_a^* relate to the thermodynamic equilibrium constant of reaction (i), K_a , by

$$\frac{k_a}{k_a^* c_7} = K_a \frac{p_o}{p_{H_2}} \tag{4.9}$$

where $p_o = 1$ atm is the standard pressure and p_{H_2} is the partial pressure of hydrogen.

Since around the temperature of interest K_a is very small, e.g., at 600^oK $K_a \simeq 0.45 \times 10^{-6}$, for any reasonable p_{H_2} ,

$$k_a << k_a^* c_7 \tag{4.10}$$

Given this relative magnitude of rate constants and the irreversibility of step (4.4), steady state approximations on olefin and its corresponding carbonium ion is justified, and thus

$$c_a = k_b^* s_2 c_b / (k_b s_2 - k_c s_2 c_b) \tag{4.11}$$

$$c_b = [(k_a^* c_7 s_1 + k_b s_2) c_a - k_a c_2 s_1] / (k_b^* s_2 - k_c s_2 c_a) \tag{4.12}$$

If it is assumed that formation of the carbonium ion, i.e., step (4.3) is rate determining, then

$$k_b s_2,\ k_b^* s_2 << k_c s_2,\ k_a s_1,\ k_a^* s_1 \tag{4.13}$$

The solution of Eqs. (4.11), (4.12) can be simplified upon utilization of the inequalities (4.10) and (4.13) as

$$c_a = \tilde{k}_2 c_2 \quad , \quad c_b = \tilde{k}_3 c_2 \tag{4.14}$$

where

$$\tilde{k}_2 = k_a / k_a^* c_7 \quad , \quad \tilde{k}_3 = k_a k_b / (k_a^* k_b^* c_7) \tag{4.15}$$

Therefore, the reaction rate of coke formation can be obtained from Eq. (4.8) as

$$r_c = \tilde{k}_c s_2 c_2^2 \tag{4.16}$$

where

$$\tilde{k}_c = k_c \tilde{k}_2 \tilde{k}_3 = \tilde{k}_{co} \exp(-E_{d2}/RT) \tag{4.17}$$

and the deactivation of the alumina site density due to coke formation has the form

$$\frac{ds_2}{dt} = - k_{d2} s_2 c_2^2 \exp(-E_{d2}/RT) \tag{4.18}$$

where k_{d2} is proportional to $\tilde{k}_{co}$.

Based on this deactivation model the coke formation reaction can be represented schematically by

$$2\ n\text{-}c_7 \xrightarrow{s_2 k'_{d2}} \text{coke} \tag{4.19}$$

where

$$k'_{d2} = k_{d2} \exp(-E_{d2}/RT) \tag{4.20}$$

In this work both the simplest model of Eq. (4.1) and the more general one of Eq. (4.18) are used to represent the deactivation of alumina due to coking. However, it should be noted that so far only the nonselective type of coke formation (i.e., uniform poisoning) has been considered. This involves uniform deposition of coke throughout the pellet, so that sites at the center of the pellet are exposed to the same conditions of coking as those at the surface. This kind of poisoning is expected to prevail in the naphtha reforming process, because of the low reaction rate of coking. For the more complicated pore-mouth poisoning, the rates of the main reactions catalyzed by alumina sites should be modified as discussed in Appendix A.

Deactivation of the Metal Component

The hydrogenation-dehydrogenation activity of the metal component of a bifunctional catalyst relates directly to its adsorptive capacity, which is usually characterized by the macroscopic average hydrogen-to-platinum atomic ratio obtained from hydrogen chemisorption

experiments. Since the hydrogen-to-platinum ratio is proportional to the specific surface area of platinum [100,101], the platinum activity relates directly to its specific area. On this basis, a deactivation model for platinum activity can be expressed by the reduction of the specific area of platinum.

As the temperature of the reforming process is high (900 $\sim$ 950°F) and the size of the platinum crystallites is small ($\sim$ 10 angstroms initially), platinum particles diffuse along the catalyst surface and collide with each other. Due to the metallurgic behavior of platinum, two colliding particles tend to change the shape of their collision boundaries and coalesce together like two liquid drops [102]. This phenomenon is called sintering. As a result of sintering, the average size of platinum particles grows and the specific surface area decreases.

A large number of studies on sintering phenomena have been reported in the literature. They deal primarily with the process of coalescence for particles of large size. However, in naphtha reforming the size of platinum particles remains small (< 200 angstrom) during the period between two successive catalyst regenerations. The process of coalescence for particles of such a small size is accomplished almost instantaneously compared to that of surface migration, according to Herrmann et al. [103] and Duwez [104]. Therefore, the rate determining process for surface reduction is surface migration. The velocity of the surface migration should in principle be determined by the size of the particles, the net microforces acting upon them, and the induced solid phase viscous drag, for which no exact theory has been available.

Therefore, in this work the following empirical platinum deactivation model reported by Hermann et al. [105] is adopted:

$$\frac{ds_1}{dt} = - k_{d1} s_1^2 \exp(-E_{d1}/RT) \qquad (4.21)$$

The above equation states that the rate of decrease in platinum chemisorptive capacity is second-order with respect to the prevailing chemisorptive capacity. It should also be noted that platinum activity declines very slowly compared to the acidic activity in naphtha reforming. For practical purposes, platinum activity can usually be approximated as a constant between two successive catalyst regenerations.

5. MODELING OF NAPHTHA REFORMING IN FIXED BED REACTORS

Industrial Significance of Naphtha Reforming Processes

The oil industry employs extensively catalytic methods, such as catalytic cracking, reforming, desulfurization, isomerization, dehydrogenation, hydrogenation, hydrocracking, and chlorination. Among them catalytic cracking of high boiling petroleum fractions and reforming of naphthas are the most significant in terms of their economic value in the petroleum industry.

Naphtha reforming is a catalytic process for producing high octane gasoline from crude naphthas. It provides a ready and convenient route to a range of aromatic hydrocarbons from readily available and relatively inexpensive starting materials. As the demand for high octane number fuels with little or no lead increases, the future prospects of catalytic reforming are bright and the technology of improving reforming processes is urgently needed in the decade ahead.

Theoretical Significance of Studies of Naphtha Reforming

The use of bifunctional catalysts in the reforming of petroleum naphthas represents one of the most outstanding applications of modern heterogeneous catalysis over the past decade. In order to facilitate the application of bifunctional catalysts, the principles embodied in bifunctional catalysis have to be understood. For this purpose, the catalytic behavior involved in naphtha reforming, apart from its intriguing kinetics and mechanisms, has attracted the attention of chemical engineers as well as catalytic chemists.

The catalytic reforming process is carried out in fixed bed reactors which can be represented by a set of nonlinear partial differential equations. It is the author's belief that this mathematical representation and the associated estimation techniques can be extended to treat a great deal of chemical systems such as the desulfurization on Co-Mo catalysts, the oxidation of butene over Bi-Mo catalysts, the catalytic oxidation of xylene using V_2O_5 catalysts, etc.

Description of the Naphtha Reforming Processes

Crude naphthas consist mainly of various naphthenes (i.e., cycloparaffins) and paraffins along with some minor amounts of aromatics and olefins. The detailed composition varies quantitatively from one geographical feed source to another. The content of naphthenes decreases significantly from Gulf Coast naphthas ($\sim$ 60% in volume) to Mid-Continent naphthas ($\sim$ 45%), and then to Arkansas naphthas ($\sim$ 15%). The typical compositions of the three types of naphtha feed stock mentioned are listed in Table 2, and the detailed composition of a typical Mid-Continent naphtha is described in Table 3. Due to the stable chemical nature of aromatics and the presence of olefins in very small amounts ($<$ 0.05% usually), only cycloparaffins and paraffins with total content of about 95% in volume are considered in this study.

Naphtha reforming is carried out in adiabatic fixed bed reactors. Due to the highly endothermic dehydrogenation of cycloparaffins to aromatics, a multi-bed reactor is used, and heat is supplied in between the reactors to keep the inlet streams at desirable temperatures. The exact engineering layout of a reforming plant varies from one commercial process to another. In general, three fixed bed

TABLE 2

TYPICAL COMPOSITION OF DIFFERENT NAPHTHAS*

Composition (Volume Percent)	Gulf Coast	Mid-Continent	Arkansas
Naphthenes	55.5	41.5	15.0
Paraffins	26.0	50.0	77.0
Aromatics	18.5	8.5	8.0
Octane No. (Research, Clear)	59.4	44.5	45.3

*Data from Petroleum Refiner 33, No. 4, p. 153 (1954).

TABLE 3

COMPOSITION OF A TYPICAL MID-CONTINENT NAPHTHA

Component	Volume Percent*
Methylcyclohexane	12.5%
Cyclohexane	14.0%
Methylcyclopentane	16.5%
Aromatics	5.1%
Olefins	0.4%
Paraffins	51.5%

*Refer to Beyler, et al. [55]

catalytic reactors are connected in series, each reactor preceded by a fired heater. The first reactor is usually the smallest and the last is the largest. An additional reactor, called a "swing" reactor, is used for substitution of any reactor whose catalyst is fouled. Since dehydrogenation of naphthenes to aromatics occurs very fast, it is the dominant reaction in the first reactor. The reactions taking place in the second reactor consist mainly of dehydrogenation of cycloparaffins and isomerization of n-paraffins along with the coking and sintering deactivation reactions. These reactions essentially characterize the process of naphtha reforming. Finally, the last reactor includes the much slower dehydrocyclization and hydrocracking in addition to the above-mentioned reactions.

At temperatures in the range 400-500^{o}C, common in catalytic reforming, almost all reforming reactions are observed to occur in the reaction rate controlling regime. However, strictly speaking the global rate of dehydrogeneration of cycloparaffins to aromatics whose intrinsic reaction rate is the fastest among all reforming reactions is limited by intraparticle diffusion [106]. For a diffusion-limited reaction, its global rate is commonly expressed using the effectiveness factor. In Appendix B the effectiveness factor for dehydrogenation of cycloparaffins to aromatics is considered in detail.

Naphtha feed stock mixed with a high concentration of hydrogen-rich recycle gas, which serves the purpose of suppressing coke formation, enters the reactor inlet as a dilute hydrocarbon feed. Typical operating conditions are as follows:

(i) Reactor inlet temperature: 900-950^{o}F

(ii) Reactor pressure: 200-300 psig

(iii) Hydrogen content in the feed stream: 4-10 moles per mole of hydrocarbon

The inlet temperature is adjusted very slowly upwards during the operation as the catalyst gradually loses its activity.

Arsenic, copper, or lead compounds act as permanent poisons in platinum reforming. Basic nitrogen compounds will neutralize the activity of alumina sites and act as reversible poisons for the isomerizing and hydrocracking functions. In a similar way, sulfur compounds act as reversible poisons for the platinum. Because of these, desulfurization units preceding the reformer usually must reduce N to < 0.5 ppm and S to < 10 ppm, and the resulting NH_3 and H_2S are removed before going to the reformer. Therefore, the above trace amounts of impurities are not considered in this work.

The growth of platinum crystallites (i.e., sintering) can be inhibited by adding rhenium to the catalyst, because apparently the Re forms an alloy with the Pt that is more stable than the Pt. Furthermore, sintering is observed to be a rather slow process compared to coking except under very severe operating conditions. Therefore, the length of catalyst utilization period before successive regenerations is generally determined by the extent of coking on the acidic function of the catalyst. The catalyst regeneration cycle may vary from a few days to several months depending upon the operating pressure and hydrogen recirculating ratio, due to the fact that coking is slowed down by increasing the operating total pressure and recirculating more hydrogen. During each operating period (i.e.,

between two successive catalyst regenerations) the platinum activity decreases only slightly. For practical purposes the platinum activity profile along the reactor is usually approximated as a constant.

Dynamical Behavior in Fixed Bed Reactors

In order to formulate the mathematical equations for a catalytic process in adiabatic fixed bed reactors, the following assumptions are used.

(i) The size of catalysts is small enough so that a continuum representation is adequate.

(ii) There is no temperature gradient between solid catalyst and its neighboring gas due to a fast heat transfer rate.

(iii) The fluid flow in the reactor is in plug flow pattern with negligible pressure drop.

(iv) Mass transfer occurs only by bulk flow. This means negligible axial and infinite radial dispersion.

(v) Heat transfer also occurs only in the direction of fluid flow. This implies that there is no radial temperature gradient and the temperature distribution is uniform over the cross-section of the reactor.

Based upon the above assumptions, the dynamical behavior of fixed bed operations can be described by the following set of quasi-linear partial differential equations:

$$\frac{\partial c_i}{\partial t} + \frac{\partial}{\partial z}(uc_i) = \sum_{j=1}^{R} \nu_{ij} \tilde{f}_j(c,s) \quad , \quad i = 1,\cdots,N \tag{5.1}$$

$$\varepsilon c_p[\frac{\partial}{\partial t}(\rho T_g) + \frac{\partial}{\partial z}(\rho u\, T_g)] = Ah_t(T_s - T_g) \tag{5.2}$$

$$(1-\varepsilon)\rho_p c_{p_s} \frac{\partial T_s}{\partial t} = \varepsilon \sum_{j=1}^{R} (-\Delta H_j)\, \tilde{f}_j(c,s) - Ah_t(T_s - T_g) \qquad (5.3)$$

where T_g is the temperature in bulk gas phase

T_s is the temperature of the catalyst surface

A is the external surface area of catalyst pellets per unit volume

h_t is the heat transfer coefficient between gas phase and the catalyst surface

and ε is the bed porosity.

The energy balance equations (5.2),(5.3) can be combined to yield

$$[c_p \frac{\partial}{\partial t}(\rho T_g) + \frac{(1-\varepsilon)}{\varepsilon} \rho_p c_{p_s} \frac{\partial T_s}{\partial t}] + c_p \frac{\partial}{\partial z}(\rho u T_g) = \sum_{j=1}^{R} (-\Delta H_j)\, \tilde{f}_j(c,s) \qquad (5.4)$$

With the previously stated assumption that T_s is approximately equal to T_g, the temperature equation becomes

$$[c_p \frac{\partial}{\partial t}(\rho T) + \frac{(1-\varepsilon)}{\varepsilon} \rho_p c_{p_s} \frac{\partial T}{\partial t}] + c_p G \frac{\partial T}{\partial z} = \sum_{j=1}^{R} (-\Delta H_j)\, \tilde{f}_j(c,s) \qquad (5.5)$$

where G is the mass velocity

and $s = (s_1, \cdots, s_m)$ is the vector of slowly varying kinetic parameters, which correspond to physical quantities that do not flow along the reactor. In this work s refers to the vector of various types of active sites in a catalytic bed.

The velocity u in Eq. (5.1) may vary along the reactor due to changes in the total number of moles and in temperature. According to Gavalas [19], u can be replaced by the constant mass flux G by transforming the concentration c_i to a new composition variable y_i for ideal gas systems:

$$y_i = \frac{c_i u}{G} = \frac{c_i}{\rho} = \frac{\text{molar flux, species i}}{\text{mass flux}} \tag{5.6}$$

and

$$c_i = \frac{p}{RT} \frac{y_i}{\sum y_i} \tag{5.7}$$

One talks about slowly varying parameters when the time constant for the state variable y to adjust itself to a new steady state due to the variation in s is very small compared to the characteristic time constant of parameter variation. Therefore, as long as the dynamic disturbances have short correlation time, it is sufficient to approximate the system as a succession of steady states. In the case of a catalytic process, the characteristic time for catalyst deactivation is much longer than the time constants for the relaxation of concentrations and the temperature. Consequently, the concentrations and temperature are at steady state with respect to the catalyst activity provided the input remains constant. With this steady state approximation, the dynamic behavior of a one-dimensional catalytic reactor is described by

$$G \frac{\partial y}{\partial z} = f(y,s) \tag{5.8}$$

$$\frac{\partial s}{\partial t} = g(y,s) \tag{5.9}$$

where $$y = (y_1, \cdots, y_N, T) \tag{5.10}$$

In addition to the heterogeneous catalytic system, the above set of partial differential equations (Eqs. (5.8) and (5.9)) characterizes a great variety of chemical processes, such as ion exchange,

chromatography, adsorption, etc.

Modeling of the Catalytic Reforming Reactions

The mechanisms of the catalytic reactions in naphtha reforming have been fully presented in Figures 1 and 2 of Chapter 3. Based on these reaction mechanisms the kinetics and stoichiometric reaction expressions are formulated in this chapter. Consider a naphtha feed stock consisting essentially of C_6 and C_7 hydrocarbons. The difference between the reaction schemes of C_6 and C_7 hydrocarbons lies in the dehydrogenation of cycloparaffin to aromatics which is shown at the right side of the dashed line in Figures 1 and 2. Since the scheme for C_6 hydrocarbons contains that of C_7 hydrocarbons, the former is discussed first, then a straightforward reduction leads to the latter.

Denote the dimensionless site densities of platinum, alumina, and platinum-alumina co-site by s_1, s_2, and s_1s_2 as described previously, and the concentrations of methylcyclopentane, n-hexane, i-hexane, benzene, cyclohexane, propane, hydrogen, methylcyclohexene, n-hexene, i-hexene, and cyclohexene by c_1, c_2, c_3, c_4, c_5, c_6, c_7, c_1', c_2', c_3', and c_5' respectively. Consider first the section lying on the left of the dashed line in Figure 2. In a naphtha reforming process, the declining temperature profile and the increase in the number of moles due to the reaction compensate to some extent changes in density along the reactor. Moreover, the partial pressure of hydrogen in the feed is more than 80% of the total pressure. Thus, the variation of the linear velocity in the reactor may be neglected and the material balance equations can be written as

$$u\frac{dc_1}{dz} = -s_1(k_9c_1 - k_9^*c_7c_1') + s_1s_2(k_5c_2' + k_5^*c_3') \tag{5.11}$$

$$u\frac{dc_2}{dz} = s_1(-k_2c_2 + k_2^*c_7c_2') \tag{5.12}$$

$$u\frac{dc_3}{dz} = s_1(-k_4c_3 + k_4^*c_7c_3') \tag{5.13}$$

$$u\frac{dc_2'}{dz} = s_1(k_2c_2 - k_2^*c_7c_2') + s_2(-k_3c_2' + k_3^*c_3') - (s_2k_6 + s_1k_7 + s_1s_2k_5)c_2' \tag{5.14}$$

$$u\frac{dc_3'}{dz} = s_1(k_4c_3 - k_4^*c_7c_3') + s_2(k_3c_2' - k_3^*c_3') - (s_2k_6^* + s_1k_7^* + s_1s_2k_5^*)c_3' \tag{5.15}$$

$$u\frac{dc_6}{dz} = s_2(k_6c_2' + k_6^*c_3') + s_1(k_7c_2' + k_7^*c_3') \tag{5.16}$$

The equilibrium constants for dehydrogenation of paraffins are related to the corresponding rate constants by

$$\frac{k_2}{k_2^*c_7} = K_2\frac{p_o}{p_{H_2}} \quad , \quad \frac{k_4}{k_4^*c_7} = K_4\frac{p_o}{p_{H_2}} \tag{5.17}$$

where p_o and p_{H_2} are defined as before.

At the temperature of interest K_2 and K_4 are very small, e.g., at 600^oK $K_2 \simeq 0.45\times10^{-6}$, $K_4 \simeq 0.58\times10^{-6}$ and for any reasonable p_{H_2}, $k_2 << k_2^*c_7$ and $k_4 << k_4^*c_7$. For these relative magnitudes of the rate constants, the olefins are at steady state with respect to the paraffins, so that

$$c_2' = \{[(a + bs_2) + c\varepsilon]\ c_2 + d\varepsilon c_3\} \ / \ \text{Det} \tag{5.18}$$

$$c_3' = \{e\varepsilon c_2 + [(f + gs_2) + h\varepsilon]c_3\} \ / \ \text{Det} \tag{5.19}$$

where

$$\varepsilon = s_2/s_1 \tag{5.20}$$

$$\text{Det} = (A + Bs_2 + Cs_2^2) + (D + Es_2)\varepsilon + F\varepsilon^2 \tag{5.21}$$

$$A = (k_2^* c_7 + k_7)(k_4^* c_7 + k_7^*) \tag{5.22}$$

$$B = k_5(k_4^* c_7 + k_7^*) + k_5^*(k_2^* c_7 + k_7) \tag{5.23}$$

$$C = k_5 k_5^* \tag{5.24}$$

$$D = (k_2^* c_7 + k_7)(k_3^* + k_6^*) + (k_4^* c_7 + k_7^*)(k_3 + k_6) \tag{5.25}$$

$$E = k_5(k_3^* + k_6^*) + k_5^*(k_3 + k_6) \tag{5.26}$$

$$F = k_3 k_6^* + k_3^* k_6 + k_6 k_6^* \tag{5.27}$$

$$a = k_2(k_4^* c_7 + k_7^*) \tag{5.28}$$

$$b = k_2 k_5^* \tag{5.29}$$

$$c = k_2(k_3^* + k_6^*) \tag{5.30}$$

$$d = k_4 k_3^* \tag{5.31}$$

$$e = k_2 k_3 \tag{5.32}$$

$$f = k_4(k_2^* c_7 + k_7) \tag{5.33}$$

$$g = k_4 k_5 \tag{5.34}$$

$$h = k_4(k_3 + k_6) \tag{5.35}$$

Upon introducing (5.18) and (5.19) into (5.12) and (5.13) one obtains

$$u \frac{d}{dz} \begin{pmatrix} c_2 \\ c_3 \end{pmatrix} = - \frac{1}{Det} [s_1 F_1 + s_2(F_2 + \varepsilon F_3)] \begin{pmatrix} c_2 \\ c_3 \end{pmatrix} \tag{5.36}$$

where F_1, F_2, and F_3 are the matrices

$$F_1 = \begin{bmatrix} k_2\{(k_4^* c_7 + k_7^*)k_7 + [(k_4^* c_7 + k_7^*)k_5 + k_7 k_5^*]s_2 + k_5 k_5^* s_2^2\} & 0 \\ 0 & k_3\{(k_2^* c_7 + k_7)k_7^* + [(k_2^* c_7 + k_7)k_5^* + k_7^* k_5]s_2 + k_5 k_5^* s_2^2\} \end{bmatrix} \tag{5.37}$$

$$F_2 = \begin{bmatrix} F_{21} & -k_4 k_2^* c_7 k_3^* \\ -k_2 k_4^* c_7 k_3 & F_{22} \end{bmatrix} \tag{5.38}$$

$$F_3 = (k_3 k_6^* + k_3^* k_6 + k_6 k_6^*) \begin{bmatrix} k_2 & 0 \\ 0 & k_4 \end{bmatrix} \tag{5.39}$$

$$F_{21} = k_2\{[(k_4^* c_7 + k_7^*)(k_3 + k_6) + (k_3^* + k_6^*)k_7] + [(k_3 + k_6)k_5^* + (k_3^* + k_6^*)k_5]s_2\} \tag{5.40}$$

$$F_{22} = k_4\{[(k_2^* c_7 + k_7)(k_3^* + k_6^*) + (k_3 + k_6)k_7^*] + [(k_3 + k_6)k_5^* + (k_3^* + k_6^*)k_5]s_2\} \tag{5.41}$$

Now, each individual reaction is discussed as follows:

(i) Isomerization

Consider isomerization only, i.e.,

$$k_5 = k_5^* = k_6 = k_6^* = k_7 = k_7^* = 0 \tag{5.42}$$

Equation (5.36) simplifies to

$$u \frac{d}{dz} \begin{pmatrix} c_2 \\ c_3 \end{pmatrix} = - \frac{s_2 c_7}{Det'} \begin{bmatrix} k_2 k_4^* k_3 & -k_2^* k_4 k_3^* \\ -k_2 k_4^* k_3 & k_2^* k_4 k_3^* \end{bmatrix} \begin{pmatrix} c_2 \\ c_3 \end{pmatrix} \tag{5.43}$$

where

$$Det' = k_2^* k_4^* c_7^2 + (k_2^* c_7 k_3^* + k_4^* c_7 k_3)\varepsilon \tag{5.44}$$

If it is assumed as by Sinfelt et al. [39] that the acidic activity is rate determining, then

$$Det' = k_2^* k_4^* c_7^2$$

and

$$u \frac{d}{dz} \begin{pmatrix} c_2 \\ c_3 \end{pmatrix} = - \frac{s_2}{c_7} \begin{bmatrix} \frac{k_2 k_3}{k_2^*} & - \frac{k_4 k_3^*}{k_4^*} \\ - \frac{k_2 k_3}{k_2^*} & \frac{k_4 k_3^*}{k_4^*} \end{bmatrix} \begin{pmatrix} c_2 \\ c_3 \end{pmatrix} \tag{5.45}$$

(ii) Dehydrocyclization

Consider dehydrocyclization of paraffin to cycloparaffin only, i.e.,

$$k_3 = k_3^* = k_6 = k_6^* = k_7 = k_7^* = 0 \tag{5.46}$$

Equation (5.36) simplifies to

$$u\frac{d}{dz}\begin{pmatrix}c_2\\c_3\end{pmatrix} = -\frac{s_1 s_2}{Det''}\begin{bmatrix}k_2k_5(k_4^*c_7+k_5^*s_2) & 0\\ 0 & k_4k_5^*(k_2^*c_7+k_5s_2)\end{bmatrix}\begin{pmatrix}c_2\\c_3\end{pmatrix} \tag{5.47}$$

where

$$Det'' = k_2^*k_4^*c_7^2 + (k_2^*c_7k_5^*+k_4^*c_7k_5)s_2 + k_5k_5^*s_2^2 \tag{5.48}$$

If it is assumed that the cyclization step is rate determining, i.e.,

$$k_5, k_5^* << k_2^*c_7, k_4^*c_7 \tag{5.49}$$

then

$$Det'' = k_2^*k_4^*c_7^2 \tag{5.50}$$

and

$$u\frac{d}{dz}\begin{pmatrix}c_2\\c_3\end{pmatrix} = -\frac{s_1 s_2}{c_7}\begin{bmatrix}\frac{k_2k_5}{k_2^*} & 0\\ 0 & \frac{k_4k_5^*}{k_4^*}\end{bmatrix}\begin{pmatrix}c_2\\c_3\end{pmatrix} \tag{5.51}$$

(iii) Hydrocracking

Consider hydrocracking only, i.e.,

$$k_3 = k_3^* = k_5 = k_5^* = 0 \tag{5.52}$$

Equation (5.36) simplifies to

$$u\frac{d}{dz}\begin{pmatrix}c_2\\c_3\end{pmatrix} = -\frac{1}{Det'''}[s_1F_1' + s_2(F_2' + \varepsilon F_3')]\begin{pmatrix}c_2\\c_3\end{pmatrix} \tag{5.53}$$

where F_1', F_2', and F_3' are the matrices

$$F_1' = \begin{bmatrix} k_2k_7(k_4^*c_7 + k_7^*) & 0 \\ 0 & k_4k_7^*(k_2^*c_7 + k_7) \end{bmatrix} \tag{5.54}$$

$$F_2' = \begin{bmatrix} k_2[k_6(k_4^*c_7 + k_7^*) + k_6^*k_7] & 0 \\ 0 & k_4[k_6^*(k_2^*c_7 + k_7) + k_6k_7^*] \end{bmatrix} \tag{5.55}$$

$$F_3' = k_6k_6^* \begin{bmatrix} k_2 & 0 \\ 0 & k_4 \end{bmatrix} \tag{5.56}$$

$$\text{Det}''' = (k_2^*k_4^*c_7^2 + k_2^*c_7k_7^* + k_4^*c_7k_7 + k_7k_7^*) + [(k_4^*c_7 + k_7^*)k_6 + (k_2^*c_7 + k_7)k_6^*]\varepsilon + k_6k_6^*\varepsilon^2 \tag{5.57}$$

Suppose that the hydrocracking steps are rate determining, i.e.,

$$k_6,\ k_6^*,\ k_7,\ k_7^* \ll k_2^*c_7,\ k_4^*c_7 \tag{5.58}$$

then

$$\text{Det}''' = k_2^*k_4^*c_7^2 \tag{5.59}$$

and

$$u\frac{d}{dz}\begin{pmatrix} c_2 \\ c_3 \end{pmatrix} = -\left\{ \frac{s_1}{c_7}\begin{bmatrix} \frac{k_2k_7}{k_2^*} & 0 \\ 0 & \frac{k_4k_7^*}{k_4^*} \end{bmatrix} + \frac{s_2}{c_7}\begin{bmatrix} \frac{k_2k_6}{k_2^*} & 0 \\ 0 & \frac{k_4k_6^*}{k_4^*} \end{bmatrix} \right\} \begin{pmatrix} c_2 \\ c_3 \end{pmatrix} \tag{5.60}$$

If it is further assumed as in most of the work reported on

hydrocracking that the rate of hydrocracking over platinum sites is negligible compared to that over alumina sites, then Eq. (5.60) can be reduced to

$$u \frac{d}{dz} \begin{pmatrix} c_2 \\ c_3 \end{pmatrix} = - \frac{s_2}{c_7} \begin{bmatrix} \frac{k_2 k_6}{k_2^*} & 0 \\ 0 & \frac{k_4 k_6^*}{k_4^*} \end{bmatrix} \begin{pmatrix} c_2 \\ c_3 \end{pmatrix} \tag{5.61}$$

(iv) Dehydrogenation of cycloparaffins to aromatics

The reaction scheme for the dehydrogenation of c_6 cycloparaffins to benzene which is shown at the right side of Figure 2 is considered as follows:

$$u \frac{dc_1}{dz} = s_1(-k_9 c_1 + k_9^* c_7 c_1') \tag{5.62}$$

$$u \frac{dc_5}{dz} = s_1(-k_8 c_5 + k_8^* c_7 c_5') \tag{5.63}$$

$$u \frac{dc_1'}{dz} = s_1(k_9 c_1 - k_9^* c_7 c_1') + s_2(-k_{10} c_1' + k_{10}^* c_5') \tag{5.64}$$

$$u \frac{dc_5'}{dz} = s_2(k_{10} c_1' - k_{10}^* c_5') + s_1(k_8 c_5 - k_8^* c_7 c_5' - k_1 c_5') \tag{5.65}$$

$$u \frac{dc_4}{dz} = s_1 k_1 c_5' \tag{5.66}$$

The equilibrium constants for dehydrogenation of paraffins are related to the corresponding rate constants by

$$\frac{k_8}{k_8^* c_7} = K_8 \frac{p_o}{p_{H_2}} \quad , \quad \frac{k_9}{k_9^* c_7} = K_9 \frac{p_o}{p_{H_2}} \tag{5.67}$$

At the temperature of interest K_8 and K_9 are very small ($\sim 4.0 \times 10^{-3}$) and for any reasonable p_{H_2}, $k_8 << k_8^* c_7$ and $k_9 << k_9^* c_7$. For these relative magnitudes of the rate constants the olefins are at steady state with respect to the paraffins,

$$\begin{pmatrix} c_1' \\ c_5' \end{pmatrix} = \frac{1}{\text{Det}} (E_1 + \varepsilon E_2) \begin{pmatrix} c_1 \\ c_5 \end{pmatrix} \tag{5.68}$$

where E_1 and E_2 are the matrices

$$E_1 = \begin{bmatrix} k_9(k_8^* c_7 + k_1) & 0 \\ 0 & k_9^* c_7 k_8 \end{bmatrix} \quad , \quad E_2 = \begin{bmatrix} k_9 k_{10}^* & k_8 k_{10}^* \\ k_9 k_{10} & k_8 k_{10} \end{bmatrix} \tag{5.69}$$

$$\text{Det} = k_9^* c_7 (k_8^* c_7 + k_1) + [k_{10}(k_8^* c_7 + k_1) + k_{10}^* k_9^* c_7]\varepsilon \tag{5.70}$$

Upon introducing (5.68) into (5.62) and (5.63) one obtains

$$u \frac{d}{dz} \begin{pmatrix} c_1 \\ c_5 \end{pmatrix} = - [s_1 G_1 + s_2 G_2] \begin{pmatrix} c_1 \\ c_5 \end{pmatrix} \tag{5.71}$$

where G_1 and G_2 are the matrices

$$G_1 = \begin{bmatrix} 0 & 0 \\ 0 & k_1 k_9^* c_7 k_8 \end{bmatrix} \Big/ \text{Det} \tag{5.72}$$

$$G_2 = \begin{bmatrix} (k_8^* c_7 + k_1) k_9 k_{10} & -k_8 k_9^* c_7 k_{10}^* \\ -k_8^* c_7 k_9 k_{10} & k_8 (k_1 k_{10} + k_9^* c_7 k_{10}^*) \end{bmatrix} \Big/ \text{Det} \tag{5.73}$$

Suppose that the isomerization of olefin is rate determining as before, i.e.,

$$k_{10},\ k_{10}^{*} \ll k_8^{*}c_7,\ k_9^{*}c_7,\ k_1 \tag{5.74}$$

then

$$\text{Det} = k_9^{*}c_7(k_8^{*}c_7 + k_1) \tag{5.75}$$

and G_1 and G_2 in (5.71) simplify to

$$G_1 = \begin{bmatrix} 0 & 0 \\ 0 & g_1 \end{bmatrix} \tag{5.76}$$

$$G_2 = \begin{bmatrix} g_2 & -g_3 k_{10}^{*} \\ -g_2 k_8^{*}c_7/(k_1 + k_8^{*}c_7) & g_3(k_1 k_{10} + k_9^{*}c_7 k_{10}^{*})/k_9^{*}c_7 \end{bmatrix} \tag{5.77}$$

$$g_1 = k_1 k_8/(k_1 + k_8^{*}c_7) \tag{5.78}$$

$$g_2 = k_9 k_{10}/k_9^{*}c_7 \quad , \quad g_3 = k_8/(k_1 + k_8^{*}c_7) \tag{5.79}$$

For the dehydrogenation of c_7 hydrocarbon to aromatics, equations (5.62)-(5.66) are not applicable. Denoting the concentration of methylcyclohexane, toluene, and butane by c_1, c_4, and c_5, the material balance equations can be deduced from Eqs. (5.71) and (5.76) as

$$u\frac{d}{dz}\begin{pmatrix} c_1 \\ c_4 \end{pmatrix} = s_1 g_1 \begin{bmatrix} -1 & 0 \\ 1 & 0 \end{bmatrix} \begin{pmatrix} c_1 \\ c_4 \end{pmatrix} \tag{5.80}$$

In summary of the above modeling work, a catalytic reforming process can be represented by twelve species and nineteen reactions, among which three are reversible. These reactions are shown in Figures 3 and 4. It can be shown that the derived rate expressions for individual reactions can be combined together to form an overall reaction scheme with the following rate expressions. To distinguish the reactions of c_7 hydrocarbons from those of c_6 hydrocarbons, the conditions for c_6 hydrocarbons are designated by the superscripts * and " .

(i) The rates of dehydrogenation of methylcyclohexane, methylcyclopentane, and cyclohexane to aromatics are

$$r_1 = s_1 k_a \rho y_1 \tag{5.81}$$

$$r_1^* = s_1 k_a^* \rho y_1^* \tag{5.82}$$

$$r_2^* = (s_1 k_g^* + s_2 k_g'') \rho y_5^* \tag{5.83}$$

(ii) The rates of isomerization between c_7 paraffins, c_6 paraffins, and c_6 cycloparaffins respectively are

$$r_2 = s_2(k_b y_2 - k_b' y_3) / y_7 \tag{5.84}$$

$$r_3^* = s_2(k_b^* y_2^* - k_b'' y_3^*) / y_7 \tag{5.85}$$

$$r_4^* = s_2(k_f^* y_1^* - k_f'' y_5^*) / y_7 \tag{5.86}$$

(iii) The rates of dehydrocyclization of n-paraffins and i-parrifins to cycloparaffins are

$$r_3 = s_1 s_2 k_c y_2 / y_7 \tag{5.87}$$

$$r_4 = s_1 s_2 k_c' y_3 / y_7 \tag{5.88}$$

$$r_5^* = s_1 s_2 k_c^* y_2^* / y_7 \tag{5.89}$$

$$r_6^* = s_1 s_2 k_c'' y_3^* / y_7 \tag{5.90}$$

(iv) The rates of hydrocracking to low molecular weight hydrocarbons from n-paraffins and i-paraffins respectively are

$$r_5 = (s_2 k_d + s_1 k_e) y_2 / y_7 \tag{5.91}$$

$$r_6 = (s_2 k_d' + s_1 k_e') y_3 / y_7 \tag{5.92}$$

$$r_7^* = (s_2 k_d^* + s_1 k_e^*) y_2^* / y_7 \tag{5.93}$$

$$r_8^* = (s_2 k_d'' + s_1 k_e'') y_3^* / y_7 \tag{5.94}$$

The rate constants k_i throughout this section have the usual Arrhenius dependence

$$k_i = k_{io} \exp(-E_i/RT) \tag{5.95}$$

Mathematical Representation of the Dynamical System

Based upon the models of reaction rates derived in Chapter 5, along with the descriptions given in Chapters 3 and 4, the following mathematical representation of the dynamical system can be obtained:

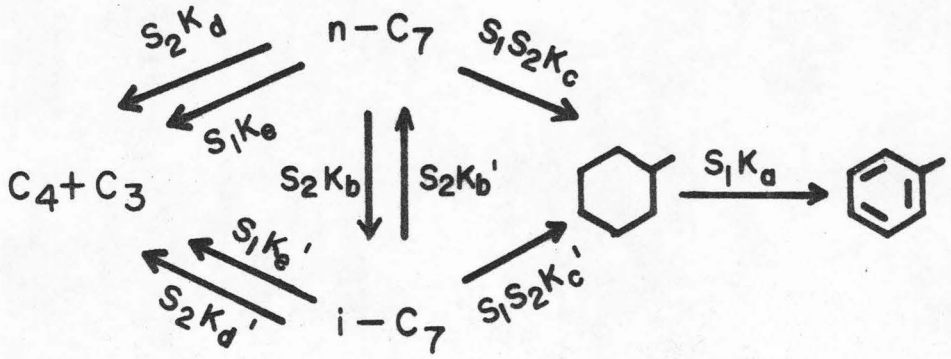

Fig. 3. Stoichiometric Reactions in the Reforming of C_7 Hydrocarbons

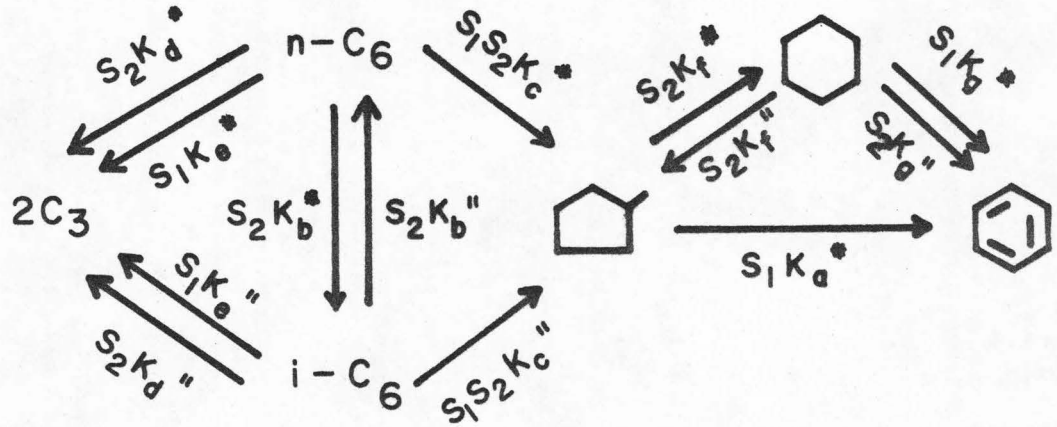

Fig. 4. Stoichiometric Reactions in the Reforming of C_6 Hydrocarbons

(i) The material balance equations describing the pseudo-steady-state operation of an adiabatic fixed bed reactor at constant pressure are

(methylcyclohexane) $$G\frac{\partial y_1}{\partial z} = -r_1 + r_3 + r_4 \tag{5.96}$$

(n-heptane) $$G\frac{\partial y_2}{\partial z} = -r_2 - r_3 - r_5 \tag{5.97}$$

(i-heptane) $$G\frac{\partial y_3}{\partial z} = r_2 - r_4 - r_6 \tag{5.98}$$

(toluene) $$G\frac{\partial y_4}{\partial z} = r_1 \tag{5.99}$$

(methylcyclopentane) $$G\frac{\partial y_1^*}{\partial z} = -r_1^* - r_4^* + r_5^* + r_6^* \tag{5.100}$$

(n-hexane) $$G\frac{\partial y_2^*}{\partial z} = -r_3^* - r_5^* - r_7^* \tag{5.101}$$

(i-hexane) $$G\frac{\partial y_3^*}{\partial z} = r_3^* - r_6^* - r_8^* \tag{5.102}$$

(benzene) $$G\frac{\partial y_4^*}{\partial z} = r_1^* + r_2^* \tag{5.103}$$

(cyclohexane) $$G\frac{\partial y_5^*}{\partial z} = -r_2^* + r_4^* \tag{5.104}$$

(butane) $$G\frac{\partial y_5}{\partial z} = r_5 + r_6 \tag{5.105}$$

(propane) $$G\frac{\partial y_6}{\partial z} = r_5 + r_6 + 2r_7^* + 2r_8^* \tag{5.106}$$

(hydrogen) $$G\frac{\partial y_7}{\partial z} = 3r_1 + r_3 + r_4 - r_5 - r_6 + 3r_1^* + 3r_2^* + r_5^* + r_6^* - r_7^* - r_8^* \tag{5.107}$$

Since the dimension in the above system is too large, the hydrogen

concentration is assumed to remain constant along the reactor during an operating period. Thus the equations for c_7 hydrocarbons, (5.96)-(5.99), are coupled with those for c_6 hydrocarbons, (5.100)-(5.104), only through the temperature dependencies in the rate constants, and they can be solved separately provided that the temperature profile along a tubular reactor is known.

(ii) The energy balance equation can be obtained as follows:

Denote the heats of reaction for r_1, r_3, r_4, r_1^*, r_2^*, r_5^*, and r_6^* by ΔH_1 to ΔH_3 and ΔH_1^* to ΔH_4^* respectively, and assume that

$$k_c = k_c' \quad , \qquad k_d = k_d' \quad , \qquad k_e = k_e' \tag{5.108}$$

$$k_c^* = k_c'' \quad , \qquad k_d^* = k_d'' \quad , \qquad k_e^* = k_e'' \tag{5.109}$$

and

$$\Delta H_2 = \Delta H_3 \quad , \qquad \Delta H_3^* = \Delta H_4^* \tag{5.110}$$

For a feed containing only c_7 hydrocarbons,

$$-c_p G \frac{\partial T}{\partial z} = h_7 \tag{5.111}$$

where

$$h_7 = (\Delta H_1) s_1 k_a \rho y_1 + (\Delta H_2) s_1 s_2 k_c (y_2 + y_3) / y_7 \tag{5.112}$$

Since the heat equation can be obtained by linear combination of (5.96) and (5.99), the following relationship can be obtained

$$-c_p (T - T_o) = (\Delta H_2)(y_1 - y_{1o}) + (\Delta H_1 + \Delta H_2)(y_4 - y_{4o}) \tag{5.113}$$

or

$$y_1 = \phi(T, y_4) \tag{5.114}$$

For a feed containing only c_6 hydrocarbons,

$$-c_p G \frac{\partial T}{\partial z} = h_6 \tag{5.115}$$

where

$$h_6 = (\Delta H_1^*) s_1 k_a^* \rho y_1^* + (\Delta H_2^*)(s_1 k_g^* + s_2 k_g'') \rho y_2^* + (\Delta H_3^*) s_1 s_2 k_c^* (y_2^* + y_3^*) / y_7 \tag{5.116}$$

Since the heat of reaction for the dehydrogenation of methylcyclopentane is approximately equal to that of cyclohexane, i.e.,

$$\Delta H_2^* \simeq \Delta H_1^* \tag{5.117}$$

(5.116) can be simplified to

$$h_6 = (\Delta H_1^*)[s_1 k_a^* \rho y_1^* + (s_1 k_g^* + s_2 k_g'') \rho y_2^*] + (\Delta H_3^*) s_1 s_2 k_c^* (y_2^* + y_3^*) / y_7 \tag{5.118}$$

Since Eqs. (5.115) and (5.118) can be obtained by a linear combination of (5.100), (5.103), and (5.104), the following expression can be obtained

$$-c_p (T - T_o) = (\Delta H_3^*)(y_1^* - y_{1o}^* + y_5^* - y_{5o}^*) + (\Delta H_1^* + \Delta H_3^*)(y_4^* - y_{4o}^*) \tag{5.119}$$

or

$$y_1^* = \psi(T, y_4^*, y_5^*) \tag{5.120}$$

Similarly, for a feed containing both c_7 and c_6 hydrocarbons, it can be shown that

$$-c_p G \frac{\partial T}{\partial z} = h_7 + h_6 \tag{5.121}$$

Now a self-contained partial differential equation system for the state variables in the reforming process of c_7 hydrocarbons consists of Eqs. (5.111), (5.112), and (5.97)-(5.99), while that of c_6 hydrocarbons consists of Eqs. (5.115), (5.118), and (5.101)-(5.104). The other state variables can be expressed as functions of the species referred to in the above equations by using a total carbon and hydrogen balance.

Simulation of the Dynamical System and Measurements

The above representation of a detailed reforming system is too complicated to permit a clear analytical conclusion on either the dynamical behavior or the estimation algorithms. To simplify the mathematical representation and still retain the essential dynamical behavior, naphtha reforming can be characterized by the following two major reactions, according to the description in the first part of this chapter:

(i) The dehydrogenation of cycloparaffin

$$G \frac{\partial y_1}{\partial z} = - s_1 y_1 k_{1o} \exp(- E_1/RT) \tag{5.122}$$

(ii) The isomerization of n-paraffin

$$G \frac{\partial y_2}{\partial z} = - s_2 y_2 k_{2o} \exp(- E_2/RT) \tag{5.123}$$

The temperature distribution along the reactor is determined by the endothermic dehydrogenation reaction as follows:

$$c_p G \frac{\partial T}{\partial z} = (-\Delta H) s_1 y_1 k_{1o} \exp(- E_1/RT) \tag{5.124}$$

Note that isomerization is expressed in terms of an irreversible reaction for simplicity. It is more convenient to write the above three equations in dimensionless form as

$$v \frac{\partial x_1}{\partial \xi} = -\alpha_1 s_1 x_1 \exp[-p_1(\frac{1}{\theta} - 1)] \tag{5.125}$$

$$v \frac{\partial x_2}{\partial \xi} = -\alpha_2 s_2 x_2 \exp[-p_2(\frac{1}{\theta} - 1)] \tag{5.126}$$

$$v \frac{d\theta}{d\xi} = -\frac{\alpha_1}{\lambda} s_1 x_1 \exp[-p_1(\frac{1}{\theta} - 1)] \tag{5.127}$$

where

$$x_i = \frac{y_i}{y_{io}} \ (i = 1,2) \quad , \quad \theta = \frac{T}{T_o} \ , \quad \xi = \frac{z}{L} \tag{5.128}$$

$$p_i = \frac{E_i}{RT_o} \ , \quad \alpha_i = \frac{L}{G_o} k_{io} \exp(-p_i) \quad (i = 1,2) \tag{5.129}$$

$$v = \frac{G}{G_o} \ , \quad \lambda = \frac{c_p T_o}{(\Delta H) y_{1o}} \tag{5.130}$$

By eliminating the right side between Eqs. (5.125), (5.127) one obtains

$$v \frac{\partial \theta}{\partial \xi} = -\frac{\alpha_1}{\lambda} s_1[(x_{1f} - \lambda\theta_f) + \lambda\theta] \exp[-p_1(\frac{1}{\theta} - 1)] \tag{5.131}$$

where the subscript f denotes feed conditions. Equations (5.126) and (5.131) completely describe the steady state operation of the reactor.

For the unsteady state operation due to catalyst deactivation, the dynamical system should also include the accompanying deactivation reactions, which have been described by Eqs. (4.18) and (4.21). Thus, the platinum particles undergo sintering whereby the site density of platinum decreases at a rate

$$\frac{\partial s_1}{\partial \tau} = -\beta_1 s_1^2 \exp[-q_1(\frac{1}{\theta} - 1)] \tag{5.132}$$

The acidic alumina activity declines due to coking at a rate

$$\frac{\partial s_2}{\partial \tau} = -\beta_2 s_2 x_2^2 \exp[-q_2(\frac{1}{\theta} - 1)] \tag{5.133}$$

$$\tau = t/t_o \quad , \qquad q_i = E_{di}/RT \quad (i = 1,2) \tag{5.134}$$

where

$$\beta_1 = t_o k_{d1} \exp(-q_1) \ , \quad \beta_2 = t_o k_{d2} \exp(-q_2) \rho^2 y_{2o}^2 \tag{5.135}$$

and t_o is a characteristic time for deactivation.

To simulate the system, Eqs. (5.131), (5.132), which form a pair of first order hyperbolic partial differential equations, are solved numerically using the method of characteristics. Then, with a knowledge of the temperature profile, the second pair of partial differential equations, i.e., Eqs. (5.126), (5.133) is solved similarly. A typical set of solution profiles is plotted in Figures 5-8 to demonstrate the dynamical behavior of this system.

As to the numerical scheme used for integration of partial differential equations along their characteristic lines, both the implicit scheme using the trapezoidal rule with Newton-Raphson iteration and the explicit scheme using the fifth order Adams-Moulton predictor-corrector method have been adopted. They gave almost the same accuracy up to the fourth or fifth digit after the decimal point. However, the stability of the implicit scheme allows large step size, and hence shortens the computing time considerably. Note that due to the slowly varying

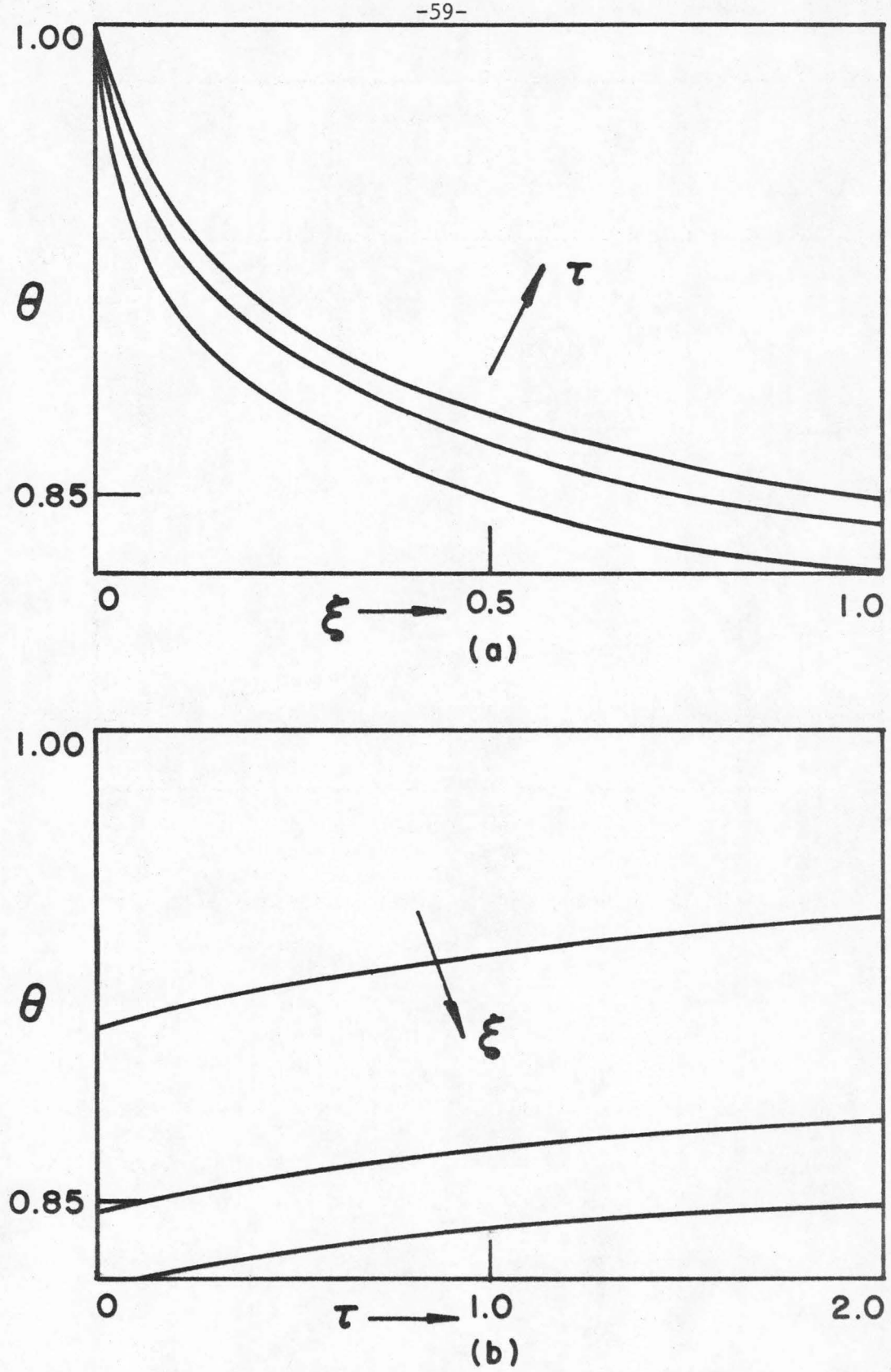

Fig. 5. Typical Temperature Profiles for a Fixed Bed Reforming System

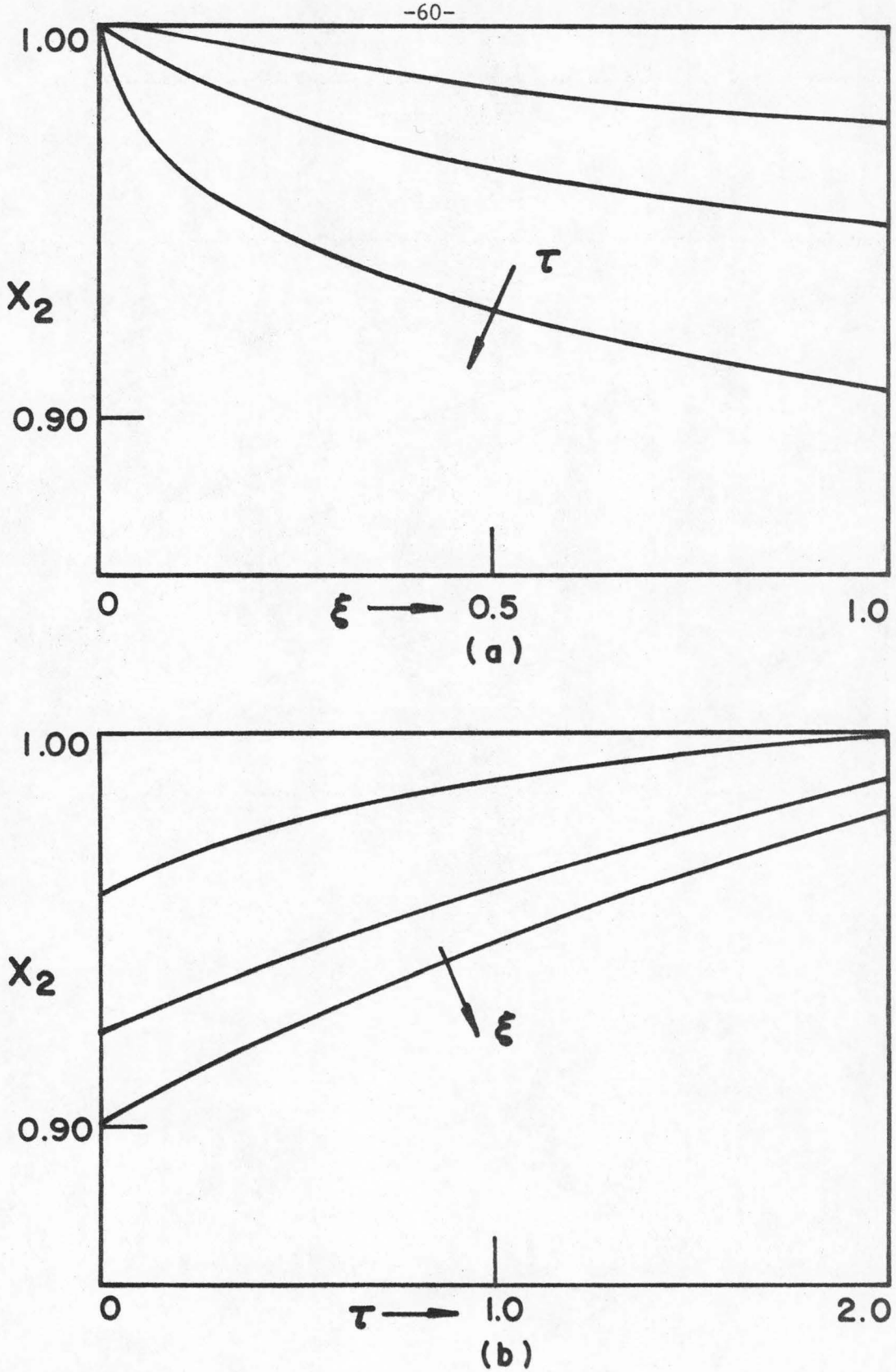

Fig. 6. Typical Concentration Profiles of n-Paraffin

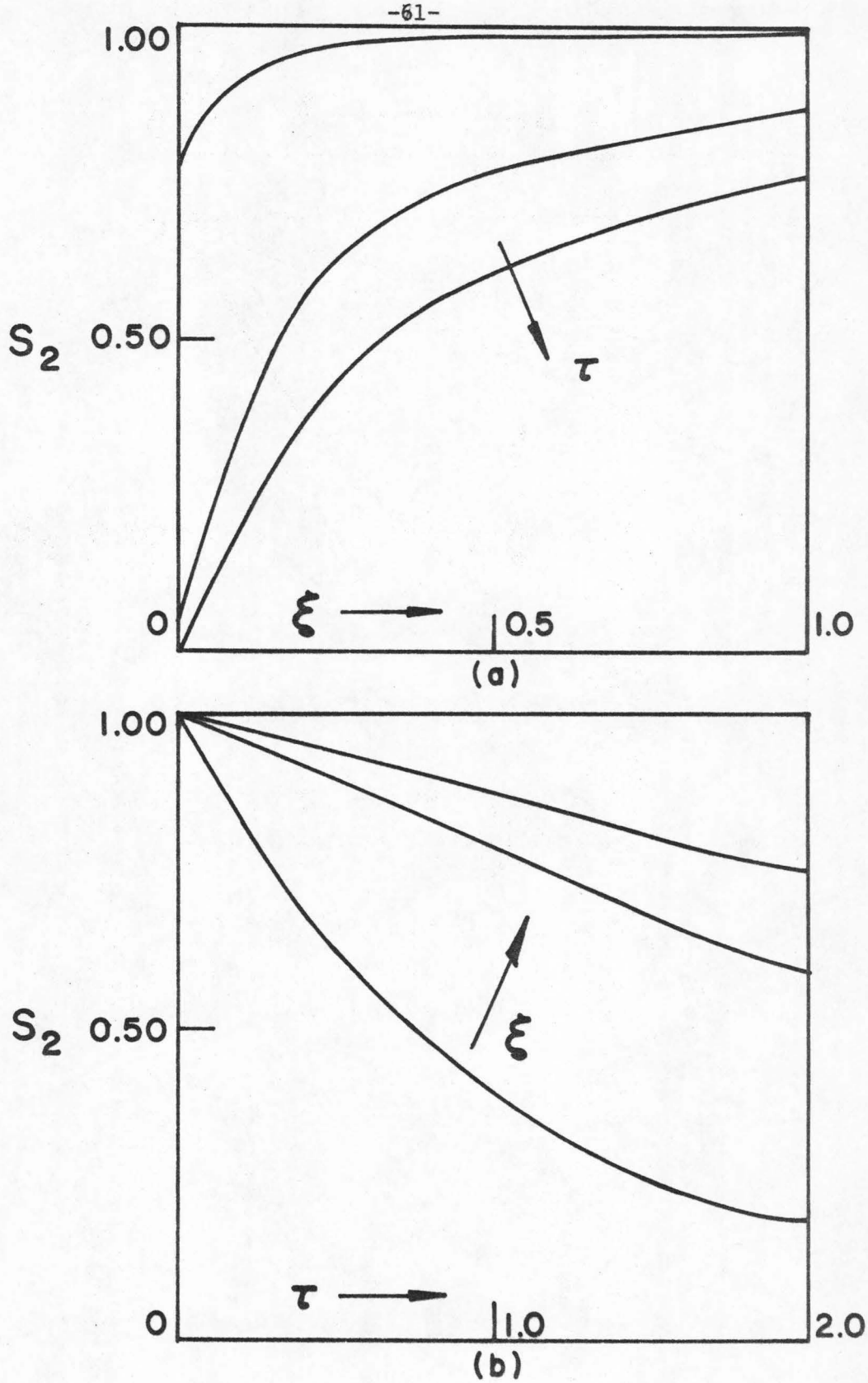

Fig. 7. Typical Profiles of Alumina Activity

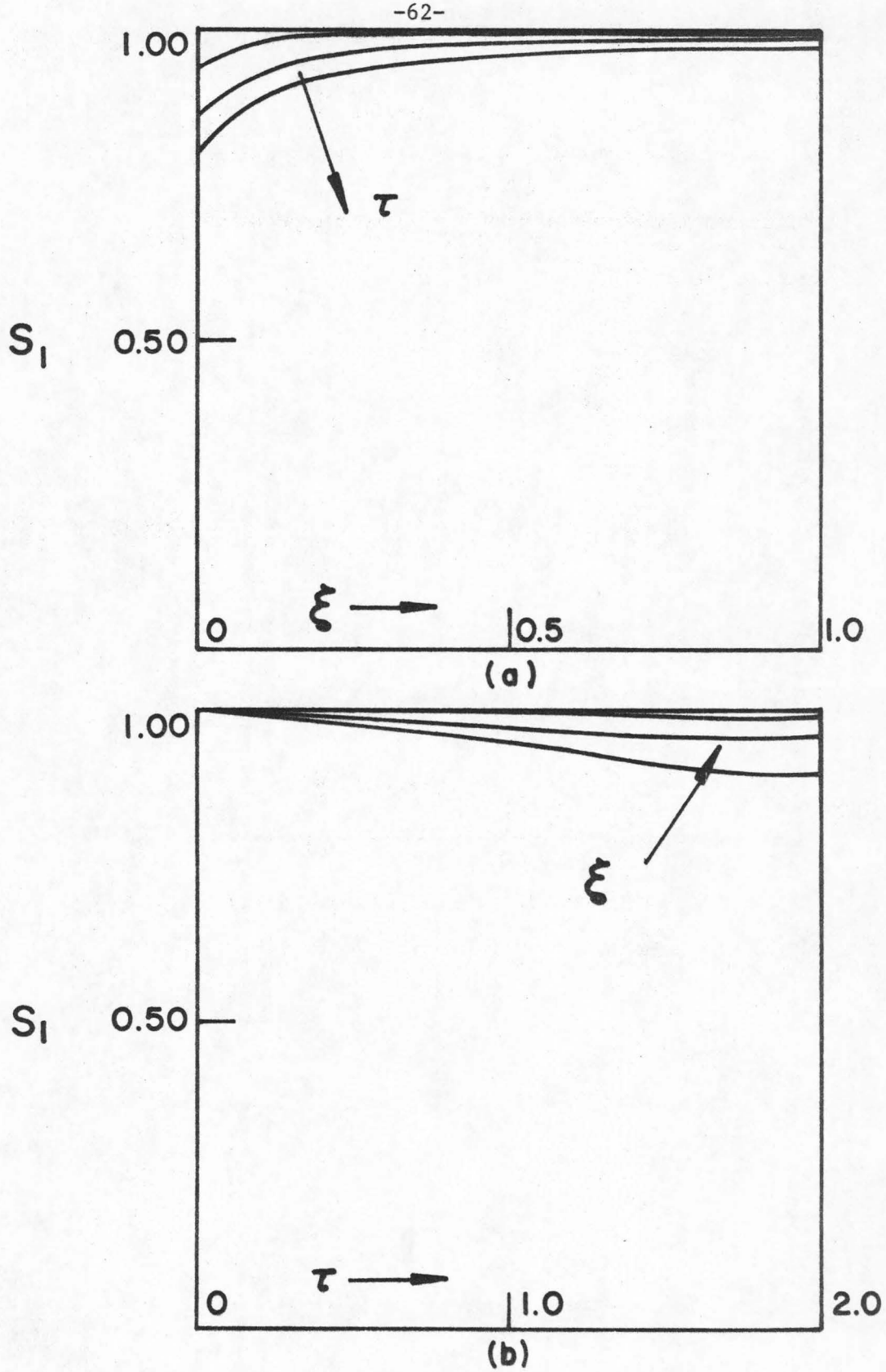

Fig. 8. Typical Profiles of Platinum Activity

property of this system in the direction of time, Euler's approximation can be used as a starting guess in Newton-Raphson iteration. A typical ratio of computing time for the implicit scheme over the explicit scheme is about 1 to 5. Therefore, the implicit scheme is strongly recommended for this type of systems.

The principle adopted in this work for determining which quantities are to be measured depends on what operating data are available in actuality. Based on this principle, temperature measurements realized by continuous thermocouple recordings and concentration observations of certain selected species accomplished by discrete gas chromatographic analysis are chosen as the measured quantities. Moreover, the number of measurement points along the reactor are determined as the minimum necessary for the estimation purposes dealt with in Part II.

Since an enormous amount of temperature data are obtained during each day along the reactor from continuous thermocouple readings, it is reasonable to assume that the daily averages of the temperature distribution are known exactly. On the other hand, simulated concentration measurements are generated at m points along the reactor by adding random measurement error to the "true" values

$$\tilde{x}_2(\xi_j) = x_2(\xi_j)[1 + n(0,\sigma)] \quad , \quad j = 1,\cdots,m \tag{5.133}$$

where $n(0,\sigma)$ is a normally distributed random variable with zero mean and variance σ^2. Supposing that concentration measurements are taken ℓ times a day, the variance of daily averages is $\sigma^2 = \sigma_o^2/\ell$ where σ_o^2 is the variance of individual measurements.

Now, after gathering the temperature and concentration measurements from the simulated dynamical system, the information about catalyst activity profiles and deactivation parameters, which are inaccessible for observations, may hopefully be obtained from the coupling relation between the state variables and catalyst activities. This is explored in detail in Part II.

APPENDICES

A. REDUCTION OF THE OVERALL REACTION RATES DUE TO PORE-MOUTH COKE FORMATION

B. EFFECTIVENESS FACTOR FOR CYCLOPARAFFIN DEHYDROGENATION

APPENDIX A

REDUCTION OF THE OVERALL REACTION RATES DUE TO PORE-MOUTH COKE FORMATION

As was described in Chapter 4, uniform poisoning is expected to prevail for coking due to its low reaction rate. However, for the sake of a complete study, pore-mouth poisoning is discussed in this appendix. As a result of pore-mouth coke formation, the overall rates of the main reactions catalyzed by alumina sites decrease. It is the purpose of this appendix to seek an expression for the reduction ratio of reaction rates.

Pore-mouth poisoning is defined as the poison deposition process which commences at the catalyst pellet exterior surface and progresses inward along pore walls until the center of the pellet is reached. It is the outcome of instantaneous irreversible adsorption of poisons on a catalyst surface. For example, a coking species c which is adsorbed both rapidly and tightly at the alumina sites of reforming catalysts, causes a pore-mouth poisoning of the alumina centers.

A sketch of the pore subject to pore-mouth coking is shown in Figure A-1. The work of Petersen [78] is followed with slight modifications. Instead of a parallel pore model, this appendix adopts a random pore model which employs the effective diffusivity D_e. The pore is at any time divided into two zones. The first zone starts at the pore mouth and extends some distance, say $r_o - \bar{r}$, into the pore to form a tube of no catalytic activity. The second zone, i.e., from $r_o - \bar{r}$ to r_o contains no adsorbed coke. Denote the number of moles

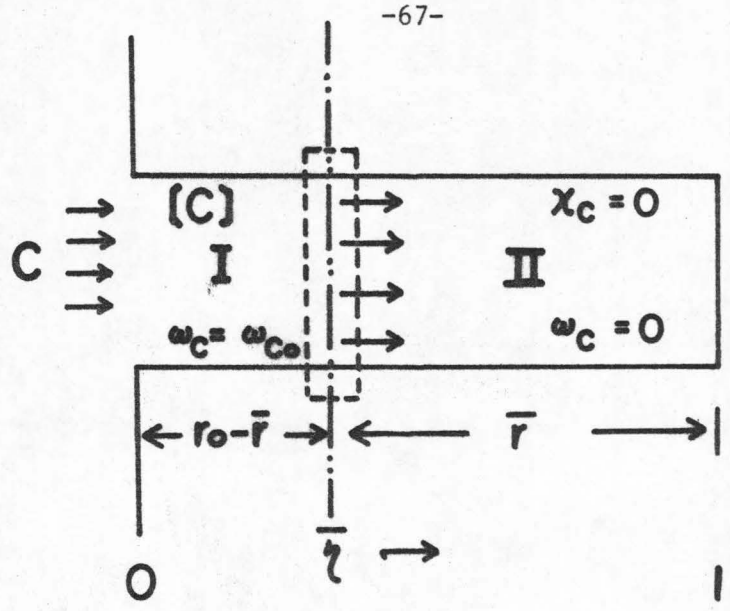

Fig. A-1. Schematic Diagram of Pore-Mouth Poisoning

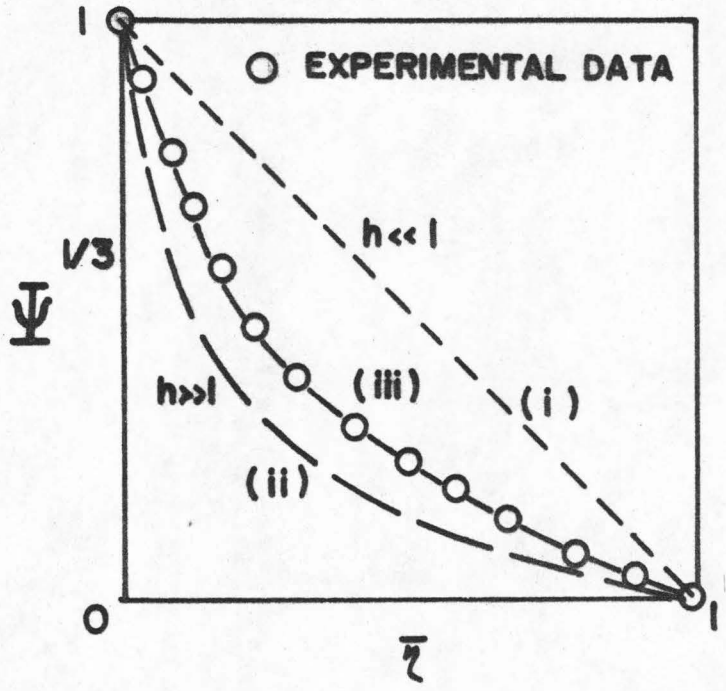

Fig. A-2. Effects of Coking on the Overall Reaction Rate

of coke adsorbed per unit area of catalyst surface by ω_c , whereas ω_{co} is the numerical value of ω_c when adsorption sites are completely occupied. The rate of adsorption per unit area for an irreversible adsorption process can be expressed by

$$\frac{\partial \omega_c}{\partial t} = k_c\left(1 - \frac{\omega_c}{\omega_{co}}\right)c_c \tag{A.1}$$

With steady state assumption, the material balance of the coking species c in the pore is

$$D_e \frac{1}{r^2}\frac{\partial}{\partial r}\left(r^2 \frac{\partial c_c}{\partial r}\right) = \rho_p s_p \frac{\partial \omega_c}{\partial t} \tag{A.2}$$

The system of equations (A.1) and (A.2) can be more easily examined by letting

$$x_c = \frac{c_c}{c_{co}} \quad , \qquad \phi = \frac{\omega_c}{\omega_{co}} \quad , \qquad \eta = 1 - \frac{r}{r_o} \tag{A.3}$$

$$\tau = \left(\frac{c_{co} k_c}{\omega_{co}}\right)t \quad , \quad h = r_o\left(\rho_p s_p \frac{k_c}{D_e}\right)^{1/2} \tag{A.4}$$

where c_{co} is the surface concentration of coking species, to obtain upon substitution

$$\frac{\partial^2 x_c}{\partial \eta^2} = h^2 \frac{\partial \phi}{\partial \tau} \tag{A.5}$$

$$\frac{\partial \phi}{\partial \tau} = (1 - \phi)x_c \tag{A.6}$$

Equation (A.5) is valid for small η . In reality, η is indeed kept small as catalysts are regenerated periodically.

Mathematically, pore-mouth poisoning means that in

$$\text{zone I} : \quad 0 < \eta < \bar{\eta} \quad , \quad \phi = 1 \tag{A.7}$$

$$\text{zone II} : \quad \bar{\eta} < \eta < 1 \quad , \quad \phi = 0 \ , \ x_c = 0 \tag{A.8}$$

The Expression for the Coking Front

Substituting conditions (A.7),(A.8) into Eqs. (A.6) and (A.5), it is clear that

$$\frac{\partial x_c}{\partial \eta} = \text{constant} = \frac{0 - 1}{\bar{\eta} - 0} = - \frac{1}{\bar{\eta}} \tag{A.9}$$

Now, a differential mass balance in the volume between $\bar{\eta}$ and $\bar{\eta} + \Delta\bar{\eta}$ becomes

$$- [(\frac{\partial x_c}{\partial \eta})_{\bar{\eta},\tau} - (\frac{\partial x_c}{\partial \eta})_{\bar{\eta}+\Delta\bar{\eta},\tau}]\Delta\tau = h^2[\phi(\bar{\eta},\tau+\Delta\tau) - \phi(\bar{\eta},\tau)]\Delta\bar{\eta} \tag{A.10}$$

Substituting the boundary conditions (A.7),(A.9) in Eq. (A.10) gives

$$- (- \frac{1}{\bar{\eta}} - 0)\Delta\tau = h^2(1 - 0)\Delta\bar{\eta} \tag{A.11}$$

which upon simplification and integration becomes

$$\bar{\eta} = \frac{(2\tau)^{1/2}}{h} \tag{A.12}$$

In the original coordinates Eq. (A.12) can be written as

$$r_o - \bar{r} = \beta' t^{1/2} \tag{A.13}$$

where $$\beta' = (2D_e c_{co} / \rho_p s_p \omega_{co})^{1/2} \tag{A.14}$$

This means that the moving front of coked section in a pore extends towards the center of the catalyst pellet with a speed of half order with respect to the catalyst on-stream time as well as the surface concentration of the coking species.

Expressions for the Reduction Ratio of the Overall Reaction Rates

As a result of coke formation, a portion of alumina sites is occupied by coke and the acidic activity of a reforming catalyst decreases as the coking reaction proceeds. Define the reduction ratio of the overall catalytic reaction rate subject to pore-mouth coking to the original coke-free reaction rate as Ψ . In the case of very small Thiele modulus h (i.e., $h << 1$), the reaction rate within the unpoisoned pore is not diffusion influenced, and the overall catalytic reaction rate falls off in direct proportion to the volume of poisoned shell. Thus, for a spherical pellet

$$\Psi = (\frac{\bar{r}}{r_o})^3 = (1 - \bar{\eta})^3 \qquad (A.15)$$

Introducing the expression for the moving coke front, Eq. (A.15) becomes

$$\Psi = (1 - \beta t^{1/2})^3 \quad , \quad \text{for } h << 1 \qquad (A.16)$$

where $\beta = \beta'/r_o$. When the unpoisoned pore is operated in the diffusion-influenced region (i.e., $h >> 1$), the activity falls much faster, due to the transport resistance, than given by Eq. (A.16). In this case the relationship between $\bar{\eta}$ and t should be obtained through the equality of diffusion rate and reaction rate at the poisoning front. A solution is shown schematically as curve (ii) in Figure

A-2. Petersen and co-workers [78,80] have shown that the usual experimental data lie in between the above two theoretical extremes, namely $h << 1$ and $h >> 1$. Therefore, a typical experimental curve for $\Psi^{1/3}$ behaves as a hyperbola, curve (iii) in Figure A-2. For simplicity, it is suggested here that the following straightforward geometric approximation be adopted,

$$(\Psi^{1/3})^{-nh} + \overline{\eta}^{-nh} = 1 \ , \quad \text{where} \quad nh > 1 \tag{A.17}$$

Here, n is an empirical parameter obtained experimentally from a fit of the data curve with a hyperbola. Therefore, an approximate expression for the reduction ratio of the overall reaction rates due to pore-mouth coke formation is

$$\Psi = \left(1 - \beta^{-nh}\, t^{-\frac{n}{2}h}\right)^{-3/nh} \tag{A.18}$$

APPENDIX B

EFFECTIVENESS FACTOR FOR CYCLOPARAFFIN DEHYDROGENATION

Detailed accounts of the theoretical-mathematical aspects of diffusion in catalyst pellets have been given by Satterfield [107], Gavalas [108], Weisz and Hicks [109], Wakao and Smith [110], and Gunn and Thomas [111]. Many other studies deal particularly with the subject of effectiveness factors for porous catalysts [112,113,114,115].

An effectiveness factor is defined as the ratio

$$\text{Eff} = \frac{-s_p D_e [\frac{\partial}{\partial r} c(c,T)]_{r=r_o}}{v_p \, r(c_s,T_s)} \qquad \text{(B.1)}$$

where c,T are the local concentration and temperature inside of the catalyst pellet,

$r(c_s,T_s)$ is the reaction rate evaluated at the surface of the pellet,

s_p,v_p are the external surface and the volume of the catalyst pellet respectively,

r_o is the radius of the catalyst pellet,

and D_e is the effective diffusivity of that species with respect to the porous structure

For a reforming feed stock consisting of methylcyclohexane and n-heptane, the essential behavior can be characterized by the dehydrogenation of methylcyclohexane to toluene and the isomerization of n-heptane. The material and energy balances within a spherical catalyst pellet can thus be set up as follows:

$$D_e \frac{1}{r^2} \frac{d}{dr} \left(r^2 \frac{dc}{dr}\right) = k_o s \exp(-E/RT)\, c \qquad (B.2)$$

$$k_e \frac{1}{r^2} \frac{d}{dr} \left(r^2 \frac{dT}{dr}\right) = (\Delta H) k_o s \exp(-E/RT)\, c \qquad (B.3)$$

where k_e is the effective heat conductivity.

The boundary conditions are

$$\text{(i)} \quad \text{at} \quad r = 0 \qquad \frac{dc}{dr} = 0 \quad , \quad \frac{dT}{dr} = 0 \qquad (B.4)$$

$$\text{(ii)} \quad \text{at} \quad r = r_o \qquad c = c_s \quad , \quad T = T_s \qquad (B.5)$$

Here the dimensionless site density of platinum s is uniform over the catalyst pellet.

From Eqs. (B.2) and B.3) one obtains

$$T = T_s + \frac{(\Delta H) D_e}{k_e} (c - c_s) \qquad (B.6)$$

Defining

$$\theta = \frac{T_s - T}{T_s} \quad , \quad \lambda = \frac{E}{RT} \frac{(\Delta H) D_e c_s}{k_e T_s} \qquad (B.7)$$

Eq. (B.6) becomes

$$\frac{E}{RT_s} \theta = \lambda \left(1 - \frac{c}{c_s}\right) \qquad (B.8)$$

Introducing Eqs. (B.7),(B.8) and the following approximation

$$\frac{1}{1-\theta} \simeq 1 + \theta \qquad \text{, for small } \theta \qquad (B.9)$$

(B.2) can be rewritten as

$$D_e \frac{1}{r^2} \frac{d}{dr} \left(r^2 \frac{dx}{dr}\right) = k f(x) \qquad (B.10)$$

where

$$x = c/c_s \quad , \quad k = k_o s \exp(-E/RT) \tag{B.11}$$

and

$$f(x) = x \exp[-\lambda(1-x)] \tag{B.12}$$

Now for large h, Eq. (B.10) can be simplified approximately according to Petersen [78] as

$$\frac{d^2x}{d\eta^2} = h^2 f(x) \tag{B.13}$$

where

$$\eta = 1 - \frac{r}{r_o} \quad , \quad h = r_o \left(\frac{k}{D_e}\right)^{1/2} \tag{B.14}$$

For large h the reaction goes to completion in a thin surface layer, and the boundary conditions for Eq. (B.14) become

$$\text{(i)} \quad \text{at} \quad \eta = 0 \quad , \quad x = 1 \tag{B.15}$$

$$\text{(ii)} \quad \text{at} \quad \eta = 1 \quad , \quad x = 0 \tag{B.16}$$

Following the procedure suggested by Amundson and Raymond [116], and using x as a new independent variable and $dx/d\eta$ as a new dependent variable, one obtains from Eq. (B.13)

$$\frac{dx}{d\eta} = -h \left[2 \int_0^1 f(x)\, dx \right]^{1/2} \tag{B.17}$$

Substituting the above expression into Eq. (B.1), the effectiveness factor of cycloparaffins for a spherical catalyst pellet can be obtained as

$$Eff = 3[2\int_0^1 f(x)dx]^{1/2} / h \qquad (B.18)$$

$$= 3[2(e^{-\lambda} + \lambda - 1)]^{1/2} / \lambda h \qquad (B.19)$$

If the quantity $\lambda(1-x)$ is smaller than one, a simplification can be made by approximating expression (B.12) as

$$f(x) = x[1 - \lambda(1-x)] = (1-\lambda)x + \lambda x^2 \qquad (B.20)$$

and the resulting effectiveness factor becomes

$$Eff = [3(3-\lambda)]^{1/2} / h \qquad (B.21)$$

A Modification Due to Coke Formation

In the case of uniform poisoning, the average pore radius is gradually reduced due to the presence of coke. As a result, the value of the effective diffusivity, which is a function of pore radius, also decreases. From the definition of effectiveness factor, it is clear that a diffusion factor d should be incorporated in the expression (B.1) as follows

$$Eff = Eff(0) \cdot d \qquad (B.22)$$

where Eff(0) is the effectiveness factor obtained from a coke-free system, i.e., Eq. (B.21), with effective diffusivity $D_e(0)$

and $$d = D_e/[D_e(0)] \qquad (B.23)$$

According to Levinter et al. [117], the type of diffusion occurring in the porous media is Knudsen diffusion. Therefore, an effective diffusivity can be written in terms of the Knudsen diffusivity

as

$$D_e = D_k \varepsilon_p(t) \frac{\sigma}{\tau} \tag{B.24}$$

where σ is an empirical parameter called the constriction factor,

τ is an empirical parameter called tortuosity,

and $\varepsilon_p(t)$ is the porosity of the catalyst pellet at time t,

while

$$D_k = \frac{8}{3\rho_p s_p} \left(\frac{2RT}{\pi M}\right)^{1/2} \varepsilon_p(t) \tag{B.25}$$

where M is the molecular weight of diffusing species,

and ρ_p, s_p are the density and specific area of the catalyst pellet

Combining the above two expressions gives

$$D_e = a\, \varepsilon_p^2(t) \tag{B.26}$$

where

$$a = \frac{8}{3\rho_p s_p} \left(\frac{\sigma}{\tau}\right) \left(\frac{2RT}{\pi M}\right)^{1/2} \tag{B.27}$$

and thus

$$d = \left(\frac{\varepsilon_p(t)}{\varepsilon_p(0)}\right)^2 \tag{B.28}$$

Now, the decrease of catalyst porosity due to coke formation is equal to the weight of coke deposited at time t per unit catalyst weight divided by the ratio of coke and catalyst density, i.e.,

$$\Delta\varepsilon_p(t) = \varepsilon_p(0) - \varepsilon_p(t) = \frac{\delta_c(t)}{(\rho_c/\rho_p)} \tag{B.29}$$

and

$$\delta_c(t) = M_c s_p \omega_c(t) \tag{B.30}$$

where M_c is the molecular weight of coke,

and $\omega_c(t)$ is the surface concentration of coke at time t .

Supposing that this porosity change is small compared to $\varepsilon_p(t)$, the square of porosity can be approximated by

$$\varepsilon_p^2(t) \simeq \varepsilon_p^2(0) - (2M_c\rho_p s_p/\rho_c)\ \varepsilon_p(0)\ \omega_c(t) \tag{B.31}$$

Substituting the above expression into (B.28) gives

$$d = 1 - k_c\omega_c(t) \tag{B.32}$$

where

$$k_c = 2M_c\rho_p s_p\ /\ \rho_c\varepsilon_p(0) \tag{B.33}$$

Expression (B.32) is physically reasonable as it states that the diffusivity factor is a decreasing function of the amount of coke deposited on the catalyst pellet.

Finally, according to expression (B.22), one obtains

$$\text{Eff} = \frac{[3(3-\lambda)]^{1/2}}{h}\ (1 - k_c\omega_c) \tag{B.34}$$

This means that the effectiveness factor of cycloparaffins as well as the resulting global dehydrogenation rate in a reforming process decreases almost linearly as the coking reaction proceeds. However, since in practice the surface concentration of coke ω_c will be kept small by the regeneration of catalysts, the decay of effectiveness factors due to coke formation will also remain small.

PART II

ESTIMATION OF CATALYST ACTIVITY PROFILES AND DEACTIVATION PARAMETERS IN FIXED BED REACTORS

6. ESTIMATION OF CATALYST ACTIVITY PROFILES IN FIXED BED REACTORS

A certain amount of information about the catalyst activity distribution is required for the description as well as the control of the steady state operation of a catalytic reactor. For industrial processes the activities are not measurable. Instead, a large amount of operating data is available in the form of temperature and concentration measurements at the reactor exit and, perhaps, at several positions along the reactor. The interest of this chapter centers on how these operating data are utilized to estimate catalyst activity profiles. This estimation relates to actual operating conditions, and hence it can be used directly for optimization purposes.

System with a Single Activity Profile

For a monofunctional system or a special bifunctional system with two activities that decline at the same relative rate, the balance equation for the state $x = (y_1,\cdots,y_N,T)$ may be written as

$$G \frac{dx}{dz} = sf(x) \tag{6.1}$$

under the assumptions of uniformity of the catalyst surface and the absence of transport limitations. The case of transport limitations was discussed by Gavalas et al. [6]. Note that G in Eq. (6.1) is the mass velocity, y_i is the molar flux of species i per unit mass flux, and s represents the dimensionless density of active sites.

Defining a cumulative activity

$$S(z,t) = \int_0^z s(z',t)dz' \tag{6.2}$$

Eq. (6.1) can be written as

$$\frac{dx}{d(S/G)} = f(x) \tag{6.3}$$

which yields, after integration,

$$x = F(S/G, x_f) \tag{6.4}$$

The estimation algorithm depends on the types of measurements used. If a single component x_i is measured at the reactor exit, integration of Eq. (6.3) from $x_i = x_{if}$ to $x_i = \tilde{x}_i$, the measured value, yields an estimate of the total activity $S(L,t)$. If more components of x are measured at $z = L$, $S(L,t)$ can be determined by least squares.

The total activity $S(L,t)$ estimated from the measurement at the reactor exit is sufficient for predicting the reactor output $x(L,t)$ for any input x_f, G. However, it will seldom be possible to estimate the deactivation parameters from the deactivation equation utilizing the knowledge of $S(L,t)$ alone. For this case it is necessary to take measurements at several positions $z_1, \cdots, z_N$ and thus estimate the quantities $S(z_1,t), \cdots, S(z_N,t)$ which provide a more detailed representation of the activity profile. In reactions with large heat effects, thermocouple recordings at several points along the reactor are most convenient for this type of estimation.

The aforementioned estimation scheme is illustrated numerically by a simplified kinetic model of naphtha reforming. In this case, the platinum activity distribution changes independently of the alumina activity, and the energy equation involves only the Pt activity

profile.

According to the description in Part I, a simplified model of naphtha reforming consists of the following major reactions:

(i) Dehydrogenation of cycloparaffins to aromatics

(ii) Isomerization of n-paraffins to isoparaffins

accompanied by two catalyst deactivation reactions:

(iii) Coking on alumina sites

(iv) Sintering of platinum crystallites

The essential dynamical behavior of naphtha reforming can be characterized by the following set of partial differential equations in terms of dimensionless quantities:

$$v \frac{\partial \theta}{\partial \xi} = - \frac{\alpha_1}{\lambda} s_1 [(x_{1f} - \lambda\theta_f) + \lambda\theta] \exp[-p_1(\frac{1}{\theta} - 1)] \tag{6.5}$$

$$v \frac{\partial x_2}{\partial \xi} = -\alpha_2 s_2 x_2 \exp[-p_2(\frac{1}{\theta} - 1)] \tag{6.6}$$

$$\frac{\partial s_1}{\partial \tau} = - \beta_1 s_1^2 \exp[-q_1(\frac{1}{\theta} - 1)] \tag{6.7}$$

$$\frac{\partial s_2}{\partial \tau} = -\beta_2 s_2 x_2^2 \exp[-q_2(\frac{1}{\theta} - 1)] \tag{6.8}$$

with boundary conditions

$$\text{(i)} \quad \text{at } \xi = 0 : \quad \theta = \theta_f \ , \ x_2 = x_{2f} \tag{6.9}$$

$$\text{(ii)} \quad \text{at } \tau = 0 : \quad s_1 = s_{1o} \ , \ s_2 = s_{2o} \tag{6.10}$$

Here s_1, s_2 represent the activities of the platinum function and acidic alumina function. $\theta(\xi,\tau)$ and $x_2(\xi,\tau)$ are the local temperature

and concentration of n-paraffin at position ξ and time τ. p_i, q_i (i=1,2) denote dimensionless activation energies.

The estimation of the total platinum activity S_1 is obtained from the integrated form of Eq. (6.1) as

$$S_1(\xi_j) = \int_0^{\xi_j} s_1(\xi)d\xi = \frac{\lambda v}{\alpha_1} \int_{\theta(\xi_j)}^{\theta_f} \frac{\exp[p_1(\frac{1}{\theta} - 1)]}{x_{1f} - \lambda\theta_f + \lambda\theta} d\theta \qquad (6.11)$$

This cumulative activity profile fully characterizes the activity level of metallic sites, and is sufficient for predicting the temperature profile $\theta(\xi_j)$ subject to new inlet conditions θ_f' and v'. In the above estimation, knowledge of the activation energy p_1 of the main reaction is assumed. In the absence of this knowledge, an alternative estimation scheme is suggested in the next section.

Simultaneous Estimation of Activity Profile and the Activation Energy of the Main Reaction

Utilizing the temperature measurements alone, an analytical estimation scheme for obtaining estimates on both activity profile and activation energy is not conceivable. Instead, a qualitative method must be sought. Based on a priori information about the geometric shape of the catalyst activity distribution along the reactor and how it is affected by the activation energy, a simple graphical estimation scheme may be established. The reasoning and estimation algorithm are presented in this section, and no attempt is made to make the estimation scheme rigorous.

An activity profile $s_1(\xi)$, which has been deactivated from an initially flat distribution, has the following four basic geometric properties as shown in Figure 9:

(i) parabolic shape

(ii) monotonically increasing

(iii) positive slope at $\xi = 0$

(iv) $0 < s_1(\xi) \leq 1$

An activity profile $s_1(\xi)$ can be obtained by first curve-fitting a set of estimated cumulative activities $S_1(\xi_j)$'s with a third order curve which, upon differentiation, yields a second order parabola for $s_1(\xi)$. Due to the general nature of the parabola, a maximum often appears within the range of interest, i.e., $0 \leq \xi \leq 1$. This makes the tail of the parabola bend down somewhat. Therefore, the second basic requirement has to be relaxed. On modification, $s_1(\xi)$ becomes a monotonically increasing function over most of the reactor length.

Now, in the early stage of catalyst deactivation, the activity profile is expected to be close to unity for large ξ . If the estimate $\hat{p}_1$ is chosen too large, the resulting activity estimates would have values larger than one, as shown by curve (i) in Figure 10. On the other hand, if $\hat{p}_1$ is chosen too small, the slope of the activity profile at the beginning of the reactor will become negative, as shown in curve (ii) in Figure 10. Only a narrow range of activation energy estimates around the true p_1^* will give activity profiles whose geometric shapes possess the previously stated properties. As the deactivating reaction proceeds, the catalyst activities deviate

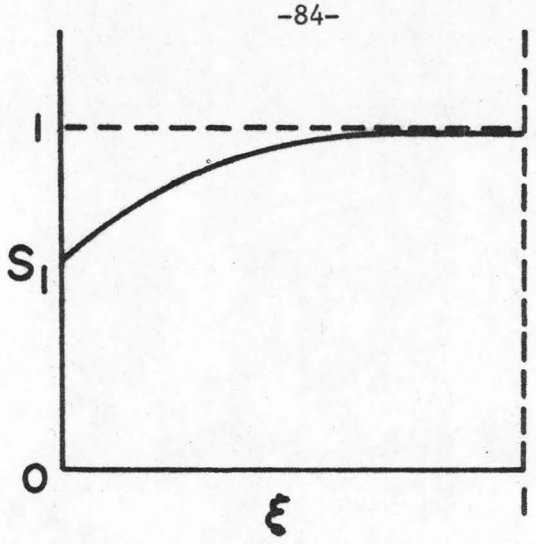

Fig. 9. "True" Platinum Activity Profile

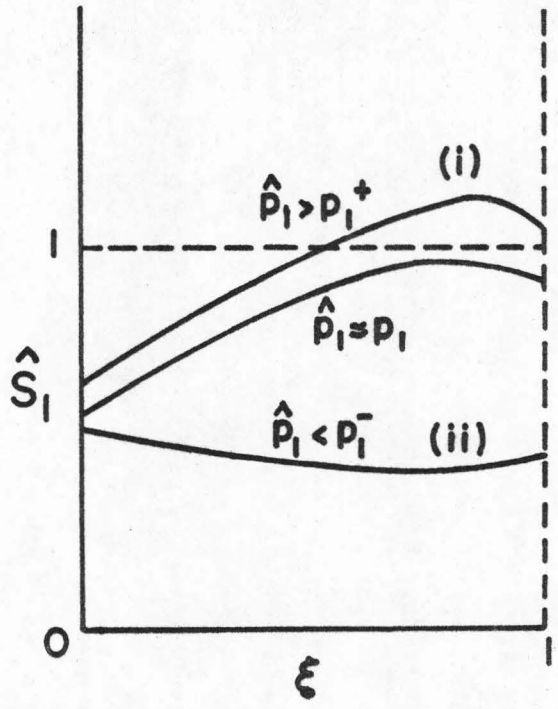

Fig. 10. Estimated Platinum Activity Profiles

more and more from unity. However, the basic behavior of the activity profile remains the same so that the following estimation algorithm is still applicable.

(i) Guess a value for the activation energy, i.e., $\hat{p}_1$.

(ii) Calculate $S_1(\xi_j)$, $j=1,\cdots,m$ from Eq. (6.11).

(iii) Fit $S_1(\xi_j)$'s with a third order curve.

(iv) Differentiate the third order curve $S_1(\xi)$ to get the activity profile $s_1(\xi)$.

(v) Check for the basic properties of initial positive slope and $0 < s_1(\xi) \leq 1$.

(vi) Calculate the amount of negative slope according to a reasonable criterion, e.g., the summation of negative slope at several sampling points along the reactor.

(vii) Repeat steps (i)-(vi) with other $\hat{p}_1$'s .

(viii) Obtain the desirable estimate of activation energy as the $\hat{p}_1$ which yields the least amount of negative slope.

(ix) The corresponding activity profile has already been calculated in step (iv).

Finally, it should be noted that the shape of the activity profile is much more sensitive to the choice of activation energy than is the cumulative activity profile. Therefore, it is better to carry out the graphical estimation on the activity profile rather than on the cumulative activity profile.

Now suppose that the estimate of activation energy obtained in the above manner is not accurate. How this inaccuracy will affect the

prediction of the temperature profile subject to changes in feed conditions becomes an important question. This question is answered by the following analysis.

Consider the simplified model of naphtha reforming consisting of the temperature distribution equation, Eq. (6.5), and the catalyst deactivation equation, Eq. (6.7). The activation energy of the dehydrogenation reaction is p_1^*, and the initial feed conditions are $\theta_f = 1$, $v = 1$. From the simulated temperature measurements $\theta(\xi_j, p_1^*)$ and Eq. (6.11), the cumulative activities are calculated as $S_1(\xi_j, p_1^*)$. Following the proposed estimation algorithm the estimate $\hat{p}_1$ and the resulting $S_1(\xi_j, \hat{p}_1)$ from Eq. (6.11) are obtained. Now, if the operating conditions are changed into new inlet temperature θ_f' and dimensionless mass velocity v', different sets of temperature profiles $\hat{\theta}'(\xi)$ are obtained according to whether $S_1(\xi_j, \hat{p}_1)$ or $S_1(\xi_j, p_1^*)$ is used:

$$\frac{\lambda v'}{\alpha_1} \int_{\hat{\theta}'(\xi_j, \hat{p})}^{\theta_f'} \frac{\exp[\hat{p}_1(\frac{1}{\theta} - 1)]}{x_{1f} - \lambda\theta_f' + \lambda\theta} \, d\theta = S_1(\xi_j, \hat{p}_1) \tag{6.12}$$

$$\frac{\lambda v'}{\alpha_1} \int_{\hat{\theta}'(\xi, p^*)}^{\theta_f'} \frac{\exp[p_1^*(\frac{1}{\theta} - 1)]}{x_{1f} - \lambda\theta_f' + \lambda\theta} \, d\theta = S_1(\xi_j, p_1^*) \tag{6.13}$$

Numerical results in Table 4 show that the average percentage error for temperature predictions along the reactor ranges from 0.06% to 9.0% corresponding to a wide range of values for $\hat{p}_1$. In fact, in most of the cases, the error is less than 1%. This may be due to the insensitivity of the temperature to the activation energy in Eq. (6.11).

TABLE 4

EFFECT OF THE ESTIMATION OF ACTIVATION ENERGY ON

THE AVERAGE TEMPERATURE PREDICTION

** $\hat{p}_1$	θ'_f	v'	Average % error in $\hat{\theta}'(\xi_j, \hat{p}_1)$
30.6	0.80	2.00	0.60%
	1.10	1.60	1.3%
26.2	0.80	0.80	0.20%
	1.05	0.80	0.32%
21.5	0.92	0.53	0.10%
	1.05	0.80	0.06%
	0.80	0.80	3.2%
10.0	0.92	0.53	2.0%
	1.05	0.80	0.86%
	0.80	0.80	9.0%
2.0	1.05	0.80	1.7%
	1.10	1.60	6.5%

**True activation energy $p_1^* = 20.6$

It can be concluded from the above analysis that the temperature resulting from changes in operating conditions can usually be satisfactorily predicted even if the estimated activation energy is subject to error.

System with Two Activity Profiles

In the case of bifunctional catalysts with the two activities declining at different relative rates, the balance equation for the state x takes the form

$$G \frac{dx}{dz} = s_1 f_1(x) + s_2 f_2(x) \qquad (6.14)$$

under the assumptions described in Part I.

The transformation defined in Eq. (6.2) cannot be performed for Eq. (6.14) and thus the determination of the reactor output in terms of cumulative activities is not possible. In principle, the steady state input-output characterization requires the complete information of $s_1(z)$ and $s_2(z)$. Alternatively, the activity profiles can be approximated by certain functions containing a small number of parameters to be estimated from the measurements. The success of this method depends on the choice of the approximating function. No general rules can be formulated. Some possibilities are illustrated in the following section.

Estimation of Activity by Parametrization

Consider the estimation of the alumina activity profile for the simplified model of naphtha reforming. In order to predict the reactor output $x_2(1)$ for arbitrary inputs such as feed conditions θ_f, x_{1f},

x_{2f}, and flow rate v, it is necessary to obtain information about the alumina activity distribution $s_2(\xi)$. Integration of Eq. (6.6) yields

$$\frac{v}{\alpha_2} \log \frac{x_{2f}}{x_2(1)} = \int_0^1 s_2(\xi) \exp[-p_2(\frac{1}{\theta(\xi)} - 1)] \, d\xi \qquad (6.15)$$

where the temperature θ is measured at a sufficient number of points along the reactor to allow the numerical evaluation of the integral.

It is obvious from Eq. (6.15) that the prediction of $x_2(1)$ requires knowledge of the complete activity profile $s_2(\xi)$, which in turn requires an infinite number of concentration measurements. The necessity of an approximation based on parametrization of $s_2(\xi)$ thus becomes apparent, and the subsequent estimation of the necessary parameters is sufficient for all practical purposes.

Numerical calculations were made using simulated measurements. It should be noted here that the decrease of platinum activity due to sintering is much slower than that of acidic activity by coking so that between successive regenerations the platinum activity remains essentially constant and needs to be estimated only once. Therefore, a constant profile for $s_1(\xi)$ is assumed for simplicity in the present case. The "true" values of θ, x_2, and s_2 were obtained numerically from Eqs. (6.5)-(6.8) for the following values of the parameters:

$$\alpha_1 = 0.216 \, , \quad \alpha_2 = 5.0 \, , \quad \lambda = 0.108 \, , \quad p_1 = 21.6$$

$$p_2 = 20.0 \, , \quad q_2 = 15.0 \, , \quad \beta_1 = 0 \, , \quad \beta_2 = 6.0$$

$$s_1 = 0.95 \, , \quad s_2(\xi,0) = 1.0, \; \theta_f = 1.0 \, , \quad x_{2f} = 1.0$$

Then the simulated measurements of x_2 were generated at m positions along the reactor ($m \geq 3$, e.g., $\xi_1 = 0.1$, $\xi_2 = 0.4$, $\xi_3 = 1.0$), by adding random measurement error to the "true" values. It is interesting to notice that in the history of alumina activity decay there are two possible shapes for an activity profile:

(i) In the early stage of catalyst life, the profile looks like a portion of the increasing part of a parabola;

(ii) In the later stage of catalyst life, the profile looks like an S shaped curve.

The proposed parametrization schemes have been tested for both cases.

Figure 11a,b indicates two simple parametrizations that have been found adequate. In the first the activity profile $s_2(\xi)$ is approximated by a curve $\hat{s}_2(;p_1',p_2',p_3')$ consisting of two segments of straight lines as follows:

$$\hat{s}_2(\xi;p_1',p_2',p_3') = \begin{cases} \xi p_2'/p_1' & \text{for } 0 \leq \xi \leq p_1' \quad (6.16) \\ p_2' + (p_3'-p_2')(\xi - p_1')/(1-p_1') & \text{for } p_1' \leq \xi \leq 1 \quad (6.17) \end{cases}$$

where p_1', p_2', and p_3' are three length parameters shown in Figure 11a. These parameters can be estimated by minimizing the following sum of squared errors:

$$J = \sum_{j=1}^{m} [\tilde{g}(\xi_j) - \phi(\xi_j;p_1',p_2',p_3')]^2 \quad (6.18)$$

where

$$\tilde{g}(\xi_j) = \frac{v}{\alpha_2} \log \frac{x_{2f}}{\tilde{x}_2(\xi_j)} \quad (6.19)$$

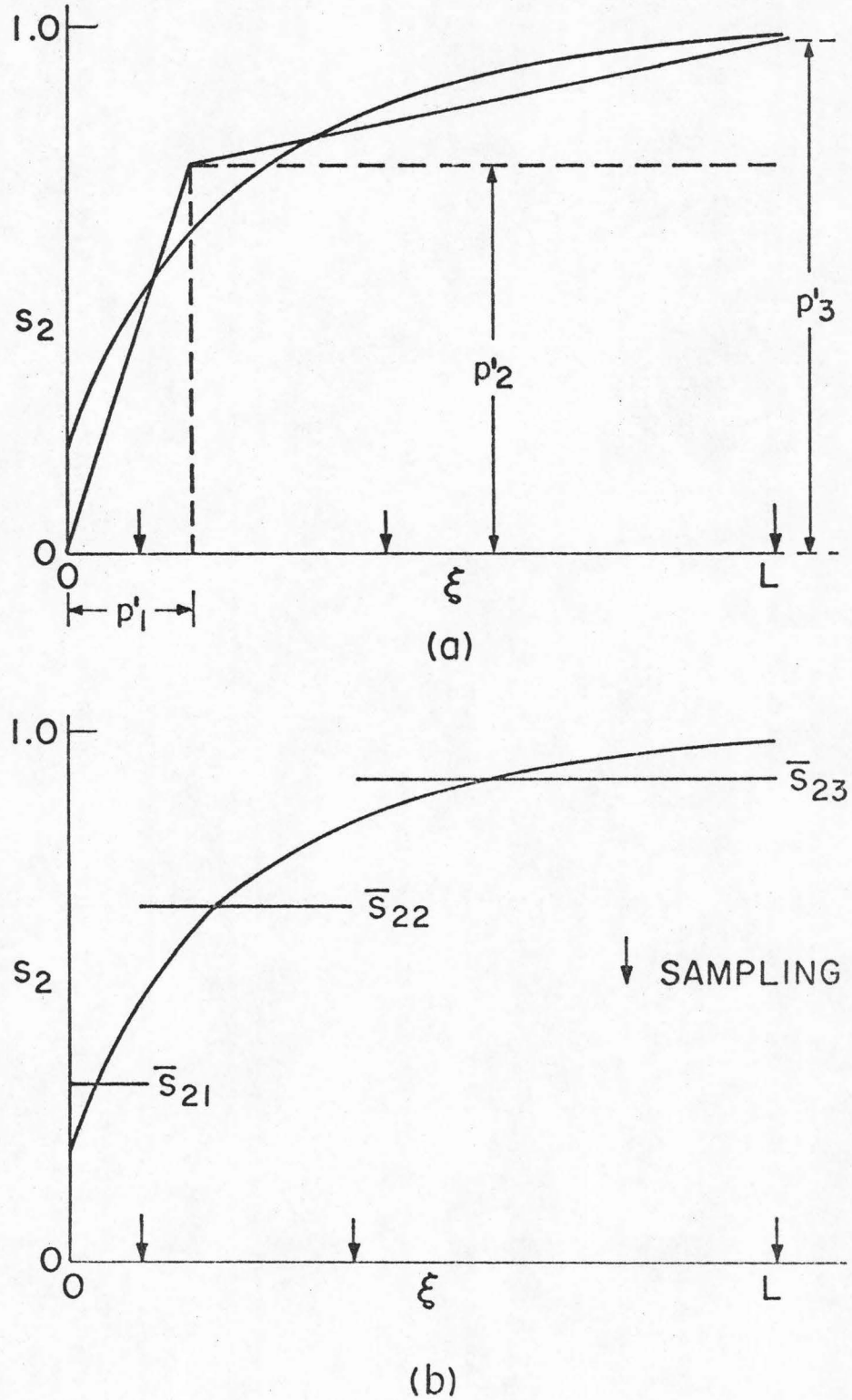

Fig. 11. Two Parametrizations of a Catalyst Activity Profile

$$\phi(\xi_j;p_1',p_2',p_3') = \int_0^{\xi_j} \hat{s}_2(\xi;p_1',p_2',p_3') \exp[-p_2(\frac{1}{\tilde{\theta}(\xi)} - 1)]d\xi \quad (6.20)$$

subject to the physical constraints

$$0 \leq p_1' \leq 1 \qquad \text{and} \qquad 0 \leq p_2' \leq p_3' \leq 1 \quad (6.21)$$

The estimation was carried out for three measurements $m = 3$ using a first order gradient method. The results are given in Figures 12 and 13.

Now the predictions of the reactor response $x_2(\xi)$ to changes in inputs can be obtained as

$$\hat{x}_2(\xi_j) = x_{2f}' \exp\{ - \frac{\alpha_2}{v'} \int_0^{\xi_j} \hat{s}_2(\xi ; p_1',p_2',p_3') \exp[-p_2(\frac{1}{\tilde{\theta}'(\xi)} - 1)]d\xi\} \quad (6.22)$$

where the predicted value of x_2 is denoted by $\hat{x}_2$, and the conditions corresponding to the new input are designated by primes. Figures 14 and 15 present the results of predictions using the parametrized activity profiles corresponding to $\tau = 0.3$ and $\tau = 0.5$, respectively. Even with the large difference between the initial feed conditions ($\theta_f = 1.0$, $v = 1.0$) and the feed conditions used for testing the prediction ($\theta_f' = 1.2$, $v' = 2.0$), good agreement was obtained between the "true" profile and predicted values. For the input $\theta_f' = 1.0$, $v' = 2.0$, and $\theta_f' = 1.2$, $v' = 1.0$, the predicted values also agree satisfactorily with the "true" profiles as shown in Table 5. The error is less than 3% in all cases and less than 1.5% in most cases. Moreover, it is observed that the prediction of the output concentration is usually more accurate than that of the average concentration

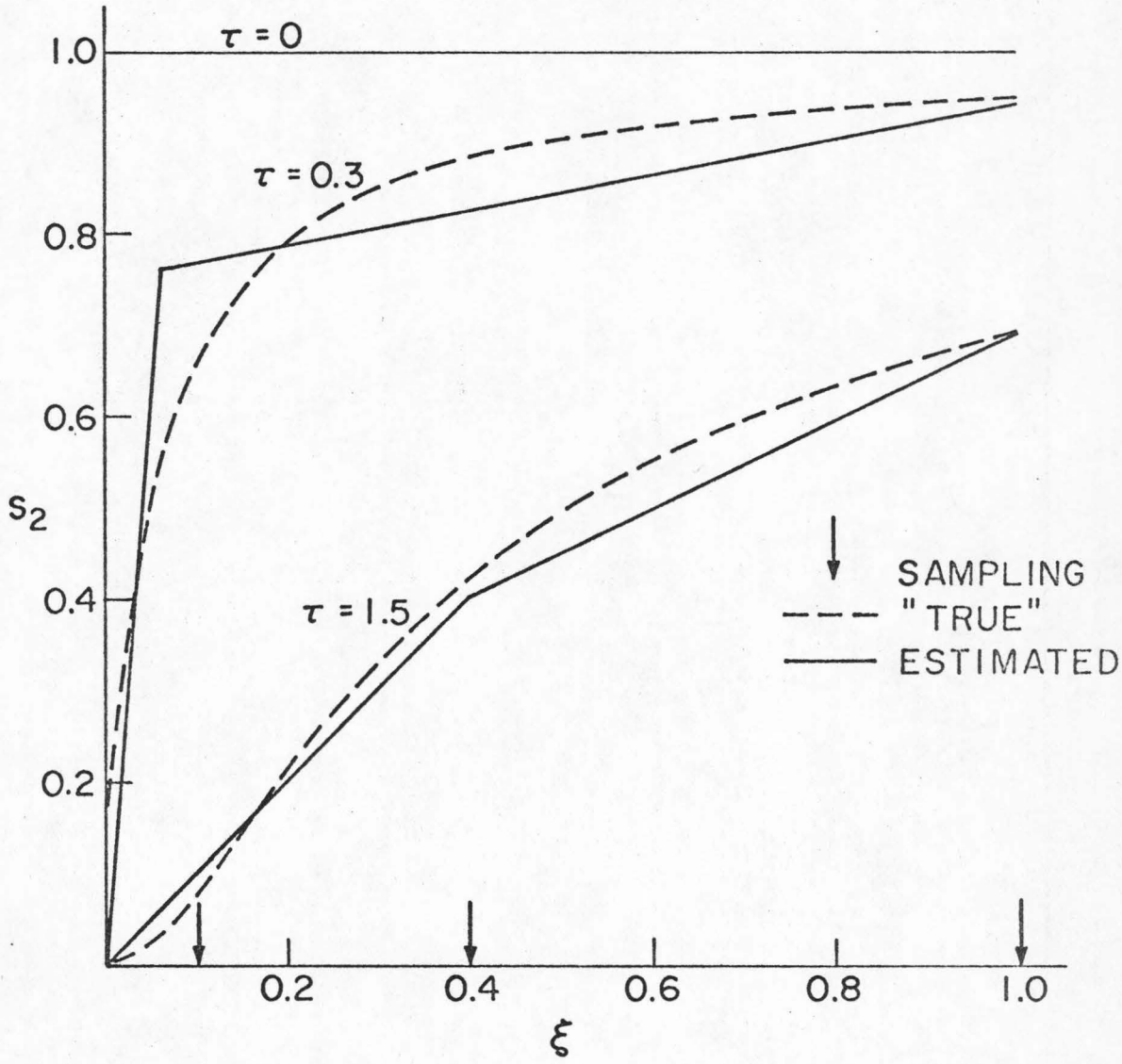

Fig. 12. "True" and Estimated Activity Profiles

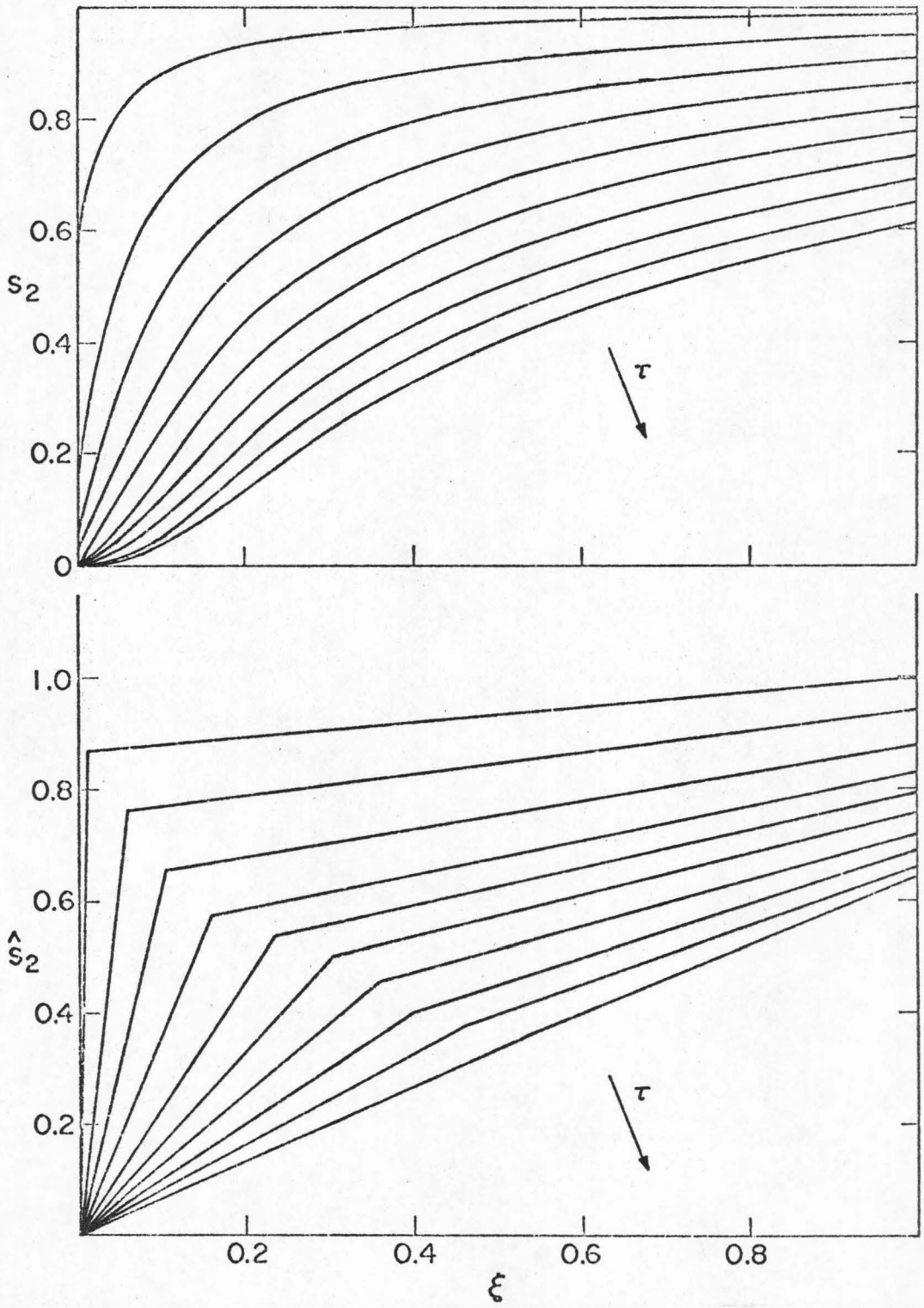

Fig. 13. Time Evolution of "True" and Estimated Activity Profiles

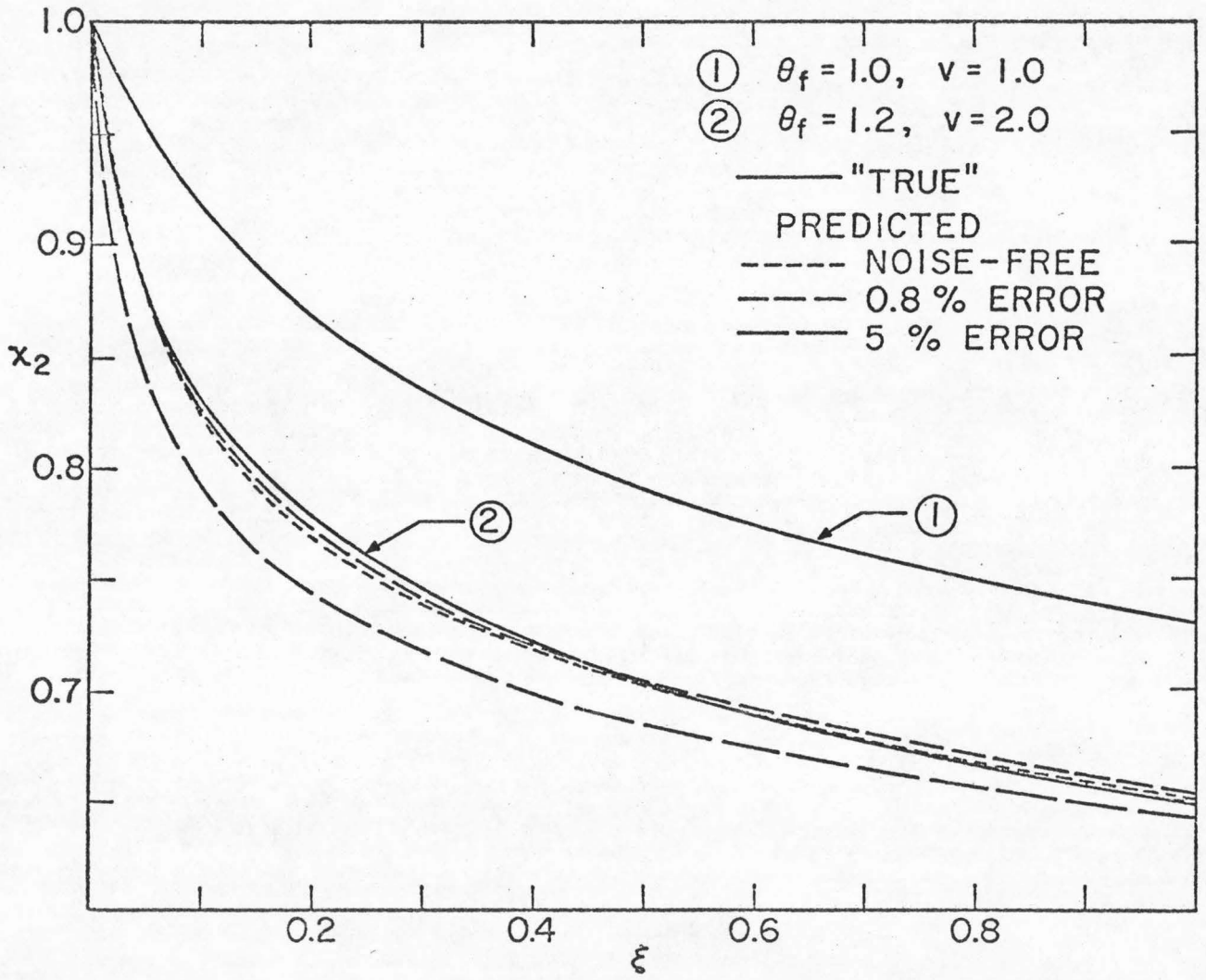

Fig. 14. Comparison between "True" and Estimated Concentration Profiles of n-Paraffin at $\tau = 0.3$

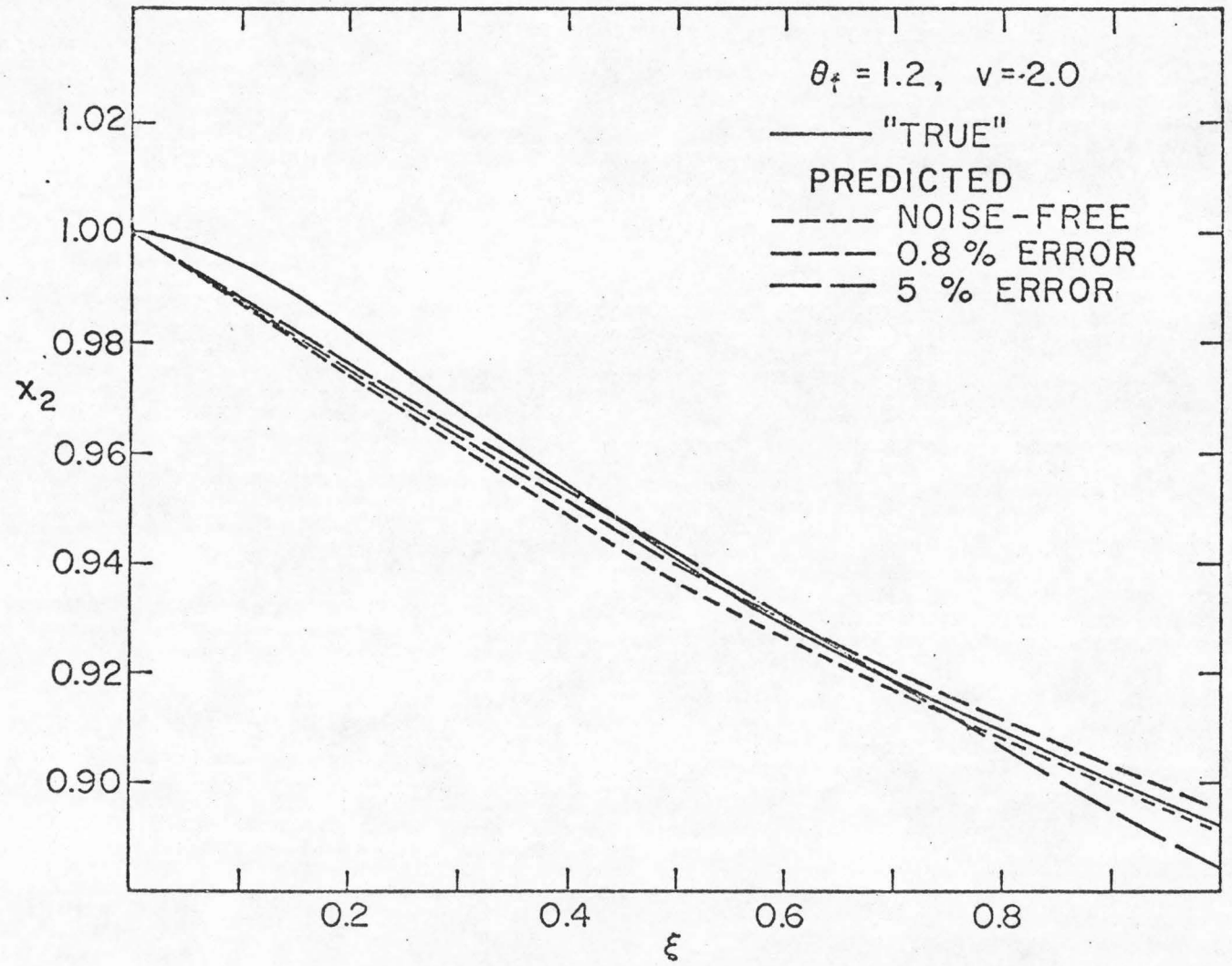

Fig. 15. Comparison between "True" and Estimated Concentration Profiles of n-Paraffin at $\tau = 1.5$

Percentage Error for prediction $\hat{x}_2$ (Absolute value)			New Operating Condition					
			$\theta_f' = 1.0$, $v' = 2.0$			$\theta_f' = 1.2$, $v' = 1.0$		
			Noise Level in Measurements					
			Noise-free	0.8%	5%	Noise-free	0.8%	5%
$\hat{s}_2(\xi)$ in Figure 12	$\tau = 0.3$	Output ($\xi = 1$)	0.61	0.38	1.30	2.50	2.90	0.60
		Avg. ($0 \leq \xi \leq 1$)	1.47	1.36	1.49	1.58	1.93	2.18
	$\tau = 1.5$	Output ($\xi = 1$)	0.26	0.60	0.58	0.15	0.29	0.92
		Avg. ($0 \leq \xi \leq 1$)	0.49	0.55	0.43	0.65	0.51	0.64

TABLE 5. COMPARISON BETWEEN "TRUE" AND PREDICTED VALUES BY THE PARAMETRIZATION OF FIGURE 11a

along the reactor. From the above results the adequacy of this parametrization scheme is established. The parametrized curve gives a closer approximation to the activity profile with decreasing measurement error. Furthermore, the prediction error decreases as the deactivation proceeds. This behavior probably results from the fact that the activity distribution function $s_2(\xi)$ becomes smoother and thus is better approximated by the proposed parametrization scheme. One interesting point that has resulted from this estimation scheme is that even though the set of measurements containing smaller noise yields a better approximation to the activity profile in general, the resulting prediction of $x_2(\xi)$ does not necessarily yield significantly improved results. This may be due to the fact that an exponentially decreasing factor is weighted along the reactor as shown in Eq. (6.22), and thus a poor activity approximation at the latter part of the reactor is hardly revealed by the weighted integral.

Another promising parametrization involves the approximation of the activity profile by a piecewise constant function

$$\hat{s}_2(\xi) = \bar{s}_{2j} \qquad , \qquad \xi_{j-1} \leq \xi \leq \xi_j \tag{6.23}$$

This is indicated by Figures 11b and 16.

The parameters $\bar{s}_{2j}$ can be determined by minimizing the performance index

$$J = \sum_{j=1}^{m} [\tilde{g}(\xi_j) - \phi(\xi_j, \bar{s}_{2j})]^2 \tag{6.24}$$

where

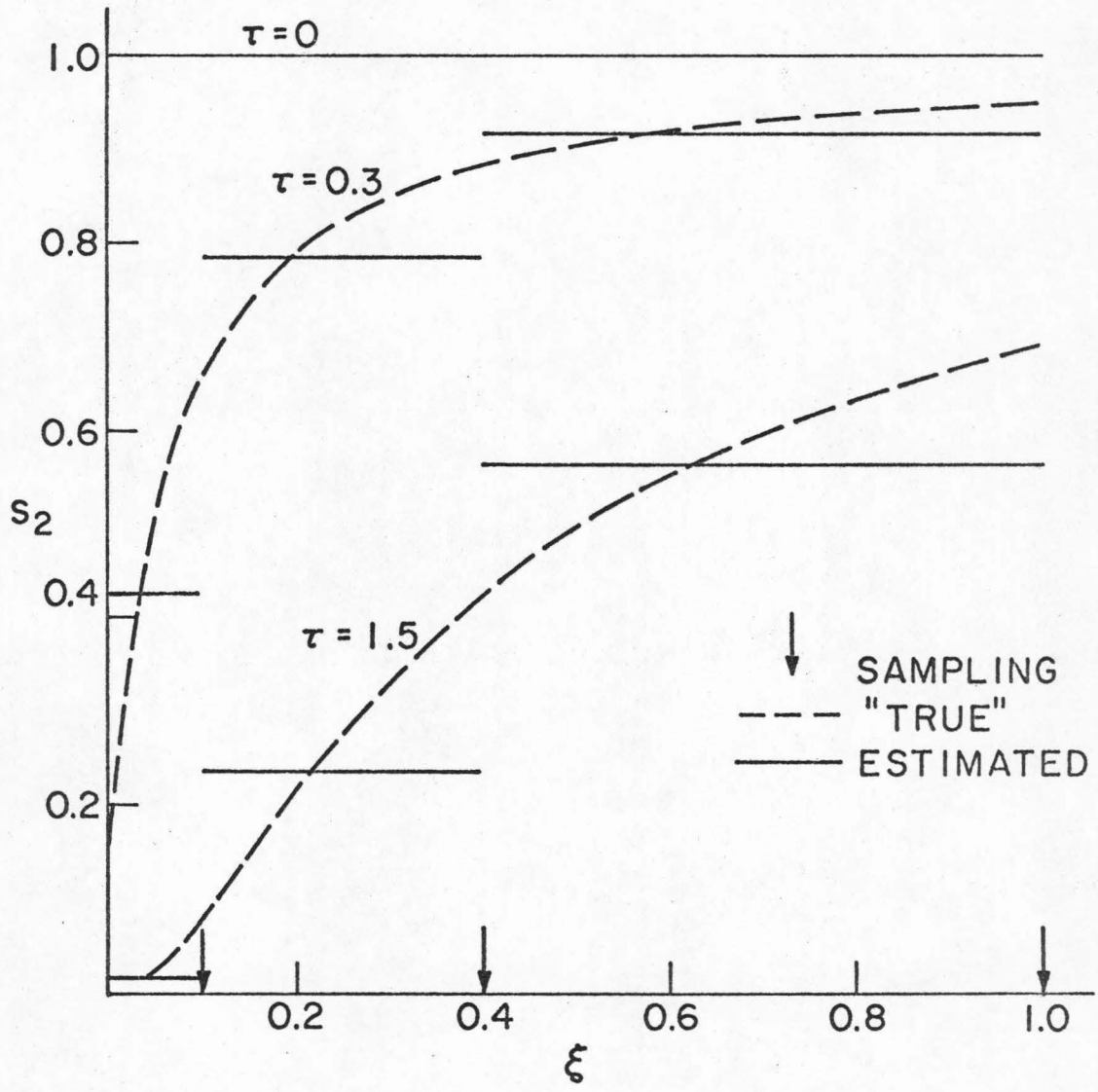

Fig. 16. "True" and Estimated Activity Profiles

$$\phi(\xi_j, \bar{s}_{2j}) = \sum_{i=1}^{j} \bar{s}_{2i} \int_{\xi_{i-1}}^{\xi_i} \exp[-p_2(\frac{1}{\tilde{\theta}(\xi)} - 1)]d\xi \qquad (6.25)$$

and $\tilde{g}$ is given by Eq. (6.19) , subject to the constraints

$$0 \leq \bar{s}_{2j} \leq 1 \ , \quad j=1,\cdots,m \qquad (6.26)$$

Since Eq. (6.25) is linear with respect to $\bar{s}_{2i}$, the minimization can be achieved easily by linear regression. Figure 16 gives two estimated profiles of s_2 . Based upon these estimated $\hat{s}_2(\xi)$, the predicted $\hat{x}_2'(\xi)$ subject to new input conditions $\theta_f' = 1.2$, $v' = 2.0$ is presented in Figures 17 and 18. Similar comparisons between predicted and "true" $x_2'(\xi)$ were also performed for inputs $\theta_f' = 1.0$, $v' = 2.0$ and $\theta_f' = 1.2$, $v' = 1.0$ as shown in Table 6. The predictions were good in all cases. The advantage of this parametrization scheme lies in the convenience of the linear regression technique. However, the error (< 5%) is somewhat higher than that obtained by the previous parametrization, i.e., Figure 11a. Based upon these results, the parametrization of Figure 11a must be preferred.

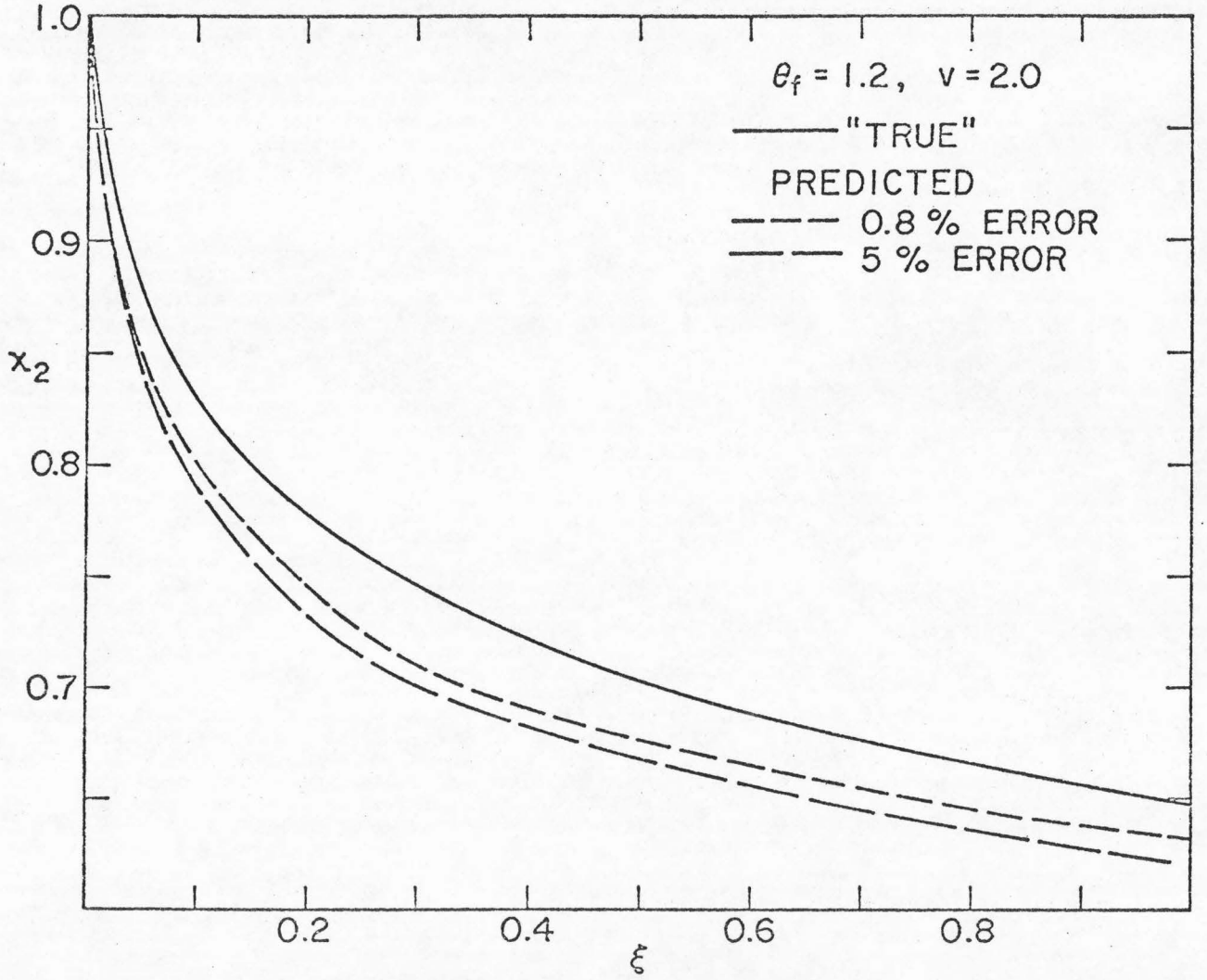

Fig. 17. Comparison between "True" and Estimated Concentration Profiles of n-Paraffin at $\tau = 0.3$

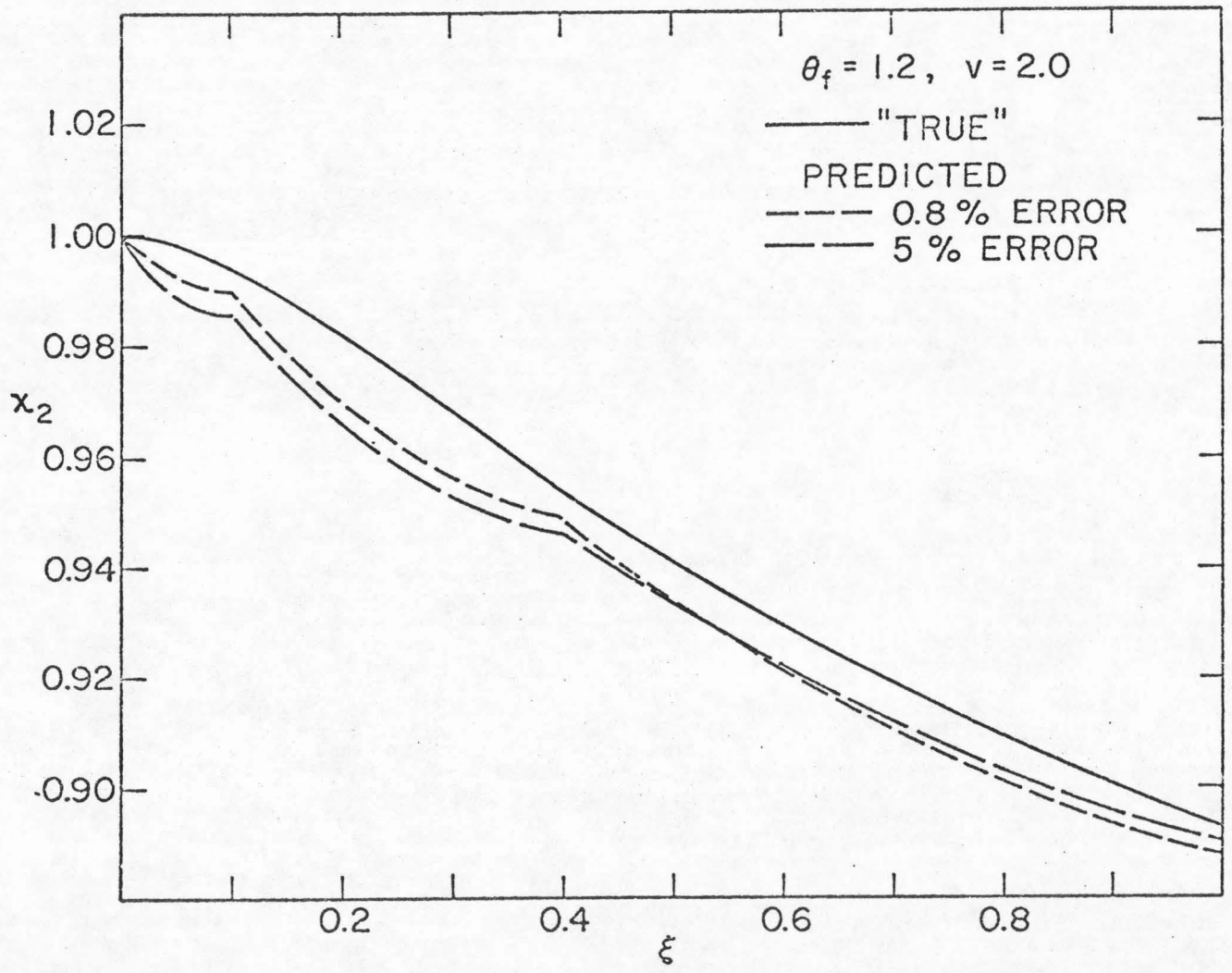

Fig. 18. Comparison between "True" and Estimated Concentration Profiles of n-Paraffin at $\tau = 1.5$

Percentage Error for prediction $\hat{x}_2$ (Absolute value)			New Operating Condition			
			$\theta_f' = 1.0$, $v' = 2.0$		$\theta_f' = 1.2$, $v' = 1.0$	
			Noise Level in Measurements			
			Noise-free	0.8%	Noise-free	0.8%
$\hat{s}_2(\xi)$ in Figure 16	$\tau = 0.3$	Output ($\xi = 1$)	0.32	1.20	7.50	4.90
		Avg. ($0 \leq \xi \leq 1$)	0.25	0.42	7.80	5.80
	$\tau = 1.5$	Output ($\xi = 1$)	0.10	0.67	0.82	0.58
		Avg. ($0 \leq \xi \leq 1$)	0.22	0.28	1.10	1.30

TABLE 6. COMPARISON BETWEEN "TRUE" AND PREDICTED VALUES BY THE PARAMETRIZATION OF FIGURE 11b

7. ESTIMATION OF DEACTIVATION PARAMETERS FOR MONOFUNCTIONAL CATALYSTS

For a fixed bed catalytic process using monofunctional catalysts, deactivation is usually slow so that under the previously stated assumptions for the factorization of activity s the plug-flow equations can be written as

$$G(t)\,\frac{\partial y}{\partial z} = sf(y,T) \tag{7.1}$$

$$G(t)\,\frac{\partial T}{\partial z} = sg(y,T) \tag{7.2}$$

where y is the vector of composition variables y_i.

To achieve the purposes of long-term reactor optimization such as optimal catalyst utilization and regeneration policies, the estimation of deactivation parameters is necessary. On the other hand, in some cases it is desirable to have an on-line process control. There, the updated information about catalyst deactivation parameters would be useful in obtaining optimal or suboptimal control policies. Two separate estimation schemes are presented, one for first order catalyst deactivation and the other for a general power model. Emphasis is on the case of first order deactivation as it can result in a sequential estimation scheme.

First Order Deactivation

Considering first a single reaction, the steady reactor operation can be described by the single equation

$$G(t)\,\frac{\partial T}{\partial z} = s\tilde{g}(T,y_o(t),T_o(t)) \tag{7.3}$$

where $\tilde{g}$ is obtained from $g(y,T)$ of Eq. (7.2) by expressing y in terms of y_o, T_o, and T.

According to the description of Chapter 2, the simplest deactivation model is first order with respect to the catalyst activity and independent of concentration

$$\frac{\partial s}{\partial t} = -s\ k_d\ \exp(-E_d/RT) \tag{7.4}$$

Equations (7.3) and (7.4) form a system of partial differential equations. However, mathematically, it is generally much easier to solve a system of ordinary differential equations than a system of partial differential equations in many respects, i.e., accuracy, computing time, stability, etc. Furthermore, the estimation of several parameters in partial differential equations usually requires lengthy computations and may involve convergence problems. On the other hand, parameter estimation in ordinary differential equations is a well developed topic. Therefore, the transformation of partial differential equations to a system of ordinary differential equations is highly desired.

In general, there are two approaches to estimate deactivation parameters. The first is to combine Eqs. (7.3) and (7.4) and obtain a relationship between the deactivation parameters and the measured state variables. This relationship, which may not be direct or explicit, relates state variables to catalyst decay parameters through a function of catalyst activities. Often, this function has a significant physical interpretation, and makes the transformation to a system of ordinary differential equations feasible. The transformation is

described in the following paragraph, while some examples are included in the remaining sections. The second way of estimating decay parameters is to deal with Eqs. (7.3) and (7.4) one by one. By parametrization of the activity profile, one can generate local activity estimates, which in turn can be fed into the catalyst deactivation equation to yield estimates of the decay parameters. This estimation scheme is illustrated by a simple example in Appendix C. In general, the latter approach, involving an approximation by parametrization, gives less accurate results than the former.

Now, combining Eqs. (7.3) and (7.4) and integrating the resulting expression one obtains

$$\frac{dS(L,t)}{dt} = -k_d G(t) \int_{T_o(t)}^{T(L,t)} \frac{e^{-E_d/RT'}}{\tilde{g}(T',y_o(t),T_o(t))}\, dT' \qquad (7.5)$$

where the cumulative activity $S(z,t)$ is defined as

$$S(z,t) = \int_0^z s(z')dz' \qquad (7.6)$$

The integration of Eq. (7.3) gives

$$G(t) \int_{T_o(t)}^{T(L,t)} \frac{dT'}{\tilde{g}(T',y_o(t),T_o(t))} = S(L,t) \qquad (7.7)$$

which defines implicitly $T(L,t)$, the measured quantity, as a function of S :

$$T(L,t) = F(y_o(t),T_o(t),S/G) \qquad (7.8)$$

Substituting Eq. (7.8) into (7.5), the latter becomes an ordinary differential equation in $S(L,t)$:

$$\frac{dS}{dt} = -k_d G(t)\, P(S/G(t), y_o(t), T_o(t), E_d) \tag{7.9}$$

where

$$P(S/G(t), y_o(t), T_o(t), E_d) = \int_{T_o(t)}^{F} \frac{e^{-E_d/RT'}}{\tilde{g}(T', y_o(t), T_o(t))}\, dT' \tag{7.10}$$

The differential equation Eq. (7.9) can be used with Eq. (7.8), which represents the measurements for a sequential or nonsequential estimation of the parameters E_d and k_d.

When the feed conditions y_o, T_o, and G are constant, an ordinary differential equation in $T(L,t)$ can be obtained by introducing Eq. (7.7) in Eq. (7.5):

$$\frac{dT(L,t)}{dt} = -k_d\, \tilde{g}(T(L,t), y_o, T_o) \int_{T_o}^{T(L,t)} \frac{e^{-E_d/RT'}}{\tilde{g}(T', y_o, T_o)}\, dT' \tag{7.11}$$

This equation is simpler than (7.9) because it does not require the evaluation of the function F defined by Eq. (7.8) and because it can be used directly with the measurements of $T(L,t)$ for the estimation of the deactivation parameters k_d, E_d. Equations (7.9) and (7.11) apply also when $S(L,t)$ or $T(L,t)$ are replaced by $S(z,t)$ and $T(z,t)$. Such equations may be used for estimation with measurements of T at intermediate points along the reactor.

The system of partial differential equations, (7.3) and (7.4), were transformed to ordinary differential equations. The system of Eqs. (7.3),(7.4) is more general than the system treated by Bischoff

[90], where the right hand sides of the two equations are proportional to each other. The latter situation occurs only in isothermal operation. For the special case of isothermal operations, for example in a laboratory reactor, the integral in the ordinary differential equations similar to Eq. (7.9) or (7.11) can be written in closed form. This is discussed in Appendix D.

Now, consider the case of more than one reaction, i.e., Eqs. (7.1) and (7.2), and a concentration-dependent deactivation:

$$\frac{\partial s}{\partial t} = -sk_d\, \phi(y)\, \exp(-E_d/RT) \tag{7.12}$$

For fixed time, dividing Eq. (7.1) by Eq. (7.2) yields

$$\frac{dy}{dT} = \frac{f(y,T)}{g(y,T)} \tag{7.13}$$

Integration of Eq. (7.13) gives y as a function of T and the feed conditions

$$y = h(T,y_o(t),T_o(t)) \tag{7.14}$$

Combining Eqs. (7.2), (7.12), and (7.14) one obtains

$$G(t)\, \frac{\partial T}{\partial z} = s\, \tilde{g}(T,y_o(t),T_o(t)) \tag{7.15}$$

$$\frac{\partial s}{\partial t} = -sk_d\, \exp(-E_d/RT)\, \tilde{\phi}(T,y_o(t),T_o(t)) \tag{7.16}$$

where

$$\tilde{g}(T,y_o(t),T_o(t)) = g(h(T,y_o(t),T_o(t)),T) \tag{7.17}$$

$$\tilde{\phi}(T,y_o(t),T_o(t)) = \phi(h(T,y_o(t),T_o(t)),T) \tag{7.18}$$

Now Eqs. (7.15) and (7.16) have the form of the system consisting of Eqs. (7.3) and (7.4). Thus, the aforementioned transformation to an ordinary differential equation can be followed exactly, although the estimation algorithm will be more tedious due to the need of evaluating the function h at each time.

A Sequential Estimation Scheme

Many estimation schemes can be used with a system of ordinary differential equations. They can be classified into two types, i.e., sequential and non-sequential. Non-sequential estimation can be performed by the well-known methods of hill climbing, e.g., Rosenbrock and Storey [118], Kittrell, Mezaki, and Watson [119], and by quasi-linearization, e.g., Heineken, Tsuchiyah and Aris [120], Seinfeld and Gavalas [121], E. S. Lee [122]. However, sequential estimation should in general be favored for the estimation of slowly varying parameters as in the case of catalyst decay for the following reasons. Firstly, in a non-sequential estimation, every time an additional observation is to be included, the entire calculation must be repeated. Secondly, in sequential estimation the parameters are immediately updated as additional data become available so that the estimated parameters can be provided for "on-line" control purposes.

The earliest work on sequential estimation was done by Wiener [123] and is often referred to as the Wiener filter. However, the basic theories for linear systems in the literature are those of Kalman [124] for the discrete case and Kalman and Bucy [125] for the continuous case. In these theories the problem of estimation is ingeneously reduced to the solution of a system of ordinary difference or

differential equations, and the method is usually known as "Kalman filter". Cox [126] has developed a formulation applicable to both linear and nonlinear systems using the discrete forms and has suggested the use of dynamic programming as a computational approach. The above papers are all based upon the statistical point of view, hence the resulting estimates are optimal. However, another practical approach to sequential estimation based on classical least squares criteria has been taken by Bellman and co-workers [127] and Detchmendy and Sridhar [128] for continuous systems and by Sridhar and Pearson [129] for discrete systems. Their filters, which contain certain approximations, are not optimal but are sufficient for many engineering purposes. Seinfeld [130] has extended the sequential estimation technique to the systems described by nonlinear parabolic and hyperbolic partial differential equations. For applications to chemical engineering problems, see Gavalas and Seinfeld [12], Wells [131] and Lee [132]. For further background information on filtering theory, the reader may consult the books by Bryson and Ho [133] and Meditch [134], and the reviews by Schwartz et al. [135] and Seinfeld [136].

In general, all the filters proposed in the literature are alike in functionality, but differ only in the estimation criteria or approximations adopted. In this study a modified Kalman's sequential filter described by Meditch [134] is adopted, and the discrete version of that filter is chosen for its convenience in digital computer operations. For reference purposes, the discrete filter of Cox [126] and the continuous filter of Detchmendy and Sridhar [128] are sketched briefly in Appendix E.

To formulate the sequential filter, the following difference equation and linear measurements are considered:

$$x(i+1) = f(x(i)) \tag{7.19}$$

$$y(i) = H(i)\, x(i) + \varepsilon(i) \tag{7.20}$$

It is required to minimize the performance index

$$J \triangleq \|x(0) - x_o\|^2_{D_o^{-1}} + \sum_{i=1}^{N} \|y(i) - H(i)\, x(i)\|^2_{R^{-1}(i)} \tag{7.21}$$

with respect to $x(0),\cdots,x(N)$ subject to the constraint equation (7.19). Omitting the derivation procedures, the resulting Kalman's linearized filter is sketched as follows:

$$\hat{x}(k+1 \mid k+1) = f(\hat{x}(k|k)) + K(k+1)[y(k+1) - H(k+1)\, f(\hat{x}(k|k)] \tag{7.22}$$

$$P(k+1 \mid k) = f_x(\hat{x}(k|k))\, D(k|k)\, f_x^T(\hat{x}(k|k)) \tag{7.23}$$

$$K(k+1) = P(k+1 \mid k)\, H^T(k+1)[H(k+1)\, P(k+1 \mid k)\, H^T(k+1) + R(k+1)]^{-1} \tag{7.24}$$

$$D(k+1 \mid k+1) = P(k+1 \mid k) - K(k+1)\, H(k+1)\, P(k+1 \mid k) \tag{7.25}$$

where the matrices P and D can be interpreted qualitatively as the covariance matrices of errors in estimates for the state at stage $k+1$ given k observations and $k+1$ observations, respectively. They represent approximately the measures of present uncertainty about the state x. Finally, since D and P are symmetric matrices, the

total number of initial estimates required for an n-dimensional system is $n + n(n+1)/2 = n(n+3)/2$.

Numerical Examples

(i) Example 1

The oxidative dehydrogenation of 1-butene to butadiene using bismuth molybdate catalysts is carried out in fixed bed reactors in the presence of air as follows:

$$C_4H_8 + \frac{1}{2} O_2 \xrightarrow{sk} C_4H_6 + H_2O \qquad (7.26)$$

According to Adams et al. [137], the reaction rate is first order with respect to butene,

$$r_o = sk_o \exp(-E/RT)c_1 \qquad (7.27)$$

Note that a detailed kinetic model for the catalytic oxidation of 1-butene must include the following side reactions:

(i) a consecutive oxidation of butadiene to CO_2 and H_2O

(ii) a parallel direct oxidation of 1-butene to CO_2 and H_2O

(iii) a parallel isomerization of 1-butene to cis- and trans-2-butene along with the isomerization between the 2-butenes

Under the operating conditions of atmospheric pressure and 400-500°C, it has been reported [137,138,139] that the ratios of the rates of the side reactions (i)-(iii) to that of the main reaction are approximately 1/20, 1/400, and 1/10 respectively so that these side reactions can be neglected for practical purposes. In industry, this exothermic process is carried out in an adiabatic fixed bed reactor. At steady state and

constant pressure the reactor equations are

$$G(t)\,\frac{\partial y_1}{\partial z} = -\,\tilde{r}_1(s,y_1,T) \tag{7.28}$$

$$G(t)\,\frac{\partial T}{\partial z} = \frac{(-\Delta H)}{c_p}\,\tilde{r}(s,y_1,T) \tag{7.29}$$

where y_1 is the molar flux of butene per unit mass flux of feed, and

$$\tilde{r}_1 = sk_o \exp(-E/RT)\,\frac{Py_1}{RT\,\sum y_i} \tag{7.30}$$

By eliminating the right side between Eqs. (7.28) and (7.29) one obtains in dimensionless form

$$\frac{\partial\theta}{\partial\xi} = s\,\frac{c[a - \lambda(\theta-1)]}{[b+\frac{\lambda}{2}(\theta-1)]}\exp[p(1 - \tfrac{1}{\theta})] \tag{7.31}$$

where

$$\theta = T/T_o\ , \qquad \xi = z/L\ , \qquad p = E/RT_o \tag{7.32}$$

$$a = M_1 y_{1o}\ , \qquad b = M_1 \Sigma\, y_{io}\ , \qquad \lambda = c_p T_o M_1/(-\Delta H) \tag{7.33}$$

$$M_m = \Sigma\, M_i y_{io} / \Sigma y_{io}\ , \quad \alpha = \frac{L}{u}\,k_o \exp(-p)\ , \quad c = \frac{\alpha M_1}{\lambda M_m} \tag{7.34}$$

For simplicity, consider the case of constant G, y_{io}, T_o and a first order deactivation such as

$$\frac{\partial s}{\partial t} = -sk_d \exp(-E_d/RT) \tag{7.35}$$

or in dimensionless form as

$$\frac{\partial s}{\partial\tau} = -s\beta \exp(p(1 - \tfrac{1}{\theta})] \exp(-q/\theta) \tag{7.36}$$

where

$$\tau = t/t_o \ , \quad \beta = k_d t_o \exp(-p) \ , \quad q = (E_d - E)/RT_o \tag{7.37}$$

Numerical calculations were performed using simulated measurements. First, "true" values of the temperature at the end of the reactor were obtained numerically from Eqs. (7.31) and (7.36) using the following set of parameters:

$$a = 0.28 \ , \quad b = 1.68 \ , \quad \lambda = 2.08 \ , \quad p = 17.87 \ , \quad c = 0.4$$

$$\beta = 2.0 \ , \quad q = 2.75 \ , \quad \theta(0,\tau) = 1.0 \ , \quad s(\xi,0) = 1.0$$

Then simulated measurements were generated by adding random measurement error to the "true" values

$$\tilde{\theta}(1,\tau) = \theta(1,\tau)\ [1 + n(0,\sigma)] \tag{7.38}$$

Since the temperature is usually measured very frequently during a day, its daily average value can be considered to contain a very small random error.

Consider the estimation of the deactivation constants k_d and E_d from the record of the outlet temperature. By using the scheme outlined previously, the following ordinary differential equation is obtained from Eqs. (7.31) and (7.36):

$$\frac{d\theta}{d\tau} = -\frac{\beta[a - \lambda(\theta-1)]}{\theta[b + \frac{\lambda}{2}(\theta-1)]} \exp[-p(\frac{1}{\theta} - 1)] \int_1^{\theta} \frac{x[b + \frac{\lambda}{2}(x-1)]}{[a - \lambda(x-1)} \exp(-q/x)dx \tag{7.39}$$

To Eq. (7.39) the following equations for the parameters are adjoined

$$\frac{d\beta}{d\tau} = 0 \quad , \quad \frac{dq}{d\tau} = 0 \tag{7.40}$$

A complete system of dynamical equations along with the temperature measurements $\tilde{\theta}(1,\tau)$ for constructing an estimator is thus obtained.

The sequential filtering scheme described in the last section has been applied to the estimation of the deactivation parameters β and q. The numerical results are presented in Figures 19-21. Calculations have been performed with noise-free, 1% error and 5% error in the measurements $\tilde{\theta}(1,\tau)$, which are taken at time intervals of 0.02 corresponding to five times daily. The unrealistically high error level of 5% was used solely to test the effectiveness of the filter. Figure 19 compares the filtered temperature signal with the "true" signal for the error level of 5%. The two signals are indistinguishable for the two lower error levels. Figures 20 and 21 show the estimates of the decay parameters β and q as functions of time. The initial estimates were chosen to contain a large error in both cases. The error is rapidly reduced in a short initial interval of time and then it changes very slowly. At large times, the mean of the error does not become zero but remains roughly proportional to the measurement error. This behavior is commonly observed in nonlinear filters, especially when two signals such as β and q are correlated. Even at the high measurement error of 5%, however, the estimation results are adequate for the intended applications.

(ii) Example 2

Consider an isothermal catalytic operation in a fixed bed reactor. The catalysts used in the reactor are subject to deactivation at a rate

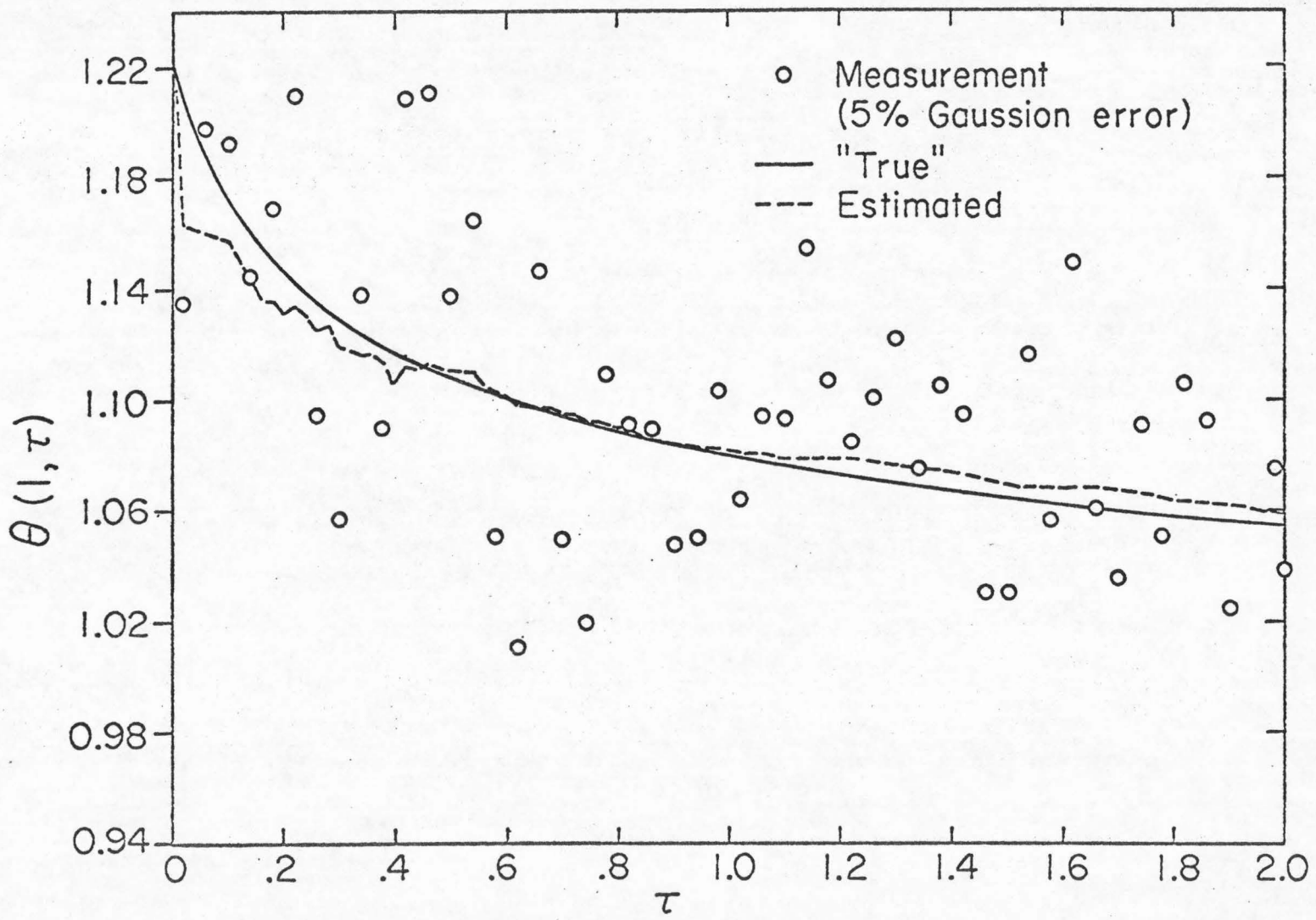

Fig. 19. Sequential Filtering of the Outlet Temperature

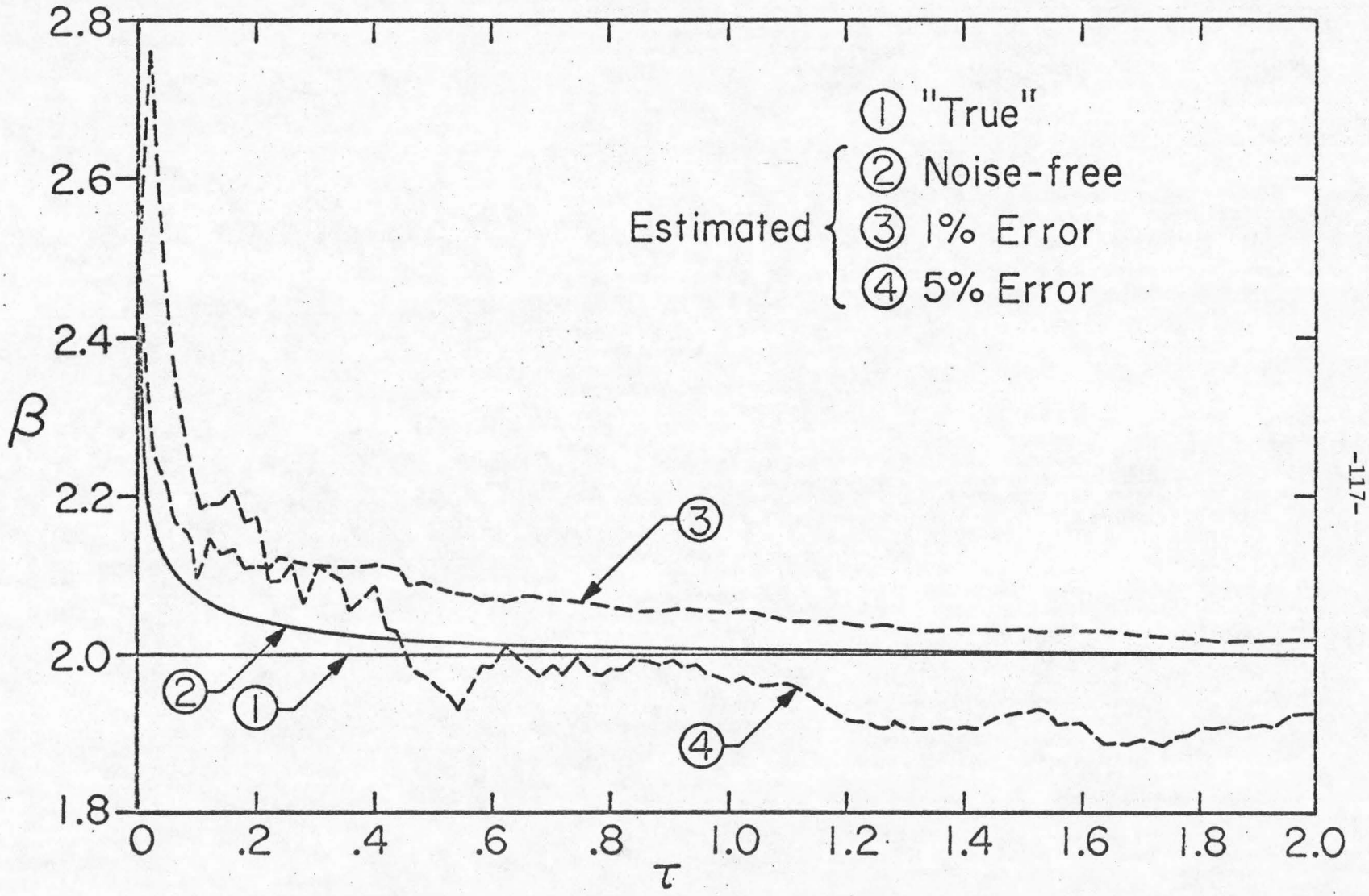

Fig. 20. Sequential Estimation of the Deactivation Parameter β

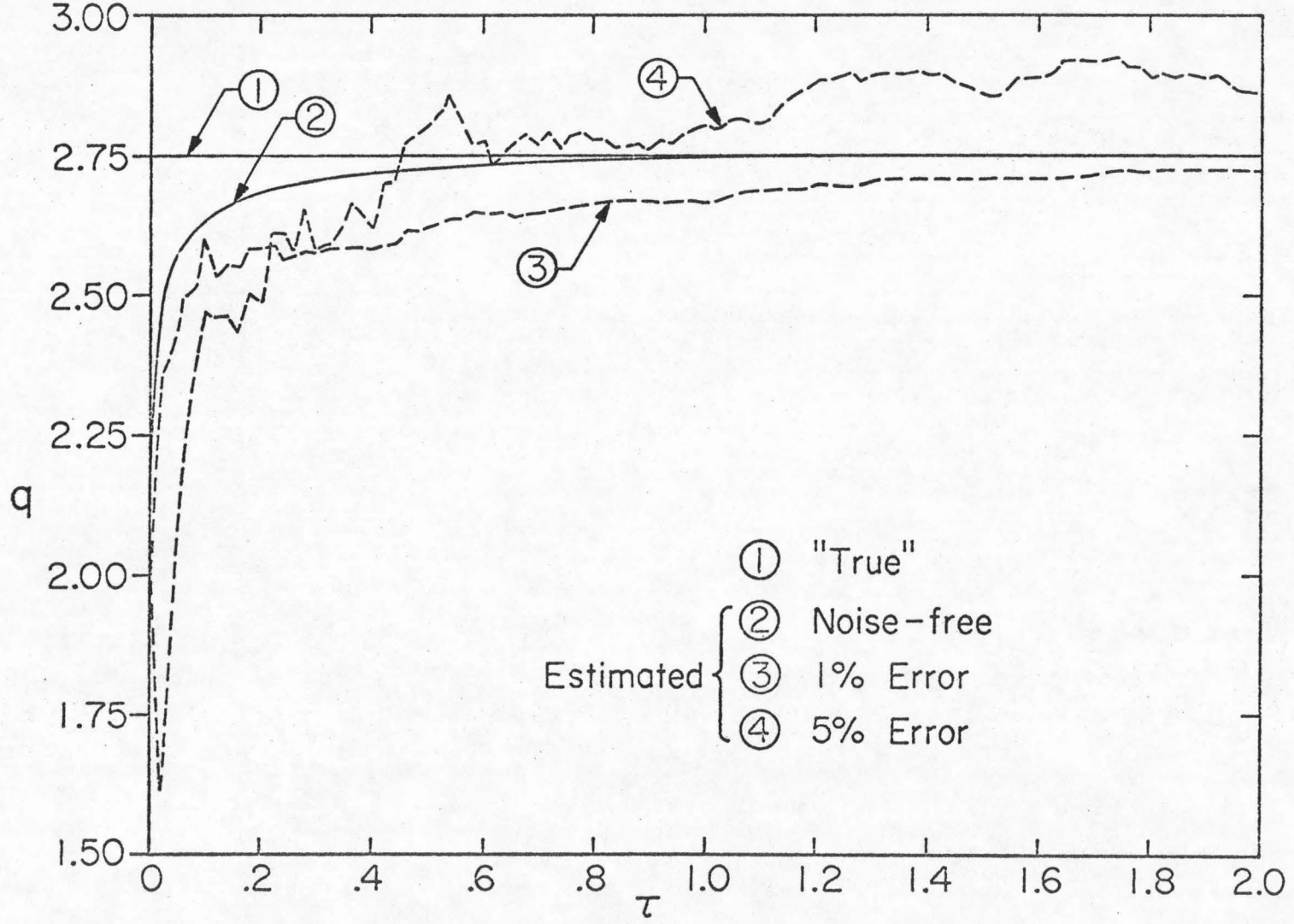

Fig. 21. Sequential Estimation of the Deactivation Parameter q

controlled by the absorption-desorption of the reactant. The dynamical system is characterized by the following set of partial differential equations:

$$\frac{\partial x}{\partial \xi} = - \alpha s \, x^{1/2} \tag{7.41}$$

$$\frac{\partial s}{\partial \tau} = - \beta s \, \left(\frac{x}{1+mx}\right)^{1/2} \tag{7.42}$$

with boundary conditions

$$\text{(i)} \quad \text{at} \quad \xi = 0 : \qquad x = x_f \tag{7.43}$$

$$\text{(ii)} \quad \text{at} \quad \tau = 0 : \qquad s = s_o \tag{7.44}$$

Consider the estimation of the deactivation parameters β and m from the reactor outlet concentration measurements. The "true" values of the output concentration $x(1,\tau)$ were obtained numerically from Eqs. (7.41) and (7.42) using the following values of the parameters:

$$\alpha = 0.6 \, , \quad \beta = 2.0 \, , \quad m = 0.5 \, , \quad x_f = 1.0 \, , \quad s_o = 1.0$$

The noisy measurements are simulated in the way described previously. Following the proposed transformation technique, an ordinary differential equation is obtained:

$$\frac{dx}{d\tau} = \frac{2\beta}{m} \, x^{1/2} [(1+mx_f)^{1/2} - (1+mx)^{1/2}] \tag{7.45}$$

Equation (7.45) and the following equations for the unknown parameters

$$\frac{d\beta}{d\tau} = 0 \qquad , \qquad \frac{dm}{d\tau} = 0 \tag{7.46}$$

constitute a complete dynamical system for the sequential filter. The

filtering results for the state x using the set of measurements containing 5% standard error are shown in Figure 22. Satisfactory results were also obtained for the deactivation parameters β and m as shown in Figures 23 and 24. Two different sets of initial estimates for the parameters are included in both figures. All the results indicate the feasibility of the proposed transformation scheme and the adequacy of the filtering technique.

Should there exist some interaction between neighboring occupied sites to make the rate dependency on the activity nonlinear, the proposed transformation scheme may still give a fair approximation after a simple linearization process. For instance, if the system equations are changed into

$$\frac{\partial x}{\partial \xi} = -\alpha s^2 x^{1/2} \tag{7.47}$$

$$\frac{\partial s}{\partial \tau} = -\beta s^2 \left(\frac{x}{1+mx}\right)^{1/2} \tag{7.48}$$

The term s^2 can be linearized as follows:

$$s^2 \tilde{=} s^*(2s - s^*) \tag{7.49}$$

Defining a new variable

$$\tilde{s} = s - s^*/2 \tag{7.50}$$

the system equations can be transformed to

$$\frac{\partial x}{\partial \xi} = -\tilde{\alpha}\ \tilde{s} x^{1/2} \tag{7.51}$$

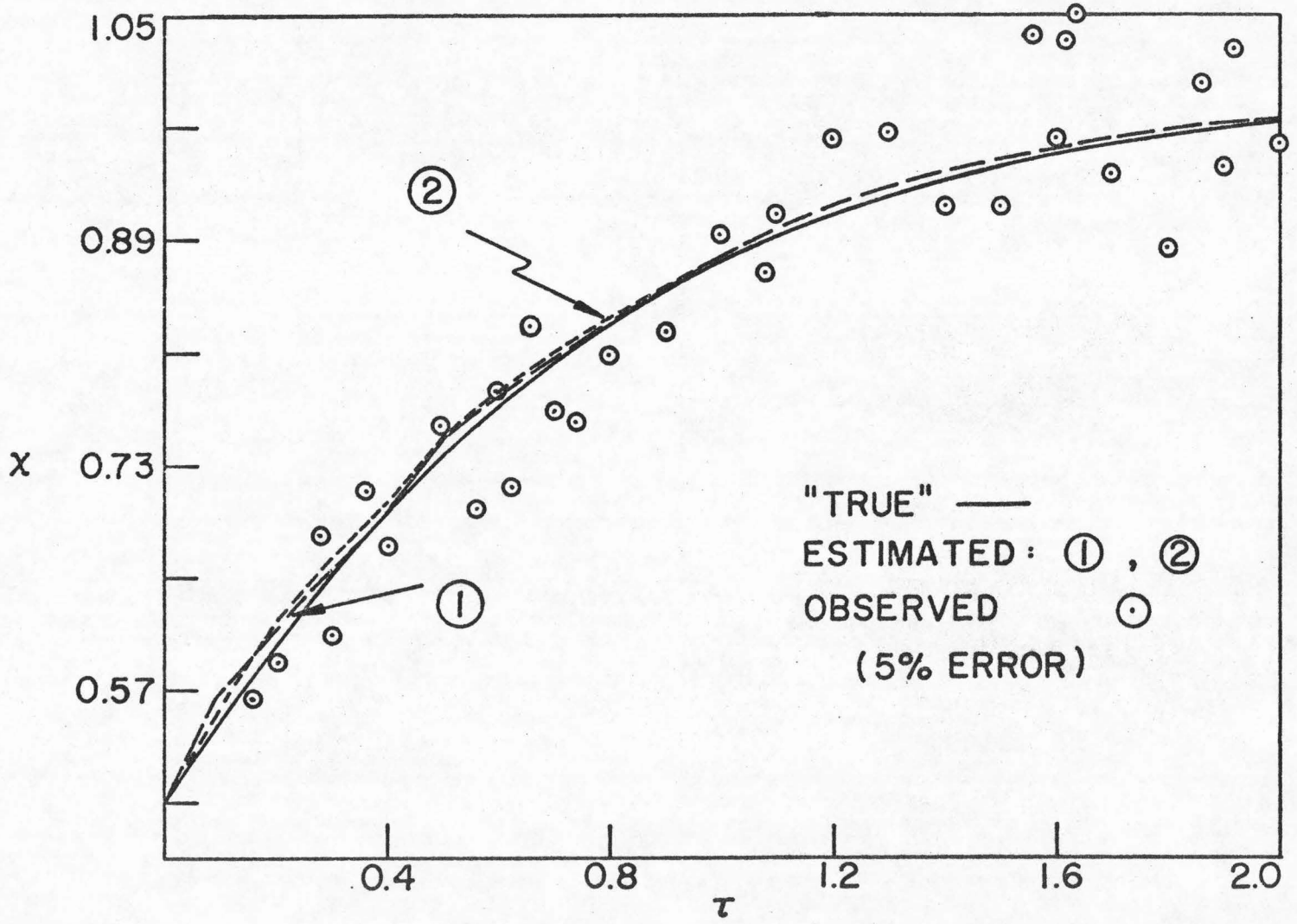

Fig. 22. Sequential Estimation of the State x

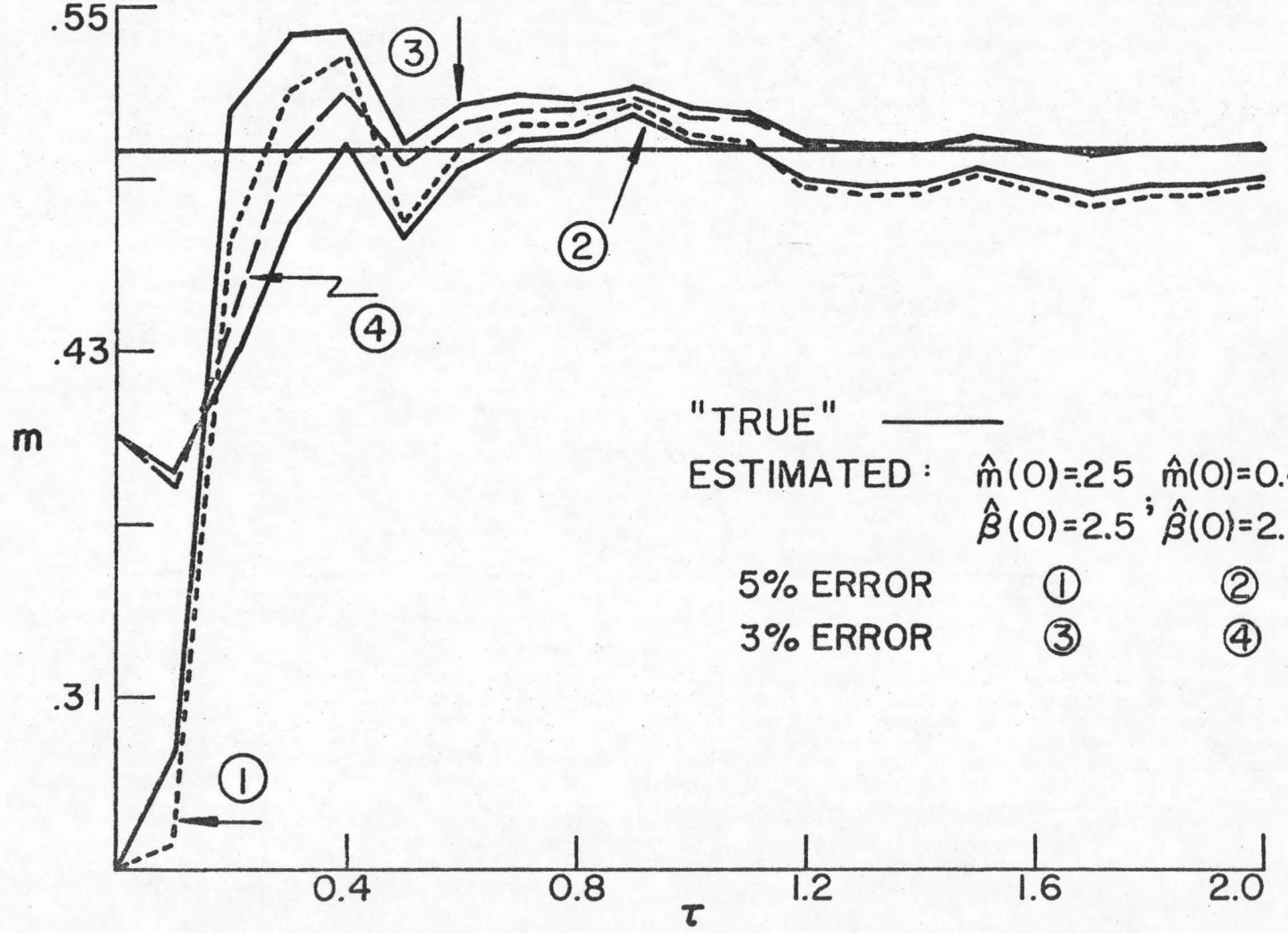

Fig. 23. Sequential Estimation of the Parameter m

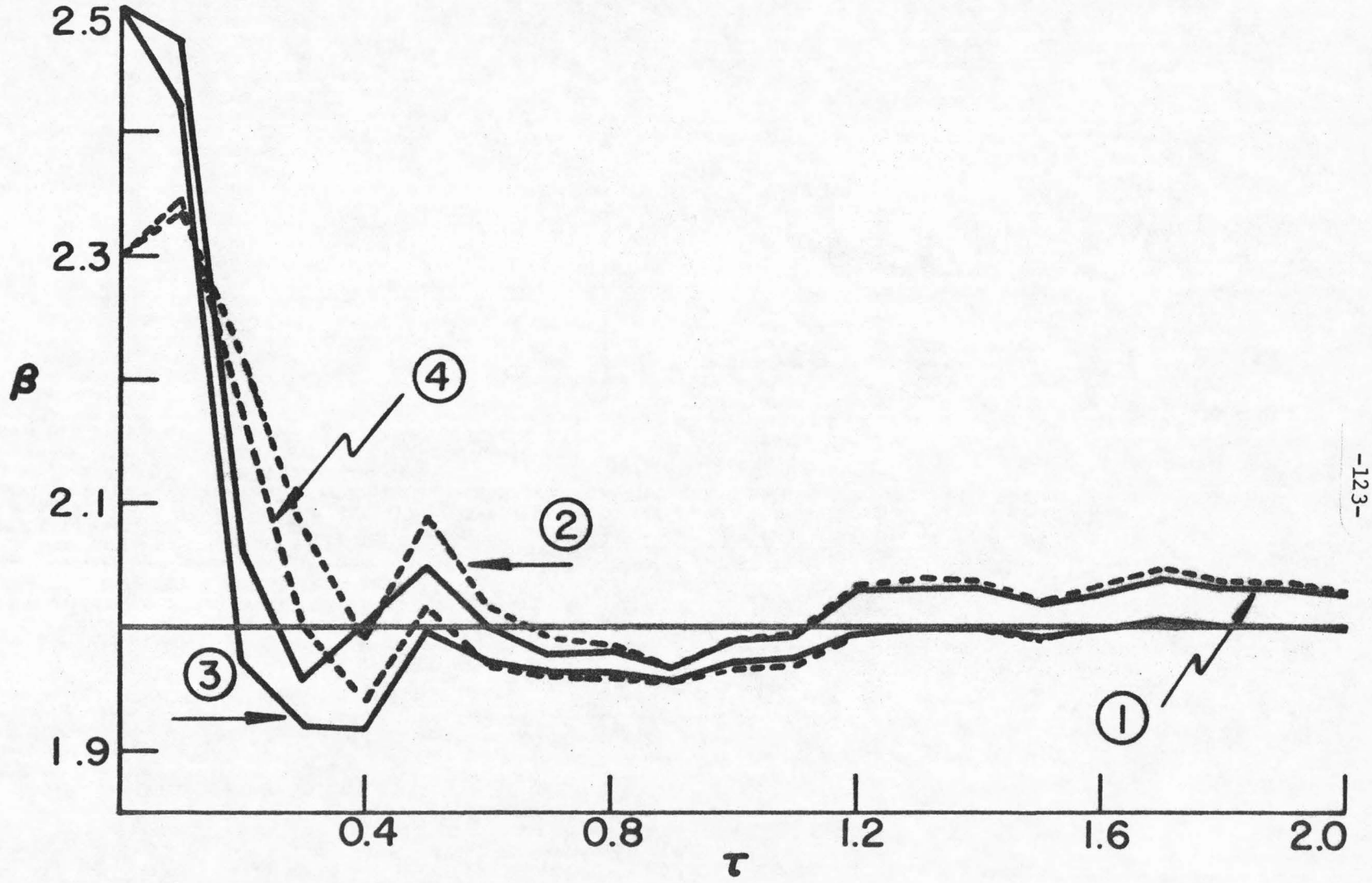

Fig. 24. Sequential Estimation of the Parameter β

$$\frac{\partial \tilde{s}}{\partial \tau} = -\tilde{\beta}\,\tilde{s}\left(\frac{x}{1+mx}\right)^{1/2} \tag{7.52}$$

where

$$\tilde{\alpha} = 2s^*\alpha \quad , \quad \tilde{\beta} = 2s^*\beta \tag{7.53}$$

The boundary condition (7.44) is changed into

$$\text{(ii)} \quad \text{at} \quad \tau = 0 \; : \qquad \tilde{s} = s_o - s^*/2 \tag{7.54}$$

Now Eqs. (7.51) and (7.52) have the same form as Eqs. (7.41) and (7.42), and thus they accept the same estimation scheme.

General Power Model

For simplicity, consider only the case of a concentration independent deactivation model

$$\frac{\partial s}{\partial t} = -\,k_d \exp(-E_d/RT)\,s^m \tag{7.55}$$

with three parameters k_d, E_d, m . The presence of a concentration-dependent term increases the amount of required computation but does not present additional conceptual difficulties.

The dynamical system (i.e., Eqs. (7.3) and (7.55), is a set of coupled partial differential equations, and is nonlinear with respect to both temperature and catalyst activity. For such a system, it is seldom possible to carry out an exact and rigorous estimation of both k_d and E_d . Therefore, in this section no attempt is made to derive an anlytically rigorous estimation scheme. Instead, approximations are introduced.

Consider the following approximation for the activity profile

$$s(z,t) = \sum_{i=1}^{n} \sigma_i(t)\, p_i(z) \tag{7.56}$$

where the p_i's are polynomials or other suitable functions. Equation (7.56) can be rewritten as

$$s(z,t) = \sum_{i=1}^{n} s(z_i,t)\, q_i(z) \tag{7.57}$$

where q_i is a rational function of $p_1,\cdots,p_n$ and hence a known function of z.

A combination of Eqs. (7.57) and (7.3) gives

$$G(t) \int_{T_o(t)}^{T(z_j,t)} \frac{dT'}{\tilde{g}(T',y_o(t),T_o(t))} = \sum_{i=1}^{n} M_{ji}\, s(z_i,t) \tag{7.58}$$

where

$$M_{ji} = \int_0^{z_j} q_i(z)dz \tag{7.59}$$

On the other hand, at a measurement position z_j the deactivation equation is expressed as

$$\frac{ds(z_j,t)}{dt} = -k_d \exp[-E_d/RT(z_j,t)]\, s^m(z_j,t) \tag{7.60}$$

which can be integrated to yield

$$s(z_j,t) = \left\{ \frac{1}{(s(z_j,t_o)} + (m-1)k_d \int_{t_o}^{t} \exp(-E_d/RT(z_j,t'))]dt' \right\}^{-\frac{1}{m-1}}, \qquad m \neq 1 \tag{7.61}$$

From Eqs. (7.58) and (7.61), deactivation parameters m, k_d, E_d can be

estimated by nonlinear regression using the temperature measurements $T(z_j,t)$. It should be noted that these deactivation parameters are strongly correlated so that their simultaneous estimation presents numerical difficulties. It is thus suggested to estimate k_d and E_d for a fixed m and then repeat the calculations for various values of m .

Suppose that there is more than one reaction involved in the catalytic process. The procedures described by Eqs. (7.13)-(7.15) should be followed first to obtain a single equation. Based on that equation, the estimation scheme of the present section can then be used.

8. ESTIMATION OF DEACTIVATION PARAMETERS FOR BIFUNCTIONAL CATALYSTS

For a bifunctional catalytic process taking place in a fixed bed reactor under the assumptions discussed in Part I, the system equation can be written as

$$G \frac{\partial y}{\partial z} = s_1 f_1(y,T) + s_2 f_2(y,T) \tag{8.1}$$

$$G \frac{\partial T}{\partial z} = s_1 g_1(y,T) + s_2 g_2(y,T) \tag{8.2}$$

where f_1, f_2, g_1, g_2 are vector rate functions with possibly some zero components.

First, the special case where two activities decline by the same relative rate (i.e., $s_i = s_{io}\sigma(z,t)$ where s_{io} are constants) can be handled by the techniques of the previous chapter with σ playing the role of s.

In general, the two activities decay with rates

$$\frac{\partial s_1}{\partial t} = -k_{d1} s_1^{m_1} \exp(-E_{d1}/RT) \tag{8.3}$$

$$\frac{\partial s_2}{\partial t} = -k_{d2} s_2^{m_2} \exp(-E_{d2}/RT) \tag{8.4}$$

The estimation problem cannot be approached as in the previous chapter because Eqs. (8.1) and (8.2) cannot be reduced to expressions of the type (7.7) or (7.58). Nevertheless, in special cases it is often possible to simplify the problem as illustrated by the following example of naphtha reforming.

The estimation scheme varies according to how detailed the kinetic model is. To illustrate a variety of estimation schemes, three different models of naphtha reforming are discussed separately in this chapter. The discussion starts with a simplified model, then proceeds with a more detailed one, and finally concludes with one of general scope.

An Essential Kinetic Model of Naphtha Reforming

As discussed in Part I, the essential dynamical behavior of naphtha reforming can be characterized by the two most important reactions, i.e., naphthene dehydrogenation and n-paraffin isomerization.

The platinum particles undergo sintering at a rate

$$\frac{\partial s_1}{\partial \tau} = -\beta_1 s_1^2 \exp[-q_1(\frac{1}{\theta} - 1)] \tag{8.5}$$

and the acidic alumina activity decays due to coking at a rate

$$\frac{\partial s_2}{\partial \tau} = -\beta_2 s_2 x_2^2 \, y(\theta) \tag{8.6}$$

Two functional forms of $y(\theta)$ are used in this study, and the corresponding estimation schemes are discussed separately:

(i) $y(\theta) = 1$ if the deactivation rate constant is independent of temperature;

(ii) $y(\theta) = \exp[-q_2(\frac{1}{\theta} - 1)]$, if the rate constant has the usual Arrhenius dependence.

The estimation of β_1, q_1 can be achieved by considering Eqs. (6.5) and (8.5) as follows. The activity profile $s_1(\xi,\tau)$ is

approximated by a summation of polynomials

$$s_1(\xi,\tau) = \sum_{i=1}^{n} \sigma_{1i}(\tau)\, p_{1i}(\xi) = \sum_{i=1}^{n} s_1(\xi_i,\tau)\, q_{1i}(\xi) \qquad (8.7)$$

Integration of Eq. (6.5) with Eq. (8.7) yields

$$\frac{\lambda v}{\alpha_1} \int_{\theta(\xi_j,\tau)}^{\theta_f} \frac{\exp[p_1(\frac{1}{\theta} - 1)]}{x_{1f} - \lambda\theta_f + \lambda\theta}\, d\theta = \sum_{i=1}^{n} M_{ji} s_1(\xi_i,\tau) \qquad (8.8)$$

where

$$M_{ji} = \int_0^{\xi_j} q_{1i}(\xi)\, d\xi \qquad (8.9)$$

Meanwhile, Eq. (8.5) can be integrated to give

$$s_1(\xi_j,\tau) = \{\frac{1}{s_1(\xi_j,\tau_o)} + \beta_1 \int_{\tau_o}^{\tau} \exp[-q_1(\frac{1}{\theta(\xi_j,t)} - 1)]dt\}^{-1} \qquad (8.10)$$

Using nonlinear regression, the estimation of β_1, q_1 can thus be accomplished from Eqs. (8.8) and (8.10) with $\theta(\xi_j,\tau)$ being the measured quantity along the bed. Since the Pt activity declines very slowly compared to the acidic activity, it needs to be estimated only once between successive regenerations. Thus, in practice, the knowledge of the detailed kinetic model of Pt deactivation is much less important than that of alumina deactivation, and the former is usually neglected.

For the estimation of the alumina deactivation parameters, consider Eqs. (6.6) and (8.6) in the following functional form

$$\frac{\partial x_2}{\partial \xi} = s_2 w[\theta(\xi)]\, \phi(x_2) \qquad (8.11)$$

$$\frac{\partial s_2}{\partial \tau} = s_2 \psi(x_2, \underset{\sim}{k}) \tag{8.12}$$

where

$$w[\theta(\xi)] = \exp[-p_2(\frac{1}{\theta(\xi,\tau)} - 1)], \quad \phi = -\alpha_2 x_2 \tag{8.13}$$

$$\psi = -\beta_2 x_2^m \qquad , \; y(\theta) = 1 \tag{8.14}$$

Consider $\underset{\sim}{k} = [m, \beta_2]$ as the deactivation vector to be estimated. The estimation is realized through the introduction of a modified cumulative activity

$$S_m(\xi,\tau) = \int_0^{\xi} s_2(\xi')\, w[\theta(\xi')] d\xi' \tag{8.15}$$

where the integrand represents the distribution of a weighted catalyst activity in a non-isothermal reactor. From Eqs. (8.11) and (8.12)

$$w[\theta(\xi)] \frac{\partial s_2}{\partial \tau} = \frac{\psi(x_2, \underset{\sim}{k})}{\phi(x_2)} \frac{\partial x_2}{\partial \xi} \tag{8.16}$$

and its integration yields

$$\frac{\partial S_m}{\partial \tau} = \int_{x_{2f}}^{x_2} \frac{\psi(u, \underset{\sim}{k})}{\phi(u)} \, \partial u \tag{8.17}$$

Again, from Eq. (8.11)

$$S_m = \int_{x_{2f}}^{x_2} \frac{du}{\phi(u)} \tag{8.18}$$

which is differentiated to yield

$$\frac{dS_m}{d\tau} = \frac{1}{\phi(x_2)} \frac{dx_2}{d\tau} \tag{8.19}$$

Substituting Eq. (8.19) into Eq. (8.17) along the characteristic lines, an ordinary differential equation is obtained:

$$\frac{dx_2}{d\tau} = \phi(x_2) \int_{x_{2f}}^{x_2} \frac{\psi(u,\underset{\sim}{k})}{\phi(u)} du \tag{8.20}$$

The above derivation of equation (8.20), based on the concentration is quite similar to that of Eq. (7.11), based on the temperature. The corresponding functions S_m and S play a central role in realizing the transformation to an ordinary differential equation.

Equation (8.20) can be written explicitly as

$$\frac{dx_2}{d\tau} = \frac{\beta_2}{m} x_2(x_{2f}^m - x_2^m) \tag{8.21}$$

The system is simulated by Eqs. (6.5), (6.6), and (8.6) for the following values of the parameters:

$$\alpha_1 = 2.0 \ , \quad \alpha_2 = 5.0 \ , \quad p_1 = 21.6 \ , \quad p_2 = 20.0 \ , \quad \beta_2 = 1.0 \ ,$$

$$m = 2.0 \ , \quad \lambda = 0.108 \ , \quad v = 1.0 \ , \quad \theta_f = x_{1f} = x_{2f} = 1.0$$

$$s_1 \equiv 0.95 \ , \quad s_{2o} = 1.0$$

The concentration measurements are generated from the "true" concentrations at $z = L$. Again, since daily average values are used, the noise level of the actual measurements is greater than that of the average measurements which are indicated in these figures. The

filtering results shown in Figures 25-27 are very satisfactory. These results are particularly significant in view of the fact that only one concentration measurement at each time is required to carry out the filtering for both x_2, m, and β_2 in this nonlinear system.

For case (ii) (i.e., $y(\theta) = \exp[-q_2(\frac{1}{\theta} - 1)]$, the above estimation scheme must be modified due to the fact that the resulting ordinary differential equation contains the variable θ instead of a single dependent variable x_2.

$$\frac{dx_2}{d\tau} = \beta_2 x_2 \int_{x_{2f}}^{x_2} u^{m-1} \exp[-q_2(\frac{1}{\theta} - 1)]\, du \qquad (8.22)$$

This modification is accomplished by expressing θ as a function of x_2 (i.e., $\theta = \theta(x_2)$) in the following way: A curve (e.g., a parabola or piece-wise linear function) is fitted through the m measured concentration points along the reactor. Now, a cross plot can be made between this curve and the temperature profile along the reactor. In this manner θ is expressed by x_2 directly and the position variable z is eliminated from the expression. It should be noted that more than one point concentration measurement is required to carry out the estimation in this case, whereas one point measurement was enough in the case of $y(\theta) = 1$. The sequential estimates of the state x_2 and the deactivation parameters can be obtained from the weighted average over the individual filtering results at the measurement points along the reactor.

A piecewise linear function connecting the three measured points along the bed (i.e., $\xi_j = 0.1, 0.4, 1.0$) is chosen for

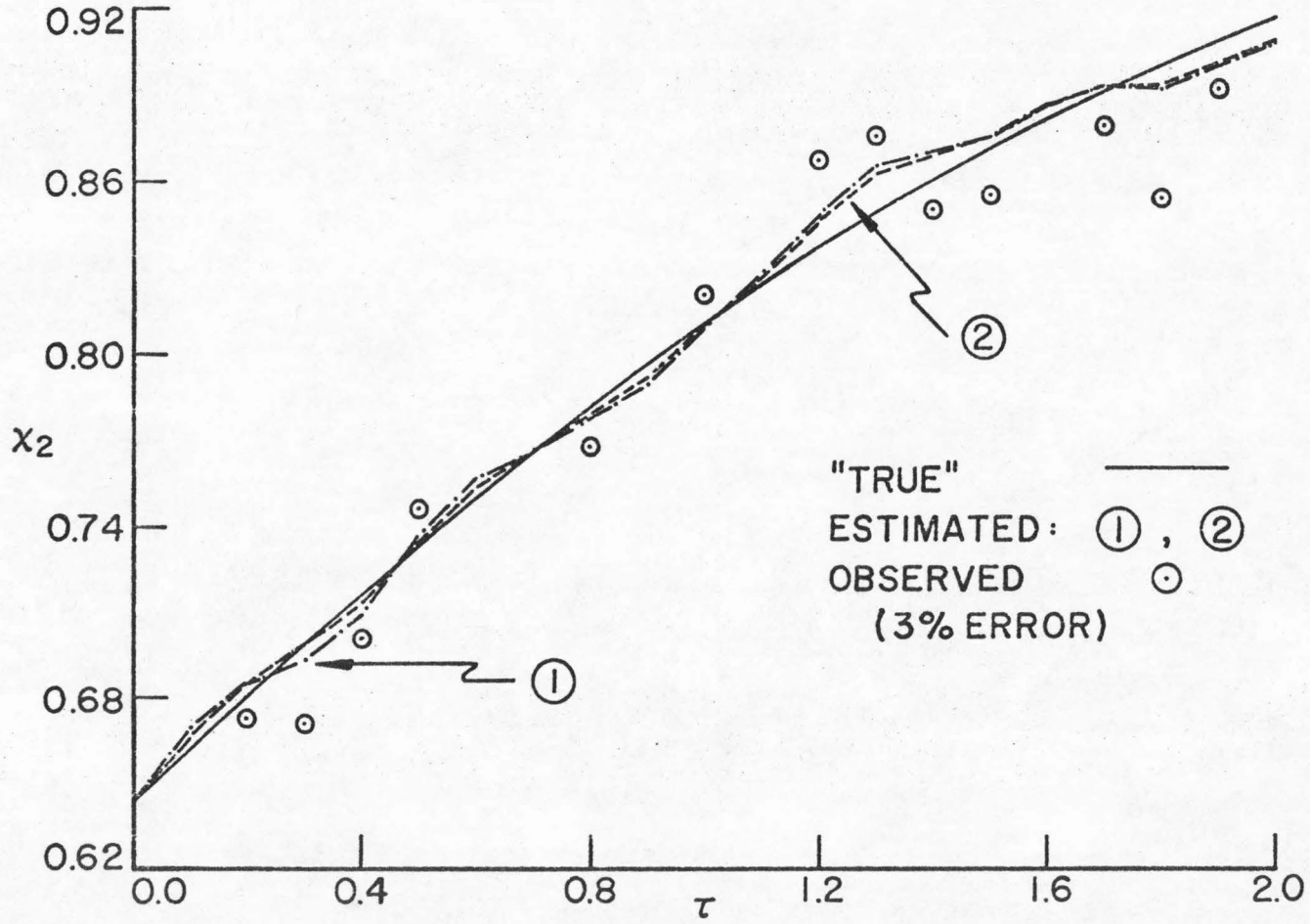

Fig. 25. Sequential Estimation of the State x_2 in Naphtha Reforming, Case (i)

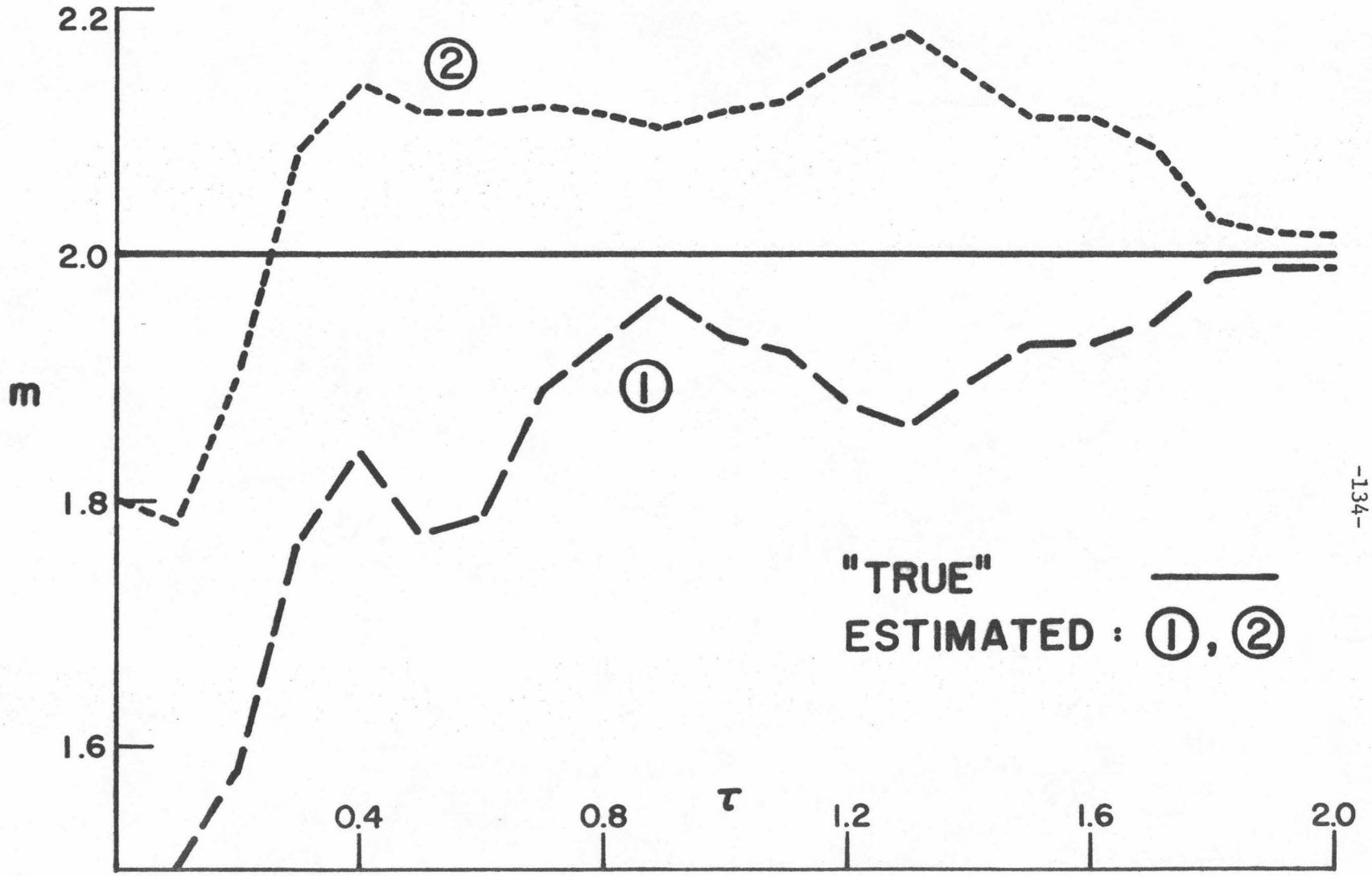

Fig. 26. Sequential Estimation of the Parameter m in Naphtha Reforming, Case (i)

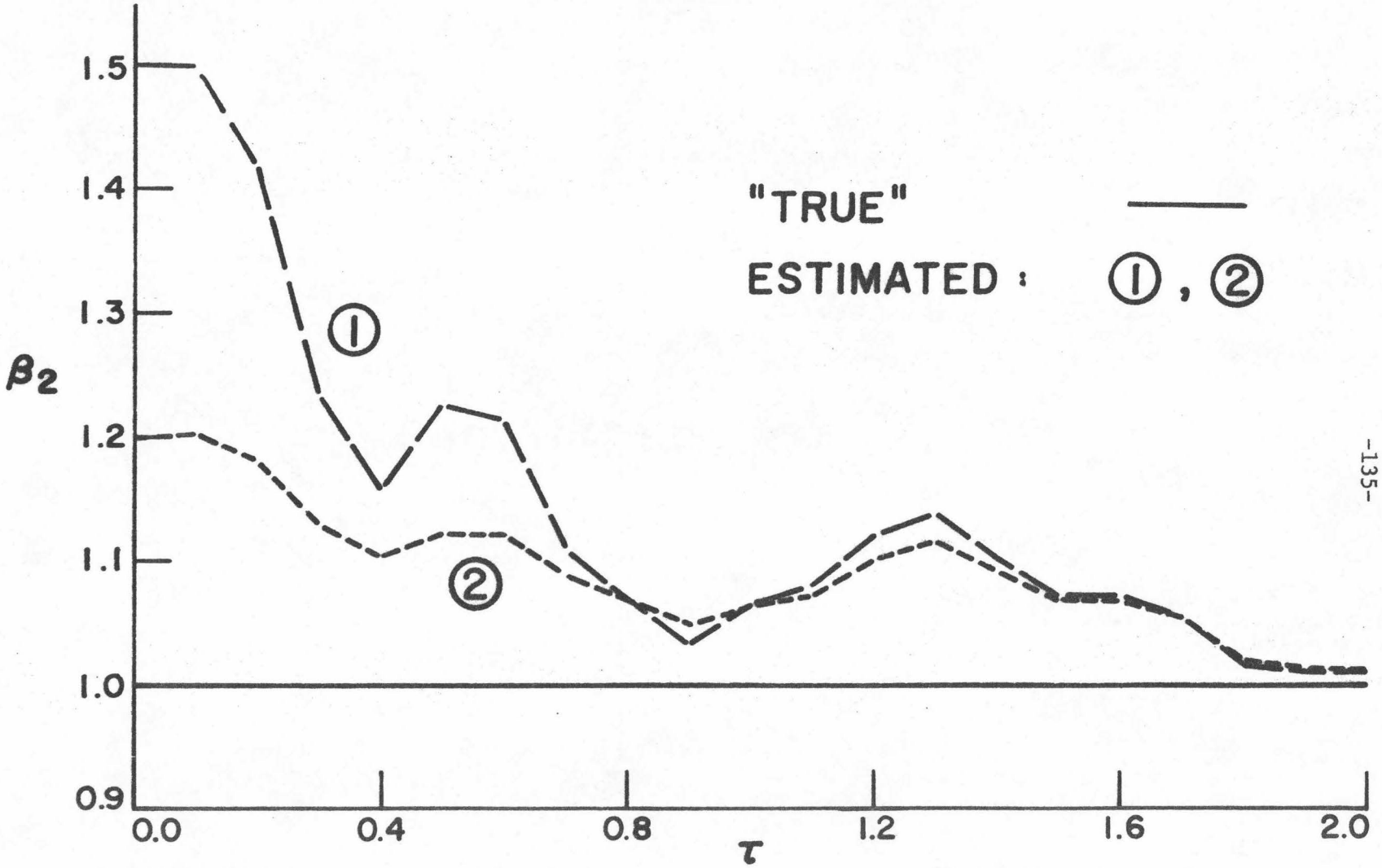

Fig. 27. Sequential Estimation of the Parameter β_2 in Naphtha Reforming, Case (i)

illustration to approximate x_2 as a function of ξ. Figures 28-31 present the filtering results for this case. Figures 28 and 29 are the estimation results for the state x_2 at $\xi = 0.1$ and $\xi = 1.0$ respectively. Since the activity near the entrance of the reactor decays more rapidly due to the endothermic Arrhenius rate, the decay parameter estimates obtained from the earlier measurement point should be more accurate. This observation is supported by Figures 28 and 29. Figures 30 and 31 present average q_2 and β_2 estimates along the reactor for different initial guesses, noise levels, and initial P matrices for the filters. These results indicate that satisfactory estimates can be obtained quite early ($\tau \simeq 1.2$) in the decay history ($\tau \simeq 6.0$ for 80% deactivation of alumina activity). This means that the information obtained from the above study would be available in time for determining long-term operating and regenerating policies. Meanwhile, the fact that the filtering process of curve (6) converges faster than that of curve (3) indicates that the estimation can be improved by assigning a more appropriate initial P matrix. Finally, the slow convergence for β_2 and q_2 estimates is probably due to the strong correlation existing between β_2 and q_2 in the dynamic system and to the approximation introduced for $x_2(\xi)$.

A More Detailed Kinetic Model of Naphtha Reforming

Consider a more detailed kinetic model of naphtha reforming containing the additional feature of hydrocracking relative to the essential kinetic model described in the last section. Suppose that a mixture of separate platinum and alumina particles is employed as the catalyst. Dehydrocyclization cannot take place as its occurrence

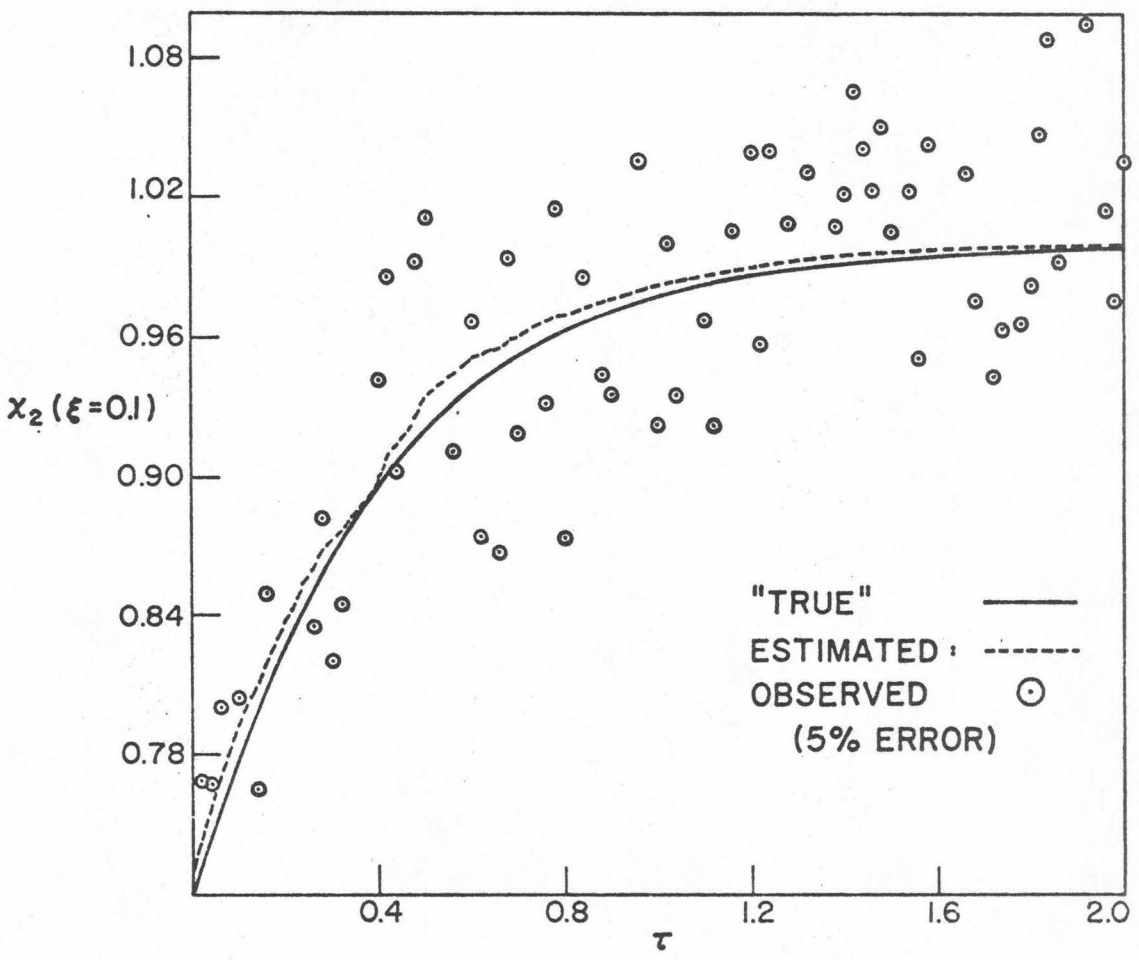

Fig. 28. Sequential Estimation of the State x_2 at $\xi = 0.1$ in Naphtha Reforming, Case (ii)

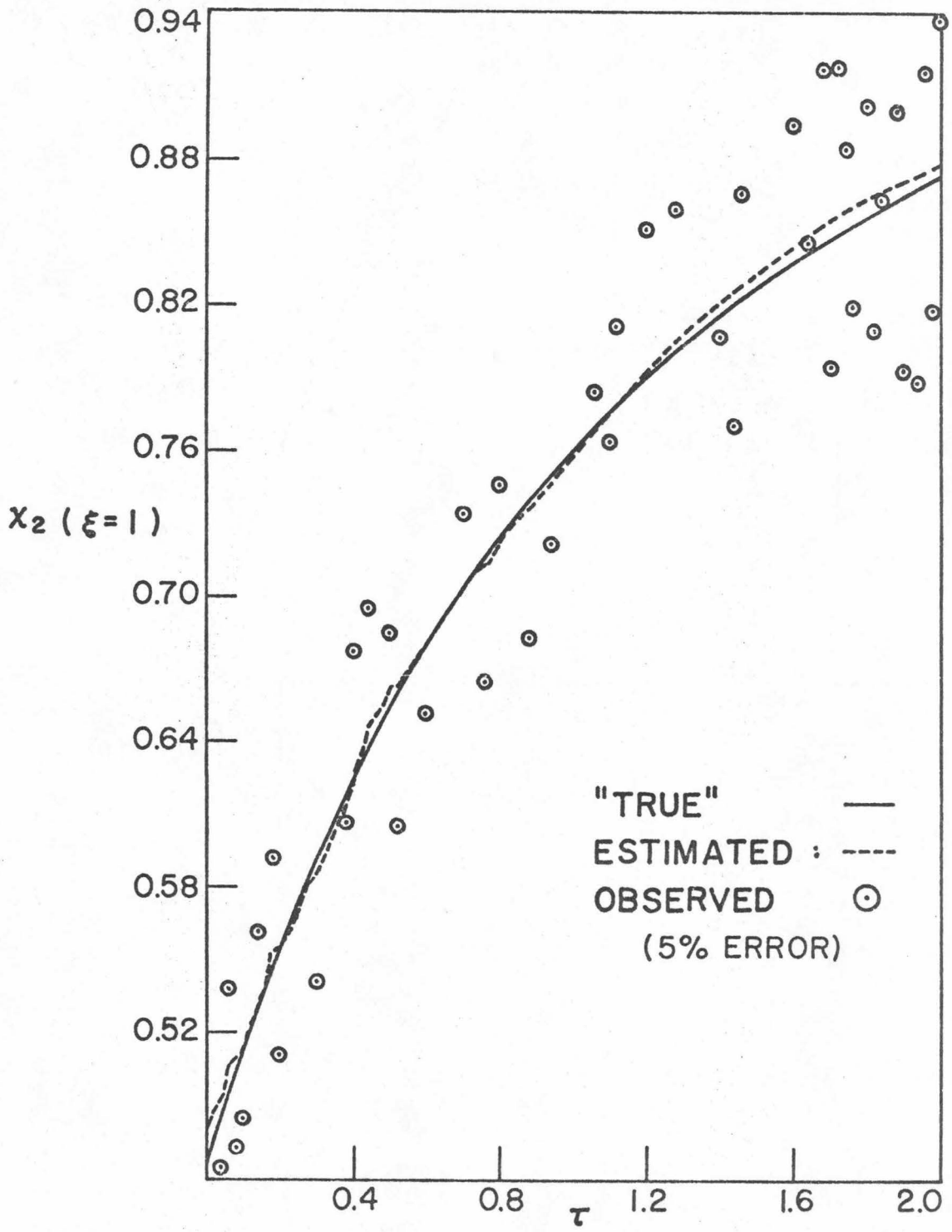

Fig. 29. Sequential Estimation of the State x_2 at $\xi = 1.0$ in Naphtha Reforming, Case (ii)

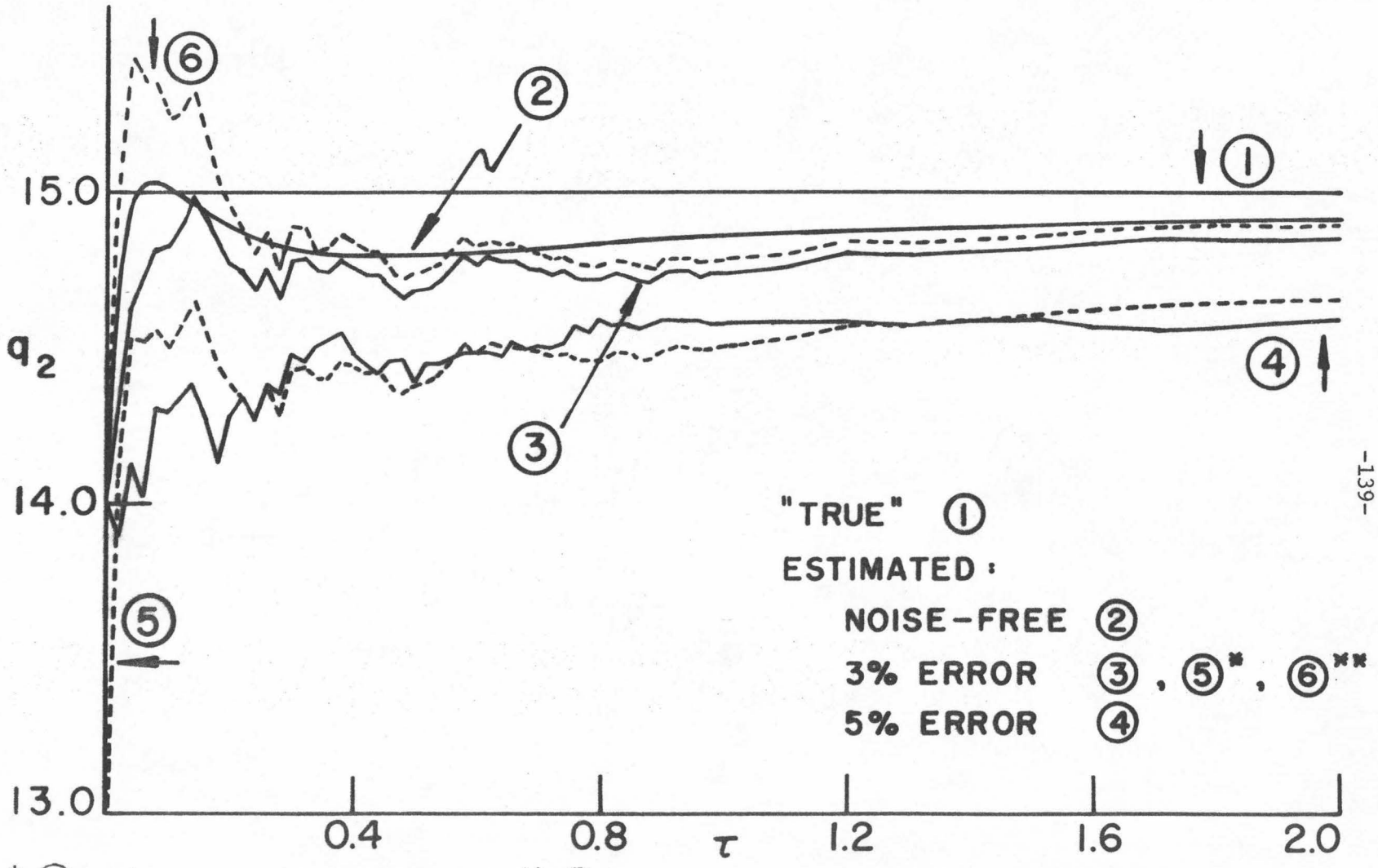

* ⑤ : $\hat{\beta}_2(0) = 7.0$, $\hat{q}_2(0) = 13.0$; ** ⑥ : All elements of the initial P matrix are four times larger than those for the other cases.

Fig. 30. Sequential Estimation of the Parameter q_2 in Naphtha Reforming, Case (ii)

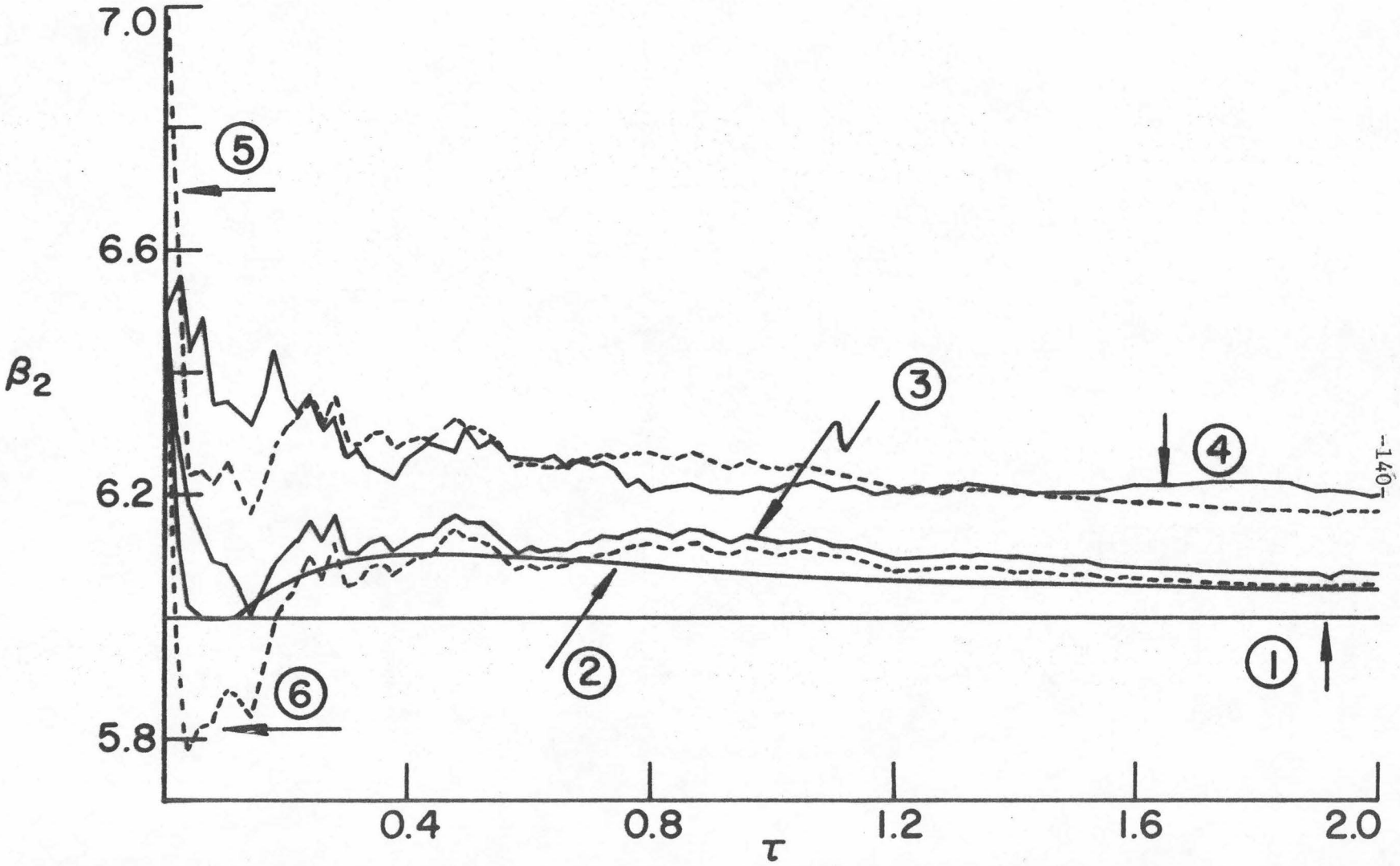

Fig. 31. Sequential Estimation of the Parameter β_2 in Naphtha Reforming, Case (ii)

requires the close proximity of two functional sites in a compound bifunctional catalyst. The reaction scheme of such a model is sketched as follows:

$$N \longrightarrow A + 3H_2 \tag{8.23}$$

$$p \rightleftharpoons ip \tag{8.24}$$

$$H_2 + p \longrightarrow 2\ LHC \tag{8.25}$$

$$H_2 + ip \longrightarrow 2\ LHC \tag{8.26}$$

where N, A, p, ip, LHC denote naphthene, aromatic, n-paraffin, iso-paraffin, and lower hydrocarbons.

The platinum activity s_1 and the acidic alumina activity s_2 are assumed to deactivate according to Eqs. (8.3) and (8.4). The rates of reactions (8.23)-(8.26) can be written as formulated in Chapter 5, part I,

$$r_a = s_1 k_a \rho y_1 \tag{8.27}$$

$$r_b = s_2 (k_b y_2 - k_b' y_3) / y_7 \tag{8.28}$$

$$r_d = s_2 k_d y_2 / y_7 \tag{8.29}$$

$$r_d' = s_2 k_d' y_3 / y_7 \tag{8.30}$$

where y_1, y_2, y_3, y_6, y_7 denote the concentration variables of N, p, ip, LHC, H_2, and

$$k_i = k_{io} \exp(-E_i/RT) \tag{8.31}$$

The conservation equations for y_1, y_2, and y_3 are

$$G \frac{\partial y_1}{\partial z} = -s_1 k_a \rho y_1 \tag{8.32}$$

$$G \frac{\partial y_2}{\partial z} = \frac{s_2}{y_7} (-k_b y_2 + k_b' y_3 - k_d y_2) \tag{8.33}$$

$$G \frac{\partial y_3}{\partial z} = \frac{s_2}{y_7} (k_b y_2 - k_b' y_3 - k_d' y_3) \tag{8.34}$$

Since only the dehydrogenation reaction has significant heat effect, the energy equation can be written in terms of the dehydrogenation rate as

$$G \frac{\partial T}{\partial z} = \frac{(-\Delta H)}{c_p} s_1 k_a \rho y_1 \tag{8.35}$$

Due to the fact that only reaction (8.23) changes the number of moles, the fluid density ρ can be expressed in terms of y_7, T and the feed conditions. Equations (8.32) and (8.35) can be combined in a single equation for the temperature. Using the resulting equation, the estimation of the deactivation parameters for s_1 can be carried out following the procedures described in the first section of this chapter.

The estimation of the deactivation parameters for s_2 is based on Eqs. (8.33), (8.34), and (8.4). Supposing that y_2, y_3, and T are measured at points $z_1 = 0, z_2, \cdots, z_n = L$, then Eqs. (8.33) and (8.34) can be integrated to

$$G \int_{y_{2o}}^{y_2(z_j)} \frac{y_7 \, dy_2}{-k_b y_2 + k_b' y_3 - k_d y_2} = \sum_{i=1}^{n} M_{ji} \, s_2(z_i, t) \tag{8.36}$$

$$G \int_{y_{3o}}^{y_3(z_j)} \frac{y_7 \, dy_3}{k_b y_2 - k_b' y_3 - k_d' y_3} = \sum_{i=1}^{n} M_{ji} \, s_2(z_i, t) \tag{8.37}$$

After evaluating the above integrals numerically, the activity $s_2(z_i, t)$

can be obtained as the solution of the matrix equations (8.36) and (8.37). The resulting $s_2(z_i,t)$ are then used as the measurements to estimate the deactivation parameters of s_2 using the integrated form of the deactivation equation (i.e., Eq. (7.61)) via a least squares criterion. It must be noted that the present estimation scheme requires measurement of certain concentrations and the temperature at several points along the reactor.

A Generalized Kinetic Model of Naphtha Reforming

Now, consider a generalized model of naphtha reforming which consists of all the individual reactions, namely dehydrogenation and dehydroisomerization of cycloparaffins, isomerization, dehydrocyclization and hydrocracking of paraffins, together with coking over alumina sites, and sintering of platinum crystallites. For convenience of description, the system of C_7 hydrocarbons is considered first. Then the discussion proceeds with the system of C_6 hydrocarbons, and finally concludes with a system of C_6 and C_7 hydrocarbon mixtures.

(i) C_7 hydrocarbons

Refer to Figure 3 of Part I for a schematic representation of naphtha reforming of C_7 hydrocarbons. Denote the concentrations of methylcyclohexane, n-heptane, i-heptane, tolunene by y_1, y_2, y_3, y_4 respectively. For simplicity, the density of the gas is assumed to be constant along the reactor as justified in Part I. The material and energy balance equations derived in Chapter 5 of Part I become

$$G \frac{\partial y_1}{\partial z} = -s_1 k_{ao} \exp(-E_1/RT) y_1 + s_1 s_2 k_{co} \exp(-E_3/RT)(y_2 + y_3) \quad (8.38)$$

$$G \frac{\partial y_2}{\partial z} = -s_1 k_{eo} \exp(-E_5/RT) y_2 - s_2 [k_{bo} \exp(-E_2/RT) y_2 - k'_{bo} \exp(-E'_2/RT) y_3 + k_{do} \exp(-E_4/RT) y_2] - s_1 s_2 k_{co} \exp(-E_3/RT) y_2 \quad (8.39)$$

$$G \frac{\partial y_3}{\partial z} = -s_1 k_{eo} \exp(-E_5/RT) y_3 + s_2 [k_{bo} \exp(-E_2/RT) y_2 - k'_{bo} \exp(-E'_2/RT) y_3 - k_{do} \exp(-E_4/RT) y_3] - s_1 s_2 k_{co} \exp(-E_3/RT) y_3 \quad (8.40)$$

$$G \frac{\partial y_4}{\partial z} = s_1 k_{ao} \exp(-E_1/RT) y_1 \quad (8.41)$$

$$G \frac{\partial T}{\partial z} = -\frac{(\Delta H_1)}{c_p} s_1 k_{ao} \exp(-E_1/RT) y_1 - \frac{(\Delta H_2)}{c_p} s_1 s_2 k_{co} \exp(-E_3/RT)(y_2 + y_3) \quad (8.42)$$

Since the heat equation (8.42) can be obtained from a linear combination of (8.38) and (8.41), the following relationship holds

$$-c_p (T - T_o) = (\Delta H_2)(y_1 - y_{1o}) + (\Delta H_1 + \Delta H_2)(y_4 - y_{4o}) \quad (8.43)$$

and thus

$$y_1 = y_{1o} - \frac{c_p}{\Delta H_2} (T - T_o) - \frac{\Delta H_1 + \Delta H_2}{\Delta H_2} (y_4 - y_{4o}) \quad (8.44)$$

Substituting Eq. (8.44) into (8.41) gives

$$G \frac{\partial y_4}{\partial z} = s_1 \phi(y_4, T) \quad (8.45)$$

where

$$\phi = [y_{1o} - \frac{c_p}{\Delta H_2}(T - T_o) - \frac{\Delta H_1 + \Delta H_2}{\Delta H_2}(y_4 - y_{4o})]\, k_{ao} \exp(-E_1/RT) \quad (8.46)$$

Supposing that the concentration of toluene y_4 is measured at several points along the reactor, the activity s_1 can be estimated using the previously stated polynomial parametrization as follows:

$$G(t) \int_{y_{4o}(t)}^{y_4(z_j,t)} \frac{dy_4'}{\phi(y_4', \tilde{T})} = \sum_{i=1}^{n} M_{ji} s_1(z_i,t) \quad (8.47)$$

where

$$s_1(z,t) = \sum_{i=1}^{n} s_1(z_i,t) q_{1i}(t) \ , \quad M_{ji} = \int_0^{z_j} q_{1i}(z)dz \quad (8.48)$$

and $\tilde{T}$ represents the daily average temperature measurements along the reactor.

The catalyst deactivation parameters k_{d1}, E_{d1} can be estimated by nonlinear regression from the following equation:

$$s_1(z_j,t) = \left[\frac{1}{s_1(z_j,t_o)} + k_{d1} \int_{t_o}^{t} \exp(-E_{d1}/RT)dt \right]^{-1} \quad (8.49)$$

Having estimated $s_1(z)$, the estimation of $s_2(z)$ and the parameters k_{d2}, E_{d2} can be obtained as follows. First, combination of Eqs. (8.39) and (8.40) yields

$$G \frac{\partial y_{23}}{\partial z} = -[s_1 k_{eo} \psi_5 + s_2 (k_{do} \psi_4 + s_1 k_{eo} \psi_3)] y_{23} \quad (8.50)$$

where

$$y_{23} = y_2 + y_3 \quad (8.51)$$

$$\psi_i = \exp(-E_i/RT) \tag{8.52}$$

Integration of Eq. (8.50) gives

$$G \log \frac{y_{23o}}{y_{23}(z_j)} = \int_0^{z_j} [s_1 k_{eo}\psi_5 + s_2(k_{do}\psi_4 + s_1 k_{co}\psi_3)]dz \tag{8.53}$$

Introducing the parametrization of s_2 as

$$s_2(z,t) = \sum_{i=1}^{n} s_2(z_i,t)\ q_{2i}(z) \tag{8.54}$$

Eq. (8.53) can be rewritten as a matrix equation

$$\sum_{i=1}^{n} M'_{ji}\ s_2(z_i,t) = \tilde{g}_{1j} \tag{8.55}$$

where

$$M'_{ji} = k_{do} \int_0^{z_j} q_{2i}(z')\psi_4(\tilde{T})dz' + k_{co} \int_0^{z_j} s_1(z',t) q_{2i}(z')\psi_3(\tilde{T})dz' \tag{8.56}$$

$$\tilde{g}_{1j} = G \log \frac{y_{23o}}{\tilde{y}_{23}(z_j)} - k_{eo} \int_0^{z_j} s_1(z',t)\psi_5(\tilde{T})dz' \tag{8.57}$$

Therefore, estimates on $s_2(z)$ can be obtained as the solution of Eq. (8.55). Subsequently, the deactivation parameters k_{d2}, E_{d2} can be obtained by carrying out nonlinear regression on the following equation:

$$\log \frac{s_2(z_j,t_o)}{s_2(z_j,t)} = k_{d2} \int_{t_o}^{t} \tilde{y}_2^2(z_j)\ \exp(-E_{d2}/R\tilde{T}(z_j,t'))dt' \tag{8.58}$$

It should be noted that the present estimation algorithm requires the

knowledge of the temperature, toluene concentration, and total concentration of n-heptane and i-heptane at several points along the reactor.

(ii) C_6 hydrocarbons

Refer to Figure 4 of Part I for a schematic representation of the reforming of C_6 hydrocarbons. Denote the concentrations of methylcyclopentane, n-hexane, i-hexane, benzene and cyclohexane by $y_1^*,\cdots,y_5^*$ respectively. With the same simplifications described in Part I, the material and energy balance equations become

$$G\frac{\partial y_1^*}{\partial z} = -s_1 k_{ao}^* \exp(-E_1^*/RT)y_1^* - s_2[k_{fo}^* \exp(-E_6^*/RT)y_1^* - k_{fo}'' \exp(-E_6''/RT)y_5^*] + s_1 s_2 k_{co}^* \exp(-E_3^*/RT)(y_2^* + y_3^*) \quad (8.59)$$

$$G\frac{\partial y_2^*}{\partial z} = -s_1 k_{eo}^* \exp(-E_5^*/RT)y_2^* - s_2[k_{bo}^* \exp(-E_2^*/RT)y_2^* - k_{bo}''\exp(-E_2''/RT)y_3^* + k_{do}^*\exp(-E_4^*/RT)y_2^*] - s_1 s_2 k_{co}^*\exp(-E_3^*/RT)y_2^* \quad (8.60)$$

$$G\frac{\partial y_3^*}{\partial z} = -s_1 k_{eo}^* \exp(-E_5^*/RT)y_3^* + s_2[k_{bo}^*\exp(-E_2^*/RT)y_2^* - k_{bo}''\exp(-E_2''/RT)y_3^* - k_{do}^*\exp(-E_4^*/RT)y_3^*] - s_1 s_2 k_{co}^*\exp(-E_3^*/RT)y_3^* \quad (8.61)$$

$$G\frac{\partial y_4^*}{\partial z} = s_1[k_{ao}^*\exp(-E_1^*/RT)y_1^* + k_{go}^*\exp(-E_7^*/RT)y_5^*] + s_2 k_{go}''\exp(-E_7''/RT)y_5^* \quad (8.62)$$

$$G\frac{\partial y_5^*}{\partial z} = -s_1 k_{go}^* \exp(-E_7^*/RT) y_5^* - s_2[k_{go}'' \exp(-E_7''/RT) y_5^* - k_{fo}^* \exp(-E_6^*/RT) y_1^* + k_{fo}'' \exp(-E_6''/RT) y_5^*] \quad (8.63)$$

$$G\frac{\partial T}{\partial z} = -\frac{\Delta H_1^*}{c_p}\{s_1[k_{ao}^* \exp(-E_1^*/RT) y_1^* + k_{go}^* \exp(-E_7^*/RT) y_5^*] + s_2 k_{go}'' \exp(-E_7''/RT) y_5^*\} - \frac{\Delta H_3^*}{c_p} s_1 s_2 k_{co}^* \exp(-E_3^*/RT)(y_2^* + y_3^*) \quad (8.64)$$

From Eqs. (8.59), (8.62), (8.63), and (8.64), it is clear that

$$-c_p(T-T_o) = (\Delta H_3^*)(y_1^* - y_{1o}^* + y_5^* - y_{5o}^*) + (\Delta H_1^* + \Delta H_3^*)(y_4^* - y_{4o}^*) \quad (8.65)$$

or

$$y_1^* = L^*(y_4^*, y_5^*, T) \quad (8.66)$$

Now, the combination of Eqs. (8.60) and (8.61) gives

$$G\frac{\partial y_{23}^*}{\partial z} = -[s_1 k_{eo}^* \psi_5^* + s_2(k_{do}^* \psi_4^* + s_1 k_{co}^* \psi_3^*)] y_{23}^* \quad (8.67)$$

and the combination of Eqs. (8.59), (8.62), and (8.63) results in

$$G\frac{\partial y_{45}^*}{\partial z} = s_1 s_2 k_{co}^* \psi_3^* \, y_{23}^* \quad (8.68)$$

where

$$y_{23}^* = y_2^* + y_3^* \quad (8.69)$$

$$y_{45}^* = y_1^* + y_4^* + y_5^* = L^*(y_4^*, y_5^*, T) + y_4^* + y_5^* \quad (8.70)$$

and

$$\psi_i^* = \exp(-E_i^*/RT) \quad (8.71)$$

Equations (8.67) and (8.68) thus form the basis for the estimation of s_1 and s_2. Since s_1 and s_2 are correlated strongly, the following iterative estimation scheme may be tried:

(a) Guess a polynomial profile for s_1, i.e.,

$$s_1(z,t) = \sum_{i=1}^{n} s_1(z_i,t) q_{1i}(z) \tag{8.72}$$

(b) Estimate $s_2(z,t)$ [i.e., $\sum_{i=1}^{n} s_2(z_i,t) q_{2i}(z)$] by solving the following matrix equation:

$$\sum_{i=1}^{n} M^*_{ji}\, s_2(z_i,t) = \tilde{g}^*_{2j} \tag{8.73}$$

where

$$M^*_{ji} = k^*_{do} \int_0^{z_j} q_{2i}(z')\psi^*_4(\tilde{T}))dz' + k^*_{co} \int_0^{z_j} s_1(z',t) q_{2i}(z')\psi^*_3(\tilde{T})dz' \tag{8.74}$$

$$\tilde{g}^*_{2j} = G \log \frac{y^*_{23o}}{\tilde{y}^*_{23}(z_j)} - k^*_{eo} \int_0^{z_j} s_1(z',t)\psi^*_5(\tilde{T})dz' \tag{8.75}$$

(c) Improve $s_1(z,t)$ from the solution of the following matrix equation

$$\sum_{i=1}^{n} \tilde{M}^*_{ji}\, s_1(z_i,t) = \tilde{g}^*_{1j} \tag{8.76}$$

where

$$\tilde{M}^*_{ji} = \int_0^{z_j} s_2(z',t)\, q_{1i}(z')dz' \tag{8.77}$$

$$\tilde{g}^*_{ij} = \int_{y^*_{45o}}^{\tilde{y}^*_{45}} \frac{dy_{45}}{\psi^*_3(\tilde{T})\tilde{y}^*_{23}} \tag{8.78}$$

(d) Iterate by repeating steps (b) and (c).

In this case, in addition to the temperature, the concentrations of y^*_4 and y^*_5 and the sum of concentrations y^*_2 and y^*_3 should be observed at several points along the reactor. Compared to the case of C_7 hydrocarbons, the present estimation scheme requires the additional measurements of y^*_5. Once $s_1(z,t)$ and $s_2(z,t)$ are known, the estimation of the corresponding deactivation parameters can be achieved in the same way as described before.

(iii) A mixture of C_7 and C_6 hydrocarbons

A generalized kinetic model of the reforming of a mixture consisting of C_7 and C_6 hydrocarbons includes all individual reactions as shown in Figures 3 and 4. The energy equation becomes

$$-c_p G \frac{\partial T}{\partial z} = s_1[(\Delta H_1)k_{ao}\psi_1 y_1 + (\Delta H^*_1)(k^*_{ao}\psi^*_1 y^*_1 + k^*_{go}\psi^*_7 y^*_5)]$$
$$+ s_2(\Delta H^*_1)k''_{go}\psi''_7 y^*_5 - s_1 s_2[(\Delta H_2)k_{co}\psi_3(y_2+y_3) + (\Delta H^*_3)k^*_{co}\psi^*_3(y^*_2+y^*_3)] \tag{8.79}$$

All the material balance equations remain the same, i.e., Eqs. (8.38)-(8.41) and (8.59)-(8.63). They are coupled through the temperature in the Arrhenius rate constants.

From a linear combination of the reactor equations for material and energy balances, it can be shown that

$$y^*_1 = L^*_1(y^*_4, y^*_5, y_1, y_4, T) \tag{8.80}$$

where L_1^* is a linear operation.

Now, since Eq. (8.44) is no longer valid, y_1 must also be observed. Therefore it is necessary to measure T, y_1, y_4, y_4^*, y_5^* together with the total concentrations of y_2, y_3 and y_2^*, y_3^* at several points along the reactor, and the estimation schemes discussed in the above sections (i) and (ii) remain valid with the only modification being that ϕ in (8.47) is taken as

$$\phi = \tilde{y}_1(z') \; k_{ao} \exp(-E_1/R\tilde{T}(z') \tag{8.81}$$

Appropriate estimates of the activities s_1, s_2 and the resulting deactivation parameters k_{di}, E_{di}, i=1,2 can be obtained by taking a weighted average over the individual estimates obtained in Section (i) and Section (ii).

Conclusion

In summary, the estimation of catalyst deactivation parameters for bifunctional catalysts requires measurements at several points along the reactor, whereas that for monofunctional catalysts needs only measurements at the reactor exit. In special cases, the transformation to an ordinary differential equation may be applied on a simplified model with certain approximations. However, in general, the case of a bifunctional catalyst must be treated by special methods. A scheme which combines the parametrization of activity profile in terms of a polynomial form and nonlinear regression over the integrated form of the deactivation equation, provides a promising solution to the complicated estimation problem. The utilization

of this scheme should depend on the particular structure of the pertinent system equations as has been illustrated systematically in this chapter by various models of catalytic naphtha reforming.

APPENDICES

C. SEQUENTIAL ESTIMATION OF A SINGLE DECAY CONSTANT IN THE LINEAR DEACTIVATION MODEL

D. ESTIMATION OF DEACTIVATION PARAMETERS FOR ISOTHERMAL OPERATION OF NAPHTHA REFORMING

E. DISCRETE AND CONTINUOUS SEQUENTIAL FILTERS

APPENDIX C

SEQUENTIAL ESTIMATION OF A SINGLE DECAY CONSTANT IN THE LINEAR DEACTIVATION MODEL

Consider a simplified model of naphtha reforming which consists of dehydrogenation and isomerization reactions along with coking and sintering deactivation reactions. The dynamical system for the estimation of the decay constant β_2 contains the following two equations

$$\frac{\partial x_2}{\partial \xi} = -\frac{\alpha_2}{v} s_2 x_2 \exp[-p_2(\frac{1}{\theta(\xi)} - 1)] \qquad (C.1)$$

$$\frac{\partial s_2}{\partial \tau} = -\beta_2 s_2 x_2^2 \exp(-q_2(\frac{1}{\theta(\xi)} - 1)] \qquad (C.2)$$

Through the parametrization of the activity profile using Eq. (C.1) as described in Chapter 7, estimates of the local alumina activities (i.e., $\hat{s}_2(\xi_j)$ s) at m positions along the reactor are obtained. These estimates can be treated as pseudo measurements to carry out the following sequential estimation of β_2 using least squares.

Along $\xi = \xi_j$, Eq. (C.2) can be written in the form of an ordinary differential equation:

$$\frac{d\hat{s}_2(\xi_j)}{d\tau} = -\beta_{2j} \hat{s}_2(\xi_j)\tilde{x}_2^2(\xi_j) \exp[-q_2(\frac{1}{\theta(\xi)_j} - 1] \quad , \quad j=1,\cdots,m \qquad (C.3)$$

where $\hat{x}_2(\xi_j)$ are local concentration measurements,

and $\theta(\xi_j)$ are assumed to be known for temperature measurements. Integration of Eq. (C.3) gives

$$\log \frac{\hat{s}_2(\xi_j,\tau_{i-1})}{\hat{s}_2(\xi_j,\tau_i)} = \beta_{2j}(\tilde{x}_2^2(\xi_j)\ \phi_j\Delta\tau)\ ,\ j=1,\cdots,m \tag{C.4}$$

where

$$\phi_j \triangleq \exp[-q_2(\frac{1}{\theta(\xi_j)} - 1)] \tag{C.5}$$

Since Eq. (C.4) is linear with respect to β_{2j}, the estimation of β_2 can be carried out sequentially by minimizing the following least squares function at each measurement position ξ_j :

$$J_j \triangleq \sum_{i=1}^{N} \{\log \frac{\hat{s}_2(\xi_j,\tau_{i-1})}{\hat{s}_2(\xi_j,\tau_i)} - \beta_{2j}(\tilde{x}_2^2(\xi_j)\ \phi_j\Delta\tau)\}^2 \tag{C.6}$$

The resulting sequential estimation algorithm is

$$\hat{\beta}_{2j}(\tau_n) = \frac{\hat{\beta}_{2j}(\tau_{n-1}) \sum_{i=1}^{n} \tilde{x}_2^2(\xi_j)\phi_j\Delta\tau + \tilde{x}_2^2(\xi_j,\tau_n)\phi_j(\tau_n)\Delta\tau \log \frac{\hat{s}_2(\xi_j,\tau_{n-1})}{\hat{s}_2(\xi_j,\tau_n)}}{\sum_{i=1}^{n} (\tilde{x}_2^2(\xi)\phi_j\Delta\tau)^2 + \tilde{x}_2^2(\xi_j,\tau_n)\phi_j(\tau_n)\Delta\tau} \tag{C.7}$$

Now an average β_2 estimate, denoted by $\hat{\beta}_2$, is obtained as a weighted average over $\hat{\beta}_{2j}$'s

$$\hat{\beta}_2(\tau_n) = \sum_{j=1}^{m} \omega_j \hat{\beta}_{2j}(\tau_n) \tag{C.8}$$

The activity near the entrance to the reactor decays more rapidly due to the higher temperature, so that the decay constant estimate $\hat{\beta}_{2j}$

obtained from the earlier section is in general more accurate and should be weighted more heavily.

Another minimization criterion, similar to expression (C.6), is

$$J \triangleq \sum_{i=1}^{N} \sum_{j=1}^{m} \omega_j \left\{ \log \frac{\hat{s}_2(\xi_j, \tau_{i-1})}{\hat{s}_2(\xi_j, \tau_i)} - \beta_{2j} (\tilde{x}_2^2(\xi_j) \phi_j \Delta\tau) \right\}^2 \qquad (C.9)$$

The resulting estimation algorithm is similar to (C.7).

Numerical calculations were performed using the same simulated system as that in Chapter 6. Estimates on local activities were first obtained according to the procedures in Chapter 6. The subsequent estimation results for β_2 are shown to be satisfactory by Figure C-1. The estimation via criterion (C.6) is indicated by the dashed line, while the estimate obtained from criterion (C.9) is represented by a solid line. The advantages of this scheme are that the estimation is accomplished in a sequential manner and that the computation takes very little time.

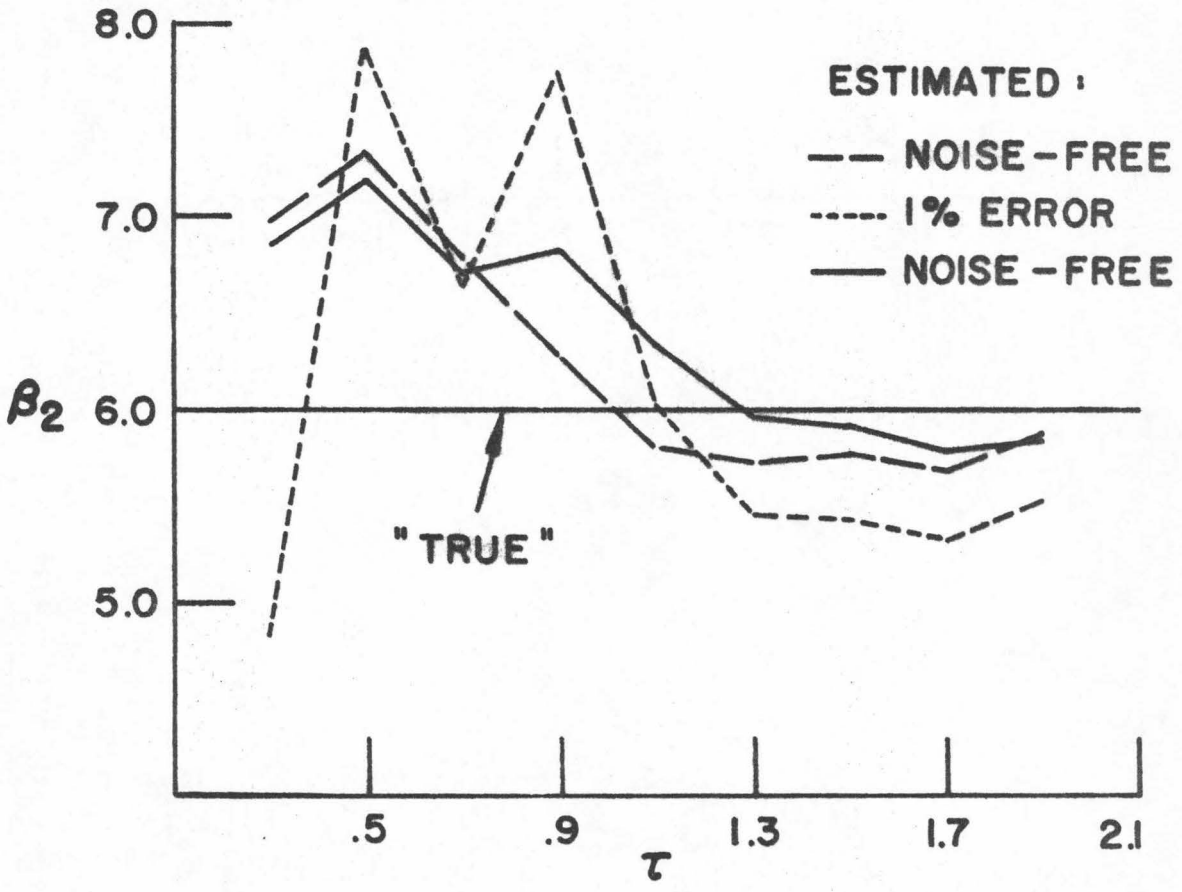

Fig. C-1. Sequential Estimation of Decay Constant β_2 by Least Squares Minimization

APPENDIX D

ESTIMATION OF DEACTIVATION PARAMETERS FOR ISOTHERMAL OPERATION OF NAPHTHA REFORMING

Under isothermal operation, utilized in laboratory kinetic studies, the estimation of catalyst deactivation parameters for a simplified model of naphtha reforming can be achieved from the following system of equations:

$$\frac{\partial x_2}{\partial \xi} = - \frac{\alpha_2}{v} s_2 x_2 (1 + \alpha_c x_2) \tag{D.1}$$

$$\frac{\partial s_2}{\partial \tau} = - \beta_2 s_2 x_2^2 \tag{D.2}$$

where n-paraffin is consumed by isomerization and coking reactions according to Eq. (D.1)

and alumina activity s_2 deactivates at a rate described by (D.2).

The boundary and initial conditions are

$$\text{(i)} \quad \text{at } \xi = 0 : \qquad x_2 = x_{2f} \tag{D.3}$$

$$\text{(ii)} \quad \text{at } \tau = 0 : \qquad s_2 = s_{2o} \tag{D.4}$$

The partial differential equations (D.1) and (D.2) can be transformed to an ordinary differential equation by the same transformation introduced in Chapter 7 for the non-isothermal operation.

Define

$$S_2 = \int_0^{\xi} s_2(\xi') \, d\xi' \tag{D.5}$$

From Eqs. (D.1) and (D.2)

$$\frac{\partial s_2}{\partial \tau} = \frac{v\beta_2}{\alpha_2} \left(\frac{x_2}{1+\alpha_c x_2}\right) \frac{\partial x_2}{\partial \xi} \tag{D.6}$$

Integration of (D.6) from 0 to ξ gives

$$\frac{\partial S_2}{\partial \tau} = \frac{v\beta_2}{\alpha_2\alpha_c} \left[x_2 - x_{2o} - \frac{1}{\alpha_c} \log\left(\frac{1+\alpha_c x_2}{1+\alpha_c x_{2o}}\right)\right] \tag{D.7}$$

Since from (D.1)

$$\int_{x_{2o}}^{x_2} \frac{dx}{x(1+\alpha_c x)} = -\frac{\alpha_2}{v} S_2 \tag{D.8}$$

the following relationship between S_2 and x_2 is obtained,

$$x_2 = \frac{1}{\left(\frac{1}{x_{2o}} + \alpha_c\right) \exp\left(\frac{\alpha_2}{v} S_2\right) - \alpha_c} \tag{D.9}$$

Denoting the right hand side of (D.9) as $f(\tilde{S}_2)$, Eq. (D.7) can be written in the form of an ordinary differential equation as

$$\frac{dS_2}{d\tau} = \frac{v\beta_2}{\alpha_2\alpha_c} \left[x_2 - x_{2o} - \frac{1}{\alpha_c} \log\left(\frac{1+\alpha_c f(S_2)}{1+\alpha_c x_{2o}}\right)\right] \tag{D.10}$$

for each reactor position ξ, with initial condition

$$S_2(0) = S_{2o}\xi \tag{D.11}$$

If Eq. (D.8) is substituted into (D.7), an ordinary differential equation in terms of x_2 is obtained, valid for an arbitrary fixed value of ξ :

$$\frac{dx_2}{d\tau} = -\beta_2 x_2(1 + \alpha_c x_2)\left[x_2 - x_{2o} - \frac{1}{\alpha_c}\log\left(\frac{1+\alpha_c x_2}{1+\alpha_c x_{2o}}\right)\right] \quad (D.12)$$

where

$$x_2(0) = \frac{1}{\left[\left(\frac{1}{x_{2o}} + \alpha_c\right)\exp\left(\frac{\alpha_2 \xi}{v}\right) - \alpha_c\right]} \quad (D.13)$$

Now, based on the ordinary differential equation (D.12) or (D.10), the estimation of the deactivation parameter β_2 can be carried out according to the scheme described in Chapter 7 or Appendix C.

APPENDIX E

DISCRETE AND CONTINUOUS SEQUENTIAL FILTERS

A discrete filter presented by Cox [126] and a continuous filter presented by Detchmendy and Sridhar [128] are described in this appendix for reference. The derivations and other background information can be found in the references listed in Chapter 7.

A Discrete Nonlinear Filter

Consider a process described by the following vector difference equation:

$$x_{k+1} = f_k(x_k) + G_k \eta_k \tag{E.1}$$

The observed signal is

$$y_k = h_k(x_k) + \varepsilon_k \tag{E.2}$$

where x_k is the n-dimensional state vector;

y_k is the p-dimensional observational vector;

f_k is an n-dimensional vector-valued function;

h_k is a p-dimensional vector-valued function;

G_k is an $n \times m$ matrix;

η_k is the m-dimensional dynamical disturbance vector where $m \leq n$;

ε_k is the p-dimensional observational disturbance vector

$\{\eta_k\}, \{\varepsilon_k\}$ are assumed to be independent Gaussian random sequences with zero mean

and $$\varepsilon\{\eta_k \eta_j^T\} = M_k \delta_{kj}, \quad \varepsilon\{\varepsilon_k \varepsilon_j^T\} = N_k \delta_{kj}, \quad \varepsilon\{\eta_k \varepsilon_j^T\} = 0 \tag{E.3}$$

where ε is the expectation operator and δ_{kj} is the Kronecker delta.

Given the information about the dynamical equations and a sequence of noisy observations, the goal is to estimate sequentially the true state variables and some unknown constant parameters.

A nonlinear system with linear observations can be treated by the following linearization:

$$x_{k+1} \simeq f(x^*(k|k),k) + F_x(x^*(k|k),k)\cdot(x_k - x^*(k|k)) + G_k\eta_k \qquad (E.4)$$

where $F_x(x^*(k|k),k)$ is the matrix of partial derivatives and the point $x^*(k|k)$, about which the expansion is made, is the estimate of x_k produced by the linearized scheme to be developed, given the sequence of observations $\{y_o,\cdots,y_k\}$.

Now the minimization function is defined as

$$J^* = \frac{1}{2}\left[\|x_o - m_o\|^2_{P_o^{-1}} + \sum_{k=0}^{R}\|y_k - H_k x_k\|^2_{N_k^{-1}}\right] + \sum_{k=0}^{R-1}\left\{\frac{1}{2}\|\eta_k\|^2_{M_k^{-1}} + \lambda_k^T\left[x_{k+1} - f(x^*(k|k),k) - F_x(x^*(k|k),k)(x_k - x^*(k|k)) - G_k\eta_k\right]\right\} \qquad (E.5)$$

where the initial state of the process is assumed to have a normal probability distribution of the form $P_{x_o} = n\{m_o,p_o\}$.

Setting dJ^* equal to zero, the solution of the resulting two-point boundary-value problem is obtained as

$$x^*(k|r) = x^*(k|k) + C_k F_x^T(x^*(k|k),k)\,\lambda_k \qquad (E.6)$$

where

$$C_k^* = [I + P_k^* H_k^T N_k^{-1} H_k]^{-1} P_k^* \qquad (E.7)$$

$$P^*_{k+1} = F_x(x^*(k|k))\ C^*_k F^T_k(x^*(k|k)) + G_k M_k G^T_k \qquad (E.8)$$

$$x^*(r|r) = f(x^*(r-1|r-1)) + C^*_r H^T_r\ N^{-1}_r [y(r) - H_r f(x^*(r-1|r-1),r-1)] \qquad (E.9)$$

The recurrence relation (E.9) can be interpreted intuitively as follows:

$C^*(r)$ = a measure of present uncertainty;

$H^T(r)$ = sensitivity of observation to changes in x_r ;

$N^{-1}(r)$ = reliability of measurement y_r ;

$f(x^*(r-1|r-1),r-1)$ = a prediction of x_r ;

$H(r)f(x^*(r-1|r-1),r-1)$ = a prediction of y_r

The error in the prediction of y_r is weighted in proportion to the present uncertainty, sensitivity of the observation, and reliability of the measurement. This weighted error is then used to modify the predicted value of x_r to obtain an up-to-date estimate of x_r . Equations (E.7)-(E.9) are particularly suitable for real time implementation on a digital computer.

A Continuous Nonlinear Filter

Consider a process described by

$$\frac{dx}{dt} = f(t,x) + G(t)\ \eta(t) \quad \text{(dynamical disturbance)} \qquad (E.10)$$

$$y(t) = h(t,x) + \varepsilon(t) \quad \text{(observational disturbance)} \qquad (E.11)$$

The p vector observation $y(t)$ is known in an interval $0 \leq t \leq T$. Based on this observation, it is required to estimate the

n dimensional state $x(t)$ for $0 \leq t \leq T$.

The cost associated with the estimate $\hat{x}(t)$ is defined as

$$J \triangleq \int_0^T [\, \|y(t) - h(t,x)\|^2_{Q(t)} + \|\dot{\hat{x}} - f(t,x)\|^2_{R(t)}]dt \qquad (E.12)$$

where $Q(t)$ can be interpreted as the inverse of the covariance matrix $N(t)$ of the observational error $\varepsilon(t)$, and $R(t)$ is $[G(t)\, M(t)\, G^T(t)]^{-1}$ where $M(t)$ is the covariance matrix of $\eta(t)$. By definition, the optimal estimate $\hat{x}(t)$, $0 \leq t \leq T$ minimizes J .

The above minimization problem is reformulated as an optimal control problem. If it is assumed that an a priori distribution of the initial state is known, the cost for an initial estimate $\|x_o - m_o\|^2_{P_o^{-1}}$ which is not included in the cost for observational errors, should be added in the performance index, and then the return function for the control problem is defined as:

$$J^*(T,C) = \underset{0 \leq t \leq T}{\underset{u(t)}{\text{Min}}} \{ \|x_o - m_o\|^2_{P_o^{-1}} + \int_0^T [\, \|y(t) - h(t,x)\|^2_{Q(t)} + \|u\|^2_{R(t)}]dt \qquad (E.13)$$

where $T \geq 0$, $-\infty < C_i < \infty$, $i = 1,2,\cdots n$

with $\dot{x} = f(t,x) + u$, $x(T) = C$ (E.14)

The above optimal control problem can be treated by dynamic programming.

Detchmendy and Sridhar [128] have approximated J^* by a quadratic function of x in the neighborhood of $\hat{x}(t)$ to derive the

following filter

$$\frac{d\hat{x}}{dT} = f(T,\hat{x}) + P(T)h_{\hat{x}}^{T}(T,\hat{x})\ Q[y(T) - h(T,\hat{x})] \tag{E.15}$$

$$\frac{dP}{dT} = f_{\hat{x}}(T,\hat{x})P + Pf_{\hat{x}}^{T}(T,\hat{x}) + P\{h_{\hat{x}}^{T}Q[y(T) - h(T,\hat{x})]_{\hat{x}}\}P + R^{-1} \tag{E.16}$$

where the $n \times n$ matrix $P(T)$ is defined by

$$P(T) \triangleq 2[J_{cc}^{*}(T,\hat{x})]^{-1} \tag{E.17}$$

The initial conditions are

$$x_o = m_o$$

$$P_o = 2[J_{cc}^{*}(0,m_o)]^{-1} \tag{E.18}$$

NOMENCLATURE

A	external surface area of catalyst pellets per unit volume
c	vector of concentration
c_i	concentration of the i^{th} species
c_p	heat capacity
D_e	effective diffusivity
D_k	Knudsen diffusivity
$D(i+1\|i+1)$	covariance matrix of the error in estimate for state at stage i+1 given i+1 observations
E, E_i	activation energies
Eff	effectiveness factor defined by Eq. (B.1)
E_d, E_{di}	activation energies of catalyst decay reactions
$f, f_i, \tilde{f}$	rate expressions
G	mass velocity
$g, g_i, \tilde{g}$	rate expressions
$H(i)$	linear observation matrix defined by Eq. (7.20)
ΔH	heat of reactions
h	Thiele modulus defined by Eq. (B.14)
h_t	heat transfer coefficient
J	criterion function
K_i	thermodynamic equilibrium constants
k, k_i	rate constants
k_e	effective heat conductivity
k_d, k_{di}	rate constants of catalyst decay reactions
k_o, k_{io}	frequency factors of rate constant
L	length of reactor

M_i	molecular weight of the i^{th} species
M_m	mean molecular weight defined by Eq. (7.34)
M_{ji}	matrix defined by Eq. (7.59)
m, m_i	catalyst deactivation parameters
n	total number of temperature or concentration measurements along the reactor
$P(i+1\|i)$	covariance matrix of the error in estimate for state at stage i+1 given i observations
p, p_1, p_2	dimensionless activation energies
p_i	function of z defined by Eq. (7.56)
p_o	reference pressure, 1 atm.
p_1', p_2', p_3'	parameters in the approximation of Figure 11a
q, q_1, q_2	dimensionless activation energies of catalyst decay reactions
R	gas constant
r	radial position within pellet
$\bar{r}$	position of front between poisoned and active parts of pellet
r'	intrinsic reaction rate
r_i	global reaction rates
r_o	radius of catalyst pellet
S, S_i	cumulative activities
S_m	modified cumulative activity, defined by Eq. (8.18)
s, s_1, s_2	dimensionless densities of active sites, catalyst activities
s_p	specific surface area of the catalyst pellet
$\bar{s}_{2i}$	parameters in the approximation of Figure 11b
T	temperature

T_g temperature in bulk gas phase

T_s temperature of the catalyst surface

t time

u linear velocity

v dimensionless velocity

x $= (c_1, \cdots, c_N, T)$ vector of composition and temperature

x_i dimensionless concentration variables defined by Eq. (5.128)

y, y_i composition variable defined by Eq. (5.6)

z length along the reactor

Greek Symbols

α_i dimensionless rate constant defined by Eq. (5.129)

β_i dimensionless frequency factor of catalyst decay reactions defined by Eq. (5.135)

ε bed porosity

ε_p porosity of the catalyst pellet

$\overline{\eta}$ dimensionless poisoning front

θ dimensionless temperature

λ dimensionless group defined by Eq. (5.130)

ξ dimensionless position

ξ_j j^{th} dimensionless position of temperature or concentration measurements

ρ fluid density

ρ_p density of the catalyst pellet

τ dimensionless time

Ψ reduction ratio of the global reaction rate subject to poisoning to the poison-free reaction rate

ω_c surface molar concentration of coke

Subscripts

f denotes feed conditions

o denotes reference or initial conditions

Superscripts

$\hat{}$ estimated quantities

$\tilde{}$ measured quantities

' new feed conditions

* true quantities

LIST OF FIGURES

LIST OF TABLES

BIBLIOGRAPHY

1. Butt, J. B., Chem. Eng. Sci. 25, 801 (1970).

2. Butt, J. B. and Rohan, D. M., Chem. Eng. Sci. 23, 489 (1968).

3. Lee, W., paper presented at AIChE 62nd Annual Meeting, Washington, D.C., November 1969.

4. Ogynye, A. F. and Ray, W. H., AIChE Jour. 17, 43 (1971).

5. Ogynye, A. F. and Ray, W. H., AIChE Jour. 17, 365 (1971).

6. Gavalas, G. R., Hsu, G. C., and Seinfeld, J. H., Chem. Eng. Sci., in press.

7. Gavalas, G. R., Hsu, G. C., and Seinfeld, J. H., submitted to Chem. Eng. Jour.

8. Seinfeld, J. H., Gavalas, G. R., and Hwang, M., J. Dynamic Systems Meas. Control, in press.

9. Seinfeld, J. H. and Chen, W. H., Chem. Eng. Sci. 26, 753 (1971).

10. Seinfeld, J. H. and Hwang, M., Chem. Eng. Sci. 25, 741 (1970).

11. Pell, T. M. Jr. and Aris, R., I and EC Fundl. 9, 15 (1970).

12. Gavalas, G. R. and Seinfeld, J. H., Chem.Eng.Sci. 24, 625 (1969).

13. Thomas, J. M. and Thomas, W. J., Introduction to the Principles of Heterogeneous Catalysis, Academic Press (1967).

14. Maatman, R. W., J. Catal. 19, 64 (1970).

15. Finch, J. N. and Clark, A., J. Catal. 19, 292 (1970).

16. Robertson, A.J.B., Catalysis of Gas Reactions by Metals, Springer-Verlag, New York, Inc. (1970).

17. Ashmore, P. G., Catalysis and Inhibition of Chemical Reactions, Butterworths, London (1963).

18. Imperial Chemical Industries, Ltd., Catalyst Handbook, Springer-Verlag, New York, Inc. (1970).

19. Gavalas, G. R., I and EC Fundamentals, in press.

20. Halsey, G. D., J. Chem. Phys. 19, 658 (1948).

21. Boudart, M., Kinetics of Chemical Processes, Prentice-Hall, Englewood Cliffs, N.J. (1968).

22. Weller, S., AIChE Jour. 2, 59 (1956).

23. Kabel, R. L., AIChE Jour. 14, 358 (1968).

24. Kwan, T., J. Phys. Chem. 60, 1033 (1956).

25. Ozaki, A., Taylor, H.S., and Boudart, M., Proc. Roy. Soc. (London) A258, 47 (1960).

26. Temkin, M. and Pyzhev, V., Acta Phys. Chim. USSR 12, 327 (1940).

27. Wojciechowski, B.W., Can. J. Chem. Eng. 46, 48 (1968).

28. Wojciechowski, B. W., Can. J. Chem. Eng. 47, 338 (1969).

29. Szepe, S. and Levenspiel, O., Chem. Eng. Sci. 23, 831 (1968).

30. Szepe, S. and Levenspiel, O., Proc. 4th Sympos. Reaction Engineering, Brussels (1968).

31. Ciapetta, F. G., Dobres, R. M., and Baker, R. W., Catalysis VI, Reinhold Pub. Co., New York (1962).

32. Weisz, P. B., Advances in Catalysis XIII, Academic Press (1962).

33. Haensel, V., Chem. Eng. 68, No.11, 105 (1961).

34. Sinfelt, J. H., Advances in Chemical Engineering V, Academic Press (1964).

35. Thomson, S. J. and Webb, G., Heterogeneous Catalysis, John Wiley (1968).

36. Keulemans, A.I.M. and Schuit, G.C.A., The Mechanism of Heterogeneous Catalysis, Elsevier, Amsterdam (1960).

37. Pollitzer, E. L., Hayes, J. C., and Haensel, V., Refining Petroleum for Chemicals, Advances in Chemistry Series No. 97, ed. Gould, R.F. ACS (1970).

38. Thomas, C. L., Catalytic Processes and Proven Catalysts, Academic Press (1970).

39. Sinfelt, J. H., Hurwitz, H., and Rohrer, J. C., J. Phys. Chem. 64, 892 (1960).

40. Lyster, W. N., Hobbs, J. L., and Prengle, H. W. Jr., AIChE Jour. 10, 907 (1964).

41. Sinfelt, J. H., Hurwitz, H., and Rohrer, J. C., J. Catal. 1, 481 (1962).

42. Sinfelt, J. H. and Rohrer, J. C., J. Phys. Chem. 65, 978 (1961).

43. Nix, P. S. and Weisz, P. B., J. Catal. 3, 179 (1964).

44. Jenkins, B.G.M. and Thomas, W. J., Can. J. Chem. Eng. 48, 179 (1970).

45. Ross, R. A. and Valentine, J. H., J. Catal. 2, 39 (1963).

46. Graham, R. R., Vidaurri, F. L., and Gully, A. J., AIChE Jour. 14, 473 (1968).

47. Hawthorn, R. D., Ackerman, G. H., and Nixon, A. C., AIChE Jour. 14, 69 (1968).

48. Davis, B. H. and Venuto, P. B., J. Catal. 15, 363 (1969).

49. Rohrer, J. C., Hurwitz, H., and Sinfelt, J. H., J. Phys. Chem. 65, 1458 (1961).

50. Langlois, G. E. and Sullivan, R. F., Refining Petroleum for Chemicals, Advances in Chem. Series No. 97, ed. Gould, R. F., ACS (1970).

51. Myers, C. G. and Munns, G. W., I and EC 50, 1727 (1958).

52. Hettinger, W. P. Jr., Keith, C. D., Gring, J. L., and Teter, J. W., I and EC 47, 719 (1955).

53. Donaldson, G. R., Pasik, L. F., and Haensel, V., I and EC 47, 731 (1955).

54. Heinemann, H., Hattman, J. B., and Schall, J. W., I and EC 47, 735 (1955).

55. Beyler, D., Stevenson, D. H., and Shuman, F. R., I and EC 47, 740 (1955).

56. Hatch, L. F., Hydrocarbon Proc. 48, No. 2, 77 (1969).

57. (Flow sheet), Hydrocarbon Proc. 47, No. 9, 155 (1968).

58. Hoffman, H. L., Hydrocarbon Proc. 50, No. 2, 85 (1971).

59. (NPRA Panel Discussion), Hydrocarbon Proc. 50, No. 2, 89 (1971).

60. Anonymous, Petrol Ref. 33, No. 4, 153 (1954).

61. Anonymous, Petrol. Ref. 34, No. 9, 190 (1955).

62. Rossini, F. D., et al., Selected Values of Physical and Thermodynamic Properties of Hydrocarbons and Related Compounds, API (1953).

63. Spenadel, L. and Boudart, M., J. Phys. Chem. 64, 204 (1960).

64. Weisz, P. B., U. S. Patent 2,854,400 (1958).

65. McHenry, K. W., Bertolacini, R. J., Brennan, H. M., Wilson, J. L., and Seelig, H. S., Actes Congr. Intern. Catalyse, Paris 1960, Sect. II, Paper No. 117 (1961).

66. Weisz, P. B. and Swegler, E. W., Science 126, 31 (1957).

67. Hindin, S. G., Weller, S. W., and Mills, G. A., J. Phys. Chem. 62, 244 (1958).

68. Wheeler, A., Catalysis II, ed. Emmett, P. H., Reinhold Pub. Co., New York (1955).

69. Froment, G. F. and Bischoff, K. B., Chem. Eng. Sci. 3, 110 (1953).

70. Laidler, K. J., Catalysis I, ed. Emmett, P. H., Reinhold Pub. Co., New York (1955).

71. Tan, C. H. and Fuller, O. M., Can. J. Chem. Eng. 48, 174 (1970).

72. Forni, L., Zanderighi, L., Cavenghi, C., and Carra, S., J. Catal. 15, 153 (1969).

73. Chu, C., I and EC Fundamentals 7, 509 (1968).

74. Wheeler, A., Advances in Catalysis III, Academic Press (1950).

75. Thiele, E. W., I and EC 31, 916 (1939).

76. Carberry, J. J. and Gorring, R. L., J. Catal. 5, 529 (1966).

77. White, D. E. and Carberry, J. J., Can. J. Chem. Eng. 43, 334 (1965).

78. Petersen, E. E., Chemical Reaction Analysis, Prentice-Hall (1965).

79. Sada, E. and Wen, C. Y., Chem. Eng. Sci. 22, 559 (1967).

80. Balder, J. R. and Petersen, E. E., Chem. Eng. Sci. 23, 1287 (1968).

81. Wheeler, A. and Robell, A. J., J. Catal. 13, 299 (1969).

82. Haynes, H. W. Jr., Chem. Eng. Sci. 25, 1615 (1970).

83. Froment, G. F. and Bischoff, K. B., Chem. Eng. Sci. 16, 189 (1961).

84. Johnson, B. M., Froment, G. F., and Watson, C. C., Chem. Eng. Sci. 17, 835 (1962).

85. Masamune, S. and Smith, J. M., AIChE Jour. 12, 384 (1966).

86. Sagara, M., Masamune, S., and Smith, J. M., AIChE Jour. 13, 1226 (1967).

87. Weekman, V. W. Jr., I and EC Process Des. and Dev. 7, 90 (1968).

88. Olson, J. H., I and EC Fundamentals 7, 185 (1968).

89. Kunugita, E., Suga, K., and Otake, T., J. Chem. Eng. Japan 2, 75 (1969).

90. Bischoff, K. B., I and EC Fundamentals 8, 665 (1969).

91. Ozawa, Y., I and EC Process Des. and Dev. 8, 378 (1969).

92. Ozawa, Y., Chem. Eng. Sci. 25, 529 (1970).

93. Peri, J. B., J. Phys. Chem. 70, 1482 (1966).

94. Hall, W. K., Larson, J. G., and Gerberich, H. R., J. Am. Chem. Soc. 85, 3711 (1963).

95. Gerberich, H. R. and Hall, W. K., J. Catal. 5, 99 (1966).

96. Ozaki, A. and Kimura, K., J. Catal. 3, 395 (1964).

97. Leftin, H. P. and Hermana, E., Proc. Intern. Congr. Catal. 1964, Amsterdam 2, 1064 (1965).

98. Hightower, J. W. and Hall, W. K., J. Am. Chem. Soc. 89, 778 (1967).

99. Hightower, J. W. and Emmett, P. H., J. Am. Chem. Soc. 87, 939 (1965).

100. Zaidman, N. M., Dzisko, V. A., Karnankhov, A. P., Krasilenko, N. P., Koroleva, N. G., and Vishnyakova, G. P., Kinetics and Catalysis (translated from Russian) 9, 709 (1968).

101. Vasilevich, L. A., Boreskov, G. K., Guryanova, R. I., Ryzhak, I., Filippova, A. G., and Frolkina, N., Kinetics and Catalysis (translated from Russian) 7, 525 (1966).

102. Nichols, F. A., J. Appl. Phys. 37, 2805 (1966).

103. Herrmann, R. A., Adler, S. F., Goldstein, M. S., and DeBaun, R.M., J. Phys. Chem. 64, 204 (1960).

104. Duwez, P., Private communication.

105. Herrmann, R. A., Adler, S. F., Goldstein, M. S., and DeBaun, R.M., J. Phys. Chem. 65, 2189 (1961).

106. Barnett, L. G., Weaver, R. E. C., and Gilkeson, M. M., AIChE Jour. 7, 211 (1961).

107. Satterfield, C. N., Mass Transfer in Heterogeneous Catalysis, MIT Press (1970).

108. Gavalas, G. R., Nonlinear Differential Equations of Chemically Reacting Systems, Springer-Verlag, New York (1968).

109. Weisz, P. B. and Hicks, J. S., Chem. Eng. Sci. 17, 265 (1962).

110. Wakao, N. and Smith, J. M., Chem. Eng. Sci. 17, 825 (1962).

111. Gunn, D. J. and Thomas, W. J., Chem. Eng. Sci. 20, 89 (1965).

112. Bischoff, K. B., AIChE Jour. 11, 351 (1965).

113. Mingle, J. O. and Smith, J. M., AIChE Jour. 7, 243 (1961).

114. Kasaoka, S. and Sakata, Y., J. Chem. Eng. Japan 1, 138 (1968).

115. Kubota, H., Yamanaka, Y., and Dalla Lana, I. G., J. Chem. Eng. Japan 2, 71 (1969).

116. Amundson, N. R. and Raymond, L. R., AIChE Jour. 11, 339 (1965).

117. Levinter, M. E., Panchenkov, G. M. and Tanatarov, M. A., Intern. Chem. Eng. 7, 23 (1967).

118. Rosenbrock, H. H. and Storey, C., Computational Techniques for Chemical Engineers, Pergamon Press (1966).

119. Kittrell, J. R., Mezaki, R., and Watson, C. C., I and EC 57, 18 (1965).

120. Heineken, F. G., Tsuchiyah, M., and Aris, R., Mathem. Biosci. 1, 115 (1967).

121. Seinfeld, J. H. and Gavalas, G. R., AIChE Jour. 16, 644 (1970).

122. Lee, E. S., Quasilinearization and Invariant Imbedding, Academic Press (1968).

123. Wiener, N., The Interpolation and Smoothing of Stationary Time Series, MIT Press, Cambridge, Mass. (1949).

124. Kalman, R. E., J. Basic Eng. 82, 35 (1960).

125. Kalman, R. E. and Bucy, R. S., J. Basic Eng. 83, 95 (1961).

126. Cox, H., IEEE Trans. Autom. Control AC-9, 5 (1964).

127. Bellman, R. E., Kagiwada, H. H., Kalaba, R. E., and Sridhar, R., J. Astron. Sci. 3, 110 (1966).

128. Detchmendy, D. M. and Sridhar, R., J. Basic Eng. 88, 362 (1966).

129. Sridhar, R., private communication.

130. Seinfeld, J. H., Chem. Eng. Sci. 24, 75 (1969).

131. Wells, C. H., AIChE Jour. 17, 966 (1971).

132. Lee, E. S., I and EC Fundamental 7, 164 (1968).

133. Bryson, A. E. Jr., and Ho, Y. C., Applied Optimal Control, Blaisdell (1969).

134. Meditch, J. S., Stochastic Optimal Linear Estimation and Control, McGraw-Hill, New York (1969).

135. Schwartz, L. and Stear, E. B., IEEE Trans. on Autom. Control 17 83 (1968).

136. Seinfeld, J. H., I and EC 62, 32 (1970).

137. Adams, C. R., Voge, H. H., Morgan, C. Z., and Armstrong, W. E., J. of Catal. 3, 379 (1964).

138. Karchenko, V. K., Intern. Chem. Eng. 9, (1), 1 (1969).

139. Hightower, J. W., Gerberich, H. R., and Hall, W. K., J. of Catal. 7, 57 (1967).

PROPOSITIONS

I. TURBULENT GAS PHASE MASS TRANSFER AT ORDINARY MASS TRANSFER RATES FROM THE MOMENTUM-MASS ANALOGY

II. A BYPASS CELL MODEL FOR GAS ADSORPTION IN A PACKED BED

III. EFFECTS OF SURFACTANTS ON COALESCENCE REST TIMES OF DROPS

PROPOSITION I

TURBULENT GAS PHASE MASS TRANSFER AT ORDINARY MASS TRANSFER RATES FROM THE MOMENTUM-MASS ANALOGY

(This is a revised version of the proposition accepted by the Candidacy Examination Committee consisting of Professors Corcoran, Shair, Seinfeld, and Gavalas on February 7, 1969.)

INTRODUCTION

In chemical engineering operations such as evaporation, humidification, gas adsorption and desorption, the mass transfer may often be characterized as a process involving the diffusion of a species through a stationary carrier gas. The role played by the concentration of the non-diffusing gas, insofar as it affects the transfer process, has been well established by Stefan and Maxwell in their classical diffusion equation. They indicated that the diffusive flux established by a concentration gradient creates a convective flow in the direction of diffusion. The magnitude of this convective transport depends upon the concentration gradient of the species and the concentration of the non-diffusing gas, which is characterized by the log-mean average density ρ_{BM}.

The role of ρ_{BM} in pure molecular diffusion has been well established, but only in recent years has attention been focussed on verifying its role in mass transfer in the turbulent flow of gases. In early work Gilliland and Sherwood [1], Cairns and Ropers [2], and Westkaemper and White [3] correlated empirically the mass transfer process in turbulent flow with the equation

$$Sh(\rho_{BM}/\rho)^a = b\ Re^c\ Sc^d \qquad (1)$$

where a, b, c, d are correlation coefficients, and the Sherwood number (Sh), Reynolds number (Re) and Schmidt number (Sc) are defined as usual (see Nomenclature).

However, the empirical studies cited above were, in general, inconclusive and did not yield a clear picture of how the parameters

affect the mass transfer process. Several interesting theoretical investigations have been made by Vivian and Behrmann [4], Hughmark [5], Longwell [6], Kays [7], Toor and Marchello [8], and Wasan and Wilke [9]. The last article suggested the approach of solving the following convective-diffusion equation directly as a boundary value problem

$$v \frac{\partial \rho_A}{\partial r} + u \frac{\partial \rho_A}{\partial z} = \frac{1}{r} \frac{\partial}{\partial r} [(D+E) r \frac{\partial \rho_A}{\partial r}] \qquad (2)$$

Since Eq. (2) is a nonlinear partial differential equation when the expression for v is substituted into it, an analytical solution is not conceivable. Numerical solution by a finite difference method was therefore adopted by Wasan and Wilke [9]. However, extensive computations were required to obtain an accurate result.

To avoid performing enormous numerical calculations but yet obtain a good estimate of the mass transfer coefficient, an analytical approach based on the momentum-mass analogy is proposed in this work. It consists of two parts. The first part contains the derivation of the following equation for convective diffusion in the special case when Schmidt number is equal to unity.

$$u_1^+ \sqrt{\frac{2}{f}}\, St = \frac{\rho}{\rho_{BM}} + \frac{1}{\delta} \log[1 - (\frac{2}{f} - u_1^+ \sqrt{\frac{2}{f}}) \delta\, St] \qquad (3)$$

where the Stanton number (St), defined as k_w/u_o, characterizes the mass transfer rate, and k_w is the mass transfer coefficient. (See Nomenclature for other notation.)

The above equation is also examined in the limiting case where it reduces to the well-known j-factor analogy.

The second part of this proposition deals with the problem in the more general situation where the Schmidt number is not unity. In this case the expression for the Stanton number is

$$St = \frac{\sqrt{f/2}}{\frac{\rho_{BM}}{\rho}\left\{\int_0^{y_1^+}\left[1 \Big/ \left(\frac{1}{Sc} + k\,\frac{\nu_e}{\nu}\right)\right] dy^+ + \frac{2{\cdot}5}{k}\log\frac{y_o^+}{y_1^+}\right\}} \qquad (4)$$

Wasan and Wilke [10] have also studied the general case with the momentum-mass analogy but were led to a different result,

$$St = \frac{f/2}{1 + \sqrt{f/2}\left[\int_0^{20}\left[1 \Big/ \left(\frac{1}{Sc} + \frac{\nu_e}{\nu}\right)\right] dy^+ - 13.0\right]} \qquad (5)$$

Their expression (5) fails to demonstrate the role of the concentration level of non-diffusing species, whose contribution to turbulent mass transfer has been well recognized. Furthermore, two unjustified assumptions were involved in their work:

(i) They utilized the Reynolds analogy which holds only if $Sc = 1$ for the general case

(ii) They neglected the convective bulk flow term in the expression for the mass flux. This simplification may lead to significant errors in the region of the laminar boundary layer.

Finally, two sets of calculations are carried out to test the adequacy of the proposed equations. The data required to calculate the

parameters of the working equations are obtained from two experiments by Cairns and Roper [2] and Weskaemper and White [3]. Numerical results indicate that the simple models based on the momentum-mass analogy can predict experimental data satisfactorily. Moreover, calculations are also made to obtain the Stanton numbers from Wasan and Wilke's equation. Again, numerical comparisons support the proposed equations, which yield better predictions.

1. THEORETICAL STUDIES

Statement of the Problem and Assumptions

Species A is vaporized from the wall of a tube of infinite length into a binary mixture of A and B (inert) as the whole mixture flows steadily in the axial direction. The mass transfer occurs both by diffusion and by bulk transport in the radial direction.

The following assumptions are made in this study:

(i) The mass transfer process occurs at an ordinary transfer rate so that it does not alter the velocity profile.

(ii) The axial velocity profile is fully developed.

(iii) The diffusion process is symmetric, i.e., $\frac{\partial \rho_A}{\partial \theta} = 0$

(iv) Species B is a non-diffusing inert gas, i.e., $N_B = 0$. Wasan and Wilke [9] have justified this assumption numerically.

(v) Constant physical properties, e.g., ρ, μ, D

(vi) Diffusion in the axial direction is negligible. This is supported by Schneider's [11] theoretical analysis.

Based on these assumptions, the system can be described mathematically by the following equation

$$v \frac{d\rho_A}{dr} = \frac{1}{r} \frac{d}{dr} [(D+E)\ r \frac{d\rho_A}{dr}] \tag{6}$$

The boundary conditions are $\rho_A = \rho_{Aw}$ at the wall and $\frac{d\rho_A}{dr} = 0$ at the center.

Now, according to the momentum-mass analogy, the following conditions are valid for turbulent flow in conduits:

(i) In the radial direction the mass flux changes its value corresponding to the variation of shear stress so that the ratio of the mass flux and shear stress remains constant, i.e.,

$$\frac{N_A}{\tau g_c} = \frac{N_{Aw}}{\tau_w g_c} \tag{7}$$

where the subscript w denotes the wall conditions.

(ii) Eddy diffusivity is proportional to eddy viscosity, i.e.,

$$E = k\nu_e \tag{8}$$

The proportionality constant k depends only on the value of the Schmidt number.

The above two expressions comprise the momentum-mass analogy. In the special case of $Sc = 1$ the above analogy can be extended to the well-known Reynolds analogy

$$E = \nu_e \text{ (i.e., } k=1) \quad \text{and} \quad \nu + \nu_e = D+E \tag{9}$$

Equation (9) simply indicates that the laws governing momentum and mass transfer are exactly the same.

Derivation of the Working Equations

Consider the following expressions for mass and momentum fluxes:

$$N_A = -(D+E)\frac{d\rho_A}{dy} + \frac{\rho_A}{\rho} N_A \tag{10}$$

$$\tau g_c = \rho(\nu + \nu_e)\frac{du}{dy} \tag{11}$$

where y is the distance away from the wall towards the center of the pipe.

The viscosities ν_e and ν, whose values are obtained experimentally, include the convective term for momentum transport implicitly. Introducing the momentum-mass analogy (7) and the expression $\rho - \rho_A = \rho_B$, Eqs. (10) and (11) can be combined to yield

$$d \log \frac{\rho_B}{\rho} = \frac{N_{Aw}}{\tau_w g_c}\left(\frac{\nu+\nu_e}{D+E}\right) du \tag{12}$$

According to the value of Schmidt number, the remaining derivations are described in two parts which yield different working equations.

(i) The Case of $Sc = 1$

In this case the Reynolds analogy (Eq. (9)) holds and Eq. (12) becomes

$$\log \frac{\rho_B}{\rho} = \frac{N_{Aw}}{\tau_w g_c} du \tag{13}$$

Integration of Eq. (13) from the wall to y_1 yields

$$\log \frac{\rho_{B1}}{\rho_{Bw}} = \frac{N_{Aw}}{\tau_w g_c} u_1 \tag{14}$$

where y_1 is the boundary separating the turbulent core from the buffer

and laminar zone.

In the turbulent core, under the restriction that the mass transfer process takes place at an ordinary rate, the convective mass transfer in the radial direction can often be neglected when compared with the radial diffusive mass transfer. Hence,

$$N_A = -(D+E)\frac{d\rho_A}{dy} \quad , \qquad y_1 \leq y \leq y_o \tag{15}$$

where the subscript o denotes the conditions in the center of tube.

Dividing Eq. (15) by Eq. (11), and then integrating from y_1 to y_o gives

$$\frac{\rho_{Bo} - \rho_{B1}}{\rho} = \frac{N_{Aw}}{\tau_w g_c}(u_o - u_1) \tag{16}$$

To evaluate u_1 the following three models for the velocity distribution in the region near the wall were adopted in the present work:

(a) $u^+ = y^+ - 1.04\times10^{-4}\, y^{+4} + 3.03\times10^{-6}\, y^{+6}$, $0 \leq y^+ \leq 20$ (17)

This u^+-y^+ correlation was presented by Wasan, Tien, and Wilke [12].

(b) $u^+ = \frac{1}{0.0695}\tanh 0.0695\, y^+$, $0 \leq y^+ \leq 26.7$ (18)

This u^+-y^+ correlation was presented by Corcoran and Sage [13].

(c) The graphical velocity distribution ($u^+ \sim y^+$) presented by Schlinger and Sage [14].

The superscript "+" used in the above equations designates dimensionless quantities, and u^+ and y^+ are defined as

$$u^+ \triangleq \sqrt{2/f}\ \frac{u}{u_o} \tag{19}$$

$$y^+ \triangleq \frac{y}{\sqrt{2/f}\ \frac{\nu}{u_o}} \tag{20}$$

The value of u_1^+ varies slightly according to which model is used. For instance, $y_1^+ = 20$ and $u_1^+ = 13$ for model (a); $y_1^+ = 26.7$ and $u_1^+ = 13.7$ for model (b). If u^+ is known, then ρ_{B1} can be obtained from Eq. (16) as

$$\rho_{B1} = \rho_{Bo} - \rho u_o(1 - u_1^+ \sqrt{f/2})(\frac{N_{Aw}}{\tau_w g_c}) \tag{21}$$

The combination of Eqs. (14), (19), (21) yields

$$\log \frac{\rho_{Bo} - \rho u_o(1 - u_1^+ \sqrt{f/2})(N_{Aw}/\tau_w g_c)}{\rho_{Bw}} = (\frac{N_{Aw}}{\tau_w g_c}) u_o u_1^+ \sqrt{f/2} \tag{22}$$

By using the following expressions

$$\tau_w g_c = \frac{f}{2}\rho u_o^2 \quad , \quad \rho_{Aw} - \rho_{Ao} = \rho_{Bo} - \rho_{Bw} \tag{23}$$

and

$$N_{Aw} = k_w(\rho_{Aw} - \rho_{Ao}) \tag{24}$$

Eq. (22) can be written as

$$\log\left[\frac{\rho}{\rho_{Bo}} - (\frac{2}{f} - u^+\sqrt{2/f})\ \frac{k_w}{u_o}\ \frac{\rho_{Aw} - \rho_{Ao}}{\rho}\right] + \log \frac{\rho_{Bo}}{\rho_{Bw}}$$

$$= (\frac{\rho_{Aw} - \rho_{Ao}}{\rho})\ u_1^+\sqrt{2/f}\ \frac{k_w}{u_o} \tag{25}$$

Now, the dimensionless driving force of the transfer process is defined

as

$$\delta \triangleq \frac{\rho_{Aw} - \rho_{Ao}}{\rho} \tag{26}$$

The dimensionless log-mean concentration of the non-diffusing species B is

$$\alpha \triangleq \frac{\rho_{BM}}{\rho} \triangleq \frac{(\rho_{Bo} - \rho_{Bw})}{\log(\rho_{Bo}/\rho_{Bw})} \Big/ \rho \tag{27}$$

For mass transfer with an ordinary transfer rate, the material in the center of the tube consists essentially of species B so that for simplicity $\rho_{Bo} = \rho$. This simplification along with the two definitions (26) and (27) allows the reduction of Eq. (25) to the following equation in dimensionless form

$$u_1^{+}\sqrt{2/f}\ St = \frac{1}{\alpha} + \frac{1}{\delta} \log[1 - \delta(\frac{2}{f} - u_1^{+}\sqrt{2/f})\ St] \tag{28}$$

From the above equation, the Stanton number St, which represents the mass transfer rate, can be easily obtained by a simple arithmetical iteration scheme. It can also be seen specifically from Eq. (28) which parameters affect the mass transfer and what these effects are. This is discussed qualitatively in Appendix A.

The Limiting Case of Zero Driving Force

Consider the limiting case when a very large amount of species B flows through a tube. The fluid in the tube is essentially uniform and there is no radial concentration gradient, i.e., $\rho_{Aw} = \rho_{Ao}$, $\rho_{BM} = \rho$. In this case, the so-called j-factor analogy holds, i.e.,

$$St = \frac{f}{2} \qquad (\simeq j_D \text{ , j-factor}) \tag{29}$$

On the other hand, taking the limit of Eq. (28) as δ approaches zero by using L'Hôspital's rule yields

$$St = \frac{f}{2} \tag{30}$$

This confirms the validity of the proposed equation in the limiting case. Since $St \triangleq Sh/(Re \cdot Sc)$ and $\rho_{BM}/\rho = 1$ in this case, Eq. (30) can be written as

$$Sh(\rho_{BM}/\rho) = \frac{f}{2} Re\ Sc \tag{31}$$

which has the same form as the empirical correlation equation (Eq. (1)).

(ii) The General Case

Without the restriction on the Schmidt number, the derivation can be carried out generally starting from the following rewritten form of Eq. (12)

$$d \log \frac{\rho_B}{\rho} = \frac{N_{Aw}}{\tau_w g_c} \left(\frac{1 + \frac{\nu_e}{\nu}}{\frac{1}{Sc} + \frac{E}{\nu}}\right) du \tag{32}$$

By using the chain rule, Eq. (11) can be written in dimensionless form as

$$\frac{du^+}{dy^+} = \frac{\tau}{\tau_w} \left(\frac{1}{1 + \frac{\nu_e}{\nu}}\right) \tag{33}$$

Near the wall region $\tau \simeq \tau_w$, Eq. (33) can be simplified to

$$\frac{du^+}{dy^+} = \frac{1}{1 + \frac{\nu_e}{\nu}} \tag{34}$$

In the turbulent core, however, the above simplification cannot be used.

Instead, von Karman's empirical logarithmic distribution law is adopted, i.e.,

$$u^+ = 2{\cdot}5 \log y^+ + 5{\cdot}5 \quad , \qquad y_1^+ \leq y^+ \leq y_o^+ \tag{35}$$

Therefore

$$\frac{du^+}{dy^+} = \frac{2{\cdot}5}{y^+} \qquad , \qquad y_1^+ \leq y^+ \leq y_o^+ \tag{36}$$

Integration of Eq. (32) from the wall to the center of the tube, combined with Eqs. (34) and (36), yields

$$\log \frac{\rho_{Bo}}{\rho_{Bw}} = \left(\frac{N_{Aw}}{\tau_w g_c}\right) u_o \sqrt{f/2} \left[\int_0^{y_1^+} \frac{1}{\frac{1}{Sc}+\frac{E}{\nu}} dy^+ + \int_{y_1^+}^{y_o^+} \frac{1+\frac{\nu_e}{\nu}}{\frac{1}{Sc}+\frac{E}{\nu}} \frac{2{\cdot}5}{y^+} dy^+ \right] \tag{37}$$

Using (24) and (27), Eq. (37) can be rewritten as

$$\frac{k_w}{u_o} = \frac{\sqrt{f/2}}{\frac{\rho_{BM}}{\rho}\left[\int_0^{y_1^+} \frac{1}{\frac{1}{Sc}+\frac{E}{\nu}} dy^+ + 2{\cdot}5 \int_{y_1^+}^{y_o^+} \frac{1+\frac{\nu_e}{\nu}}{\frac{1}{Sc}+\frac{E}{\nu}} \frac{dy^+}{y^+} \right]} \tag{38}$$

To simplify Eq. (38), it is noted that in the turbulent core

$$\frac{1}{Sc} << \frac{E}{\nu} \qquad \text{and} \qquad \frac{\nu_e}{\nu} >> 1 \tag{39}$$

Therefore, the final equation for the general case can be obtained using Eq. (39) and the mass-momentum analogy (Eq. (8))

$$St = \frac{\sqrt{f/2}}{\alpha \left[\int_0^{y_1^+} \frac{dy^+}{\frac{1}{Sc} + k \frac{\nu_e}{\nu}} + \frac{2.5}{k} \log \frac{y_o^+}{y_1^+} \right]} \tag{40}$$

where the ratio of eddy and molecular kinematic viscosity ν_e/ν is obtained from one of the following two models in this study:

(a) $$\frac{\nu_e}{\nu} = 3.2 \times 10^{-4} \, y_o^{+3} \quad , \quad 0 \leq y^+ \leq 10 \tag{41}$$

This empirical model was presented by Tien and Wason [15].

(b) $$\frac{\nu_e}{\nu} = (1 - \frac{y^+}{y_o^+}) \cosh^2 0.0695 \, y^+ - 1 \, , \quad 0 \leq y^+ \leq 26.7 \tag{42}$$

This correlation was proposed by Schlinger et al [16].

Therefore, the Stanton number St can be obtained explicitly from Eq. (40) by carrying out the necessary numerical integration.

2. COMPARISONS OF THEORETICAL AND EXPERIMENTAL VALUES

The Proposed Equation (28)

$$u_1^+ \sqrt{2/f} \, St = \frac{1}{\alpha} + \frac{1}{\delta} \log[1 - \delta(\frac{2}{f} - u_1^+ \sqrt{2/f}) \, St]$$

where u_1^+ is determined from one of the following three models:

(a) $$u^+ = y^+ - 1.04 \times 10^{-4} y^{+4} + 3.03 \times 10^{-6} \, y^{+6}$$

at $y_1^+ = 20$, $u_1^+ = 13.0$

(b) $u^+ = \frac{1}{0.0695} \tanh 0.0695\, y^+$

at $y_1^+ = 26.7$, $u_1^+ = 13.7$

(c) The experimental graph of u^+ versus y^+ presented by Schlinger and Sage (see Reference [14]). u_1^+ is determined from the curves in that graph according to the specific Reynolds number.

(i) Experiment 1: "Mass Transfer at High Humidities in a Wetted Wall Column" by R. C. Cairns and G. H. Ropers [2]. Process description: Mass transfer data were obtained from the operation of an adiabatic wetted wall column with counter-current flow of air and water. The Schmidt number equals 0.55 for each run.

The experimental Stanton number was obtained as illustrated in Appendix B. The comparisons between theoretical Stanton numbers calculated from the above equation and experimental values are listed in Table 1. The average percentage error is 16.3%. Comparisons were also made between the Stanton number obtained from Wasan and Wilke's equation (5) and the experimental value. They are tabulated in Appendix C with an average percentage error of 47.1%. The theoretical predictions in Table 1 were based upon the velocity distribution given by Model (a). The percentage errors between the Stanton numbers calculated from Models (a), (b), (c) and the experimental values are listed for comparison in Table 2. The results from these models differ from each other by insignificant amounts. This also indicates that the above three velocity distributions are quite similar and the Stanton

TABLE 1

COMPARISONS OF THEORETICAL AND EXPERIMENTAL STANTON NUMBERS

Run No.	Re	f	δ	α	St	St_{exp}	% Error
1	2389	0.0113	0.0427	0.469	0.01204	0.01430	15.8
2	3417	0.0103	0.0625	0.587	0.00877	0.01080	18.8
3	8517	0.0082	0.0696	0.583	0.00702	0.00755	7.0
4	6520	0.0088	0.0580	0.501	0.00878	0.01040	15.6
5	5304	0.0093	0.0432	0.413	0.01125	0.01310	14.1
6	3987	0.0098	0.0358	0.269	0.01735	0.01720	0.9
7	5100	0.0094	0.0705	0.685	0.00686	0.00908	24.4
8	6826	0.0087	0.0864	0.735	0.00591	0.00695	14.9
9	9095	0.0081	0.0805	0.779	0.00520	0.00715	27.3
10	3137	0.0106	0.0198	0.153	0.03465	0.03880	10.7
11	3273	0.0104	0.0254	0.175	0.02971	0.02800	6.1
12	3511	0.0103	0.0272	0.212	0.02429	0.03090	21.4
13	3662	0.0102	0.0343	0.230	0.02432	0.02410	0.9
14	4157	0.0098	0.0372	0.301	0.01636	0.02000	18.3
15	4531	0.0096	0.0407	0.337	0.01427	0.01870	23.7
16	4301	0.0098	0.0404	0.315	0.01555	0.02090	25.6
17	3995	0.0100	0.0357	0.280	0.01785	0.02380	25.0
18	4828	0.0095	0.0426	0.371	0.01280	0.01700	24.7
19	4641	0.0096	0.0481	0.355	0.01351	0.01590	15.0

TABLE 2

COMPARISONS OF PREDICTED STANTON NUMBERS BASED ON DIFFERENT VELOCITY DISTRIBUTION MODELS

Run No.	Percentage Error		
	Model (a)	Model (b)	Model (c)
1	15.8	15.8	16.0
2	18.8	18.8	18.9
3	7.0	6.9	6.9
4	15.6	15.6	15.6
5	14.1	14.1	14.1
6	0.9	1.0	0.9
7	24.4	24.4	24.4
8	14.9	14.9	14.8
9	27.3	27.2	27.2
10	10.7	10.7	11.0
11	6.1	6.1	5.8
12	21.4	21.4	21.6
13	0.9	0.9	1.1
14	18.3	18.3	18.4
15	23.7	23.6	23.7
16	25.6	25.6	25.7
17	25.0	25.0	25.1
18	24.7	24.7	24.7
19	15.0	15.0	15.0
Average	16.33	16.32	16.36

number in the proposed equation is affected weakly by the difference in u_1^+ .

(ii) Experiment 2: "Effect of Concentration Level on Mass Transfer Rates" by L. E. Westkaemper and R. R. White [3]. Process description: Carbon tetrachloride was evaporated into a stream of air in turbulent flow. The comparisons between the theoretical predictions from the proposed equation and the experimental values are listed in Table 3. In this case the average percentage error is 10.29%, while that of Wasan and Wilke's equation yields 15.59%. Again, it is shown in Table 4 that there is no significant difference between the three velocity distribution models described before.

The Proposed Equation (40)

$$St = \frac{\sqrt{f/2}}{\alpha\left[\int_0^{y_1^+} \frac{dy^+}{\frac{1}{Sc} + k\frac{\nu_e}{\nu}} + \frac{2.5}{k}\log\frac{y_o^+}{y_1^+}\right]}$$

where ν_e/ν is obtained from one of the following two models:

(a) $$\frac{\nu_e}{\nu} = 3.2\times10^{-4}\ y^{+3} \qquad , 0 \le y^+ \le 10$$

(b) $$\frac{\nu_e}{\nu} = \left(1 - \frac{y^+}{y_o^+}\right)\cosh^2 0.0695\ y^+ - 1 \qquad , 0 \le y^+ \le 26.7$$

Experiment 1:

The integral in the proposed equation is evaluated graphically in this study. Figures 1 and 2 sketch the functionality of the integrand based on the different viscosity ratio distributions given by

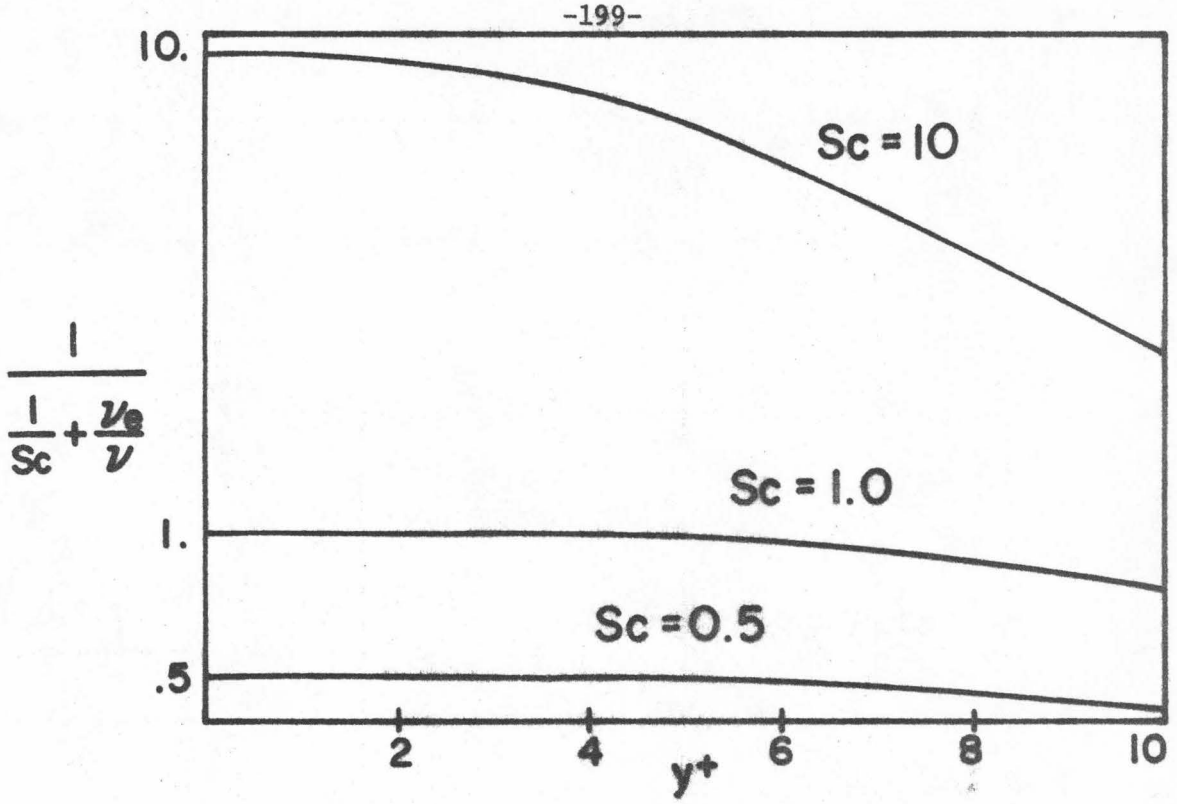

Fig. 1. Graphical Representation of the Integrand in Eq. (40) by Model (a)

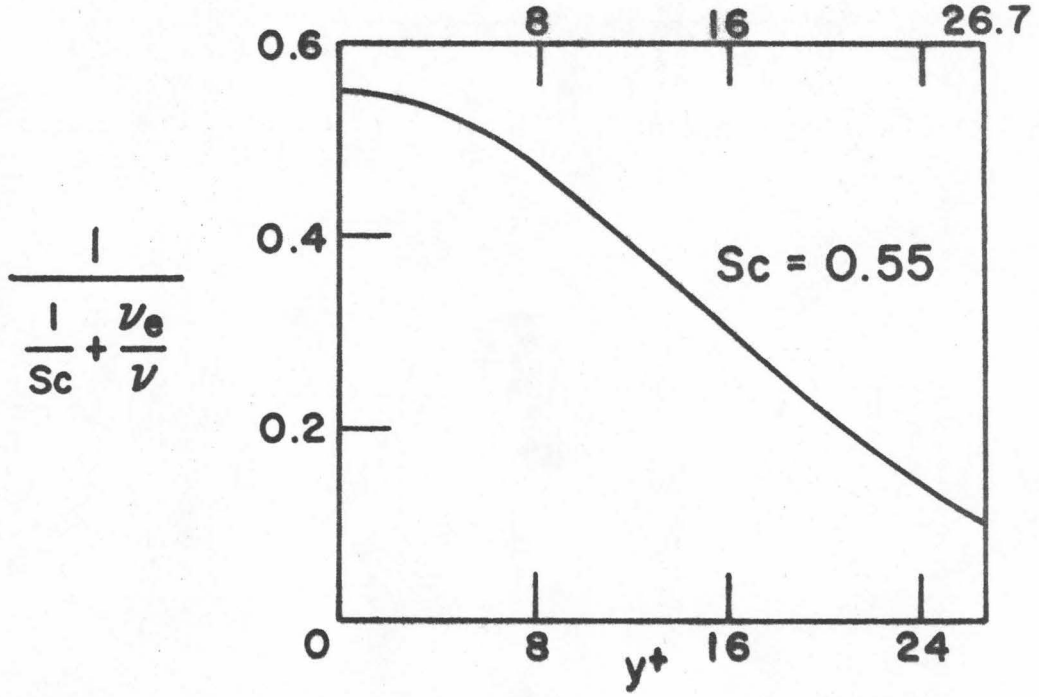

Fig. 2. Graphical Representation of the Integrand in Equation (40) by Model (b)

TABLE 3

COMPARISON OF THEORETICAL AND EXPERIMENTAL STANTON NUMBERS

Sc	Re	f	δ	α	St	St_{exp}	% Error
0.348	11800	0.0076	0.1300	0.502	0.00758	0.00840	9.80
0.471	5980	0.0090	0.1619	0.630	0.00702	0.00670	4.75
0.470	6020	0.0090	0.1590	0.625	0.00739	0.00820	9.85
0.478	5790	0.0091	0.1647	0.625	0.00721	0.00700	2.90
0.505	7800	0.0084	0.1681	0.642	0.00668	0.00685	2.50
0.640	5570	0.0091	0.1440	0.734	0.00622	0.00630	1.30
0.700	4770	0.0095	0.1526	0.747	0.00630	0.00560	12.50
1.110	1100	0.0137	0.2800	0.798	0.00845	0.00530	59.50*
1.020	600	0.0160	0.3405	0.782	0.01010	0.00995	1.52
0.432	11800	0.0076	0.1655	0.471	0.00810	0.00980	17.30
0.242	14700	0.0071	0.0955	0.312	0.01149	0.01460	21.30
0.333	4690	0.0096	0.0722	0.520	0.00930	0.01005	7.45
0.353	7490	0.0085	0.0722	0.535	0.00800	0.01000	20.05
0.368	9660	0.0080	0.0841	0.551	0.00760	0.00980	22.50

*This value is excluded in taking the average.

TABLE 4

COMPARISONS OF PREDICTED STANTON NUMBERS BASED ON DIFFERENT VELOCITY DISTRIBUTION MODELS

Percentage Error		
Model (a)	Model (b)	Model (c)
9.80	9.80	9.80
4.75	4.85	4.95
9.85	9.85	9.75
2.90	3.00	3.10
2.50	2.40	2.20
1.30	1.20	1.10
12.50	12.60	12.50
59.50*	59.40*	56.50*
1.52	1.15	1.50
17.30	17.00	17.00
21.30	21.10	21.20
7.45	7.45	7.45
20.05	19.90	19.90
22.50	22.30	22.30
10.29	10.20	10.21

*This value is excluded in taking the average.

models (a) and (b) respectively. y_o^+ is determined as follows:

For run number 13: $f = 0.0102$, $R = 0.45$ inches, $\mu = 0.0448$ lb/ft-hr , $\rho u_o = G_m/A = 2.16 \times 10^3$ lb/hr-ft^2 . Therefore

$$y_o^+ = \frac{R}{\sqrt{2/f}\ (\frac{\mu}{\rho u_o})} = 129$$

For simplicity, k is taken as unity in the proposed equation. The resulting comparisons between the predicted Stanton numbers and the experimental values are tabulated in Table 5. The average percentage error for the predicted Stanton number calculated by using model (a) is 10.3%, while the error in using model (b) is 9.4%. The difference is small, although the viscosity distribution of model (b) gives slightly better predictions.

Conclusions

(i) The proposed equations, i.e., Eqs. (28) and (40), are based upon the simple momentum-mass analogy which is purely theoretical. One expects that the calculated values would deviate from the experimental values to some extent. However, the numerical results are surprisingly good as they differ from the empirical values only by 10-16%.

(ii) The proposed schemes yield significantly better predictions than Wasan and Wilke's equation, i.e., Eq. (5).

(iii) The proposed general equation which includes the effect of Sc gives better numerical results (10% versus 16% in average error) than the equation derived for $Sc = 1$.

TABLE 5

COMPARISON ON PREDICTED AND EXPERIMENTAL STANTON NUMBER

Run No.	St_{exp}	St Model (a)	St Model (b)	% Error (a)	% Error (b)
1	0.01430	0.01430	0.01230	0	14.0
2	0.01080	0.01080	0.00945	0	12.5
3	0.00755	0.00980	0.00855	29.8	13.2
4	0.01040	0.01180	0.01040	13.4	0
5	0.01310	0.01260	0.01290	3.8	1.5
6	0.01720	0.02310	0.01885	34.2	9.6
7	0.00908	0.00894	0.00785	1.5	13.5
8	0.00695	0.00800	0.00655	15.1	6.5
9	0.00715	0.00730	0.00648	2.1	9.3
10	0.03880	0.04200	0.03670	8.3	5.4
11	0.02800	0.03700	0.03170	32.0	13.2
12	0.03090	0.03020	0.02620	2.3	15.1
13	0.02410	0.02780	0.02400	15.3	4.1
14	0.02000	0.02080	0.01840	4.0	8.0
15	0.01870	0.01740	0.01640	7.0	12.3
16	0.02090	0.01880	0.01740	10.1	16.7
17	0.02380	0.02260	0.01975	5.1	17.0
18	0.01700	0.01660	0.01465	2.3	13.7
19	0.01590	0.01730	0.01530	8.8	3.7

(iv) The mass transfer rate of convective diffusion in turbulent flow is determined by the following parameters.

(a) Schmidt number, Sc, which relates molecular diffusivity D, to kinematic viscosity ν;

(b) Reynolds number, Re, which determines the friction factor f;

(c) Radius of the tube, which determines directly the dimensionless radius y_o^+;

(d) Degree of turbulence, which influences the value assigned to the turbulent-laminar boundary y_1^+;

(e) Mass transfer driving force $\delta \triangleq (\rho_{Aw} - \rho_{Ao})/\rho$;

(f) Concentration level of the non-diffusing component

$$\alpha \triangleq \rho_{BM}/\rho \triangleq \frac{\rho_{Bo}-\rho_{Bw}}{\log \frac{\rho_{Bo}}{\rho_{Bw}}} \Big/ \rho \quad .$$

Once the system and the flow pattern have been specified, the first four factors are fixed. Then the effects of δ and α on the mass transfer rate can be studied directly. The general effects are shown diagramatically in Appendix A.

APPENDIX A

EFFECTS OF PARAMETERS ON THE STANTON NUMBER IN EQUATION (28)

Equation (28): $u_1^+\sqrt{2/f}\ St = \frac{1}{\alpha}+\frac{1}{\delta}\log[1 - \delta(\frac{2}{f} - u_1^+\sqrt{2/f})St]$

(i) Effect of concentration level of the non-diffusing component, as shown in Figure 3 plotting St versus α while fractional driving force δ varies as a parameter.

(ii) Effect of Reynolds number, as shown in Figure 4 plotting St versus α keeping δ constant.

(iii) Effect of fractional driving force, as shown in Figure 5 plotting St versus δ while concentration level α varies as a parameter.

From Figures 3, 4, and 5, some qualitative comments can be deduced such as:

a) From Figure 3, the effect of α decreases rapidly (almost like exponential decay) as α increases for a given Re, δ and Sc.

b) From Figure 4, for a given α, the higher the Reynolds number, the lower the mass transfer rate.

c) From Figure 5, for high concentration level of the non-diffusing component ($\simeq$ 1.0) the mass transfer rate is a weak function of fractional driving force δ.

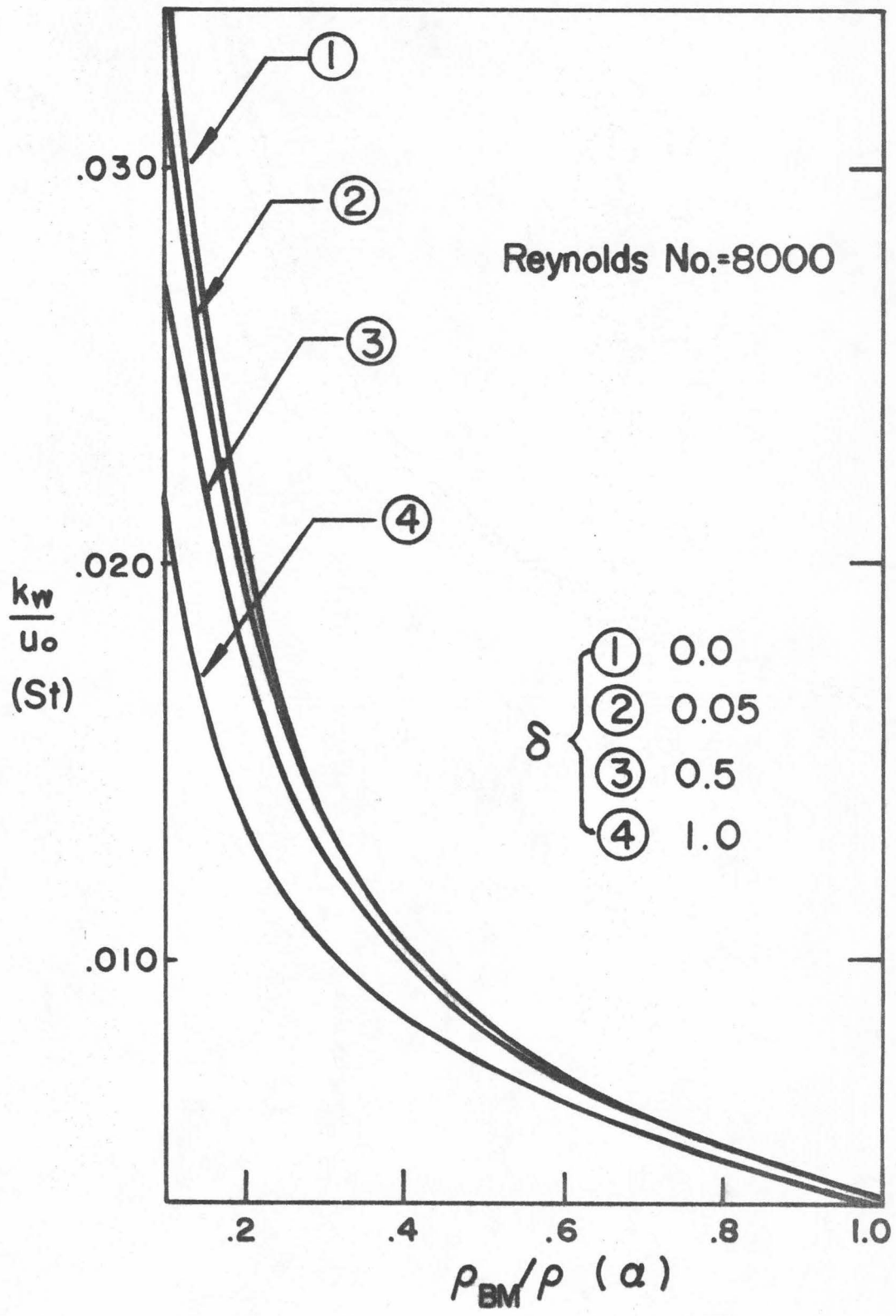

Fig. 3. Effect of Concentration Level of the Non-Diffusing Component α on the Stanton Number

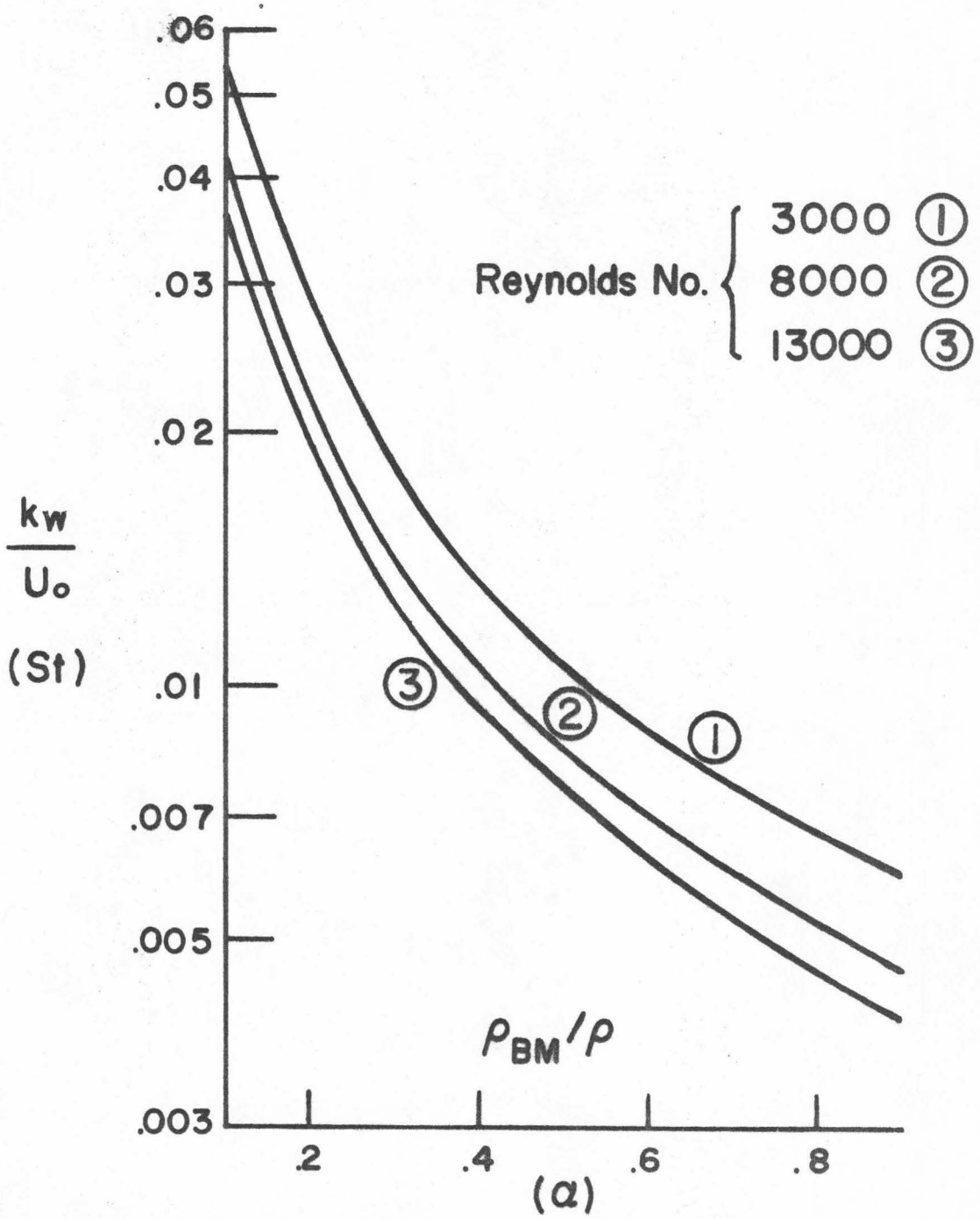

Fig. 4. Effect of Reynolds Number Re on the Stanton Number

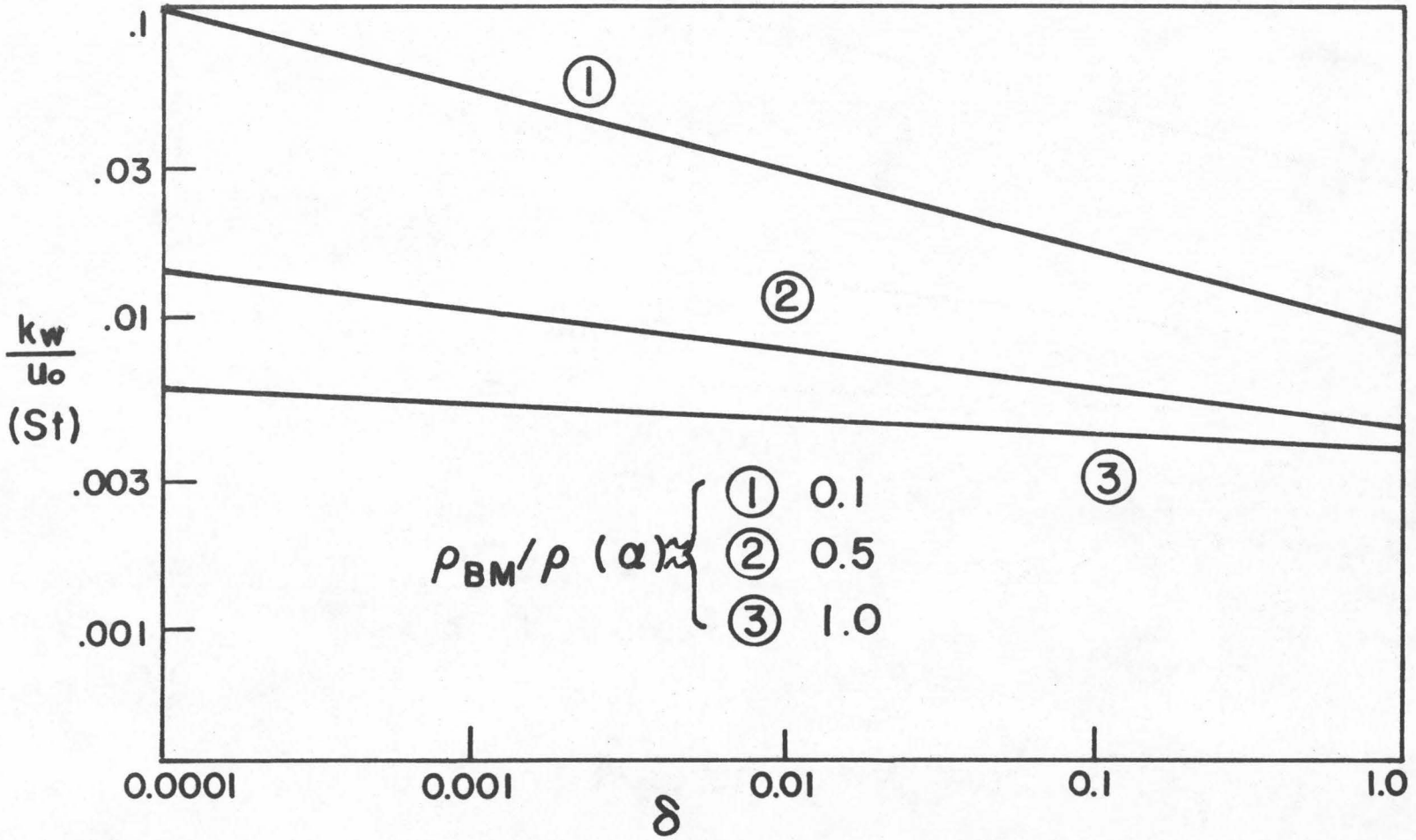

Fig. 5. Effect of Mass Transfer Driving Force δ on the Stanton Number

APPENDIX B

CALCULATION OF EXPERIMENTAL STANTON NUMBERS

i) Experiment 1 (see Reference [2]):

Demonstrated example: Run No. 13

a) Film temperature: at column inlet = $(813+200)/2 = 507\ ^{o}F$

at column outlet = $(454+200)/2 = 327\ ^{o}F$

mean value = $(507+327)/2 = 417\ ^{o}F$

b) Air density $\rho_{air} = 0.0808 \times 492/(460+417) = 0.045\ lb/ft^3$

c) Specific volume of air $v_{air} = 22.1\ ft^3/lb$ dry air

d) Specific volume of steam (from steam table) $v_{steam} = 35.36\ ft^3/lb$

e) Average humidity $\bar{H} = (H_{in} + H_{out})/2 = 1.89\ lb/lb$

f) Specific volume of the mixture $v_{mix} = (v_{steam} \times \bar{H} + v_{air} \times 1)$ / $(\bar{H}+1)$, thus $\rho_{mix} = 1/v_{mix} = 0.0321\ lb/cu.ft.$

g) Mean mass flow rate, w = dry air rate + vapor entering column + rate of evaporation/2 = $3.34+5.73+1.16/2 = 9.65\ lb/hr$

h) $u_o = w/(\rho_{mix} A) = 9.65/(0.0321 \times 0.00442) = 6.8 \times 10^4 ft/hr$

i) $k_w = k_G RT = 2.59 \times 0.73 \times 877 = 1658\ ft/hr$

Therefore

$$St = \frac{k_w}{u_o} = 1658/(6.8 \times 10^4) = 0.02410$$

ii) Experiment 2 (see Reference [3]):

a) $K_x = K_G P$ lb moles/(hr)(sq.ft), where k_G is provided as data and all the runs are carried out under atmospheric pressure

b) $G_m (=cu_o)$ is provided as data

Therefore

$$St = \frac{k_x}{G_m}$$ can be obtained directly.

APPENDIX C

CALCULATION OF STANTON NUMBER FROM WASAN AND WILKE'S EQUATION (5)

Equation (5) (see Reference [10]):

$$St_o = \frac{f/2}{1 + \sqrt{f/2}\left[\int_0^{20} \frac{dy^+}{\frac{1}{Sc} + \frac{\nu_e}{\nu}} - 13.0\right]}$$

where the integral $\int_0^{20} \frac{dy^+}{\frac{1}{Sc} + \frac{\nu_e}{\nu}}$ is tabulated as a table in Reference [10].

(i) Experiment 1: Since Sc = 0.55 for all runs, the integral has the constant value 8.0 . The comparisons of calculated results and experimental values are tabulated in Table 6. The average percentage error is 47.1%.

(ii) Experiment 2: The numerical results are shown in Table 7 for comparison with the empirical values. The average percentage error is 15.59%.

TABLE 6

COMPARISONS OF EXPERIMENTAL AND PREDICTED St FROM WASAN AND WILKE'S EQUATION

Run No.	f	$\sqrt{f/2}$	St_o	St_{exp}	% Error
1	0.01130	0.0753	0.00908	0.01430	36.5
2	0.01030	0.0719	0.00804	0.01080	25.5
3	0.00820	0.0640	0.00603	0.00755	20.6
4	0.00880	0.0665	0.00660	0.01040	36.5
5	0.00926	0.0581	0.00653	0.01310	50.1
6	0.00980	0.0700	0.00754	0.01720	56.0
7	0.00935	0.0685	0.00710	0.00908	21.8
8	0.00870	0.0660	0.00647	0.00695	6.9
9	0.00810	0.0637	0.00594	0.00715	16.9
10	0.01055	0.0726	0.00827	0.00388	113.0*
11	0.01044	0.0725	0.00820	0.02800	70.5
12	0.01026	0.0718	0.00800	0.03090	74.0
13	0.01026	0.0718	0.00800	0.02410	58.5
14	0.00984	0.0703	0.00760	0.02000	62.0
15	0.00960	0.0656	0.00640	0.01870	65.7
16	0.00976	0.0662	0.00653	0.02090	68.5
17	0.01000	0.0708	0.00775	0.02380	67.5
18	0.00950	0.0690	0.00725	0.01700	57.3
19	0.00955	0.0690	0.00729	0.01590	54.0

*Run No. 10 is excluded in taking the average.

TABLE 7

COMPARISON OF EXPERIMENTAL AND PREDICTED St FROM WASAN AND WILKE'S EQUATION

f	$\sqrt{f/2}$	$\int_0^{20} \frac{dy^+}{\frac{1}{Sc}+\frac{\nu_e}{\nu}}$	St_o	St_{exp}	% Error
0.00758	0.0616	5.44	0.00710	0.00840	15.50
0.00898	0.0671	7.02	0.00750	0.00670	11.90
0.00897	0.0671	7.02	0.00750	0.00820	8.55
0.00906	0.0676	7.11	0.00753	0.00700	7.56
0.00840	0.0649	7.46	0.00655	0.00685	4.39
0.00915	0.0677	9.04	0.00625	0.00630	0.80
0.00950	0.0690	9.70	0.00615	0.00560	8.72
0.01370	0.0829	14.10	0.00626	0.00530	15.40
0.01600	0.0895	13.20	0.00785	0.00995	21.10
0.00758	0.0616	6.52	0.00632	0.00980	35.50
0.00717	0.0600	3.93	0.00787	0.01460	46.00
0.00955	0.0692	5.23	0.01033	0.01005	2.78
0.00850	0.0653	5.49	0.00835	0.01000	16.50
0.00797	0.0633	5.68	0.00745	0.00980	24.00

NOMENCLATURE

Roman:

A	cross-sectional area of a tube
D	molecular diffusivity
E	eddy diffusivity
f	friction factor
g_c	gravitational conversion factor, 32.2 (lb.mass/lb.force) · $(ft/sec)^2$
G_m	molar flow rate
H	humidity
k	the proportionality constant defined by Eq. (8)
k_w	mass transfer coefficient
N_A, N_B	mass fluxes of species A and B
R	radius of a tube
r	distance in radial direction away from the center of tube
Re	Reynolds number
Sc	Schmidt number (ν/D)
Sh	Sherwood number (St·Re·Sc)
St	Stanton number (k_w/u_o)
u	axial velocity
u^+	the dimensionless velocity defined by Eq. (19)
v	radial velocity
w	mass flow rate
y	distance away from the wall
y^+	the dimensionless distance defined by Eq. (20)
z	distance along the tube

Greek:

α	the dimensionless concentration levels of non-diffusing species defined by Eq. (27)
δ	the dimensionless driving force defined by Eq. (26)
μ	absolute viscosity
ν	kinematic viscosity
ν_e	eddy viscosity

ρ, ρ_A, ρ_B	densities of the fluid, species A and B
ρ_{BM}	log-mean concentration of species B, $(\rho_{Bo}-\rho_{Bw})/\log \frac{\rho_{Bo}}{\rho_{Bw}}$
τ	shear stress

Subscripts:

o	denotes the conditions at the center of tube
w	denotes the conditions at the wall
1	denotes the conditions at the boundary separating the turbulent core from the laminar zone

BIBLIOGRAPHY

1. Gilliland, E. R. and Sherwood, T. K., I and EC 26, 516 (1934).

2. Cairns, R. C. and Roper, G. H., Chem. Eng. Sci. 3, 97 (1954).

3. Westkaemper, L. E. and R. R. White, AIChE Jour. 3, 69 (1957).

4. Vivian, J. E. and Behrmann, W. C., AIChE Jour. 11, 656 (1965).

5. Hughmark, G. H., I and EC Fundamentals 8, 31 (1969).

6. Longwell, P. A., Mechanics of Fluid Flow, McGraw Hill, New York (1966).

7. Kays, W. M., Convective Heat and Mass Transfer, McGraw-Hill, New York (1966).

8. Toor, H. L. and Marchello, J. M., AIChE Jour. 4, 97 (1958).

9. Wasan, D. T. and Wilke, C. R., AIChE Jour. 14, 577 (1968).

10. Wasan, D. T. and Wilke, C. R., Int. Jour. Heat and Mass Transfer 7, 87 (1964).

11. Schneider, P. J., Trans. Am. Soc. Mech. Engrs. 79, 765 (1957).

12. Wasan, D. T., Tien, C. L., and Wilke, C. R., AIChE Jour. 9, 567 (1963).

13. Corcoran, W. H. and Sage, B. H., AIChE Jour. 2, 251 (1956).

14. Schlinger, W. G. and Sage, B. H., I and EC 45, 2636 (1953).

15. Tien, C. L. and Wasan, D. T., Phys. Fluids 6, 144 (1963).

16. Schlinger, W. G., Berry, V. J., Mason, J. L., and Sage, B. H., I and EC 45, 662 (1953).

PROPOSITION II

A BYPASS CELL MODEL

FOR GAS ADSORPTION IN A PACKED BED

INTRODUCTION

The adsorption of a chemical component from a fluid stream flowing through a stationary packed bed is an important operation in chemical processing, as in the drying of gases by silica gel, softening of water by passing it through a zeolite bed, clarification of liquids by charcoal, and recovery of casing-head gasoline by solid adsorbents. The excellent review article by Thiele [1] summarizes many of the problems that are encountered in the adsorption field.

The study of adsorption-desorption dynamics in both isothermal and adiabatic processes is of fundamental as well as of practical interest in process design. Much has been done in the way of obtaining solutions of the partial differential equations, which represent the dynamical system of an adsorption-desorption process. Except in certain special cases of isothermal adsorption (see Vermeulen [2] and Lightfoot et al [3] for summaries), no analytical solution has been obtained for the general case of a fluid having a nonlinear expression for the equilibrium absorbate content at the surface of adsorbent. Many graphical and numerical methods have been proposed by Hougen and Marshall [4], Acrivos [5], Van Arsdel [6], and others. Among them, the method of characteristics commonly appears in the literature [7,8]. However, this method, being popularly employed nowadays for a large variety of mathematical problems, was actually derived for general partial differential equations, whereas the particular characteristics of adsorption in packed beds were not built into it. It is the author's belief that a model taking into consideration the particular

functional behavior of a dynamic system will yield a better computational scheme.

As to the dynamic models available in the literature for adsorption in packed beds, they were all constructed in oversimplified plug flow form. Acrivos [5] pointed out that mass diffusion or heat conduction along the bed is usually overlooked in the studies of adsorption processes, whereas their contributions are well recognized in the studies of packed bed dynamics [9].

Furthermore, the existence of non-ideal flow patterns in a packed bed in terms of channeling flow among the pellets and local mixing around each packing is well accepted in reactor analysis.

Therefore, the purpose of this study is to introduce a good dynamic model incorporating channeling, axial diffusion and local mixing effects, and to present a computational scheme better than the presently available adsorption models both in terms of computation and accuracy. The model proposed in this study is a bypass cell model. This particular model with its subsequent theoretical analysis has not been studied in any field. The idea of a simple cell model without bypassing streams has often been adopted in the literature. However, it has never been used in adsorption studies. The suitability of the proposed model is demonstrated not only by the numerical results presented in the later sections, but also by the convenience of the resulting computational scheme. Moreover, certain intriguing functional relationships between the adsorption variables are shown analytically in this study.

1. Formulation of the Problem

Consider a gas passing through a uniformly packed reactor. The adsorption rate may be limited by one or more of the following mechanisms: the diffusion of adsorbate from the fluid to the gross surface of adsorbent; the diffusion from the gross surface of the adsorbent into the interior surface; or the kinetic adsorption rate on the surface of the adsorbent. It is generally accepted that the rate controlling steps are the two diffusion processes due to the comparative inaccessibility of the adsorbate to the surface of the adsorbent [10], and that the overall adsorption rate can be represented by the mass transfer rate through the following linear-driving-force expression:

$$\text{adsorption rate per unit volume} = k_m a_s (x - x^*)$$

where x is the adsorbate content in the fluid, with units of lb_x/lb_f;

x^* is the equilibrium adsorbate content at the surface of adsorbent;

a_s is the external area of adsorbent per unit volume;

k_m is the overall mass transfer coefficient with units of $lb_x/(ft^2 sec)(lb_x/lb_f)$, and it obeys a basic assumption that the overall resistance to mass transfer is the sum of the diffusional resistances in the gas phase and the solid phase.

The main chapters of this work deal with the regular adsorption processes with the above rate expression. In certain special cases (e.g., a water softening process), kinetic rate controlling is observed. Although the same modelling technique can be extended to them,

a separate analytical method is recommended in Appendix A.

The following basic assumptions are used in formulating a simplified fixed bed adsorption system:

(a) The feed contains only one adsorbable component;

(b) The adsorbate is present in small amounts. For practical purposes, the flow rate and density of the fluid through the bed are assumed to be constant;

(c) The flow pattern is one-dimensional;

(d) Momentum, mass, and heat transfer in the radial direction are negligible;

(e) The gas phase behaves as an ideal gas mixture, and pressure drop along the bed is negligible;

(f) Mass transfer coefficient and diffusivity are both independent of position and state variables.

However, due to the inherent nature of the proposed model, the following restrictions usually adopted in the literature are not assumed in this work:

(a) Longitudinal diffusion is negligible;

(b) A linear equilibrium relationship exists between the adsorbate at the surface of adsorbent and the adsorbate content in the adsorbent;

(c) The initial adsorbate concentration in the adsorbent is uniform throughout the bed;

(d) The inlet adsorbate concentration of the fluid is constant.

The relaxation of the above assumptions is certainly a significant advantage of the present study; other advantages are brought out in the following chapters.

2. Isothermal Adsorption Analysis

The analysis of isothermal adsorption is based on material balances and the functional relationship between the adsorbates at the surface of and in the adsorbent. The application of this analysis is restricted to systems that have low inlet adsorbate concentrations and high mass velocity. In practice, this will correspond to cases where only a trace amount of adsorbate is adsorbed and the heat generated is dissipated or transferred rapidly from the system and to systems that have small heats of adsorption.

Mathematical Formulation and Modelling

Referring to a standard control volume with unit cross sectional area, the material balances on the adsorbate are given by Eqs. (1) and (2) in the fluid and adsorbent respectively:

$$\rho_f \varepsilon \frac{\partial x}{\partial t} + G \frac{\partial x}{\partial z} - \rho_f \varepsilon D_e \frac{\partial^2 x}{\partial z^2} = -k_m a_s (x - x^*) \tag{1}$$

$$(1 - \varepsilon)\rho_s \frac{\partial \omega}{\partial t} = k_m a_s (x - x^*) \tag{2}$$

where

$$x^* = f(\omega) \tag{3}$$

ω is the adsorbate content in the adsorbent, lb_x/lb_s

D_e is the effective diffusivity

f the functionality of equilibrium isotherm, is non-linear in general.

(See NOMENCLATURE for other notation.)

The initial and boundary conditions are

$$x(0,t) = x_o(t) \tag{4}$$

$$\omega(z,0) = \omega_o(z) \tag{5}$$

It is generally accepted in the literature [4,8] that for adsorption systems the rate of change of the adsorbate in the fluid is very small compared to the other terms in Eq. (1). In other words, the time constant for x to adjust itself to a new steady state is usually very small compared to the characteristic time constant of ω variation. Therefore the so-called pseudo-steady state approximation is adopted, and Eq. (1) is simplified as

$$G \frac{\partial x}{\partial z} - \rho_f \varepsilon D_e \frac{\partial^2 x}{\partial z^2} = -k_m a_s (x - x^*) \tag{6}$$

According to Levenspiel [11] a non-ideal flow with axial dispersion and local mixing can be simulated closely by a CSTR-in-series model. In this work a modified CSTR-in-series model is formulated, and the diffusion term in Eq. (6) is thus replaced by the mixing in each backmix cell. The idea of cell model is commonly used in the literature. Dean and Lapidus [12] proposed a model as an array of two-dimensional mixing cells to study the radial and axial dynamic behaviors. McGuire and Lapidus [13] extended it to the stability analysis. Vanderveen, Luss, and Amundson [14] also applied a cell model with backflow to stability study. However, their models are unnecessarily complex for a gas adsorption system, thus the resulting schemes lead to lengthy computations and loss of physical insight.

An additional feature of non-ideal flow pattern is introduced in this work. That is the channeling effect, i.e., a portion of fluid bypasses the adsorbent through the arbitrary channels in the packings. This effect has been observed experimentally to be significant in various gas adsorption systems by Bullock [8], and is incorporated by simulating a stream of bypass flow in the present work. Furthermore, the introduction of this bypass flow can improve the computation as follows.

Consider two cell models, one with bypass flow and the other without (denoted by A and B respectively). Since a realistic mixing effect is usually limited, the length of mixing cell B is kept close to the magnitude of the diameter of an adsorbent pellet (denoted as d_p). With bypassing flow, the amount of mixing in a cell of length d_p is reduced. To attain the same mixing effect as cell B, a larger cell with length $h > d_p$ must be used. On the other hand, a bypass cell model introduces a stream of higher concentration from the previous cell. In order to reduce the outlet concentration to that of cell B, a larger cell with longer residence time should be used. Since larger cell length means fewer number of cells for a fixed length packed bed, the total computation is reduced correspondingly. Therefore, in this work a bypass cell model with a series of N CSTR's and bypassing streams are used to simulate the flow process in a single packed bed with length L, where

$$N = L/h \tag{7}$$

For simplicity, consider only the case of equal volume cells, i.e.,

with identical cell length h and constant residence time $\theta = h/v$. The same technique can be applied without any conceptual difficulty to the case of arbitrary cell volumes.

A schematic description of cell i consisting of a CSTR and a bypassing stream is given in Figure 1. The quantitative ratio of bypass to overall flow is μ. This bypass flow is not a hypothetical quantity, and it relates directly to the physical dispersion and channeling effects (i.e., the effective diffusivity). This is demonstrated by the following qualitative argument.

Since μ is used to simulate a realistic flow pattern, only convective and diffusive terms which determine the flow process are considered. The mass balance on adsorbate in the fluid for cell i is

$$\varepsilon Ah \frac{dx_i}{dt} = (1 - 2\mu)vA\, x_{i-1} + \mu vA\, x_{i-2} - (1-\mu)vA\, x_i \tag{8}$$

Rewrite Eq. (8) as

$$\varepsilon \frac{dx_i}{dt} = (1 - 2\mu) \frac{v}{h} x_{i-1} + \mu \frac{v}{h} x_{i-2} - (1-\mu) \frac{v}{h} x_i \tag{9}$$

or

$$\varepsilon \frac{\partial x(z)}{\partial t} = (1-2\mu) \frac{v}{h} x(z-h) + \mu \frac{v}{h} x(z-2h) - (1-\mu) \frac{v}{h} x(z) \tag{10}$$

Provided h is small enough to make the functional variation over that cell length small, the high-order terms in the Taylor series expansion of Eq. (10) can be neglected. The resulting equation becomes

$$\varepsilon \frac{\partial x(z)}{\partial t} = -v \frac{\partial x(z)}{\partial z} + (1+2\mu) \frac{vh}{2!} \frac{\partial^2 x(z)}{\partial z^2} \tag{11}$$

Comparing Eq. (11) to the conventional description

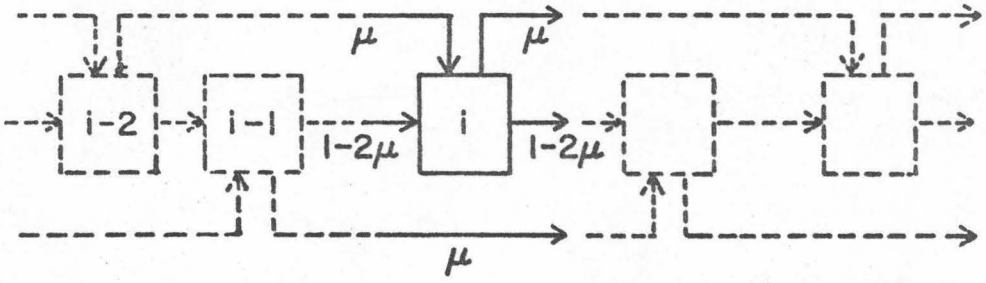

Fig. 1. A Bypass Cell Model

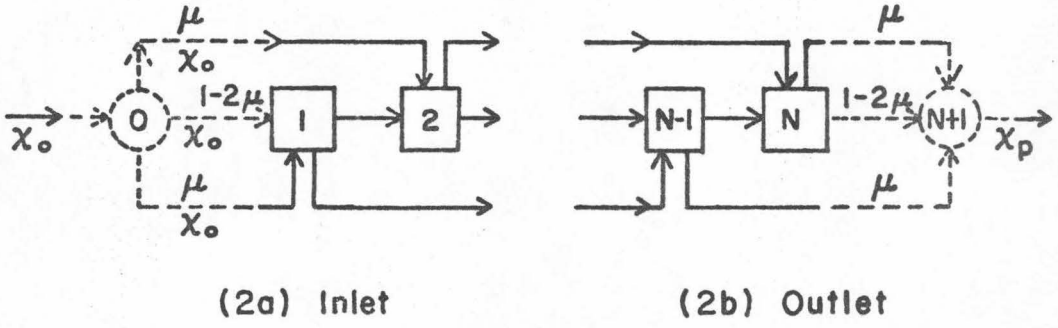

Fig. 2. The Two "Fictitious" End Cells

$$\varepsilon \frac{\partial x(z)}{\partial t} = -v \frac{\partial x(z)}{\partial z} + \varepsilon D_e \frac{\partial^2 x(z)}{\partial z^2} \tag{12}$$

the following relationship is obtained

$$(1+2\mu) \frac{vh}{2} = \varepsilon D_e \tag{13}$$

Therefore,

$$\mu = \frac{1}{2}\left(\frac{2D_e}{hv/\varepsilon} - 1\right) \tag{14}$$

$$= \frac{1}{2}\left(\frac{2}{Pe} \frac{d_p}{h} - 1\right) \tag{15}$$

where the Peclet number of adsorbate in packed bed

$$Pe = d_p u/D_e \quad \text{and} \quad u = v/\varepsilon \tag{16}$$

According to Deans and Lapidus [12], the Peclet number is usually less than 2, and is close to 2 for gas phase. Thus it is clear from Eq. (15) that μ is usually small. Note that the above expression for μ holds only under the condition of small h, as it is the basic requirement for truncating the Taylor series expansions. For larger h this expression only serves as an approximation.

To make the physical picture in each portion of a packed bed consistent, two "fictitious" cells are introduced at both ends as shown in Figures 2a and 2b. These two cells contribute zero volume and involve no reaction. The function of the front end cell is just to split the inlet flow into the main stream and bypassing streams while the back end cell combines the main stream with bypassing streams to form a single outlet flow. Therefore, the first cell has no effect on

the concentration, and the output concentration is obtained as

$$x_p = (1-\mu)\, x_N + \mu x_{N-1} \tag{17}$$

The Computational Schemes

Now, incorporating Eq. (3), the material balance Eqs.(6) and (2) about cell i become

$$(1-2\mu)\,\frac{G}{h}\,x_{i-1} + \mu\,\frac{G}{h}\,x_{i-2} - (1-\mu)\,\frac{G}{h}\,x_i - k_m a_s (x_i - f(\omega_i)) = 0 \tag{18}$$

$$\frac{d\omega_i}{d\tau} = x_i - f(\omega_i) \quad , \qquad 1 \le i \le N \tag{19}$$

where

$$\tau = (k_m a_s/(1-\varepsilon)\rho_s)t \tag{20}$$

and

$$\omega_i(0) = \omega_{io}$$

Equation (18) can be rewritten as

$$-\mu x_{i-2} - (1-2\mu)x_{i-1} + (1-\mu+\alpha_m)x_i = \alpha_m\, f(\omega_i) \tag{21}$$

where

$$\alpha_m = k_m a_s \frac{h}{G} = k_m a_s \frac{\theta}{\rho_f} \tag{22}$$

Given boundary condition $x_o(\tau)$, the concentration profile along the packed bed can be described by the following matrix equation:

$$\begin{bmatrix} 1 & & & & & & \\ -b_m & 1 & & & & 0 & \\ -\delta_m & -b_m & 1 & & & & \\ & \ddots & \ddots & \ddots & & & \\ & & & -\delta_m & -b_m & 1 & \\ & & 0 & & -\delta_m & -b_m & 1 \end{bmatrix} \begin{pmatrix} x_1 \\ x_2 \\ x_3 \\ \vdots \\ x_{N-1} \\ x_N \end{pmatrix} = \begin{pmatrix} (b_m+\delta_m)x_o+a_m f(\omega_1) \\ \delta_m x_o + a_m f(\omega_2) \\ a_m f(\omega_3) \\ \vdots \\ a_m f(\omega_{N-1}) \\ a_m f(\omega_N) \end{pmatrix} \tag{23}$$

where $\delta_m = \mu/(1-\mu+\alpha_m)$, $a_m = \alpha_m/(1-\mu+\alpha_m)$

$$b_m = (1-2\mu)/(1-\mu+\alpha_m) \tag{24}$$

The above matrix equation is denoted by

$$\vec{A}\, \underset{\sim}{x} = \underset{\sim}{g}_m \tag{25}$$

where $\vec{A}$ is a constant matrix with only three nonzero diagonals. Note that Eq. (23) is in fact a set of uncoupled algebraic equations in a sense that the solution of the first equation is obtained individually and the latter solutions are successively generated from the following recursion relationship

$$x_i = a_m f(\omega_i) + \delta_m x_{i-2} + b_m x_{i-1} , \qquad 1 \leq i \leq N \tag{26}$$

where $x_{-1} \triangleq x_o$. The computational algorithm is as follows:

(a) Given the distribution of ω_i's $(1 \leq i \leq N)$ at time τ , x_i's $(1 \leq i \leq N)$ are calculated from algebraic Eq. (23) or (26).

(b) These solutions together with ω_i's are substituted in the first order ordinary differential equation, Eq. (19), to obtain

ω_i's at the next time step.

Starting from $\tau = 0$, the above processes are repeated until the desired time τ_n.

The original partial differential equations are thus converted into a set of algebraic equations (Eq. (23)) and a set of first order ordinary differential equations (Eq. (19)), whereas the regular method of characteristics cannot be applied to the original differential equation in the presence of the diffusion term. Furthermore, the resulting form reduces the original complexity to a great extent due to its mathematical simplicity and its suitability to digital computer operation.

The solutions of Eq. (23) can also be found explicitly through Cramer's theorem, i.e.,

$$x_i = \det A_i \qquad \text{as} \quad \det A = 1 \tag{27}$$

where $\det A_i$ is the determinant of the matrix formed by replacing the i^{th} column of A by the vector g_m. After decomposing the determinant, the following well-behaved property can be found:

$$x_i = \ell_i x_o + \sum_{j=1}^{i} c_{i-j+1} f(\omega_j) \tag{28}$$

where

$$c_{i-j+1} = (-1)^{i+j} a_m (\det B_{ij}) \tag{29}$$

$$\ell_i = (-1)^{i+1} [(b_m + \delta_m) \det B_{i1} - \delta_m \det B_{i2}] \tag{30}$$

and matrix B_{ij} is defined as the $(i-1) \times (i-1)$ matrix

formed by deleting row j from the $(i) \times (i-1)$ matrix of upper left corner of A, and B_{1j} is defined as 1.

Equation (28) shows that x_i is a linear function of inlet feed condition x_o and the distribution of $f(\omega_j)$, where $j \leq i$. In matrix form Eq. (28) is written as $\vec{C}\,\underset{\sim}{f} = \underset{\sim}{x} - x_o \underset{\sim}{\ell}$, i.e.

$$\begin{bmatrix} c_1 & & & & 0 \\ c_2 & c_1 & & & \\ \cdot & \cdot & \cdot & & \\ c_{N-2} & \cdot & \cdot & \cdot & \\ c_{N-1} & c_{N-2} & \cdot & \cdot & \cdot \\ c_N & c_{N-1} & \cdots & c_2 & c_1 \end{bmatrix} \begin{pmatrix} f(\omega_1) \\ f(\omega_2) \\ \cdot \\ \cdot \\ \cdot \\ f(\omega_N) \end{pmatrix} = \begin{pmatrix} x_1 \\ x_2 \\ \cdot \\ \cdot \\ \cdot \\ x_N \end{pmatrix} - x_o \begin{pmatrix} \ell_1 \\ \ell_2 \\ \cdot \\ \cdot \\ \cdot \\ \ell_N \end{pmatrix} \tag{31}$$

The coefficient matrix C and vector ℓ are stationary as their elements are functions of α_m and μ, which are assumed to be constant. As the triangular matrix C is nonsingular, the inverse of $\vec{C}$ exists, and then $\underset{\sim}{f}(\omega)$ can be obtained directly in terms of $\underset{\sim}{x}$. As to the solution of ω_i, from Eqs. (28) and (19) one obtains

$$\frac{d\omega_i}{d\tau} + pf(\omega_i) = \ell_i x_o + L(f(\omega_1), \cdots, f(\omega_{i-1})) \quad , \quad 1 \leq i \leq N \tag{32}$$

where

$$p = 1 - a_m \quad , \quad L = \sum_{j=1}^{i-1} c_{i-j+1}\, f(\omega_j) \tag{33}$$

Again, Eq. (32) is a set of uncoupled first order ordinary differential equations where solutions of earlier sections of the bed (i.e., ω_j, $j < i$) are fed into the present equation to carry out the integration.

In the case that f is linear, analytical solutions can be obtained as for $i = 1$

$$\omega_1(\tau) = \omega_1(0)e^{-p\tau} + x_o(1 - e^{-p\tau})\, \ell_1/p \tag{34}$$

for $i = 2$

$$\omega_2(\tau) = [\omega_2(0) + c_2(\omega_1(0) - x_o\ell_1/p)\tau]e^{-p\tau} + x_o(1-e^{-p\tau})(\ell_2+c_2\ell_1/p)/p \tag{35}$$

Although the process of successive integration becomes cumbersome for large values of i, it is not difficult to obtain an analytical form in principle.

From the above derivations (i.e., from Eq. (18) to Eq. (35)), the following points are clearly demonstrated: how the solutions x_i and ω_i interrelate to each other, what are their functional dependences on time and position along the packed bed, and how the dynamic behavior of the system is affected by the initial conditions, boundary conditions, and the functionality of f. In short, this proposed bypass cell model allows us to gain a deep insight into the physical process and has certainly a great advantage over a strict numerical discretization method.

3. Adiabatic Adsorption Analysis

In practice most adsorbent beds are operated adiabatically. It is usually difficult to maintain isothermal conditions due to the heat effect accompanying the adsorption process. Under adiabatic operation the equilibrium adsorbate concentration at the surface of adsorbent is

a function of both the amount of adsorbate in the adsorbent ω and the temperature of local adsorbent bed T_s, that is,

$$x^* = f(\omega, T_s) \tag{36}$$

Since the mass transfer rate is a linear function of x^*, the resulting adsorption process is markedly influenced by change in the temperature.

Mathematical Formulation and Computation Schemes

For adiabatic adsorption two energy relations must be added to the continuity Eqs. (6) and (2). Again, under the pseudo-steady state approximation as before, it is found in a straightforward manner referring to a standard control volume that

$$G\, c_{p_f} \frac{\partial T}{\partial z} - \varepsilon k_e \frac{\partial^2 T}{\partial z^2} = h_t a_s (T_s - T) \tag{37}$$

$$(1-\varepsilon)\rho_s c_{p_s} \frac{\partial T_s}{\partial t} = -h_t a_s (T_s - T) + (\Delta H) k_m a_s (x - x^*) \tag{38}$$

where T is the temperature of the fluid

T_s is the temperature of the adsorbent

h_t is the heat transfer coefficient from the adsorbent to the fluid with units of $BTU/ft^2 sec\,^oF$

ΔH is the heat of adsorption in BTU/lb_x

k_e is the effective thermal conductivity, which includes actual thermal conductivity along with other heat dispersion effects, e.g., the heat transfer accompanying the channeling effect in a non-ideal flow.

Initial and boundary conditions are

$$T(0,t) = T_o(t) \tag{39}$$

$$T_s(z,0) = T_{so}(z) \tag{40}$$

Now the same approach as in the isothermal case can be adopted. To avoid repetition the detailed description is omitted, and the computational equations are written out directly after carrying out the bypass cell modelling:

$$(1-2\mu)\frac{Gc_{p_f}}{h}T_{i-1} + \mu\frac{Gc_{p_f}}{h}T_{i-2} - (1-\mu)\frac{Gc_{p_f}}{h}T_i + h_t a_s (T_{s_i} - T_i) = 0 \tag{41}$$

$$\frac{dT_{s_i}}{d\tau} = -Le\,\frac{c_{p_f}}{c_{p_s}}(T_{s_i} - T_i) + \frac{\Delta H}{c_{p_s}}(x_i - f(\omega_i, T_{s_i})) \tag{42}$$

where Le (Lewis number) = $h_t/k_m c_{p_f}$.

Define

$$\alpha_t = h_t a_s h/(Gc_{p_f}) = h_t a_s \theta/(\rho_f c_{p_f}) \tag{43}$$

Equation (41) can be written in matrix form (i.e., $\vec{D}\,\underset{\sim}{T} = \underset{\sim}{g}_t$) as

$$\begin{bmatrix} 1 & & & & & & & \\ -b_t & 1 & & & & & 0 & \\ -\delta_t & -b_t & 1 & & & & & \\ & \cdot & \cdot & \cdot & & & & \\ & & \cdot & \cdot & \cdot & & & \\ & & & \cdot & \cdot & \cdot & & \\ & & & & -\delta_t & -b_t & 1 & \\ & 0 & & & & -\delta_t & -b_t & 1 \end{bmatrix} \begin{pmatrix} T_1 \\ T_2 \\ T_3 \\ \cdot \\ \cdot \\ \cdot \\ T_{N-1} \\ T_n \end{pmatrix} = \begin{pmatrix} (b_t+\delta_t)T_o + a_t T_{s_1} \\ \delta_t T_o + a_t T_{s_2} \\ a_t T_{s_3} \\ \cdot \\ \cdot \\ \cdot \\ a_t T_{s(N-1)} \\ a_t T_{s_N} \end{pmatrix} \tag{44}$$

where

$$\delta_t = \mu / (1-\mu+\alpha_t) \ , \quad a_t = \alpha_t / (1-\mu+\alpha_t) \ ,$$

$$b_t = (1-2\mu)/(1-\mu+\alpha_t) \tag{45}$$

In other words, the following recursion relation holds

$$T_i = a_t T_{s_i} + \delta_t T_{i-2} + b_t T_{i-1} \tag{46}$$

where

$$T_{-1} \triangleq T_o \tag{47}$$

Note that for Le = 1

$$\alpha_t = \alpha_m \ , \quad \delta_t = \delta_m \ , \quad b_t = b_m \ , \quad \text{and} \quad a_t = a_m \tag{48}$$

Under usual adsorption operating conditions the Lewis number, which is also equal to $k_e/\rho_f c_{p_f} D_e$, is close to unity; see [8]. In the present study heat and mass dispersion effects come from the same channeling flow so that the Lewis number is equal to unity exactly. Therefore, the above approximating expressions in Eq. (48) can further simplify the computation scheme.

The computational algorithm is as follows:

(a) Given distributions of T_{s_i} and ω_i's $(1 \le i \le N)$ at time τ, T_i's and x_i's $(1 \le i \le N)$ are calculated from algebraic Eqs. (44) and (23).

(b) These solutions together with T_{s_i} and ω_i's are substituted into first order ordinary differential equations (42) and (19) to obtain T_{s_i} and ω_i's at the next time step.

Starting from $\tau = 0$ the above processes are repeated until the desired time τ_n. The exit fluid temperature of the packed bed is obtained as

$$T_p = (1-\mu)T_N + \mu T_{N-1} \tag{49}$$

Again, the fluid temperature can be expressed as a linear combination of the inlet temperature and the adsorbent temperatures along the bed as

$$T_i = m_i T_o + \sum_{j=1}^{i} S_{i-j+1} T_{s_j} \tag{50}$$

where

$$S_{i-j+1} = (-1)^{i+j} a_t (\det E_{ij}) \tag{51}$$

$$m_i = (-1)^{i+1} [(b_t+\delta_t)\det E_{i1} - \delta_t \det E_{i2}] \tag{52}$$

and matrix E_{ij} is defined as the $(i-1) \times (i-1)$ matrix formed by deleting row j from the $(i) \times (i-1)$ matrix of upper left corner of $\vec{D}$, and E_{ij} is defined as 1 .

In matrix form Eq. (50) is written as $\vec{S}\, \underset{\sim}{T}_s = \underset{\sim}{T} - T_o \underset{\sim}{m}$,

i.e.,

$$\begin{bmatrix} S_1 & & & & & & \\ S_2 & S_1 & & & & & \\ S_3 & S_2 & S_1 & & & & \\ \cdot & \cdot & \cdot & \cdot & & & \\ S_{N-1} & \cdot & \cdot & \cdot & \cdot & & \\ S_{N-1} & S_{N-2} & \cdot & \cdot & \cdot & \cdot & \\ S_N & S_{N-1} & \cdot & \cdot & \cdot & S_2 & S_1 \end{bmatrix} \begin{pmatrix} T_{S_1} \\ T_{S_2} \\ T_{S_3} \\ \cdot \\ \cdot \\ \cdot \\ T_{S_N} \end{pmatrix} = \begin{pmatrix} T_1 \\ T_2 \\ T_3 \\ \cdot \\ \cdot \\ \cdot \\ T_N \end{pmatrix} - T_o \begin{pmatrix} m_1 \\ m_2 \\ m_3 \\ \cdot \\ \cdot \\ \cdot \\ m_N \end{pmatrix} \tag{53}$$

That the solid temperature in earlier sections of the bed is independent of that in the latter parts is obvious from the triangular form of matrix S. Combining Eqs. (28), (46), and (42) gives

$$\frac{dT_{s_i}}{d\tau} + p(1 - a_t)T_{s_i} + q(1 - a_m)\, f(\omega_i, T_{s_i}) = pm_i T_o + q\ell_i x_o + p \sum_{j=1}^{i-1} S_{i=j+1} T_{s_j} + q \sum_{j=1}^{i-1} c_{i-j+1} f(\omega_j, T_{s_j}) \tag{54}$$

where

$$p = \text{Le}\, c_{p_f}/c_{p_s}\ , \quad q = (\Delta H)/c_{p_s} \tag{55}$$

Therefore the coupled heat and mass dynamics in the adsorbent are described in the following functional form.

$$\frac{dT_{s_i}}{d\tau} + \phi(T_{s_i}, \omega_i) = \Phi(T_{s_1}, \cdots, T_{s_{i-1}}; \omega_1, \cdots, \omega_{i-1}; T_o; x_o) \tag{56}$$

$$\frac{d\omega_i}{d\tau} + \psi(T_{s_i}, \omega_i) = \Psi(T_{s_1}, \cdots, T_{s_{i-1}}; \omega_1, \cdots, \omega_{i-1}; x_o) \tag{57}$$

These simultaneous ordinary differential equations become linear if the

equilibrium relationship f is linear, and the above computational schemes resulting from the bypass cell modelling are particularly advantageous for use with the high speed digital computer.

4. Results and Discussion

Comparison of the Proposed Model with Published Experimental Data

The literature data on the adsorption of water vapor from air by silica gel are available to verify the proposed bypass cell model. Two representative experimental runs of Bullock [8], chosen by Chi and Wasan [7] in supporting their models, are also adopted here as the comparison basis. These data are compared with the present predictions and with the results obtained by Bullock-Threlkeld [8] and Chi-Wasan [7] plus the prediction by the Hougen-Marshall model [4] as shown in Figures 3-7. The notations I and A in the plot stand for isothermal and adiabatic adsorption respectively. The line with circled points (Curve 1) shows Bullock's experimental results. The solid lines (Curve 2I and 2A) show the proposed bypass-cell-model predictions. Also shown on these plots are the results of Chi's isothermal analysis (Curve 3I), Hougen-Marshall's isothermal prediction (Curve 4I) and Bullock and Chi's identical adiabatic analysis (Curve 3A).

A general nonlinear expression used in this work for the equilibrium concentration of the adsorbate at the solid surface x^* is described in Appendix B. The experimental operating conditions and the pertinent parameters required for the equations are assembled

in Appendix C.

(a) Isothermal Adsorption - Run No. 12 of Bullock [8]

Due to the low inlet air humidity and temperature, the rate of heat release is low and the system behaves like an isothermal adsorption process. Figure 3 compares the results. According to Chi and Wasan [7] the agreement between their isothermal predictions (i.e., Curve 3I) and the experimental data was quite satisfactory. As the results from the present proposed model (Curve 2I) lie between Curve 3I and the experimental data, the validity of the proposed bypass cell model is thus established. In fact, it is shown in the figure that the present analysis yields better simulation of a real adsorption process than the other available theoretical predictions.

(b) Adiabatic Adsorption - Run No. 11 of Bullock [8]

When water vapor is adsorbed by the desiccant, heat is released because the adsorption process is exothermic. Under adiabatic operation the heat released raises the temperature of the bed and this rise in temperature decreases the adsorption rate. The results are presented in Figure 4. The effluent air temperature rises very rapidly due to the initial high rate of adsorption, after which it slowly decreases as the bed approaches equilibrium with the inlet air. Agreement between experimental and theoretical results is quite good, and the proposed scheme is again better than the other predictions.

In view of the results of both isothermal and adiabatic adsorptions, the proposed bypass cell model is believed to represent a real adsorption process in a packed bed properly. However, the most

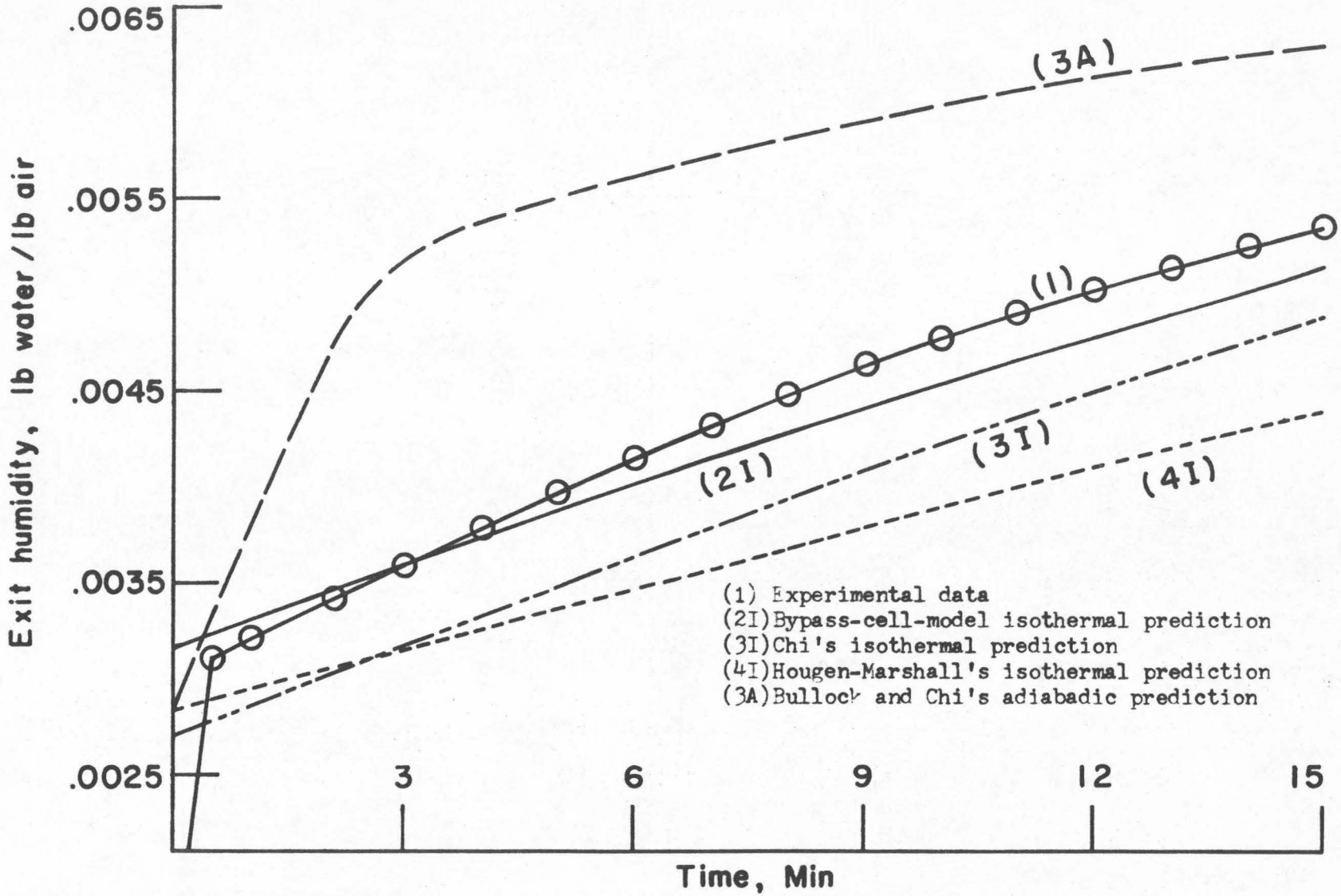

Fig. 3. Comparison between Experimental and Predicted Exit Humidities (Run No. 12)

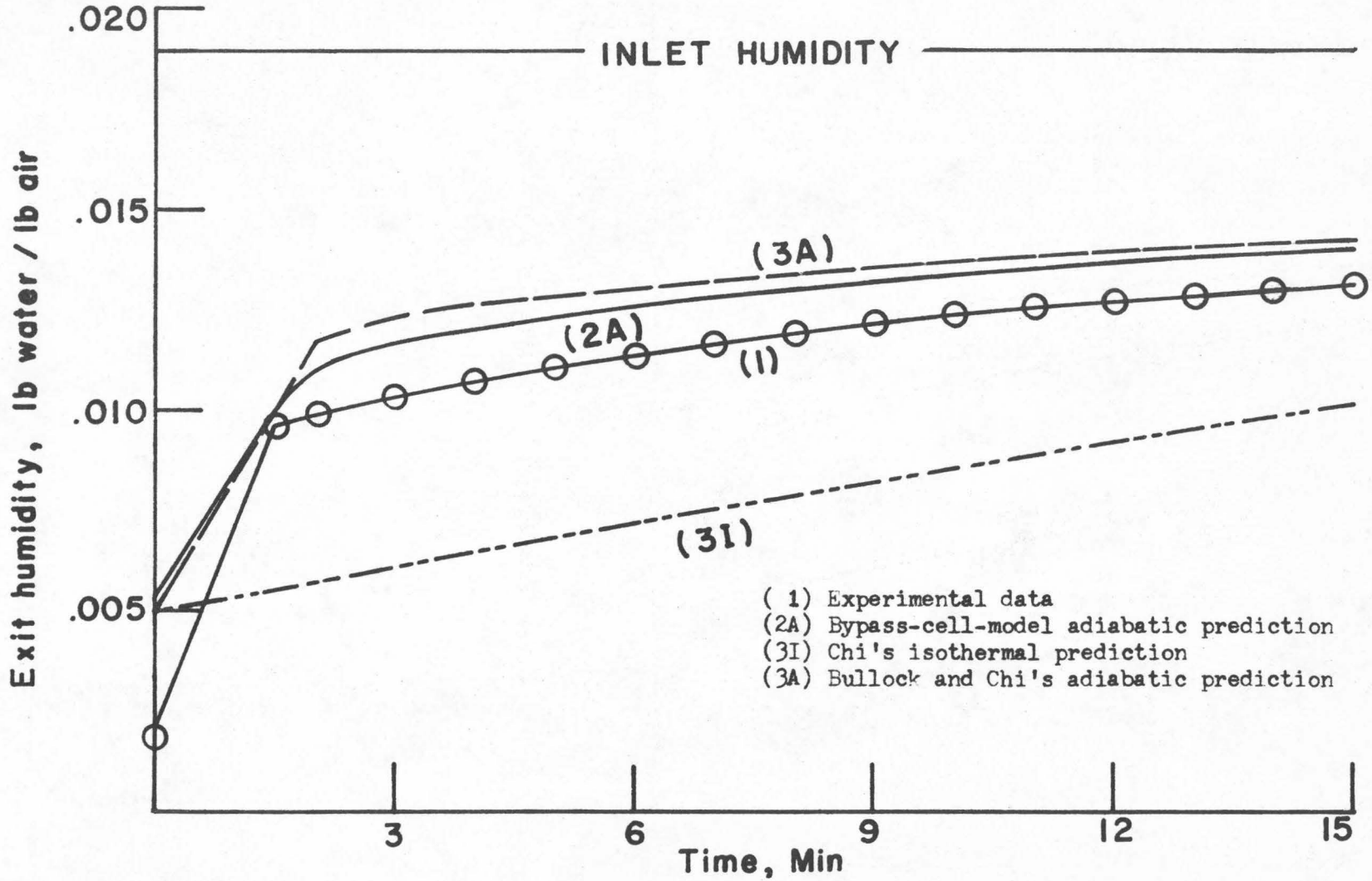

Fig. 4. Comparison between Experimental and Predicted Exit Humidities (Run No. 11)

significant advantage of this model lies in its suitability and convenience for computation. Two typical computer programs are enclosed in Appendix D for reference. A representative set of computing times on IBM 360/75 is listed in the following table for the case of five cells along the bed with the number of time increments per run denoted by K .

*K (units)	Type Isothermal	Adiabatic
100	2.06 sec	3.39 sec
300	6.20 sec	7.74 sec

*Every 20 units in K are equivalent to one minute real time in the present study.

Effects of Modelling Parameters

As shown in the above results, the local mixing around the vicinity of each pellet and the channeling flow pattern do exist in a real adsorption packed bed due to the good match of the predictions by the bypass cell model with the experimental data. However, their amounts are limited by the operating conditions. A good simulation should consist of appropriate proportions of both.

(a) Effect of cell length (h)

The CSTR part of the bypass cell model simulates the local mixing effect. The amount of mixing is revealed approximately by an optimal length of modelling cell. A typical picture of this cell

length effect, with a five percent bypass to overall stream ratio, is shown in Figure 5. Each curve refers to the approximate ratio of its cell length to the diameter of silica gel adsorbent. In this period of operation, an optimal cell length seems to lie in the vicinity of 1.5 dp , even though all the results whose cell lengths range from 0.7 dp to 2.4 dp are satisfactory compared to the other models given in the literature. As time increases, the differences between different cell lengths become smaller. For two cell lengths with similar deviations from the experimental data, a larger length is preferred as its corresponding scheme usually needs much less computing time. For instance, a simulation of adiabatic adsorption with 100 time units using five bypass cells instead of using ten cells cuts down the computing time from 4.57 sec. to 3.39 sec. That is about a 35% reduction. Since there is no integration involved in the z direction, the stability problem due to a choice of large cell length does not enter. Meanwhile, the lengths chosen in this work are all small enough to avoid any significant accumulation of truncation and round-off error. Finally, if a model with a smaller number of modelling cells for a packed bed (i.e., longer cell length) is chosen, the material transfer into the adsorbent is also less. This is consistent with the well-established theory on reactor design; namely, for a first order reaction taking place in a reactor with fixed residence time, a model with more CSTR's achieves a greater conversion and in the limit the conversion approaches that of a plug flow reactor.

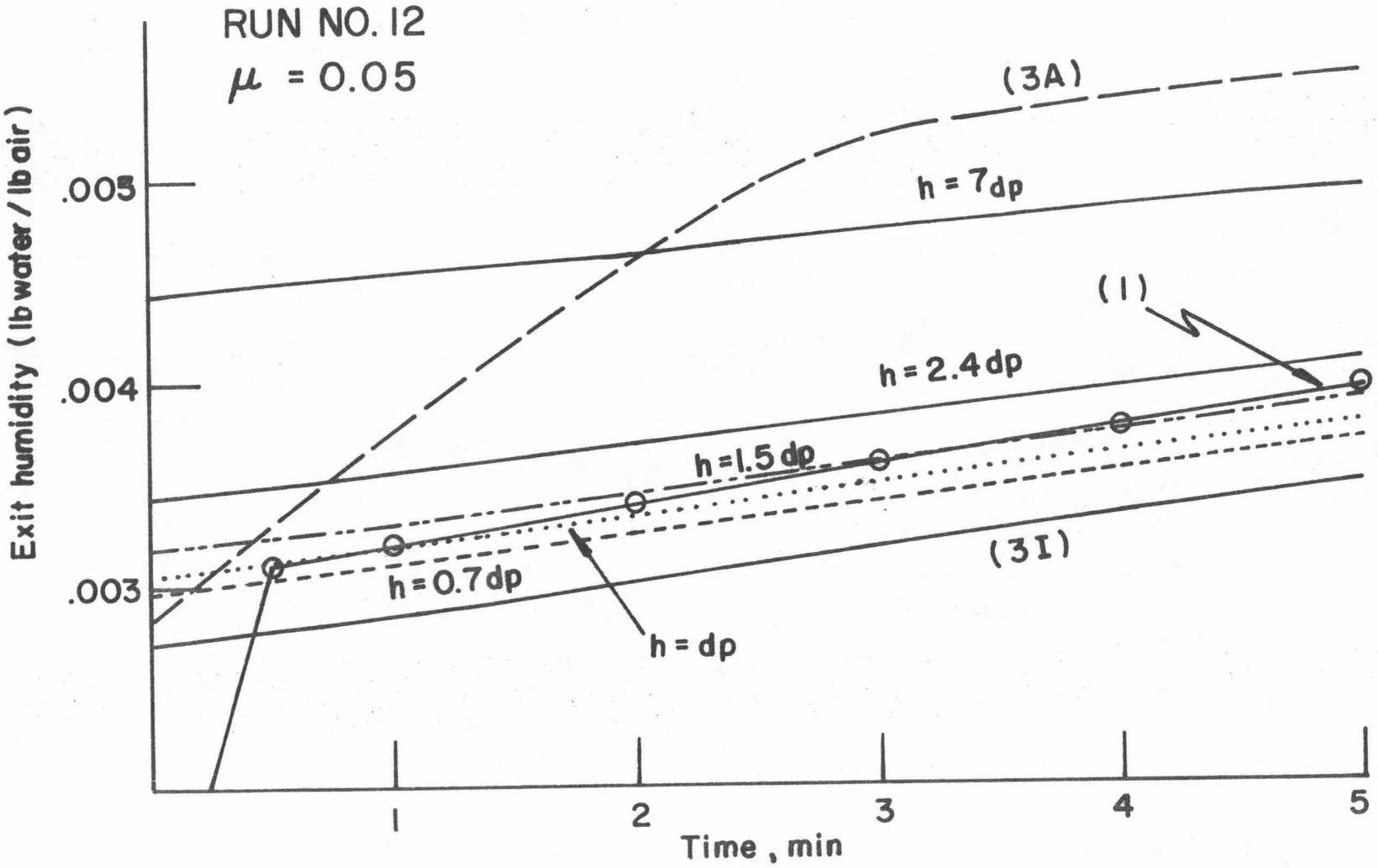

Fig. 5. Effect of Cell Length on Exit Humidities

(b) Effect of bypass ratio (μ)

The amount of channeling effect is revealed approximately by the bypass ratio. It is obvious that the greater the bypass ratio is, the less material that is transferred to the adsorbent; and then the effluent humidity is higher. The results are presented in Figure 6. For a model with more cells the effect of bypass ratio will be reduced, which is to be expected physically. This indicates that the effect of bypass ratio and that of cell length are coupled to each other. For the experimental run No. 12, it seems that an appropriate bypass ratio lies in the range of 5% to 10% with five cell modelling. As shown in the plot, the bypassing stream seems to create a parallel shift from the original curve. This shift may contribute to the parallel offset in a later period of the adsorption process as indicated in Figures 3 and 4, since bypass ratio is expected to rise when the on-stream time of adsorbents increases and the adsorbents become more saturated.

A Modification on Adiabatic Adsorption Modelling

Although the agreement between the proposed predictions and the experimental data is quite good, a common phenomenon shared with all previous investigations is observed in adiabatic silica gel adsorption processes. In the latter period of each run the theoretical predictions of effluent humidity always lie parallel to the experimental data with higher values. This discrepancy was defended in the literature as probably due to the heat losses, to uncertainties in the equilibrium vapor pressure data, the heat of wetting data, and in determining the initial bed moisture content, and to the simplifying assumptions made.

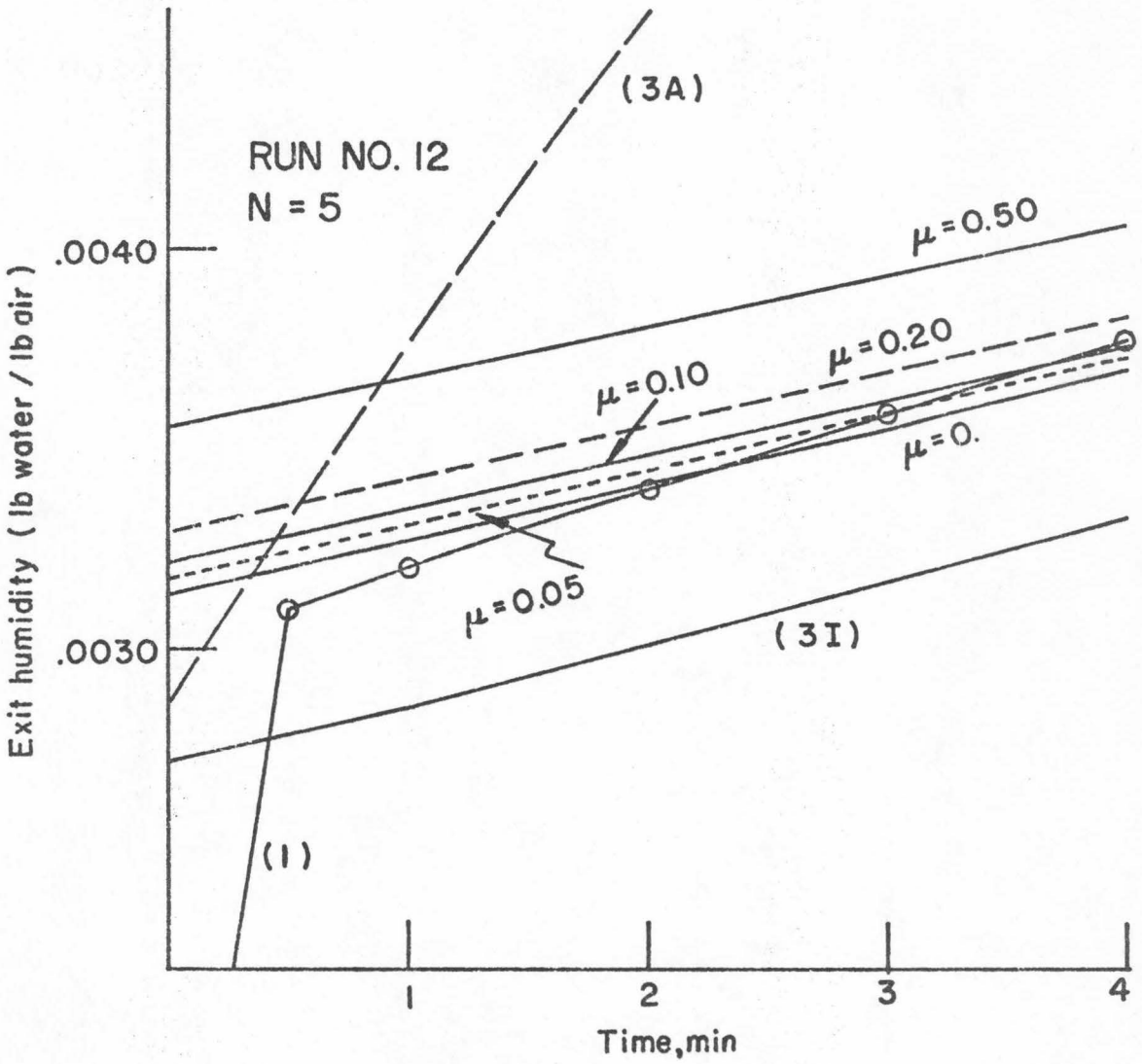

Fig. 6. Effect of Bypass Ratio on Exit Humidities

In this work the following reasoning is presented.

The function of the adsorption heat is to decrease the mass transfer rate by yielding higher equilibrium surface concentration and thereby reducing the mass transfer driving force. Thus, heat brings the adsorption level down and raises the effluent temperature. At the beginning of an adsorption run the adsorbent bed is fresh. Once the water vapor diffuses into the adsorbent, the adsorption takes place instantaneously in the form of condensed water with its latent heat released. As time goes on, the adsorbent becomes more and more saturated with water. This may cause two possible results in addition to the well-recognized decrease of mass transfer rate due to the reduced diffusion driving force. One is that the adsorption reaction rate constant becomes smaller. The other is that a portion of the adsorpted adsorbate may still remain in the vapor phase without releasing its heat in condensation. Both of these two possibilities will result in a lesser amount of adsorption heat generated. Therefore, the rate of heat released (i.e., the last term in Eq. (38)) should be built in with a decreasing functionality. This is accomplished by introducing the following simple linear function of the equilibrium adsorbate concentration at the surface of adsorbent x^* which is a function of both adsorbent water content and adsorbent temperature:

$$d_i = 1 - \left(\frac{x_i^* - x_i^*(t=0)}{x_\infty^* - x_i^*(t=0)}\right) \quad , \quad 1 \leq i \leq N \tag{58}$$

where x_∞^* is the final equilibrium concentration which is equal to the inlet concentration x_o if constant inlet condition is kept eventually

Note that at the very beginning $d_i = 1$. At the end $d_i = 0$ and the system behaves isothermally. The result is surprisingly good as indicated in Figure 7. The effluent humidity is lowered toward the experimental values. The degree of this downward curve-shifting may actually be controlled by multiplying the term in parenthesis of Eq. (58) by a scaling factor. However, this factor is not studied here as it is too arbitrary and without theoretical support. In conclusion, it is obvious now that for most adiabatic adsorptions the heat generating rate may decrease with time as the adsorbents become more saturated and may approach that of an isothermal operation in the limit.

Further Discussion

The above sections have demonstrated clearly the good representations of adsorption processes in packed beds and the corresponding fast computations. Here, additional possible applications of this model are discussed qualitatively.

(a) Determination of heat and mass transfer coefficient h_t and k_m

It is indicated by Eq. (50) that the fluid temperature $T(z)$ is an algebraic function of the adsorbent temperature T_s , and the heat transfer coefficient h_t . Suppose the temperature measurements on both T and T_s are carried out at several points along the packed bed, the heat transfer coefficient h_t can be obtained by means of nonlinear regression technique. Similarly, the mass transfer coefficient k_m can be calculated from measurements of absorbate contents both in the fluid (x) and in the absorbent (ω) at several points along the bed.

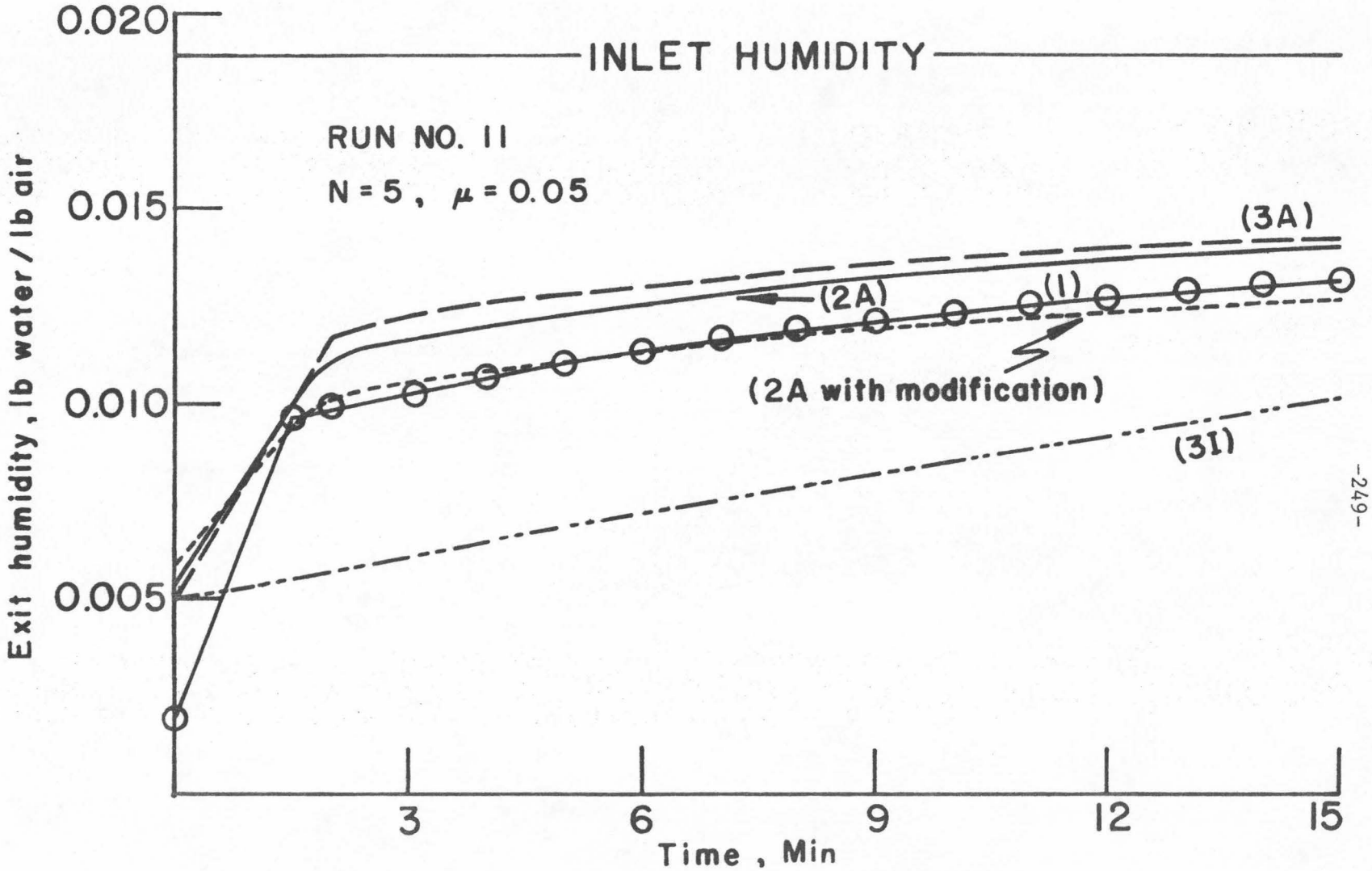

Fig. 7. Effect of the Modified Rate of Heat Generation on Exit Humidities

(b) Optimization

Due to the simplicity and linearity of the resulting scheme, the proposed bypass cell model is believed to be particularly suitable to carry out the optimization processes necessary for determining certain operating variables such as bed length, flow rate, and the adsorbent material.

(c) Estimation of adsorbate content distribution in the adsorbent

With the adsorbate content in the fluid as a known function of that in the adsorbent as indicated in Eq. (28), the latter can be estimated from the measurements on the former in a straightforward manner via least squares minimization.

Finally, because of the inherent nature of cell model, the usual assumptions of uniform initial distribution and constant inlet conditions are no longer needed. This makes possible the application to a bed containing initially several sections of different adsorbate content.

APPENDICES

A. AN ANALYTICAL SCHEME FOR RATE DETERMINING ADSORPTION PROCESS

B. A NONLINEAR EXPRESSION FOR THE EQUILIBRIUM CONCENTRATION

C. EXPERIMENTAL OPERATING CONDITIONS

D. COMPUTER PROGRAMS AND THE INTEGRATION ALGORITHM

APPENDIX A

AN ANALYTICAL SCHEME FOR RATE DETERMINING ADSORPTION PROCESS

The main chapters of this work deal with the regular adsorption processes, where diffusion is the rate determining step. However, if kinetic rate controlling is observed (e.g., a water softening process with zeolite bed [15]), a simpler analytical solution via the method of characteristics can be obtained for the case of negligible axial diffusion in the fluid.

In general, an adsorption reaction rate can be expressed as

$$r_a = kx\, g(\omega) \tag{A.1}$$

where g is a nonlinear function of ω and the dynamic system consists of the following set of quasi-linear hyperbolic partial differential equations.

$$\frac{\partial x}{\partial \xi} = -x\, g(\omega) \tag{A.2}$$

$$\frac{\partial \omega}{\partial \tau} = x\, g(\omega) \tag{A.3}$$

where

$$\xi \triangleq (k/G)z \quad , \quad \tau \triangleq (k/(1-\varepsilon)\rho_s)t \tag{A.4}$$

Combine (A.2) and (A.3) as

$$\frac{\partial x}{\partial \xi} = -\frac{\partial \omega}{\partial \tau} \tag{A.5}$$

and then integrate (A.5) along constant ξ to yield

$$\frac{\partial \theta(\xi,\tau)}{\partial \xi} = \omega_o - \omega \tag{A.6}$$

where

$$\theta(\xi,\tau) \triangleq \int_0^\tau x(\xi,\tau')d\tau' \tag{A.7}$$

On the other hand, integration along constant ξ in (A.3) gives

$$\theta(\xi,\tau) = \int_{\omega_o}^{\omega} \frac{\partial\omega'}{g(\omega')} \tag{A.8}$$

Differentiating (A.8) with respect to ξ by Leibnitz rule results in

$$\frac{\partial\theta}{\partial\xi} = \frac{1}{g(\omega)} \frac{\partial\omega}{\partial\xi} \tag{A.9}$$

Therefore, from (A.6) and (A.9) one obtains

$$\frac{d\omega}{d\xi} = (\omega_o - \omega)\, g(\omega) \quad \text{along constant } \tau \tag{A.10}$$

and its initial condition $\omega(0,\tau)$ is obtained from (A.3) as

$$\int_{\omega_o}^{\omega(0,\tau)} \frac{d\omega'}{g(\omega')} = x_o\tau \tag{A.11}$$

The solution of (A.10) and (A.11) is substituted into (A.2) to form the ordinary differential equation for x along constant τ as

$$\frac{dx}{d\xi} = -x\, g[\omega(\omega_o,\omega(0,\tau))] \tag{A.12}$$

with initial condition $x(0,\tau) = x_o$. For linear g the solutions can be readily obtained in closed form as follows:

$$\omega(\xi,\tau) = \frac{\omega_o}{1 - \exp(-\omega_o\xi)[1 - \exp(-x_o\tau)]} \tag{A.13}$$

$$x(\xi,\tau) = \frac{x_o}{1 + \exp(-x_o\tau)[1 - \exp(-\omega_o\xi)]} \qquad (A.14)$$

APPENDIX B

A NONLINEAR EXPRESSION FOR THE EQUILIBRIUM CONCENTRATION

Hubard [16] has presented data for the vapor pressure of water in equilibrium with silica gel having a given moisture content, at the same temperature. The data are fairly complete, covering a temperature range of $40^{\circ}F$ to $200^{\circ}F$, adsorbed water content from slightly above zero to 35%, and vapor pressures from slightly above zero to 16 inches of mercury, and are applicable to essentially all commonly used grades of silica gel. Figure B shows these data on semilogarithmic coordinates.

To facilitate their use in a numerical calculation procedure, the equilibrium vapor pressure data in Figure B were expressed by Bullock [8] as polynomials in temperature and moisture content over specific intervals of the latter quantity. The polynomials are of the form:

$$P^* = (AT^3 + BT^2 + CT + D)\omega^m + (ET^3 + FT^2 + GT + R)\omega^n \qquad (B.1)$$

where P^* is the equilibrium vapor pressure, inches of mercury;

T is the temperature, $^{\circ}F$;

ω is the silica gel moisture content, lb_x/lb_s ;

$A, B, \cdots, R$ are constants;

$m = 2$ and $n = 1$ for ω less than 0.05 ;

$m = 1$ and $n = 0$ for ω greater than 0.05.

Each set of constants A through R applies to a specific interval in moisture content.

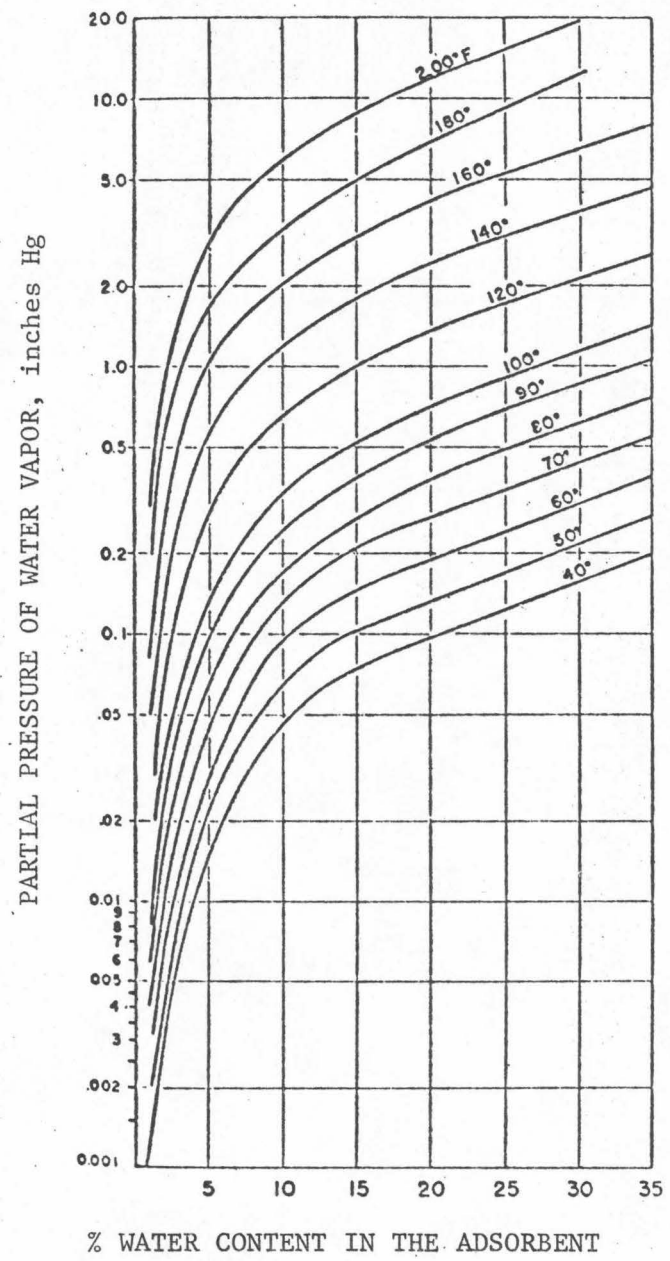

Fig. B. Adsorbed Water Capacity of Regular Silica Gel as a Function of Partial Pressure at Various Temperatures (Equilibrium Isothermals)

For constant moisture constant

$$(P^*)_\omega = aT^3 + bT^2 + cT + d \qquad (B.2)$$

(a) Quadratic segment (ω less than 0.05)

Knowing the coefficients of equation (B.2) for two values of ω within the interval; that is,

$$\text{for } \omega = \omega_1 \qquad P^* = a_1T^3 + b_1T^2 + c_1T + d_1$$

$$\text{and for } \omega = \omega_2 \qquad P^* = a_2T^3 + b_2T^2 + c_2T + d_2 \qquad (B.3)$$

one may easily show that for $k = x_1x_2(x_2-x_1)$

$$A = (a_2x_1 - a_1x_2)/k \qquad B = (b_2x_1 - b_1x_2)/k$$

$$C = (c_2x_1 - c_1x_2)/k \qquad D = (d_2x_1 - d_1x_2)/k$$

$$E = (a_1x_2^2 - a_2x_1^2)/k \qquad F = (b_1x_2^2 - b_2x_1^2)/k \qquad (B.4)$$

$$G = (c_1x_2^2 - c_2x_1^2)/k \qquad R = (d_1x_2^2 - d_2x_1^2)/k$$

(b) Straight line segments (ω greater than 0.05)

Knowing the values for the coefficients of equation (B.2) for the two end points ω_1 and ω_2 of a given interval, the coefficients of equations (B.1) may be readily calculated for $k = x_2-x_1$

$$A = (a_2-a_1)/k \ , \quad B = (b_2-b_1)/k \ , \quad C = (c_2-c_1)/k \ ,$$

$$D = (d_2-d_1)/k \ , \quad E = (x_2a_1 - x_1a_2)/k \ , \quad F = (x_2b_1 - x_1b_2)/k$$

$$G = (x_2 c_1 - x_1 c_2)/k \quad , \quad R = (x_2 d_1 - x_1 d_2)/k \qquad (B.5)$$

Equations (B.5) were evaluated for the six intervals with end points at $x = 0.05$, 0.10, 0.15, 0.20, 0.25, 0.30, and 0.35 lb_x/lb_s. Table B summarizes the values of the constants which were intended for use with P^* less than 1.0 inch mercury and temperatures between 70^oF and 180^oF, for which an accuracy of better than 2% in representing the original data may be obtained.

The equilibrium humidity ratio x^* is calculated by the perfect gas relation

$$x^* = 0.62197P^*/(P - P^*) \qquad (B.6)$$

where P is the total or barometric pressure.

TABLE B

COEFFICIENTS OF THE EQUILIBRIUM VAPOR PRESSURE

POLYNOMIAL, EQ. (B.1)

Range of Moisture Content, ω	$A \cdot 10^6$	$B \cdot 10^4$	C	D
$0 \leq \omega \leq 0.05$	402.263374	-893.827167	7.06882716	-182.152263
$0.05 \leq \omega \leq 0.10$	-7.80864197	43.1203703	-0.484787037	17.2044753
$0.10 \leq \omega \leq 0.15$	20.8333333	-38.25	0.255416667	-4.6825
$0.15 \leq \omega \leq 0.20$	53.3333333	-138.0	1.26466667	-38.0
$0.20 \leq \omega \leq 0.25$	-81.6666667	213.5	-1.75233333	47.60
$0.25 \leq \omega \leq 0.30$	40.0	-81.0	0.5990	-14.1
$0.30 \leq \omega \leq 0.35$	20.0	-37.0	0.291	-6.9

Range of Moisture Content, ω	$E \cdot 10^6$	$F \cdot 10^4$	G	R
$0 \leq \omega \leq 0.05$	11.8621399	-32.6790123	0.32929012	-10.4143621
$0.05 \leq \omega \leq 0.10$	1.98919753	-6.02453703	0.0580578703	-1.83632253
$0.10 \leq \omega \leq 0.15$	-0.875	2.1125	-0.0159625	0.352375
$0.15 \leq \omega \leq 0.20$	-5.75	17.075	-0.16735	5.35
$0.20 \leq \omega \leq 0.25$	21.25	-53.225	0.43605	-11.770
$0.25 \leq \omega \leq 0.30$	-9.1666667	20.4	-0.151783333	3.655
$0.30 \leq \omega \leq 0.35$	-3.1666667	7.2	-0.0593833333	1.495

APPENDIX C

EXPERIMENTAL OPERATING CONDITIONS

Two representative experimental runs (11 and 12 of Bullock [8]) for an adsorbent bed of silica gel were simulated on a digital computer with the models developed in the present study for isothermal and adiabatic dynamic adsorption processes.

The silica gel used in Bullock's study was the grade No. 03 commercial silica gel manufactured by the Davison Chemical Division of W. R. Grace Company with the following selected description

Gel Type	Tyler Sieve on 8
Average Diameter, d_p	0.152 in.
Individual Density, ρ_s	75 lbs/ft^3
Specific Heat, c_{p_s}	0.22 BTU/lb$_s$^{o}F
Specific external surface area, a_s	201 ft^2/ft^3

A summary of the experimental conditions is assembled in Table C. Note that the mass and heat transfer coefficients were determined from the empirical correlations for the adiabatic dynamic adsorption of water from humid air by silica gel presented by Hougen and Marshall [4] as

$$k_m = 0.704G\,(d_pG/\mu)^{-0.51} \qquad (C.1)$$

$$h_t = 0.671Gc_{p_f}(d_pG/\mu)^{-0.51}$$

where μ is the moist air viscosity.

The dimensionless Lewis number is obtained as

$$Le = h_t / k_m C_{p_f} \tag{C.3}$$

Finally, the time increment for integration is chosen as 3 sec.

TABLE C. SUMMARY OF EXPERIMENTAL CONDITIONS

		Run 11	Run 12
x_o	lb_x/lb_f	0.01896	0.00953
ω_o	lb_x/lb_s	0.0341	0.0401
T_o	^oF	81.5	71.6
T_{so}	^oF	80.2	71.9
P	in Hg	29.06	28.62
G	$lb_f/ft^2 sec$	0.05641	0.05710
ρ_f	lb_f/ft^3	0.0735	0.0748
$(1-\varepsilon)\rho_s$	lb_s/ft^3	41.81	41.81
C_{p_f}	$BTU/lb_f\ ^oF$	0.241	0.241
L	in	1.0	1.0
$k_m a_s$	$lb_f/ft^3 sec$	1.012	1.019
Le		0.953	0.953
*ΔH	BTU/lb_x	1040.0	1040.0

*Another expression for latent heat of water vapor [17] is

$\Delta H = 1060.91 + 0.44625T$ for $p < 1$ psia

APPENDIX D

COMPUTER PROGRAMS AND THE INTEGRATION ALGORITHM

Two typical computer programs for isothermal and adiabatic adsorptions respectively are listed in this appendix. The integration schemes used are described for the following system:

$$\begin{aligned} dY_i/dt &= f_i(t,Y_i) \qquad , \qquad 1 \leq i \leq N \\ Y_i(t_o) &= Y_{io} \end{aligned} \tag{D.1}$$

(a) In the early period of adsorption, a very accurate (4th order method) CIT library subroutine MODDEQ is called for integration. Since each time the integration is carried out just one step, the scheme used in MODDEQ is only the initialized Runge-Kutta-Gill method.

Let Y_{in} be the value of Y_i at $t = t_n$; f_{in} the derivative at $t = t_n$; and Δt the interval size of the independent variable t . The Runge-Kutta-Gill method uses the formulas:

$$\begin{aligned} k_{io} &= \Delta t f_i(t,Y_{in}) \\ Y_{in}^{(1)} &= Y_{in} + \frac{1}{2} k_{io} \\ q_{i1} &= k_{io} \end{aligned} \tag{D.2}$$

$$\begin{aligned} k_{i1} &= \Delta t f_i(t + \frac{\Delta t}{2}, Y_{in}^{(1)}) \\ Y_{in}^{(2)} &= Y_{in}^{(1)} + \frac{b_1}{2} (k_{i1} - q_{i1}) \\ q_{i2} &= b_1 k_{i1} + c_1 q_{i1} \end{aligned} \tag{D.3}$$

$$k_{i2} = \Delta t f_i(t + \frac{\Delta t}{2}, Y_{in}^{(2)})$$
$$Y_{in}^{(3)} = Y_{in}^{(2)} + \frac{b_2}{2}(k_{i2} - q_{i2}) \qquad (D.4)$$
$$q_{i3} = b_2 k_{i2} + c_2 q_{i2}$$

$$k_{i3} = \Delta t f_i(t + \Delta t, Y_{in}^{(3)})$$
$$Y_{i\ n+1} = Y_{in}^{(3)} + \frac{1}{6} k_{i3} - \frac{1}{3} q_{i3} \qquad (D.5)$$

where

$$b_1 = 2-\sqrt{2} \ , \quad c_1 = -2 + \frac{3\sqrt{2}}{2} \ , \quad b_2 = 2+\sqrt{2} \ , \quad c_2 = -2 - \frac{3\sqrt{2}}{2} \qquad (D.6)$$

(b) In the latter period of adsorption, a simple Predictor-Corrector method suggested by Acrivos [5] and Brand [18] is used. The numerical results obtained were compared with those from Runge-Kutta-Gill method. The agreement is excellent. The algorithm for Predictor-Corrector is as follows:

(i) Predicted value $$P_i(t_3) = Y_i(t_1) + 2\Delta t f_i(Y_i(t_2)) \qquad (D.7)$$

(ii) Corrected value

$$C_i(t_3) = Y_i(t_2) + (\frac{\Delta t}{2}) \{f_i(Y_i(t_2)) + f_i[P_i(t_3)]\} \qquad (D.8)$$

(iii) Final value

$$Y_i(t_3) = C_i(t_3) + (1/5)[P_i(t_3) - C_i(t_3)] \qquad (D.9)$$

```
C       ISOTHERMAL  ADSORPTION
C   --   BYPASS CELL MODEL  ---
        DIMENSION  X(32),W(32),F(32),BY(4),MAXK(8),MAXN(8),DT(8)
       1,WP(32,2),E(32)
        COMMON /WINTG/XX,FF
        REAL*4 H,LENGTH,KMAS
        EXTERNAL DERIV
  508 FORMAT (8I10)
  514 FORMAT (4E20.7)
  603 FORMAT (20X,4E20.7)
  606 FORMAT (/,5X,6E20.7,/)
  610 FORMAT (/,1X,10E13.6)
C       READ IN EXP. DATA & MODELING PARAMETERS; THEN CALCULATE
C       DYNAMIC PARAMETERS
        READ (5,514) LENGTH,G,KMAS,PSBULK
        CO= KMAS/PSBULK
        READ (5,514) P,XO
        READ (5,514) WIO,TSIO
        READ (5,508) KMAX,NMAX,LMAX,KPREDT,KPTM2
        READ (5,508) (MAXK(J),J=1,KMAX)
        READ (5,514) (DT(J),J=1,KMAX)
        READ (5,508) (MAXN(J),J=1,NMAX)
        READ (5,514) (BY(J),J=1,LMAX)
        WRITE (6,604) XO,WIO,P,TSIO
  604 FORMAT (/,10X,'XO; WIO; P; TSIO: ',4E16.7)
        X(1)= XO
        X(2)= XO
C KK -- EACH KK REPRESENTS A DIFFERENT TIME INTERVAL --
        DO 1000 KK=1,KMAX
        DTAU= CO*DT(KK)
        MAXKP= MAXK(KK) + 1
C    INTEGRATION OF INLET W(O); AND CALCULATE F(O)
        T= 0.0
        XX= XO
        WW= WIO
        FF= FCN(WW,TSIO,P)
        M= 1
        K=1
   20 CALL MODDEQ(DERIV,K,1,T,WW,WWDOT,DTAU,1.E-5)
        IF (K.LT.0) GO TO 99
        IF (WW.GT.0.35) GO TO 199
        FF= FCN(WW,TSIO,P)
        WRITE (6,603) T,WW,WWDOT,FF
        IF (M.GE.MAXKP) GO TO 21
        M=M+1
        GO TO 20
   21 CONTINUE
C NN -- EACH NN REPRESENTS A DIFFERENT CELL SIZE --
        DO 1000 NN=1,NMAX
        R= MAXN(NN)
        H= LENGTH/R
        MAXNP2= MAXN(NN) + 2
        TRANSF= KMAS*H/G
C LL -- EACH LL REPRESENTS A DIFFERENT BYPASS RATIO --
```

```
      DO 1000 LL=1,LMAX
      BYPASS= BY(LL)
      C= 1.0-BYPASS+TRANSF
      U= TRANSF/C
      DELTA= BYPASS/C
      B= (1.0-2.0*BYPASS)/C
C    START A BYPASS-CELL-MODEL COMPUTATION SCHEME *****
      WRITE (6,601) KK,DT(KK),DTAU,NN,H,LL,BYPASS
  601 FORMAT (//,1X,'KK=',I3,2X,'DT:DTAU:',2E16.7,/,20X,'NN=',
     1I3,2X,'LENGTH OF EACH CELL=',E16.7,10X,'LL=',I3,2X,' BYP
     2ASS RATIO=',E16.7,/,10X,'PARAMETERS (CO, TRANSF, C, U,
     3DELTA,B):')
      WRITE (6,606) CO,TRANSF,C,U,DELTA,B
      DO 101 I=3,MAXNP2
  101 W(I)= WIO
      T= 0.0
      DO 10 KT=1,MAXKP
C *ONE STEP* INTEGRATION ON THE ADSORBENT ****
      DO 2 I=3,MAXNP2
      IF (KT.EQ.1) GO TO 1
      XX= X(I)
      WW=W(I)
      FF=F(I)
      IF (KT.GE.KPREDT) GO TO 60
C *1  INTEGRATION BY MODDEQ LIB. SUBROUTINE (RUNGE/KUTTA-GILL
C     METHOD) TO KPREDT - 1
      M= 1
      K=1
   50 CALL MODDEQ(DERIV,K,1,T,WW,WWDOT,DTAU,1.E-5)
      IF(K.LT.0) GO TO 99
      WRITE(6,603)T,WW,WWDOT
      W(I)=WW
      IF (KT.LT.KPTM2) GO TO 52
      IF (M.EQ.1) GO TO 52
      MM= 2
      IF (KT.EQ.KPTM2) MM= 1
      WP(I,MM) = W(I)
   52 IF (M.GE.2) GO TO 51
      M= M+1
      GO TO 50
   51 IF (I.NE.MAXNP2) T= T - DTAU
      GO TO 1
C *2   INTEGRATION BY SIMPLE PREDICTOR-CORRECTOR METHOD
   60 IF (I.EQ.3) T= T+ DTAU
      E(I)= XX -FF
      PW= WP(I,1) + 2.0*DTAU*E(I)
      IF (PW.GT.0.35) GO TO 199
      XPW= FCN(PW,TSIO,P)
      XPX= U*XPW +DELTA*X(I-2) + B*X(I-1)
      CW= WP(I,2) + 0.5*DTAU*(E(I) + XPX- XPW)
      W(I)= CW + 0.20* (PW -CW)
      WP(I,1)= WP(I,2)
      WP(I,2)= W(I)
C     CALCULATION OF X(I),F(I)   BY RECURSION RELATIONSHIP
```

```
    1 CONTINUE
      WI= W(I)
      IF (WI.GT.0.35) GO TO 199
      F(I)= FCN(WI,TSIO,P)
      X(I)= U*F(I) + DELTA*X(I-2) + B*X(I-1)
    2 CONTINUE
      WRITE(6,610) (W(I),I=3,MAXNP2)
      XP= (1.0-BYPASS)*X(MAXNP2) + BYPASS*X(MAXNP2-1)
      WRITE (6,610) (F(I),I=3,MAXNP2)
      WRITE (6,610) (X(I),I=3,MAXNP2)
      WRITE (6,613) KT,T,XP
  613 FORMAT (/,1X,'T(',I4,2X,') =',E13.6,5X,'OUTPUT X =',E20.
     17,10X,'T=T + DTAU BELOW',/)
   10 CONTINUE
 1000 CONTINUE
      GO TO 100
   99 WRITE(6,699) KK,NN,LL,T,WW,WWDOT
  699 FORMAT(/,1X,'ERROR',3I10,3E20.7)
      GO TO 100
  199 WRITE(6,799) WI,KK,NN,LL,KT,I
  799 FORMAT(/,1X,'WI GREATER THAN .35 AS',E20.7,5X,5I10)
  100 CONTINUE
      STOP
      END
      SUBROUTINE DERIV(N,T,WW,WWDOT)
      COMMON/WINTG/XX,FF
      WWDOT=XX-FF
      RETURN
      END
```

```
C      ADIABATIC ADSORPTION
C   --  BYPASS CELL MODEL  ---
C   ***    FOR GENERAL LEWIS NUMBER  ***
       DIMENSION  W(32),TS(32),WP(32,2),TP(32,2),FW(32),ET(32),
      1BY(4),Y(2),YDOT(2),MAXK(8),MAXN(8),DT(4)
       COMMON /YINTG/X(32),TT(32),F(32),CPS,DHCS,I
       REAL*4 H,LENGTH,KMAS,LEWIS
       EXTERNAL DERIV
  508  FORMAT (8I10)
  514  FORMAT (4F20.7)
  603  FORMAT (2X,6E20.7)
  606  FORMAT (/,1X,8E16.7)
  610  FORMAT (/,1X,10E13.6)
C      READ IN EXP. DATA & MODELING PARAMETERS: THEN CALCULATE
C      DYNAMIC PARAMETERS
       READ (5,514) LENGTH,G,KMAS,PSBULK
       READ (5,514) P,XO,TO,DELTAH
       READ (5,514) WIO,TSIO,CP,CS
       READ (5,514) LEWIS
       READ (5,508) KMAX,NMAX,LMAX,KPREDT,KPTM2,INLETG
       READ (5,508) (MAXK(J),J=1,KMAX)
       READ (5,514) (DT(J),J=1,KMAX)
       READ (5,508) (MAXN(J),J=1,NMAX)
       READ (5,514) (BY(J),J=1,LMAX)
       CO= KMAS/PSBULK
       CPS= CP/CS
       DHCS= DELTAH/CS
       WRITE (6,604) XO,TO,WIO,TSIO,P,CP,CS,DELTAH
  604  FORMAT (/,1X,'XO,TO,WIO,TSIO,P,CP,CS,DELTAH:',8E12.5)
       X(1)= XO
       X(2)= XO
       TT(1)= TO
       TT(2)= TO
C KK -- EACH KK REPRESENTS A DIFFERENT TIME INTERVAL --
       DO 1000 KK=1,KMAX
       DTAU= CO*DT(KK)
       MAXKP= MAXK(KK) + 1
C    INTEGRATION OF INLET W(O);TS(O); AND CALCULATE F(O)
       IF (INLETG.NE.0) GO TO 21
       I=2
       T=0.0
       WI= WIO
       TSI= TSIO
       F(2)= FCN(WI,TSIO,P)
       M=1
       Y(1)= WIO
       Y(2)= TSIO
       K=1
    20 CALL MODDEQ(DERIV,K,2,T,Y,YDOT,DTAU,1.E-5)
       IF (K.LT.0) GO TO 99
       WI= Y(1)
       TSI= Y(2)
       IF (WI.GT.0.35) GO TO 199
       F(2)= FCN(WI,TSI,P)
```

```
      WRITE (6,603) T,(Y(J),YDOT(J),J=1,2),F(2)
      IF (M.GE.MAXKP) GO TO 21
      M=M+1
      GO TO 20
   21 CONTINUE
C NN -- EACH NN REPRESENTS A DIFFERENT CELL SIZE --
      DO 1000 NN=1,NMAX
      R= MAXN(NN)
      H= LENGTH/R
      MAXNP2= MAXN(NN) + 2
      TRANSF= KMAS*H/G
      ALPHA= TRANSF*LEWIS
      WRITE (6,603)        CO,CPS,DHCS,TRANSF,ALPHA,LEWIS
C * NOTE: NOW, CPS= LEWIS*CP/CS
      CPS= CPS*LEWIS
C LL -- EACH LL REPRESENTS A DIFFERENT BYPASS RATIO --
      DO 1000 LL=1,LMAX
      BYPASS= BY(LL)
      C= 1.0-BYPASS+TRANSF
      U= TRANSF/C
      DELTA= BYPASS/C
      B= (1.0-2.0*BYPASS)/C
      CT= 1.0-BYPASS+ALPHA
      UT= ALPHA/CT
      DELTAT= BYPASS/CT
      BT= (1.0-2.0*BYPASS)/CT
C    START A BYPASS-CELL-MODEL COMPUTATION SCHEME *****
      WRITE (6,601) KK,DT(KK),DTAU,NN,H,LL,BYPASS,CPS
  601 FORMAT (//,1X,'KK=',I3,2X,'DT;DTAU:',2E16.7,/,20X,'NN=',
     1I3,2X,'LENGTH OF EACH CELL=',E16.7,10X,'LL=',I3,2X,' BYP
     2ASS RATIO',2E15.7,/,10X,'PARAMETERS (C,U,DELTA,B -S BOTH
     3 FOR W & TS **) :')
      WRITE (6,606) C,U,DELTA,B,CT,UT,DELTAT,BT
      DO 101 I=3,MAXNP2
      TS(I)= TSIO
  101 W(I)= WIO
      T= 0.0
      DO 10 KT=1,MAXKP
C *ONE STEP* INTEGRATION ON THE ADSORBENT ****
      DO 2 I=3,MAXNP2
      IF (KT.EQ.1) GO TO 1
      IF (KT.GE.KPREDT) GO TO 60
C *1  INTEGRATION BY MODDEQ LIB. SUBROUTINE (RUNGE/KUTTA-GILL
C     METHOD) TO KPREDT - 1
      M= 1
      Y(1)= W(I)
      Y(2)= TS(I)
      K=1
   50 CALL MODDEQ(DERIV,K,2,T,Y,YDOT,DTAU,1.E-5)
      IF(K.LT.0) GO TO 99
      WRITE(6,603)T,(Y(J),YDOT(J),J=1,2)
      W(I)= Y(1)
      TS(I)= Y(2)
      IF (KT.LT.KPTM2) GO TO 52
```

```
      IF (M.EQ.1) GO TO 52
      MM= 2
      IF (KT.EQ.KPTM2) MM= 1
      WP(I,MM) = W(I)
      TP(I,MM)= TS(I)
   52 IF (M.GE.2) GO TO 51
      M= M+1
      GO TO 50
   51 IF (I.NE.MAXNP2) T= T - DTAU
      GO TO 1
C *2   INTEGRATION BY SIMPLE PREDICTOR-CORRECTOR METHOD
   60 IF (I.EQ.3) T= T+ DTAU
      EW(I)= X(I) - F(I)
      ET(I)= -CPS*(TP(I,2)-TT(I)) + DHCS*EW(I)
      PW= WP(I,1) + 2.0*DTAU*EW(I)
      PT= TP(I,1) + 2.0*DTAU*ET(I)
      IF (PW.GT.0.35) GO TO 199
      XPW= FCN(PW,PT,P)
      XPX= U*XPW +DELTA*X(I-2) + B*X(I-1)
      TPT= UT*PT + DELTAT*TT(I-2) + BT*TT(I-1)
      GP3W= XPX - XPW
      CW= WP(I,2) + 0.5*DTAU*(EW(I) + GP3W)
      CT= TP(I,2) + 0.5*DTAU*(ET(I) -CPS*(PT-TPT) + DHCS*GP3W)
      W(I)= CW + 0.20* (PW -CW)
      TS(I)=CT + 0.20* (PT -CT)
      WP(I,1)= WP(I,2)
      WP(I,2)= W(I)
      TP(I,1)= TP(I,2)
      TP(I,2)= TS(I)
C     CALCULATION OF X(I),TT(I),F(I)  BY RECURSION RELATIONSHIPS
    1 CONTINUE
      WI= W(I)
      TSI= TS(I)
      IF (WI.GT.0.35) GO TO 199
      F(I)= FCN(WI,TSI,P)
      X(I)= U*F(I) + DELTA*X(I-2) + B*X(I-1)
      TT(I)= UT*TS(I) + DELTAT*TT(I-2) +BT*TT(I-1)
    2 CONTINUE
      WRITE(6,610) (W(I),I=3,MAXNP2)
      WRITE(6,610)(TS(I),I=3,MAXNP2)
      XP= (1.0-BYPASS)*X(MAXNP2) + BYPASS*X(MAXNP2-1)
      TTP= (1.0-BYPASS)*TT(MAXNP2) + BYPASS*TT(MAXNP2-1)
      WRITE (6,610) (F(I),I=3,MAXNP2)
      WRITE (6,610) (X(I),I=3,MAXNP2)
      WRITE (6,610)(TT(I),I=3,MAXNP2)
      WRITE (6,613) KT,T,XP,TTP
  613 FORMAT (/,1X,'T(',I4,2X,') =',E13.6,5X,'OUTPUT X =',E20.
     17,10X,'OUTPUT TT =',E16.7,/)
   10 CONTINUE
 1000 CONTINUE
      GO TO 100
   99 WRITE(6,699) KK,NN,LL,T,(Y(J),YDOT(J),J=1,2)
  699 FORMAT(/,1X,'ERROR',3I5,5E16.7)
      GO TO 100
```

```
199 WRITE(6,799) WI,KK,NN,LL,KT,I,TSI
799 FORMAT(/,1X,'WI GREATER THAN .35 AS',E20.7,5X,5I5,E20.7)
100 CONTINUE
    STOP
    END
    SUBROUTINE DERIV(N,T,Y,YDOT)
    DIMENSION Y(2),YDOT(2)
    COMMON /YINTG/X(32),TT(32),F(32),CPS,DHCS,I
    XMF= X(I) - F(I)
    YDOT(1)= XMF
    YDOT(2)= -CPS*(Y(2)-TT(I)) + DHCS*XMF
    RETURN
    END
```

```
C       TO EVALUATE THE EQUILIBRIUM X CONC. AT SURFACE OF ADSORBENT
C        X* = FCN ;  WHERE THE ARGUMENTS ARE  W(I), TS(I), P
        FUNCTION FCN(WI,TSI,P)
        IF(WI-.05) 1,1,2
      1 A= 402.263374E-6
        B= -893.827167E-4
        Q= 7.06882716
        D= -182.152263
        E= 11.8621399E-6
        F= -32.6790123E-4
        G= .322929012
        R= -10.4143621
        WIV= WI
        GO TO 20
      2 WIV= 1.0
        IF(WI-.10) 3,3,4
      3 A= -7.80864197E-6
        B= 43.1203703E-4
        Q= -.484787037
        D= 17.2044753
        E= 1.98919753E-6
        F= -6.02453703E-4
        G= .0580578703
        R= -1.83632253
        GO TO 20
      4 IF(WI-.15) 5,5,6
      5 A= 20.8333333E-6
        B= -38.25E-4
        Q= .255416667
        D= -4.6825
        E= -.875E-6
        F= 2.1125E-4
        G= -0.0159625
        R= .352375
        GO TO 20
      6 IF(WI-.20) 7,7,8
      7 A= 53.3333333E-6
        B= -138.0E-4
        Q= 1.26466667
        D= -38.0
        E= -5.75E-6
        F= 17.075E-4
        G= -.16735
        R= 5.35
        GO TO 20
      8 IF(WI-.25) 9,9,10
      9 A= -81.6666667E-6
        B= 213.5E-4
        Q= -1.75233333
        D= 47.60
        E= 21.25E-6
        F= -53.225E-4
        G= .43605
        R= -11.770
```

```
      GO TO 20
   10 IF(WI-.30) 11,11,12
   11 A= 40.0E-6
      B= -81.0E-4
      Q= .5990
      D= -14.1
      E= -9.16666667E-6
      F= 20.4E-4
      G= -.151783333
      R= 3.655
      GO TO 20
   12 A= 20.0E-6
      B=-37.0E-4
      Q= .291
      D= -6.9
      E= -3.16666667E-6
      F= 7.2E-4
      G= -.0593833333
      R= 1.495
   20 PE=(((A*TSI+B)*TSI+Q)*TSI+D)*WI*WIV+(((E*TSI+F)*TSI+G)*T
     1SI+R)*WIV
      FCN=0.62197*PE/(P-PE)
      RETURN
      END
```

NOMENCLATURE

A	cross-sectional area of the packed bed
a	the dimensionless quantity defined in Eq. (24) or (45)
a_s	external area of adsorbent per unit volume
b	the dimensionless quantity defined in Eq. (24) or (45)
C_p	heat capacity
D_e	effective diffusivity
d_p	diameter of the solid adsorbent
f	functionality of the equilibrium adsorbate content at the solid surface with respect to the adsorbate content in the adsorbent
G	mass velocity
ΔH	heat of adsorption, BTU/lb_x
h	cell length
h_t	heat transfer coefficient, BTU/ft^2sec ^oF
k_e	effective thermal conductivity, BTU/ft sec ^oF
k_m	mass transfer coefficient, $lb_x/(ft^2sec)(lb_x/lb_f)$
L	length of the packed bed
N	number of cell used to simulate the packed bed
T	fluid temperature
T_s	adsorbent temperature
t	time
u	local linear velocity
v	apparent or superficial velocity
w	adsorbate content in the adsorbent, lb_x/lb_s
x	adsorbate content in the fluid, lb_x/lb_f

x^* equilibrium adsorbate content at the surface of adsorbent, lb_x/lb_f

z length along the packed bed

Greek Symbols

α the dimensionless quantity defined by Eq. (22) or (43)

δ the dimensionless quantity defined in Eq. (24) or (45)

ε bed porosity

θ cell residence time

μ bypass ratio

ρ density

τ dimensionless time

Subscripts

f denotes fluid conditions

i denotes the quantities of cell i

m denotes mass transfer quantities

o denotes boundary or initial conditions

p denotes output conditions

s denotes adsorbent conditions

t denotes heat transfer quantities

x denotes adsorbate conditions

BIBLIOGRAPHY

1. Thiele, E. W., I and EC 38, 646 (1946).

2. Vermeulen, T., Advances in Chemical Engineering 2, Academic Press, New York (1958).

3. Lightfoot, E. N., Sanchez-Palma R. J. and Edwards, D. O., New Chemical Engineering Separation Techniques, Interscience, New York (1962).

4. Hougen, O. A. and Marshall, W. R., Chem. Eng. Progr. 43, 197 (1947).

5. Acrivos, A., I and EC 48, 703 (1956).

6. Van Arsdel, W. B., Chem. Eng. Progr. Sym. Series No. 16, 47 (1955).

7. Chi, C. W. and Wasan, D. T., AIChE Jour. 16, 23 (1970).

8. Bullock, C. E., Ph.D. Thesis, University of Minnesota (1965).

9. Schneider, P. J., Trans. ASME 79, 765 (1957).

10. Meyer, O. A. and Weber, T. W., J. Am. Inst. Chem. Eng. 13, 457 (1967).

11. Levenspiel, O., Chemical Reaction Engineering, John Wiley, New York (1962).

12. Deans, H. A. and Lapidus, L., AIChE Jour. 6, 656 & 663 (1960).

13. McGuire, M. L. and Lapidus, L., AIChE Jour. 11, 85 (1965).

14. Vanderveen, J. W., Luss, D. and Amundson, N. R., AIChE Jour. 14, 636 (1968).

15. Du Domaine, J., Swain, R. L. and Hougen, O. A., I and EC 35, 546 (1943).

16. Hubard, S. S., I and EC 46, 356 (1954).

17. Keenan, J. H. and Keyes, F. G., Thermodynamic Properties of Steam John Wiley, New York (1936).

18. Brand, L., Advanced Calculus, John Wiley, New York (1955).

19. Private notes on Transport Phenomena Course at Caltech (1967).

PROPOSITION III

EFFECTS OF SURFACTANTS ON COALESCENCE REST TIMES OF DROPS

ABSTRACT

The rest time of liquid drops passing through a continuous phase with various surfactants was studied. The following surfactants were used: oil-soluble surfactants--stearic acid, oleic acid, and cholesterol; and water-soluble surfactants--ethylhexadecyldimethyl ammonium bromide, TMN, sodium lauryl sulfate, and sodium decyl-benzenesulfonate. The rest time of the liquid drops ranged from 0.874 to 397.385 seconds and the interfacial tension ranged from 1.2 to 34.2 dynes per centimeter.

It was observed that the rest time of a surfactant system was dependent primarily upon the rate of rupture of the interfaces and the drainage time of the continuous film. A Gaussian distribution which could be characterized by an arithmetic mean rest time was obtained for each run.

Reprinted from JOURNAL OF CHEMICAL & ENGINEERING DATA, Vol. 14, No. 1, January 1969, Page 67

Effects of Surfactants on Coalescence Rest Times of Drops

G. C. HSU[1] and R. C. KINTNER
Illinois Institute of Technology, Chicago, Ill. 60616

Data are reported for the rest times of drops coalescing at a flat interface in the presence of a chemically pure surface active agent. Benzene-water and water-benzene systems were used with seven surface active agents. Rest time distributions were essentially Gaussian. Film drainage time followed by a rupture time showed an exponential decay pattern. Values reported included average, minimum, maximum, median, and drainage times and the rate of rupture constant.

IF TWO nearly immiscible liquids be intimately mixed by a turbulence-creating device in the absence of a surface active agent, a temporary emulsion will form. If allowed to settle in a quiescent environment, the primary break will occur in seconds or a few minutes. A secondary emulsion, consisting of micron and submicron size droplets of the dispersed phase, will usually persist in one of the bulk phases. To separate the dispersed phase from such a dispersion it is necessary to coalesce the submicroscopic droplet into large ones of settleable size. One measure of the difficulty of the coalescence operation is the rest time of large drops at a flat interface between large volumes of the two phases. Recent reviews by Hartland (5) and Lawson (8) treat the theoretical and experimental aspects of the determination of rest time and its significance. In the present instance we are concerned not only with rest time criteria but with the effect of definable surface active agents upon them.

EXPERIMENTAL

The equipment used for the determination of drop rest time was slightly modified from that of Charles and Mason (*1*) and was similar to that used by others (*2, 3, 4*). An open-top cell design was used to facilitate construction, cleaning, and assembly. One of the two coalescent cells (*6*) was designed for using an organic continuous phase. The aqueous drops were allowed to fall to the interface. The other cell was so constructed that a light drop of an organic liquid could be released from a submerged nozzle and rise through a continuous aqueous phase to the interface. Provision was made for renewal of the interface by periodic flushing with the aqueous phase. The temperature of the water bath surrounding the cell was controlled to ±0.5° C. An electric timer was used to determine rest time. Its 0.01-second scale divisions were so spaced as to permit estimations of 0.001 second, although the accuracy of such an estimation was somewhat questionable. Drop volumes were measured with a microburet.

[1] Present address: California Institute of Technology, Pasadena, Calif.

The two cells are illustrated in Figure 1. The open top, *A*, was covered with clean hard paper during operation to prevent contamination. The continuous phase was contained in the central portion across the top of the inner cup, *B*, which was used for the renewal of the organic-aqueous interface. The side arm, *C*, permitted waste liquid to be removed from the cell. The drop was released from

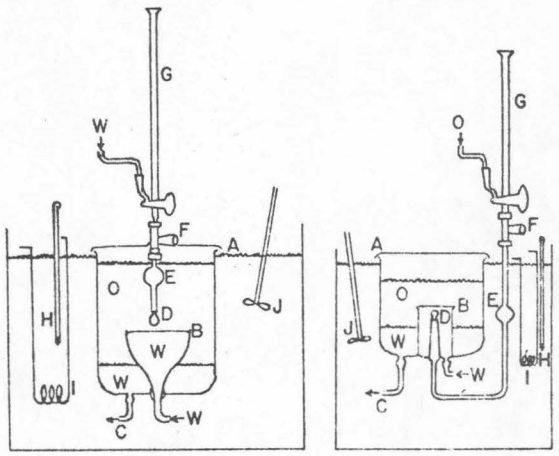

Figure 1. Diagram of coalescence cells
Left. Falling drop *Right.* Rising drop

A. Coalescence cell mouth	F. Micrometer
B. Continuous phase removal	G. Microburet
C. Waste liquid suction	H. Thermometer
D. Drop forming tip	I. Heater
E. Reservoir	J. Stirrer

the interchangeable nozzle, D, connected to a reservoir, E, which provided sufficient residence time to ensure temperature equilibrium. Fresh drop liquid was introduced from the microburet, G, through the micrometer, F, which permitted the drop formation to proceed at a desired rate. All connecting tubes were of polyethylene. Valves were of Teflon or stainless steel.

Interfacial and surface tension measurements were carried out with a Cenco-Du Nuoy Tensiometer.

The distance from the tip of the drop to the interface was kept within 5mm. to avoid impact effects. The micrometer, F, was adjusted to a desirable opening to allow the drop to remain on the nozzle for 1.5 to 2 minutes in order to come to thermal and mass equilibrium. Rest time, t, was read on the electric timer, the smallest digit being an estimated value. Drop volume was read directly on the microburet to ± 0.01 ml. After each group of eight drops, the interface was renewed and made planar. The heavier phase was periodically drawn out through side arm C.

The drop and field fluids (benzene, monochlorobenzene, styrene, and benzyl alcohol) were of the highest purity available from laboratory supply companies. Surfactants used in industrial operations are usually a mixture of rather uncertain purity. Some are soluble in both organic and aqueous phases. Some, while soluble in organic solvents, will hydrolyze when such solutions are intimately in contact with water. To avoid these uncertainties, the surfactants chosen were definite chemical compounds of the highest purity (as certified by the Fisher Scientific Co.). The sole exception was TMN (trimethyl nonyl ether of hexaethylene glycol) Tergital, supplied by the Union Carbide Chemicals Co. It is insoluble in benzene if first dissolved in water. A series of surface tension tests was carried out to be certain that the two phases were mutually saturated before the beginning of each run. The properties of the various solutions are given in Table I. The abbreviations of the proper names of all liquids used are given at the bottom of Table II.

Table I. Experimental Results of Interfacial Tensions and Surface Tensions

Oil-Soluble Surfactant				Water-Soluble Surfactant			
Surfactant (in continuous phase)	Interfacial tension, dynes/cm.	Surface tension dynes/cm.		Surfactant (in continuous phase)	Interfacial tension, dynes/cm.	Surface tension dynes/cm.	
		Benzene	Water			Benzene	Water
None	34.2	28.8	71.2	None	34.2	28.8	71.2
Stearic acid				Ethyl hexadecyl dimethyl-ammonium bromide			
0.01M	28.4	28.45	71.0	0.0005M	2.4	28.2	37.12
0.05M	25.7	28.2	69.9	0.001M	1.2	28.15	37.08
0.1M	20.0	28.2	69.7	0.01M	2.1	28.3	33.6
Oleic acid				TMN			
0.005M	24.9	28.35	63.4	0.01M	15.5	28.6	41.4
0.01M	23.1	28.35	62.0	Sodium lauryl sulfate			
0.05M	20.35	28.2	58.5	0.005M	4.2	28.5	34.0
Cholesterol				Sodium decyl benzenesulfonate			
0.001M	27.2	28.2	68.5	0.008M	3.0	28.4	31.2
0.002M	22.6	28.0	66.6				
0.005M	17.8	28.0	64.4				

Table II. Rest Time Data

Run No.	Drop Phase	Containing Phase	Surfactant	Drop Vol., Ml.	Rest Times, Sec.				Drain Time, t_o	Rate of Rupture Constant, K, Sec.$^{-1}$
					$\bar{t}$	t_{min}	t_{max}	$t_{1/2}$		
101	BA	W	...	0.128	2.538	1.050	5.966	...	...	...
103	W	S	...	0.296	1.499	0.460	2.762	...	...	...
105	CB	W	...	0.318	11.682	1.620	25.351	...	...	...
106	W	B	...	0.298	3.190	0.682	5.348	...	...	...
201	W	B	...	0.307	4.852	0.890	10.971	...	...	...
203	W	B	...	0.301	4.938	1.387	13.029	4.3	2.8	0.456
204	W	B	...	0.302	4.986	0.874	11.200	4.55	2.98	0.443
205	W	B	...	0.308	5.774	1.430	16.010	...	...	...
208	W	B	...	0.300	4.595	0.960	10.210	...	...	...
301	W	B	StA (0.01M)	0.302	7.213	3.297	13.745	6.4	4.5	0.370
303	W	B	StA (0.05M)	0.301	8.733	4.150	14.522	8.2	6.2	0.346
305	W	B	StA (0.1M)	0.300	9.626	5.274	14.872	9.05	6.95	0.329
311	W	B	OA (0.005M)	0.302	7.400	2.981	17.746	6.95	5.00	0.356
313	W	B	OA (0.01M)	0.300	8.012	4.230	15.883	7.15	5.12	0.341
314	W	B	OA (0.05M)	0.300	9.652	3.607	19.232	8.15	5.2	0.238
321	W	B	Ch (0.005M)	0.195	27.930	10.285	58.220	24	13	0.685
322	W	B	Ch (0.001M)	0.200	10.144	6.321	15.213	...	...	...
323	W	B	Ch (0.002M)	0.200	17.809	6.244	36.683	16	12	0.1658
401	B	W	EDAB (0.001M)	0.017	206.633	70.421	397.385	178	117	0.0114
402	B	W	EDAB (0.005M)	0.015	115.880	48.280	254.350	105	71	0.0202
403	B	W	EDAB (0.0005M)	0.015	155.249	57.686	312.245	146	108	0.0184
411	B	W	TMN (0.01M)	0.205	14.674	6.820	20.470	12.9	10.7	0.311
412	W	B	TMN (0.01M)	0.105	3.378	1.110	6.510	2.15	1.14	0.782
421	B	W	SLS (0.005M)	0.038	94.620	38.365	185.376	92	71	0.0338
422	B	W	SDBS (0.008M)	0.055	126.061	52.734	231.250	128	98	0.0228

BA, benzyl alcohol. W, water. S, styrene. CB, monochlorobenzene. StA, stearic acid. OA, oleic acid. Ch, Cholesterol. EDAB, ethyl hexadecyl dimethyl ammonium bromide. TMN, Trimethyl nonyl ether of hexaethylene glycol (Union Carbide Chemicals Co.). SLS, sodium lauryl sulfate. SDBS, sodium decyl benzene sulfonate.

Since the surface active chemicals used were of the highest purity available, it was assumed that the effects of the slight amounts of impurities present could be neglected. It was qualitatively estimated that such impurities, if present, acted as some low molecular weight compounds acting through the Marangoni effect. Their effect on the rest time would therefore be unobservable.

It was assumed that all drops were spherical and that the interfaces were flat. For the systems used in this work and in the apparatus employed, these were good approximations. External mechanical influences were minimized and assumed to have negligible effect on the results. Only major film-thinning forces were considered, and minor phenomena such as electroviscosity, electric double-layer repulsion, internal circulation, etc., were assumed to be negligible for the rest time evaluation.

CORRELATION OF DATA

The theoretical background and its logical application may be found in previously published papers (*1-8*). The main points are:

The relationship between the fraction of drops coalesced, f, when plotted against the rest time, t, should exhibit an approximately Gaussian distribution. When plotted on probability paper, the points should lie along a straight line. This test of the nature of the distribution of rest times is seldom reported.

The equation,

$$\ln N = \ln (1 - f) = - K (t - t_0)^x \qquad (1)$$

will generally represent the rest time distribution. Gillespie and Rideal (*4*) found x to be 1.5, while Cockbain and McRoberts (*2*) found it to be unity. Elton and Picknett (*3*) recommend $x = 1$. The present work indicates $x = 1$.

The value of t_0 can be obtained by reading it from the intercept on the t-axis of the straight-line portion of a plot of Equation 1 or calculated as

$$t_0 = t_{1/2} - (1/K) \ln 2 \qquad (2)$$

The value of $t_{1/2}$ may be read from the plot or by noting its value at the midpoint of a series of observations arranged in order of magnitude. In the latter method, it may not be on the best straight line drawn through the points.

The effect of a surfactant is to increase the rest time. The usual expression for this relationship is (*2*)

$$t_{1/2} = k_r C^m \qquad (3)$$

but the present work indicates that a better correlation is obtained by using the arithmetic mean rest time, $\bar{t}$, instead of the median value, $t_{1/2}$.

The important criteria in the present investigation are summarized in Table II. The 40 individual measurements from which the plots were made may be found in the thesis by Hsu (*6*). Values for run 204, illustrated by Figure 2, are given in Table III.

Constants in Equation 3 are given in Table IV for those surfactants for which runs at different concentrations were made. The average rest time, $\bar{t}$, was used in this correlation.

DISCUSSION OF RESULTS

For the benzene-water system the stabilities of the individual drops varied. The results followed a Gaussian distribution curve sufficiently reproducible for analysis. Initially, 50 drops were taken for a run, but it was found later that 40 coalescence measurements were enough. If the fraction of uncoalesced drops, N, was plotted against time, an exponential decay distribution was obtained as in Figure 2. Such a distribution curve indicates that the lifetimes of the drops are determined by two distinct processes—drainage of the continuous phase between the drop and the interface, followed by rupture of the adsorbed film.

Analysis of data also showed that most of the results of this investigation gave straight lines for the fraction of uncoalesced drops, N, between 0.05 and 0.60.

This work proposes that the action of a surface active agent is not only to increase the viscosity of the continuous phase, thereby decreasing the rate at which two interfaces can approach each other, but also to reduce the interfacial tension, thereby decreasing the rate of film rupture. It was observed in the experiments (Table II) that surfactants change the mean rest time more effectively than the minimum rest time. This indicates that surfactants have somewhat less effect on the drainage of liquid between interfaces than upon the nature of interface itself.

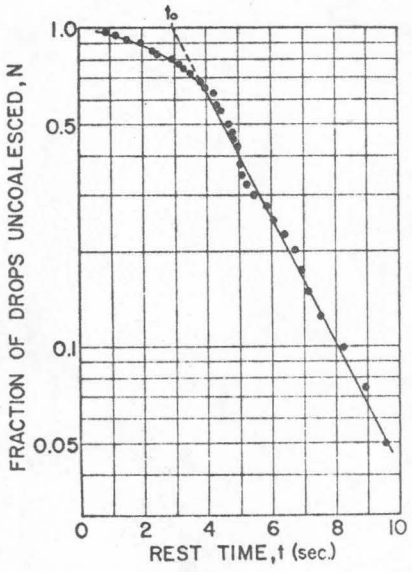

Figure 2. Semilogarithmic rest time distribution of water drops through benzene
Run 204

Table III. Rest Time of Water Drops Dispersed in Benzene

(Run 204)

	Rest Time, Sec.									
Group 1		Group 2		Group 3		Group 4		Group 5		
1	4.980	9	6.432	17	5.128	25	3.585	33	5.270
2	2.505	10	1.954	18	10.110	26	1.203	34	5.043
3	5.886	11	3.541	19	4.450	27	7.543	35	3.320
4	1.547	12	3.885	20	4.345	28	4.775	36	4.703
5	8.988	13	4.120	21	0.974	29	5.005	37	2.201
6	4.870	14	8.310	22	4.805	30	5.498	38	9.541
7	11.200	15	6.130	23	3.950	31	2.981	39	4.632
8	6.902	16	2.288	24	7.155	32	3.147	40	6.742

Table IV. Constants in Rest Time–Concentration Correlation[a]

Surfactant	m	k_r
Stearic acid	0.141	13.2
Oleic acid	0.134	14.64
Cholesterol	0.535	410

[a] Rest time concentration correlation $t = k_r C^m$.

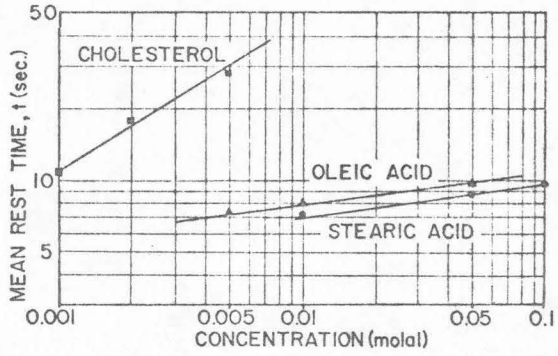

Figure 3. Mean rest time as a function of concentration of surfactant

Besides the above observations, this work led to the following:

Drainage Time, t_0. For time greater than the drainage time, t_0, a linear relationship was obtained for the logarithmic rest time distribution calculated by $t_0 = t_{1/2} - (1/K) \ln 2$. This agrees with the theory used to develop this equation, since it assumes the interfacial rupture process dominates after time t_0. Thus the use of this equation is supported by this work.

Mean Rest Time, $\bar{t}$. Table II shows that $\bar{t}$ represents the stability of the system better than $t_{1/2}$, t_{min}, or t_{max}. This has been also checked by the fact that $\bar{t}$ could be correlated to concentration of surfactant as shown in Figure 3. Thus, it is reasonable to take the arithmetic mean rest time $\bar{t}$ as the criterion to represent the stability of a system.

Concentration of Surfactant. As the concentration of surfactant increases, the rest time increases correspondingly; the K value (Table II) decreases as the range of rest time is broadened. Furthermore, the mean rest time, $\bar{t}$, could be correlated as shown in Figure 3 by the relation $\bar{t} = k_c C^m$ where parameters k_c and m are different for each system (Table IV).

Saturation or Unsaturation. Run 106 shows that the unsaturated benzene gave a shorter mean rest time of 3.19 seconds, while the saturated system gave approximately 4.94 seconds. The mutually saturated phases normally give longer lifetimes than the unsaturated phases. This effect is noticeable even when the solubility is very slight.

Stability of Water-Oil or Oil-Water Emulsion. It was clearly indicated by the nonionic surfactant study (TMN) that for the same oil-water interface, benzene drops coalesced with the bulk oil phase at a rate which differed from the rate of coalescence of water drops. This indicates that oil drops are stabilized by water-soluble surfactants, and water drops are stabilized by oil-soluble surfactants. The results of this work in general agree with the concept advanced by earlier workers that some part of the drop must "wet" the bulk liquid before coalescence can occur. If the surfactant is soluble in water and insoluble in the oil, it will collect on the outside of oil drops and tend to prevent their coalescence. However, if the drops are water instead of oil, the surfactant is inside the drops and as the molecules of surfactant are free to move into the drops, there is very little film to prevent coalescence when the drop comes in contact with the interface.

Critical Micellar Concentration (CMC). The K value decreased with increasing concentration of ethyl hexadecyl dimethyl ammonium bromide (EDAB water-soluble surfactant) from $0.0005M$ to $0.001M$ and then increased as EDAB increased to $0.005M$. This means that mean rest time reaches a maximum near the concentration of $0.001M$. Cockbain and McRoberts (2) reported that the critical micellar concentration of EDAB was about $0.0008M$. This is consistent with the previous suggestion (2) that oil drops possess maximum stabilities at concentrations slightly greater than the critical micellar concentrations.

Partial Coalescence. Through all the experiments, the drops did not coalesce completely with the bulk phase in a single stage. Partial coalescence occurred, leaving a smaller drop which, in turn, partially coalesced again. Generally speaking, this phenomenon was observed in the presence of low concentrations of surfactants. But at higher concentrations where the interfacial tensions were very low, coalescence appeared to occur in a single stage.

NOMENCLATURE

- C = concentration of surfactant, molar
- f = fraction of drops coalesced
- K = rupture constant in Equation 1, sec.$^{-1}$
- k_c = coefficient in Equation 3
- m = exponent in Equation 3
- N = $(1 - f)$ = fraction of drops uncoalesced
- t = rest time of drop at interface, sec.
- t_0 = t – intercept of straight-line portion in plot ln N *vs.* t, sec.
- $t_{1/2}$ = median rest time of large number of drops of specific size, sec.
- $\bar{t}$ = arithmetic mean rest time of large number of drops of specific size, sec.
- t_{min} = lowest value of t in series, sec.
- t_{max} = largest value of t in series, sec.
- x = exponent in Equation 1

LITERATURE CITED

(1) Charles, G.E., Mason, S.G., *J. Colloid Sci.* 15, 105, 236 (1960).
(2) Cockbain, E.G., McRoberts, T.S., *J. Colloid Sci.* 8, 440 (1953).
(3) Elton, G.A.H., Picknett, R.C., Second International Congress of Surface Activity, Vol. 1, pp. 288, 307 (1957).
(4) Gillespie, T., Rideal, E.K., *Trans. Faraday Soc.* 52, 173 (1956).
(5) Hartland, S., *Trans. Inst. Chem. Engrs. (London)* 45, T97 (1967).
(6) Hsu, G.C., M.S. thesis, Illinois Institute of Technology, Chicago, 1967.
(7) Jeffreys, G.V., Hawksley, J.L., *J. Appl. Chem.* 12, 329 (1962).
(8) Lawson, G.B., *Chem. Process Eng.* 48, No. 5, 45 (1967).

RECEIVED for review February 23, 1968. Accepted July 15, 1968. Work supported by Research Grant WP-1021, Federal Water Pollution Control Administration. For supplementary material order NAPS Document 00157 from ASIS National Auxiliary Publications Service, % CCM Information Sciences, Inc., 22 West 34th St., New York, N. Y., 10001, remitting $1.00 for microfiche or $3.00 for photocopies.